LEABHARLANN CHOLÁISTE NA TRÍONÓIDE, BAILE ÁTHA CLIATH | TRINITY COLLEGE LIBRARY DUBLIN
Ollscoil Átha Cliath | The University of Dublin

Terms and Conditions of Use of Digitised Theses from Trinity College Library Dublin

Copyright statement

All material supplied by Trinity College Library is protected by copyright (under the Copyright and Related Rights Act, 2000 as amended) and other relevant Intellectual Property Rights. By accessing and using a Digitised Thesis from Trinity College Library you acknowledge that all Intellectual Property Rights in any Works supplied are the sole and exclusive property of the copyright and/or other IPR holder. Specific copyright holders may not be explicitly identified. Use of materials from other sources within a thesis should not be construed as a claim over them.

A non-exclusive, non-transferable licence is hereby granted to those using or reproducing, in whole or in part, the material for valid purposes, providing the copyright owners are acknowledged using the normal conventions. Where specific permission to use material is required, this is identified and such permission must be sought from the copyright holder or agency cited.

Liability statement

By using a Digitised Thesis, I accept that Trinity College Dublin bears no legal responsibility for the accuracy, legality or comprehensiveness of materials contained within the thesis, and that Trinity College Dublin accepts no liability for indirect, consequential, or incidental, damages or losses arising from use of the thesis for whatever reason. Information located in a thesis may be subject to specific use constraints, details of which may not be explicitly described. It is the responsibility of potential and actual users to be aware of such constraints and to abide by them. By making use of material from a digitised thesis, you accept these copyright and disclaimer provisions. Where it is brought to the attention of Trinity College Library that there may be a breach of copyright or other restraint, it is the policy to withdraw or take down access to a thesis while the issue is being resolved.

Access Agreement

By using a Digitised Thesis from Trinity College Library you are bound by the following Terms & Conditions. Please read them carefully.

I have read and I understand the following statement: All material supplied via a Digitised Thesis from Trinity College Library is protected by copyright and other intellectual property rights, and duplication or sale of all or part of any of a thesis is not permitted, except that material may be duplicated by you for your research use or for educational purposes in electronic or print form providing the copyright owners are acknowledged using the normal conventions. You must obtain permission for any other use. Electronic or print copies may not be offered, whether for sale or otherwise to anyone. This copy has been supplied on the understanding that it is copyright material and that no quotation from the thesis may be published without proper acknowledgement.

AN INVESTIGATION OF THE FLUIDS INVOLVED IN THE FORMATION OF SOME IRISH LOWER CARBONIFEROUS DOLOMITES

CLAIRE MARIE MULHALL

A thesis submitted to the University of Dublin for the degree of Doctor of Philosophy

Department of Geology, University of Dublin, Trinity College.

November 2003

TRINITY COLLEGE
14 OCT 2004
LIBRARY DUBLIN
THESIS
7431

Declaration

Except where stated this thesis is entirely my own work. References and sources are duly acknowledged.

It has not previously been submitted for a degree at this or any other university.

C M Mulhall

Claire Marie Mulhall

DECLARATION

This thesis has not been submitted as an exercise for a degree at any other university. Except where stated, the work described therein was carried out by me alone.

I give permission for the Library to lend or copy this thesis upon request.

Signed:

Claire Marie Mulhall

To my parents

Summary

Irish Carboniferous rocks are host to an abnormally large amount of lead/zinc mineralisation and are internationally important in studies of the genesis of carbonate-hosted lead/zinc deposits. The host to mineralisation at Lisheen and Galmoy, the two most recently discovered commercial Zn-Pb deposits, is dolomitised late Tournaisian Waulsortian Limestone. This association between dolomite and base-metal sulphides has stimulated much research into the nature of the fluids responsible for the dolomitisation and the relation of dolomitisation to mineralisation. This study provides a more detailed examination of several dolomitised sections throughout the Irish Midlands, both within and outside the main mineralised zone, than carried out to date, in an effort to reconstruct their diagenetic and fluid flow history.

Dolomitisation post-dated the final porosity occlusion within the precursor limestone in all of the areas studied. Fine-grained grey dolomite occurred during the initial stages of dolomitisation and commonly selectively replaced the micrite and bryozoan material. Replacement by this dolomite was generally mimetic. Texturally later coarse-grained white dolomite has a similar luminescence to the fine-grained dolomite and is both a replacive and open space-filling dolomite. Replacement by this dolomite is non-mimetic, with the dolomite crystals being orders of magnitude greater than the precursor calcite phase. At least during the initial stages of dolomitisation dissolution seams may have been exploited as conduits, enabling the Mg bearing fluids to move through the well-cemented limestone.

In many of the areas studied, the coarse-grained white dolomite displays the curved crystal faces and sweeping extinction indicative of saddle dolomite, which suggests formation at elevated temperatures. Fluid inclusion data confirm that the coarse-grained dolomite formed from high temperature (>100°C), very saline (>17wt% combined NaCl and $CaCl_2$ equivalent) fluids. The coarse-grained dolomite is believed to have formed geothermally. It is not believed to be a hydrothermal dolomite, as it is thought to have formed at or near the same temperature as the surrounding rocks.

Halogen geochemistry data indicate that the dolomitising fluids in the majority of areas studied, were residual brines, formed by the evaporation of seawater past the point of halite precipitation. Na and K concentrations indicate that these fluids underwent interaction with feldspars and clay minerals, probably within the underlying Old Red Sandstone. Li

concentrations are substantially higher than those expected for seawater and indicate that many of these dolomitising fluids probably underwent interaction with the underlying basement lithologies.

A major unconformity at Navan and volcanic intrusions at Moyvore were used to stratigraphically date the porosity occlusion within the Waulsortian Limestone in the Irish Midlands. Petrographic data indicated an early Viséan age for both. Studies of the relationship between the basic igneous intrusions at Moyvore and carbonate and siliciclastic country rocks, showed that, at least locally, sandstones retained much of their original porosity and permeability longer than coeval carbonates and so may have formed aquifers, whereas carbonate lithologies were cemented quickly and were unlikely to be amenable to fluid flow, unless fractured.

Acknowledgements

I would like to thank Prof. George Sevastopulo for the supervision of this project, his encouragement, advice and friendship.

I would also like to thank the following:
Enterprise Ireland for funding this project and the Trinity Trust for travel assistance.

Dr Sarah Gleeson for always being there to answer my unending questions, providing me with a place to stay and being a great drinking buddy. Dr Adrian Boyce and Prof. Tony Fallick for their continued support, encouragement and willingness to help. The technicians at SUERC, especially: Andrew, Julie, Chris and Paul, for keeping me sane and providing me with the practical knowledge to run my samples.

The mining and exploration companies that granted me access to their drillcore and the many geologists that provided their time and help. In particular, Stuart Mills, Mark Cruise, Keith Henderson, Colin Chapman (Anglo American plc), Mark Holdstock (Tara Mines/Outokumpu) and Vaughan Williams (Navan Resources). Dr Michael Philcox for providing me with the Urlingford samples and for always allowing me to pick his brains.

Dr Martin Feely and Prof. Philippe Muchez for enabling me to spend time at their laboratories and adding to my knowledge of the wonderful world of fluid inclusions.

Dr Robbie Goodhue for keeping the stocks of liquid nitrogen topped up and for letting me run my final few isotopes on the new mass spectrometer. Neil, Declan, Frank and Maura, for whom nothing was ever too much trouble and Joann and Patrick for making life easy.

My postgraduate colleagues past and present, a number of whom have become and will remain close friends. In particular Becky and Niamh who remain my partners in crime and Diamond Dave and Mags for their constant willingness to help.

My family, whose love and support has always been incredible.

Chris, whose unwavering encouragement, support and patience has been wonderful.

TABLE OF CONTENTS

Declaration

Summary

Abstract

Acknowledgements

CHAPTER 1 INTRODUCTION AND REVIEW

1.1 Introduction 2

1.2 Overall aims 3

1.3 Specific objectives 3

1.4 Overview of Irish geology 4

1.5 The Irish Zn-Pb (Ba) orefield 6

1.5.1 Origin of the mineralising fluids 7

1.5.2 Timing of mineralisation 8

1.5.3 Depth of mineralisation 9

1.5.4 Mechanisms and pathways for fluid flow 13

CHAPTER 2 METHODS AND MATERIALS

2.1 Introduction 20

2.2 Sampling 20

2.3 Petrography 20

2.3.1 Transmitted light microscopy 21

2.3.2 Reflected light microscopy 21

2.3.3 Cathodoluminescence (CL) microscopy 21

2.4 Fluid inclusion microthermometry 22

2.5 Stable isotope geochemistry 23

2.5.1 Delta notation 23

2.5.2 Fractionation factor 24

2.5.3 Variables affecting the magnitude of fractionation factors 25

2.5.4 Isotopic characteristics of natural waters 27

2.5.5 Sample preparation and analysis 30

2.6 Crush-leach ion chromatography 31

2.6.1 Sample preparation and analysis 32

2.6.2 Cl/Br systematics 34
2.7 XRD 36

CHAPTER 3 LISHEEN

3.1 Introduction 39
3.2 Regional geological setting 39
3.2.1 Stratigraphy 39
3.2.2 Structure 40
3.2.3 Mineralisation and dolomitisation 40
3.3 Petrography 44
3.4 Paragenesis 47
3.5 XRD analyses of dolomitised micrite 47
3.6 Fluid inclusion microthermometry 49
3.7 Stable isotope geochemistry 53
3.7.1 Calcite 53
3.7.2 Dolomite 55
3.8 Modelling of parental fluids 56
3.9 Halogen geochemistry 57
3.10 Conclusions 59

CHAPTER 4 URLINGFORD

4.1 Introduction 70
4.2 Regional geological setting 70
4.2.1 Stratigraphy 70
4.2.2 Structure 70
4.3 Petrography 70
4.4 Paragenesis 71
4.5 Fluid inclusion microthermometry 72
4.6 Stable isotope geochemistry 73
4.6.1 Dolomite 73
4.7 Modelling of parental fluids 75
4.8 Halogen geochemistry 76
4.9 Conclusions 79

CHAPTER 5 NEWCASTLE WEST

5.1 Introduction 84

5.2 Regional geological setting 84

5.2.1 Stratigraphy 84

5.2.2 Structure 85

5.3 Petrography 85

5.4 Paragenesis 87

5.5 Fluid inclusion microthermometry 88

5.6 Stable isotope geochemistry 90

5.6.1 Calcite 90

5.6.2 Dolomite 94

5.6.3 Quartz 97

5.6.4 Pyrite 97

5.7 Modelling of parental fluids 98

5.7.1 A note on silica solubility 99

5.8 Halogen geochemistry 101

5.9 Conclusions 104

CHAPTER 6 NORTH CO. CORK

6.1 Introduction 114

6.2 Regional geological setting 114

6.2.1 Stratigraphy 114

6.2.2 Structure 115

6.3 Petrography 115

6.4 Paragenesis 117

6.5 Fluid inclusion microthermometry 118

6.6 Stable isotope geochemistry 122

6.6.1 Calcite 123

6.6.2 Dolomite 124

6.6.3 Pre-dolomite quartz 128

6.6.4 Post-dolomite quartz 129

6.7 Modelling of parental fluids 129

6.8 Halogen geochemistry 130

6.9 Conclusions 133

CHAPTER 7 CO. CARLOW

7.1 Introduction 143

7.2 Regional geological setting 143

7.2.1 Stratigraphy 143

7.2.2 Structure 144

7.2.3 Dolomitisation 144

7.3 Petrography 144

7.4 Paragenesis 148

7.5 Fluid inclusion microthermometry 149

7.6 Stable isotope geochemistry 153

7.6.1 Dolomite 153

7.6.2 Pre-dolomite quartz 155

7.6.3 Post-dolomite quartz 155

7.7 Modelling of parental fluids 155

7.8 Halogen geochemistry 158

7.9 Conclusions 161

CHAPTER 8 MULLAWORNIA

8.1 Introduction 170

8.2 Regional geological setting 170

8.2.1 Stratigraphy 170

8.2.2 Structure 171

8.3 Petrography 171

8.4 Paragenesis 174

8.5 Fluid inclusion microthermometry 175

8.6 Stable isotope geochemistry 177

8.6.1 Calcite 177

8.6.2 Dolomite 179

8.7 Modelling of parental fluids 180

8.8 Thermal history 182

8.9 Conclusions 184

CHAPTER 9 STRATIGRAPHICAL AGE OF CEMENTATION: NAVAN

9.1 Introduction 191
9.2 Regional geological setting 191
9.2.1 Stratigraphy 191
9.2.2 Structure 193
9.2.3 Mineralisation 194
9.3 Petrography 195
9.3.1 Boulder Conglomerate 195
9.3.2 'Conglomerate Complex' 196
9.4 Timing of cementation of the Tournaisian rocks 197
9.5 Depth of formation of the early calcite cements 198
9.6 Conclusions 198

CHAPTER 10 STRATIGRAPHICAL AGE OF CEMENTATION: MOYVORE

10.1 Introduction 207
10.2 Regional geological setting 207
10.2.1 Stratigraphy 207
10.2.2 Structure 208
10.3 Petrography 208
10.4 Timing of cementation and implications for fluid flow 211
10.5 Maar-diatremes or peperites? 211
10.6 Conclusions 212

CHAPTER 11 DISCUSSION

11.1 Introduction 220
11.2 Depth and timing of porosity occlusion 220
11.3 Dolomitisation – hydrothermal versus burial origin 221
11.4 Stretching of fluid inclusions 223
11.5 Trapping temperature estimation 226
11.6 Fluid geochemistry 227
11.6.1 Source of salinity 227
11.6.2 Modification by fluid-rock interaction 229
11.7 Mechanisms for fluid flow 239

11.8 Genetic models 240

CHAPTER 12 CONCLUSIONS

12.1 Regional conclusions 243

12.2 Study area specific conclusions 246

12.3 Further work 248

REFERENCES 250

APPENDICES

APPENDIX A Sample Catalogue

APPENDIX B Stable Isotope Data

APPENDIX C Fluid Inclusion Data and Histograms

APPENDIX D Crush-Leach Data

APPENDIX E XRD Traces

APPENDIX F Drillhole data from the Rathdowney Trend

List of Figures

1.1	Geological map of Ireland showing the location of areas sampled.	16
1.2	Lithostratigraphy used in this study.	17
1.3	Schematic cross sections illustrating the fluid flow models for the formation of the Irish Zn-Pb deposits.	18
2.1	Isotopic compositions and fields for the water types in the Earth's crust.	30
2.2	Cl and Br systematics in evaporating systems.	35
2.3	Na-Cl-Br systematics of formation waters.	36
3.1	Geological map of the Rathdowney Trend with the Lisheen Zn-Pb deposit.	62
3.2	Stratigraphic section of the Lisheen mine area.	63
3.3	Distribution of the Regional Dolomite along the Rathdowney Trend.	64
3.4	Paragenetic sequence at Lisheen.	47
3.5	$\delta^{13}C$ and $\delta^{18}O$ values for micrite and early calcite cement at Lisheen.	53
3.6	$\delta^{13}C$ and $\delta^{18}O$ values for the dolomites at Lisheen.	55
3.7	Mineral-water oxygen isotope fractionation curve for the dolomitised spar at Lisheen.	57
3.8	Cl and Br systematics of the coarse dolomite at Lisheen.	58
3.9	Cl-Na-Br systematics for the coarse dolomite from Lisheen.	59
4.1	Geological map of the Rathdowney Trend with Urlingford.	80
4.2	Paragenesis of the Waulsortian Limestone at Urlingford.	72
4.3	$\delta^{13}C$ and $\delta^{18}O$ values for the dolomites at Urlingford.	74
4.4	Mineral-water oxygen isotope fractionation curve for the coarse dolomite at Urlingford.	75
4.5	Mineral-water oxygen isotope fractionation curves for the minimum, maximum and mean $\delta^{18}O$ values measured for the coarse dolomite at Urlingford.	76
4.6	Cl and Br systematics of the coarse dolomite at Urlingford.	77
4.7	Cl-Na-Br systematics for the coarse dolomite from Urlingford.	78
5.1	Location of Newcastle West in relation to the Rathdowney Trend.	106
5.2	Geological map of the area surrounding Newcastle West.	107

5.3	Stratigraphic section of the Newcastle West area.	108
5.4	Paragenesis of Waulsortian Limestone and dolomite at Newcastle West.	88
5.5	$\delta^{13}C$ and $\delta^{18}O$ values for micrite and early calcite at Newcastle West.	91
5.6	$\delta^{13}C$ and $\delta^{18}O$ values for the micrite and early calcite in borehole OW28.	92
5.7	$\delta^{13}C$ and $\delta^{18}O$ values for the micrite and early calcite in borehole OW24.	93
5.8	$\delta^{13}C$ and $\delta^{18}O$ values for the dolomite at Newcastle West.	94
5.9	$\delta^{13}C$ and $\delta^{18}O$ values for the dolomite from each borehole at Newcastle West.	95
5.10	Mineral-water oxygen isotope fractionation curves for coarse dolomite and quartz at Newcastle West.	98
5.11	Cl and Br systematics of the coarse dolomite and quartz at Newcastle West.	101
5.12	Cl-Na-Br systematics for the coarse dolomite and quartz from Newcastle West.	103
6.1	Geological map of north Co. Cork with Subulter quarry and the drillholes studied.	136
6.2	Stratigraphic section of the Buttevant area.	137
6.3	The paragenetic sequence from north Co. Cork.	118
6.4	$\delta^{13}C$ and $\delta^{18}O$ values for micrite and early calcite cement at Mallow.	123
6.5	$\delta^{13}C$ and $\delta^{18}O$ values for micrite and early calcite cement phases at Fermoy.	124
6.6	$\delta^{13}C$ and $\delta^{18}O$ values for the dolomites at Mallow.	125
6.7	$\delta^{13}C$ and $\delta^{18}O$ values for the dolomites at Fermoy.	126
6.8	$\delta^{18}O$ values vs distance from Mallow (Subulter).	128
6.9	Mineral-water oxygen isotope fractionation curves for the pre-dolomite quartz, coarse dolomite and post-dolomite quartz at Mallow.	130
6.10	Cl and Br systematics of the pre-dolomite quartz, coarse-dolomite and post-dolomite quartz at Subulter.	131
6.11	Cl-Na-Br systematics for pre-dolomite quartz and coarse dolomite fluid inclusions from Subulter.	132
7.1	Geological map of the Carlow area.	163
7.2	Stratigraphic section based on the Quinagh borehole.	163

7.3	Paragenesis of the Ballysteen Limestone and dolomite in Carlow.	149
7.4	$\delta^{13}C$ and $\delta^{18}O$ values for the dolomites at Clonmelsh and Quinagh	154
7.5	Mineral-water oxygen isotope fractionation curves for the pre-dolomite and post-dolomite quartz at Quinagh.	156
7.6	Mineral-water oxygen isotope fractionation curve for the coarse dolomite at Quinagh.	157
7.7	Cl and Br systematics of the coarse dolomite and post-dolomite quartz at Quinagh and Clonmelsh.	159
7.8	Cl-Na-Br systematics for the coarse dolomite and post-dolomite quartz from both Quinagh and Clonmelsh.	160
8.1	Geological map of the area surrounding Mullawornia.	185
8.2	Paragenetic sequence inferred at Mullawornia	175
8.3	$\delta^{13}C$ and $\delta^{18}O$ values for micrite and bitumen-related calcite phases at Mullawornia.	178
8.4	$\delta^{13}C$ and $\delta^{18}O$ values for the coarse dolomites at Mullawornia.	179
8.5	Mineral-water oxygen isotope fractionation curves for the minimum, maximum and mean $\delta^{18}O$ values measured for zone 3 of the coarse dolomite at Mullawornia. See text for discussion.	181
8.6	Mineral-water oxygen isotope fractionation curves for the minimum, maximum and mean $\delta^{18}O$ values measured for zone 4 of the coarse dolomite at Mullawornia. See text for discussion.	181
9.1	Location and geological setting of the Navan Zn-Pb deposit.	200
9.2	Stratigraphic sequence as seen in the Navan mine area.	201
10.1	Geological map of the area surrounding the Moyvore Zn-Pb prospect.	213
10.2	Stratigraphic section of the Moyvore prospect area.	214
11.1	Schematic diagram showing the minimum possible age and depth of dolomitisation for all areas studied.	223
11.2	Th vs. maximum inclusion size for all inclusions measured in this study.	225
11.3	Cl and Br systematics of the fluid inclusions from all areas.	228
11.4	Cl-Na-Br systematics of the fluid inclusions from all areas.	229

11.5 Cl/Br molar ratio vs. Na/Li weight ratio of fluid inclusions from all areas. 230
11.6 Na/K weight ratio vs. Na/Li weight ratio of fluid inclusions from all areas. 231
11.7 Calculated Na vs. Cl composition of fluid inclusions from all study areas. 236
11.8 Calculated K vs. Cl composition of fluid inclusions from all study areas. 236
11.9 A schematic summary diagram of the fluid-rock interaction pathways of the dolomitising and quartz-bearing fluids from all areas studied. 238

12.1 Fluid inclusion data from the coarse white dolomite component of the dolomitised Waulsortian Limestone and Ballysteen Limestone. 245
12.2 Stable isotope data from the fine-grained and coarse-grained components of the dolomitised Waulsortian Limestone and Ballysteen Limestone 246

List of Plates

3.1	Partially dolomitised orthoconic nautiloid in hand sample (Lisheen)	65
3.2	Partially dolomitised bryozoans and micrite in hand sample (Lisheen)	65
3.3	Regional dolomite with black tops texture in hand sample (Lisheen)	65
3.4a	PPL view of a selectively dolomitised bryozoan (Lisheen)	65
3.4b	Same view in CL	65
3.5a	PPL view of a partially dolomitised fenestrate bryozoan (Lisheen)	66
3.5b	Same view in CL	66
3.6a	PPL view of a brachiopod containing early calcite cements (Lisheen)	66
3.6b	Same view in CL	66
3.7a	PPL view of a crinoid ossicle (Lisheen)	66
3.7b	Same view in CL	66
3.8a	PPL view of an early calcite-filled cavity with coarse dolomite (Lisheen)	67
3.8b	Same view in CL	67
3.9a	PPL view of non-mimetic replacement by dolomite (Lisheen)	67
3.9b	Same view in CL	67
3.10a	PPL view of the 2nd coarse-grained dolomite (Lisheen)	67
3.10b	Same view in CL	67
3.11a	PPL view of coarse white dolomite growing into open space (Lisheen)	68
3.11b	Same view in CL	68
3.12	SEM image of the black tops dolomite (Lisheen)	68
3.13	SEM image of an individual crystal within the black tops (Lisheen)	68
4.1	Regional dolomite with black tops texture in hand sample (Urlingford)	81
4.2a	PPL view the fine-grained grey dolomite (Urlingford)	81
4.2b	Same view in CL	81
4.3a	PPL view of the coarse-grained white dolomite (Urlingford)	81
4.3b	Same view in CL	81
4.4a	PPL view of the black tops dolomite (Urlingford)	82
4.4b	Same view in CL	82
4.5a	PPL view of the black tops dolomite (Urlingford)	82
4.5b	Same view in CL	82
5.1	Dolomite front in hand sample (Newcastle West)	109

5.2	Mineralisation in hand sample (Newcastle West)	109
5.3	CL view of an early calcite-filled cavity (Newcastle West)	109
5.4	CL view an early calcite-filled cavity (Newcastle West)	109
5.5a	PPL view showing relationship between Stage D and *E* (Newcastle West)	110
5.5b	Same view in CL	110
5.6	CL of Stage D partially dolomitised (Newcastle West)	110
5.7	CL of partially dolomitised micrite and bryozoans (Newcastle West)	110
5.8a	PPL view of a dissolution seam acting as a conduit (Newcastle West)	110
5.8b	Same view in CL	110
5.9a	PPL view of coarse dolomite growing into open space (Newcastle West)	111
5.9b	Same view in CL	111
5.10a	PPL view of the zonation within the coarse dolomite (Newcastle West)	111
5.10b	Same view in CL	111
5.11a	PPL view of the authigenic quartz crystals (Newcastle West)	111
5.11b	Same view in CL	111
5.12a	PPL view of quartz crystals post-dating Stage *E* (Newcastle West)	112
5.12b	Same view in CL	112
5.13a	PPL view of quartz crystals pre-dating Stage *E* (Newcastle West)	112
5.13b	Same view in CL	112
5.14	Image of a fluid inclusion within the coarse dolomite (Newcastle West)	112
5.15	Image of a fluid inclusion within the quartz (Newcastle West)	112

6.1	Vuggy dolomite hand sample (Subulter)	138
6.2	Alignment of vugs in quarry face (Subulter)	138
6.3	Euhedral quartz crystals within vugs (Subulter)	138
6.4	Pink plug dolomite within vugs (Subulter)	138
6.5	En échelon vein set filled with pink plug dolomite (Subulter)	138
6.6	En échelon vein set filled with coarse-grained white dolomite (Subulter)	138
6.7a	PPL view of an early calcite cavity partially replaced by dolomite (Lag)	139
6.7b	Same view in CL	139
6.8a	PPL view of pre-dolomite quartz crystals in the CFC cements (Lag)	139
6.8b	Same view in CL	139
6.9a	PPL view of the pre-dolomite quartz and fine-grained dolomite (Lag)	139
6.9b	Same view in CL	139

6.10a PPL view of the coarse dolomite replacing Stage D (Curtin's Farm) 140
6.10b Same view in CL 140
6.11a PPL view of the pre-dolomite quartz (Subulter) 140
6.11b Same view in CL 140
6.12a PPL view of the post-dolomite quartz (Subulter) 140
6.12b Same view in CL 140
6.13 Image of a fluid inclusion within the pre-dolomite quartz (Subulter) 141
6.14 Image of a fluid inclusion within the coarse dolomite (Subulter) 141
6.15 Image of a fluid inclusion within the post-dolomite quartz (Subulter) 141

7.1 Distribution of vugs along quarry face (Clonmelsh) 164
7.2 Detail of a vug within the dark grey dolomite (Clonmelsh) 164
7.3 Coarse dolomite filled vug fed by bed parallel veins (Clonmelsh) 164
7.4 Hydraulic fracturing and brecciation of the dark grey dolomite (Clonmelsh) 164
7.5 Vug filled with coarse pink dolomite (Clonmelsh) 164
7.6 Fluorite contained within a vug (Quinagh) 164
7.7a PPL view of a preferentially silicified bioclast (Quinagh) 165
7.7b Same view in XPL 165
7.8a PPL view of early calcite cements being replaced by dolomite (Quinagh) 165
7.8b Same view in CL 165
7.9a PPL view of fossil ghosts in a pervasively dolomitised sample (Quinagh) 165
7.9b Same view in CL 165
7.10a PPL view of the pre-dolomite quartz (Quinagh) 166
7.10b Same view in CL 166
7.11a PPL view of the grey organic and dark grey dolomites (Quinagh) 166
7.11b Same view in CL 166
7.12a PPL view of the grey organic and coarse white dolomites (Quinagh) 166
7.12b Same view in CL 166
7.13a PPL view of the coarse dolomite and post-dolomite quartz (Quinagh) 167
7.13b Same view in CL 167
7.14a PPL view of the coarse dolomite growing into open space (Quinagh) 167
7.14b Same view in CL 167
7.15 Image of a fluid inclusion within the coarse-grained dolomite (Quinagh) 167
7.16 Image of a fluid inclusion within the post-dolomite quartz (Quinagh) 167

7.17a	Hydrocarbon-bearing inclusion in the pre-dolomite quartz at 20°C (Quinagh)	168
7.17b	Hydrocarbon-bearing inclusion in the pre-dolomite quartz at -21°C (Quinagh)	168
7.17c	Hydrocarbon-bearing inclusion in the pre-dolomite quartz at –76.2°C (Quinagh)	168
7.17d	Hydrocarbon-bearing inclusion in the pre-dolomite quartz at 18.6°C (Quinagh)	168
7.17e	Hydrocarbon-bearing inclusion in the pre-dolomite quartz at 23.5°C (Quinagh)	168
7.17f	Hydrocarbon-bearing inclusion in the pre-dolomite quartz at 111°C (Quinagh)	168
8.1	Large irregularly-shaped cavity (Mullawornia)	186
8.2a	PPL view of an early calcite-filled cavity (Mullawornia)	186
8.2b	Same view in CL	186
8.3a	Base of the cavity with CFC2 and geopetal sediment (Mullawornia)	186
8.3b	Same view in CL	186
8.4a	PPL view of coarse-grained dolomite and bitumen-related calcite (Mullawornia)	187
8.4b	Same view in CL	187
8.5a	PPL view of saddle crystal shapes of the coarse-grained dolomite (Mullawornia)	187
8.5b	Same view in CL	187
8.6a	PPL view of the coarse-grained dolomite, bitumen-related calcite and bitumen. (Mullawornia)	187
8.6b	Same view in CL	187
8.7a	PPL view of bitumen contained within the bitumen-related calcite (Mullawornia)	188
8.7b	Same view in CL	188
8.8a	PPL view of bitumen with signs of brittle failure (Mullawornia)	188
8.8b	Same view in CL	188
8.9a	PPL view of bitumen and pyrite (Mullawornia)	188
8.9b	Same view in CL	188

8.10	Image of a fluid inclusion within the coarse-grained dolomite (Mullawornia)	189
9.1	Boulder Conglomerate in hand sample (Navan)	202
9.2	Boulder Conglomerate in hand sample (Navan)	202
9.3a	PPL view of collophane within the Boulder Conglomerate (Navan)	202
9.3b	Same view in XPL	202
9.4a	PPL view of apatite within the Boulder Conglomerate (Navan)	203
9.4b	Same view in CL	203
9.5a	PPL view of a Waulsortian Limestone clast (Navan)	203
9.5b	Same view in CL	203
9.6a	PPL view of a Waulsortian Limestone clast (Navan)	203
9.6b	Same view in CL	203
9.7	'Conglomerate Complex' in hand sample (Navan)	204
9.8a	Pale Beds clast within the 'Conglomerate Complex' (Navan)	204
9.8b	Same view in CL	204
9.9	Pale Beds clast within the 'Conglomerate Complex' (Navan)	204
9.10	Partially silicified crinoid ossicle (Navan)	204
10.1	Igneous intrusion in hand sample (Moyvore)	215
10.2	Igneous intrusion in hand sample (Moyvore)	215
10.3	PPL view of a phenocryst of olivine or amphibole (Moyvore)	215
10.4	PPL view of a phenocryst of feldspar (Moyvore)	215
10.5	PPL view of the spheres within the matrix of the intrusions (Moyvore)	216
10.6	PPL view an entrained fragment of Waulsortian Limestone (Moyvore)	216
10.7a	PPL of a spherulite (Moyvore)	216
10.7b	Same view in XPL	216
10.8	PPL view of sheared spheres (Moyvore)	216
10.9	PPL view of embayments in quartz (Moyvore)	216
10.10	PPL view of quartz grain with truncated trail of fluid inclusions (Moyvore)	217
10.11	PPL view of the replacement by Fe carbonate of mica crystals (Moyvore)	217
10.12a	PPL view of a Waulsortian clast containing chalcedony (Moyvore)	217
10.12b	Same view in XPL	217
10.13	PPL view of an intrusion into unconsolidated sandstone (Moyvore)	217

10.14 PPL view a Waulsortian Limestone clast entrained in intrusion (Moyvore) 217
10.15a PPL view of Waulsortian clast with early calcite cavities (Moyvore) 218
10.15b Same view in CL 218

List of Tables

2.1 Internal laboratory standards used at SUERC and their global equivalent. 31

3.1 XRD analyses of dolomitised micrite samples from the quarry near Lisheen. 48

CHAPTER 1

INTRODUCTION AND OVERVIEW

1.1 INTRODUCTION

The Irish orefield is the richest in the world per square kilometre (Singer, 1995) with the Zn-Pb deposits within it hosted almost exclusively in carbonates of Tournaisian (Mississippian) age (Phillips & Sevastopulo, 1986). The host to mineralisation at Lisheen and Galmoy (Figure 1.1), the two most recently discovered commercial Zn-Pb deposits, is dolomitised late Tournaisian Waulsortian Limestone. This association between dolomite and base-metal sulphides has stimulated much research into the nature of the fluids responsible for the dolomitisation and the relation of dolomitisation to mineralisation.

Lisheen, Galmoy and several Zn-Pb prospects occur within a northeast trending tract, 40 kilometres long, which has been termed the Rathdowney Trend (Figure 1.1). In each, pyrite-sphalerite-galena mineralisation is concentrated at the base of the Waulsortian Limestone, which is pervasively dolomitised both within the Rathdowney Trend and over a substantial area to the east. Hitzman *et al.* (1992) referred to the dolomitised Waulsortian Limestone in this region as 'Regional Dolomite' because of its areal extent. More recently Wright *et al.* (2000) and Wright (2001) have described a specific phase of dolomite (their pk2 cement) with a distinctive signature revealed by cathodoluminescence microscopy that has been identified over a wider area than the 'Regional Dolomite' *sensu* Hitzman *et al.* (1992).

Hitzman *et al.* (1998) proposed that the 'Regional Dolomite' formed as a result of replacement of Waulsortian Limestone by dolomite precipitated from heated subsurface brines flowing northwards in response to topographic uplift in the south during the early phase of the Hercynian orogeny. Gregg *et al.* (2001) on the basis of a larger regional petrographic, microthermometric and geochemical study proposed a more complex model of dolomitisation, involving early diagenetic dolomitisation by seawater, neomorphism of early dolomite, and the precipitation of dolomite cement by later diagenetic/hydrothermal fluids.

The studies by Gregg *et al.* (2001), Hitzman *et al.* (1998), Wright *et al.* (2000) and Wright (2001) used samples collected on a regional basis to construct models of dolomitisation. In contrast, the present study focuses on individual occurrences of dolomitised Waulsortian Limestone (and equivalent rocks) to elucidate the timing of dolomitisation and the

physico-chemical attributes of the dolomitising fluid(s) at these localities. Sample areas were chosen both within and outside the main mineralised zones (Figure 1.1). If the areas outside the mineralised zones are representative of dolomitisation throughout the southern half of Ireland, the absence of significant mineralisation offers an opportunity to focus solely on the details of the process of dolomitisation without the complications of the hydrothermal or geothermal overprint associated with base-metal mineralisation.

1.2 OVERALL AIMS

This research project is intended to be a multidisciplinary approach to the understanding of the thermal and chemical evolution of dolomitising fluids, and the porosity and permeability of rocks containing them, during the evolution of the Carboniferous basins in the Midlands of Ireland and the relation of the fluids to base-metal mineralisation. It is not intended to be a regional study, as both distance between and internal variation within individual sample sites preclude anything more than cursory comparisons to be made. This project is, however, a more detailed examination than carried out heretofore of the sample areas chosen in an effort to reconstruct their diagenetic and fluid flow history.

1.3 SPECIFIC OBJECTIVES

- To evaluate porosity and permeability changes in the Waulsortian Limestone (and other carbonates) and of siliciclastic rocks during burial and to compare these changes in the different lithologies.

- To compare porosity and permeability histories during burial of successions representative of mineralised and unmineralised areas.

- To investigate how dolomitising fluids migrated through large volumes of Waulsortian Limestone to form the 'Regional Dolomite'.

- To evaluate the temperature of formation of cements and replacive phases.

- To evaluate aspects of the chemistry of fluids from which cements and replacive phases precipitated.

1.4 OVERVIEW OF IRISH GEOLOGY

The following is intended only to be a brief introduction to the geological setting of the Irish Carboniferous base-metal deposits. For a more detailed discussion see Holland (2001) and the chapters therein.

The underlying crust in Ireland was assembled during the terminal closure of the Iapetus Ocean during the Caledonian orogeny (Silurian). Ireland straddles the Iapetus suture with the northwestern and southeastern parts of the island belonging to different continents (Laurentia and Avalonia respectively) prior to the Caledonian collision. Laurentian basement occurs in the northwest of Ireland and it includes granitic gneiss with a U-Pb zircon age of ~1.7Ga (Daly, 2001). The rocks of the Avalonian plate, which are exposed in the southeast of Ireland, are thought to be younger than their Laurentian counterparts with minimum Ar-Ar ages of ~620Ma (Max & Roddick, 1989). High-grade metamorphic xenoliths found within Carboniferous volcanics in the Irish Midlands, northwest of the Iapetus suture, provide direct samples of the lower crust (Strogen, 1974; Van den Berg & Daly, 2001; Gatley *et al.*, in press) and provide Sm-Nd ages of between ~2300 and 900Ma (Daly *et al.*, 2002).

During the late Proterozoic (800 to 530Ma) the opening of the Iapetus ocean resulted in the deposition of the clastic sediments of the Dalradian Supergroup (Figure 1.1). The subsequent closure of the Iapetus ocean caused the development of the Iapetus suture zone that extends across Ireland as a series of NE-SW trending structural corridors (Phillips & Sevastopulo, 1986). These NE-SW trending Caledonian basement structures are clearly visible as deep-seated linear features in regional gravity and aeromagnetic datasets and are thought to have played an important role in controlling the later structural conduits exploited by the metal-bearing fluids (Johnston *et al.*, 1996; O'Reilly *et al.*, 1999). During or slightly after the Caledonian collision (~400Ma), granitic intrusions were emplaced which include the Leinster Granite batholith, and the Donegal, Newry and Galway granites.

During the early to mid Devonian, coarse clastics, termed the Lower Old Red Sandstone, were deposited in fault bound pull-apart basins in the west and northwest of Ireland (Hitzman, 1995a). Deposition temporarily ceased during the mid Devonian, as a result of

regional uplift and peneplanation of much of central and southern Ireland. Consequently the Lower to Middle Devonian rocks are poorly represented in this part of the country. Extension in the early late Devonian resulted in the formation of the Munster Basin in the south of Ireland. This east-northeast trending half graben contains 6-7 kilometres of fluvial sediments deposited as alluvial fans and in braided river systems (Graham, 1983). In the latest Devonian, a northward migrating marine transgression occurred. Marginal marine sandstone (uppermost Old Red Sandstone) sedimentation occurred in the Munster Basin and alluvial conglomerates and red beds, lithologically similar to the alluvial facies of the Upper Old Red Sandstone were deposited immediately north of the Munster Basin in the southern part of the Irish Midlands (Hitzman, 1995a).

By the mid-Tournaisian (Courceyan) the sea covered most of the Irish Midlands. In the south and central Midlands, the basal red bed sequence (which is lithologically similar to the Upper Old Red Sandstone further south) is conformably overlain by shallow water thinly bedded mudstones, sandstones and limestones, collectively known as the Lower Limestone Shales (Figure 1.2). They include the Ballymartin, Ringmoylan Shale, Ballyvergin Shale and Mellon House Formations.

In the northern Midlands the marine sediments are more carbonate-rich than the Lower Limestone Shales and are informally termed the Navan Group (Philcox, 1984). These consist of a thin basal section of terrigenous sediments overlain by mudstones, sandstones and limestones, which contain oncolites and bird's eye textures and are indicative of deposition in a shallow peritidal environment.

Lying above the Lower Limestone Shales in the south of Ireland is the Ballysteen Limestone Formation (Shephard-Thorn, 1963; Philcox, 1984). It consists of fossiliferous packstones and grainstones, which culminate with a thin development of nodular chert (Nodular Micrite Unit; Figure 1.2). Lying above the Navan Group in the north is what is referred to in the mining industry as the Argillaceous Bioclastic Limestone (ABL). It is the lateral equivalent to the Ballysteen Limestone in the south (Figure 1.2) but, unlike the Ballysteen Limestone, is found both above and below the overlying Waulsortian Limestone (M. Philcox pers. comm.).

Throughout southern and central Ireland, the Ballysteen Limestone (and part of the ABL) is overlain by a generally non-argillaceous, largely micritic unit, termed the Waulsortian Limestone. It is comprised of coalesced mudmounds, which commonly have steep depositional dips and generally contains conspicuous masses of sparry calcite, with digitate upper surfaces and smooth lower surfaces, termed stromatactis cavities. Although they are an important component of the Waulsortian Limestone, the origin of these cavities remains enigmatic. The thickest developments of Waulsortian Limestone occur in the axial region of the Shannon Basin, with estimates of thickness in northwest Co. Limerick ranging up to as much as 1200m (Shephard-Thorn, 1963); 600m of which have been proven by drilling (Sevastopulo & Wyse Jackson, 2001).

From the latest Tournaisian onwards there is evidence for steep fault-controlled slopes and by the Viséan there was clear differentiation between shelf and deeper water basinal areas. Increased subsidence in the central Midlands led to the development of interconnecting moderate sized basins (Andrew, 1992). The margins of these basins were fault controlled, with many of the controlling faults being reactivated basement structures (Somerville & Strogen, 1992). The Upper Carboniferous marked the return of clastic sedimentation with the deposition of the Namurian sandstone and shales (Figure 1.2) and the Westphalian Coal Measures.

The Variscan orogeny was the result of a Himalayan-type collision to the south of Ireland. The resultant deformation migrated northwards through time and reached Ireland by the late Carboniferous producing large ENE-trending upright folds and a pervasive cleavage that both become less marked from south to north (Graham, 2001).

1.5 THE IRISH Zn-Pb (Ba) OREFIELD

Since the first discoveries in the 1960s, much research has been published on the Irish Zn-Pb deposits (Andrew, 1986; Bowden *et al.*, 1992; Andrew, 1993; Anderson *et al.*, 1995; Hitzman & Beaty, 1996; Johnston, 1999; Kelly *et al.*, 2003). As many of the deposits did not clearly fit into the two most important classes of Zn-Pb deposit, Mississippi Valley-type (MVT) and sedimentary exhalative (Sedex), the epithet 'Irish-type' was introduced. As the name suggests, the Irish orefield is the *locus typicus* of these deposits, which share the following characteristics:

1. Mineralisation occurs within the stratigraphically lowest, non-argillaceous, limestone unit. All of the Irish Zn-Pb deposits and prospects discovered to date are hosted within either: the Navan Group, which is host to the deposits in the northern and central part of the Irish Midlands; or the Waulsortian Limestone, which hosts the deposits in central and southern Ireland.

2. Mineralisation occurs in the hanging wall of extensional faults, which can be shown to have been active close to the time of deposition of the host rocks. The faults formed the conduits for fluid flow.

3. Pyrite, sphalerite and galena are the principal sulphides developed in association with varying amounts of barite.

4. The mineralisation is stratabound and in some cases stratiform.

It is important to note that there are deposits within the Irish orefield that, although they are genetically related to the other deposits, do not conform to the description of an Irish-type deposit. One such deposit is Harberton Bridge, which has been considered to represent an example of MVT mineralisation (Emo, 1986; Trude & Wilkinson, 2001).

Of all of the aspects of the Irish Zn-Pb deposits currently under investigation, the origin of fluids involved in mineralisation has been the most intensively researched.

1.5.1 Origin of the mineralising fluids

Constraints on the temperature and salinity of the fluids associated with mineralisation have been obtained from fluid inclusion studies within the Irish Zn-Pb deposits and prospects. Detailed studies have included Silvermines (Samson & Russell, 1983), Tynagh (Banks & Russell, 1992), Lisheen (Eyre, 1998), Navan (Everett *et al.*, 1999a) and Harberton Bridge (Trude & Wilkinson, 2001). Investigations into the origin of the mineralising fluids have benefited greatly from bulk halogen analyses of fluid inclusions from Tynagh and Silvermines (Gleeson *et al.*, 1999; Banks *et al.*, 2002) and from veins in the Lower Palaeozoic basement beneath the mineralised Carboniferous successions (Gleeson *et al.*, 1999; Everett *et al.*, 1999a).

It is now widely accepted that there were two fluids involved in the formation of the Irish base-metal deposits. The first of these (Fluid 1) was the ore-bearing, high temperature (200-280°C) fluid. This fluid, which carried the metals to the deposits, originated as seawater that was evaporated to high salinities, but did not reach halite precipitation (Banks *et al.*, 2002). It came from depth and most likely circulated in the Lower Palaeozoic basement (Russell, 1978; Banks *et al.*, 2002; Everett *et al.*, 2003), where it sourced its metals (Everett *et al.*, 2003). It was moderately saline (12-18 wt% NaCl equivalent) and was associated with hydrothermal sulphide with distinct, isotopically positive, sulphur isotope values. The second fluid (Fluid 2) was a low temperature (<140°C), highly saline (~25 wt% NaCl equivalent) fluid that contained a significant amount of bacteriogenic sulphide with low, negative sulphur isotope values. It is thought to have been residual brine that originated from evaporated seawater that had reached halite saturation (Banks *et al.*, 2002). This second fluid, although bearing little metal, was crucial to the development of economic deposits in the Irish orefield; for example, studies at Navan have demonstrated a greater than 90% contribution of bacteriogenic sulphide to ores (Fallick *et al.*, 2001). There is little argument that economic mineralisation in Ireland intimately involved the mixing of these two end-member fluids.

Despite this general consensus, there is much less agreement on the timing of mineralisation, the depth within the sediment/rock column at which it occurred, and the mechanisms and pathways of fluid transport that were involved.

1.5.2 Timing of mineralisation

As attempts to obtain radiometric dates for individual deposits have been unsuccessful (Halliday & Mitchell, 1983; Walshaw & Menuge, 1997), the timing of mineralisation, specifically in relation to the time of deposition of the host carbonates, remains one of the most controversial aspects of the Irish deposits.

It is generally agreed that the bulk of the Irish-type deposits formed beneath the seafloor and are epigenetic (post-lithification) in origin. This is clearly seen at Navan (Anderson *et al.*, 1998), the only deposit for which the age of mineralisation can be constrained, where mineralised clasts occur in a late Chadian to early Arundian aged debris flow. Younger ages of mineralisation have also been proposed for the Navan deposit (Peace & Wallace, 2000; Symons *et al.*, 2002), but they remain contentious.

Work by Taylor (1984) at Silvermines and Boast *et al.* (1981a) at Tynagh has shown that the bulk of the mineralisation at both deposits is epigenetic. However, evidence for both fossilised vent structures and vent biota at Silvermines (Boyce *et al.*, 1983a; Boyce *et al.*, 2003) and Tynagh (Banks, 1985, 1986) has shown that at least some component of the mineralisation at these deposits was syngenetic (synsedimentary). On the basis that this implies that some of the mineralisation occurred contemporaneously with the host rocks, a late Tournaisian age has been proposed for the onset of mineralisation at Silvermines (Boyce *et al.*, 2003). Banks (1985) also proposed a late Tournaisian age for the vent fauna at Tynagh, which would imply a Tournaisian age for the syngenetic mineralisation at Tynagh.

Younger age dates have also been proposed for mineralisation in the Irish orefield based on the relationship between the time of deposition of the host limestone and the subsequent onset of pre-mineralisation dolomitisation.

Using estimates, obtained from fluid inclusion and oxygen isotope data, of the temperature at which pre-mineralisation dolomitisation (Regional Dolomite) took place at Lisheen, Sevastopulo and Redmond (1999) have suggested that the depth of burial at the time of dolomitisation must have been greater than that achieved by early Arundian time. Consequently, they suggested that this indicates that the mineralisation at Lisheen is younger, perhaps considerably younger, than that at Navan.

Similarly, based on the stratigraphic occurrence of the pre-mineralisation, non-planar dolomite (their pk2 cement), Wright (2001) suggested that the high temperature fluids that formed this dolomite were substantially younger (Asbian) than the majority of the host rocks for mineralisation (Tournaisian-Arundian).

1.5.3 Depth of mineralisation

There are two contrasting hypothesis of the depth at which mineralisation took place. The first is based on the evidence for synsedimentary mineralisation in the Irish orefield and proposes that mineralisation took place either on the seafloor or at shallow depths. The opposing hypothesis proposes that since the majority of the mineralisation is epigenetic, mineralisation occurred at depth.

Mineralisation at shallow depths

As mentioned above, evidence for seafloor exhalative hydrothermal activity has been found at both Silvermines and Tynagh and provides strong evidence in support of seafloor or near-seafloor mineralisation.

In a study of ironstones (iron oxide-silica) associated with base-metal mineralisation, Cruise (2000) demonstrated that iron oxide-silica precipitation overlapped with and post-dated the precipitation of the early calcite cements within the limestone lithosome. Isotopic data from haematite in iron oxide-silica mineralisation (Cruise, 2000) suggest precipitation from a parental fluid with very heavy isotopic values ($\delta^{18}O$ of ~20 to 30‰). Cruise (2000) interpreted this as hematite mineralisation involving seawater that contained dissolved atmospheric oxygen and suggested that this was most likely to have occurred at shallow depths (within a few metres of the sediment/water interface). However, it should be noted that no data exist on the depth to which fluids containing dissolved atmospheric oxygen may penetrate into the sedimentary pile and so the assumption that iron-oxide mineralisation occurred at shallow depths may be incorrect.

The sedimentary reworking of pre-existing mineralised clasts has been used to support a near-seafloor deposition of ore. A recent study by Lee and Wilkinson (2002) in the Cooleen Zone, a sub-economic satellite of the Silvermines deposit, has shown evidence of reworked, isolated clasts of laminated pyrite, colloform sphalerite and dolomitised limestone, contained within breccias formed as a result of synsedimentary faulting. This indicates that both mineralisation and dolomitisation processes were active at shallow depths. Similarly, the observation of thin stratiform layers containing very fine-grained galena and sphalerite within the Boulder Conglomerate and the lower part of the overlying Upper Dark Limestones at Navan has been suggested as evidence for either a synsedimentary or syndiagenetic (very early diagenesis) origin for the sulphides (Ashton *et al.*, 1992).

The reported occurrence of clathrate in sphalerite-hosted fluid inclusions at Navan and sphalerite and quartz-hosted fluid inclusions from Lower Palaeozoic feeder veins (Everett *et al.*, 1999a) is highly significant. CO_2 may have played an important role in generating acidity in the mineralising fluid by hydrolysis, thereby providing a mechanism for the mineralising fluids to dissolve and replace the carbonate lithosome (Everett *et al.*, 1999b).

The presence of CO_2 is also important when considering the depth at which the deposits and associated feeder vein systems formed, because CO_2 would have raised the pressure (and thus increased the depth) at which effervescence (boiling) could have occurred. This suggests that phase separation may have been important at shallow depths of sulphide formation (Wilkinson, 2001). Apart from the occurrence of monophase vapour inclusions at Silvermines (Samson & Russell, 1987), there has been no evidence of effervescence reported in the fluid inclusion studies from the various deposits and prospects. It therefore does not appear to be a common phenomenon. This is important as it means that the vapour pressure of the mineralising fluids did not exceed the ambient fluid pressure. Effervescence-depth curves can be constructed for fluids containing low concentrations of CO_2 (Wilkinson (2001), p.244 Fig. 13) from which the minimum depth of entrapment of the fluid can be estimated. The low levels of CO_2 (up to ~4mol%) (Wilkinson *et al.*, 2003) and high salinities measured from inclusions in Ireland are consistent with shallow depths (<~300m) of fluid entrapment.

Using the alkali compositions of fluids determined from bulk fluid inclusion extraction, Everett *et al.* (1999a) were able to use alkali geothermometry to estimate the fluid trapping temperatures in Lower Palaeozoic-hosted feeder veins. They found that the temperature range derived from the geothermometers was similar to the homogenisation temperatures. They used this to suggest that fluid pressures at the time of trapping were low. This implies that vein formation probably occurred at relatively shallow (but unquantifiable) depths.

Mineralisation at depth

In their study of the Waulsortian Limestone of Britain and Ireland, Lees and Miller (1995) suggested that the early calcite cements (Stages A-D) formed at relatively shallow depths of burial (within approximately 500m of the seafloor). A minimum depth of dolomitisation and thus mineralisation can be estimated by establishing the relationship between final porosity occlusion and dolomitisation. Sevastopulo and Redmond (1999) observed that pre-mineralisation dolomitisation (Regional Dolomite) at Lisheen post-dated almost complete porosity occlusion within the limestone lithosome and noted the presence of sutured contacts between skeletal grains that were subsequently overgrown by dolomite. They used this to support the hypothesis that dolomitisation occurred under an appreciable thickness of overlying rocks.

Furthermore, one of the components of the Regional Dolomite, the coarse-grained white dolomite, displays the curved crystal faces and exhibits the sweeping extinction indicative of saddle dolomite. This suggests formation at elevated temperatures in the range of 60-150°C (Radke & Mathis, 1980), a suggestion borne out by the homogenisation temperatures of fluid inclusions.

In order to calculate the depth of burial at the time of dolomitisation, Sevastopulo and Redmond (1999) calculated the palaeogeothermal gradient needed for the Regional Dolomite at Lisheen to have formed at 70°C (the lower end of the range of inferred temperatures of dolomitisation based on oxygen isotope analyses (Allan *et al.*, 1992)) during the Arundian and Asbian. This was done by calculating the cumulative thickness of overlying rocks and assuming an ambient seafloor temperature of 10°C. They found that the palaeogeothermal gradient required for dolomitisation at the base of the Waulsortian at Lisheen by the beginning of the Arundian was >100°C km^{-1} and for the beginning of the Asbian was 45-50°C km^{-1}. They concluded that the inferred temperature of formation of the Regional Dolomite was sufficiently high to suggest that it could not have been attained under the stratigraphical cover, which had accumulated by the early Arundian, as a result of either conductive or advective transport of heat.

Stylolites and solution seams, which pre-date mineralisation, have been used to infer minimum estimates of the depth at which mineralisation took place (Peace, 1999; Peace & Wallace, 2000; Reed & Wallace, 2001). Reed and Wallace (2001) in their study of the Courtbrown Zn-Pb deposit, invoke the use of "macrostylolite" formation (Lind, 1993; Nicolaides & Wallace, 1997) as a tool for estimating the amount of burial the sediment package had undergone. Based on the timing of early calcite cements (Stage C and D cements) relative to stylolite formation they suggested that the sequence at Courtbrown attained a minimum burial depth of 800m prior to the onset of mineralisation, which they stated was contemporaneous with the development of the Stage D porosity occluding cements. Similarly, Peace and Wallace (2000) suggested that the mineralisation at Navan occurred at depths in excess of 800m and that burial cementation prior to mineralisation occurred at a minimum of 400-500m (Peace, 1999). However, Railsback (1993b) has shown that pressure dissolution features can form at depths as shallow as 30 metres and so the use of these features as depth indicators may not be reliable. Gregg *et al.* (2001) also reported pressure solutions seams that post-dated or were contemporaneous with planar

dolomite (their pk1 cement) and pre-dated non-planar dolomite (their pk2 cement). As Gregg *et al.* (2001) interpreted the pk1 cement as having formed from early diagenetic dolomitisation by seawater prior to final porosity occlusion within the precursor limestones, this implies that the pressure solution seams formed relatively early and at shallow depths and contradicts the work by Peace (1999), Peace and Wallace (2000) and Reed and Wallace (2001).

1.5.4 Mechanisms and pathways for fluid flow

Three models currently exist that try to explain the driving mechanisms behind the mineralising fluids and their fluid flow pathways (Figure 1.3). These are the density-driven convection model (Russell, 1978, 1986), the basin compaction model (Lydon, 1986) and the topographically driven flow model (Hitzman & Beaty, 1996).

Density-Driven Convection Model

Part of this model suggests that high heat flow, caused by extension during the Lower Carboniferous, enabled hydrothermal convection cells to develop. This initiated density-driven flow, whereby wide-scale convection caused seawater to penetrate the crust to depths of 15 kilometres (Figure 1.3a). The fluids are then thought to have risen via deep-seated normal faults to the near surface where they combined with surface brines to form the ore deposits.

This model is strongly supported by Pb isotope studies, which suggest the circulation of fluids into the Lower Palaeozoic basement and/or the Precambrian crystalline basement (Caulfield *et al.*, 1986; O'Keeffe, 1986; LeHuray *et al.*, 1987; Mills *et al.*, 1987; Dixon *et al.*, 1990; Everett *et al.*, 2003). The main problem with this model is the difficulty in circulating large volumes of seawater through the Lower Palaeozoic basement rocks. The heat source for driving the convection cells is also in question, as volcanic activity during the Lower Carboniferous was largely confined to the Limerick syncline and Croghan Hill, Co. Offaly. Both volcanic centres have no mineralisation associated with them (except for the Zn-Pb mineralisation recently discovered but not described from Pallas Green, Co. Limerick) and the volcanism is younger than the first appearance of hydrothermal activity at either Tynagh or Silvermines (Cruise, 2000).

Basin Compaction Model

This model (Lydon, 1986) suggested that metal-rich, saline pore waters within the Old Red Sandstone were delivered by a combination of compaction and heat conducted from the basement to the site of ore deposition (Figure 1.3b). Lydon (1986) suggested that clay minerals and iron oxide pigments within the Old Red Sandstone were the source of the metals (although there may have been some minor basement involvement as well) and that the high salinities of the formation waters were the result of saline ground waters at the time of the Carboniferous marine transgression.

The main problem with this model is that data from fluid inclusions indicate that two fluids were present at the time of mineralisation (Samson & Russell, 1983, 1987; Banks & Russell, 1992; Banks *et al.*, 2002). The basin compaction model assumes that only one fluid is involved and that this fluid evolved to become hotter and less saline through time. This model also requires that the Old Red Sandstone sequence is on the order of 2 kilometres thick in basins adjacent to both Navan and Silvermines, whereas drilling in the mine area at Navan and Silvermines has shown that the Old Red Sandstone is only 0-100m (Andrew & Ashton, 1985) and 120m (Samson & Russell, 1987) thick respectively.

Topographically Driven Flow Model

This model is similar to the fluid flow models developed for the North American Mississippi Valley-type deposits (Garven & Freeze, 1984a, 1984b; Garven, 1985) and invokes topographic head, developed due to the Variscan orogenic uplift to the south of Ireland, as the driving mechanism for the fluid flow (Figure 1.3c). The fluids are thought to have circulated in minor convection cells within the sedimentary succession itself with no interaction with the basement. These fluids are then thought to have exploited reactivated normal faults to reach the overlying carbonate host rocks, where they mixed with brines from the near surface to precipitate the ore deposits.

The main problem with this model is that it implies that the Old Red Sandstone was the main source of the metals for the Irish Zn-Pb deposits. Recent work by Everett *et al.* (2003) has shown that the Old Red Sandstone is more likely to have acted as a sink for lead during mineralisation rather than a source. Another criticism of this model is that it fails to explain how the fluids remained confined within the Old Red Sandstone aquifer over such large distances (c. 400-600km) across a pre-existing structural grain.

Furthermore, the Old Red Sandstone is not considered to have been conducive to fluid flow at this time. However, work by L. Chapman (pers. comm.) has shown ubiquitous large-scale alteration in the Old Red Sandstone throughout the Irish Midlands, which suggests that fluids were circulating within the Old Red Sandstone. In addition, work in this study at Moyvore (Chapter 10) has shown that, at least locally, sandstones retained much of their original porosity and permeability longer than coeval carbonates and so may have formed aquifers, whereas carbonate lithologies were cemented quickly and were unlikely to be amenable to fluid flow, unless fractured. This highlights the mistake of assuming that the Old Red Sandstone was impermeable at the time of mineralisation.

The apparent contradictions concerning syngenesis versus epigenesis and shallow versus deep depths of mineralisation within individual deposits such as Tynagh, Silvermines and Navan may point to an extended history of hydrothermal activity. It seems obvious to consider that mineralisation may not have occurred in one pulse, but may in fact have occurred intermittently over millions of years providing evidence for both syngenetic-shallow mineralisation and epigenetic-deeper mineralisation arguments. Using estimates of the age of mineralisation at Navan (~345 Ma) and Silvermines (~352 Ma), Boyce *et al.* (2003) suggested that hydrothermal activity in the Irish orefield must have occurred over a period of >7 Ma. However, they did not discuss whether the activity was intermittent or continuous. At Navan, although mineralisation occurs mainly within the Tournaisian (Courceyan) Pale beds it also occurs in the Arundian Upper Dark Limestones (UDL). This UDL-hosted mineralisation is not just the framboidal pyrite reported by Ashton (1995), but also developments of sphalerite similar to that found within the Pale Beds (G. Sevastopulo pers. comm.). This suggests that mineralisation, at least at Navan, may have occurred over more prolonged time periods than those suggested by Boyce *et al.* (2003) and that it may have also been more intermittent.

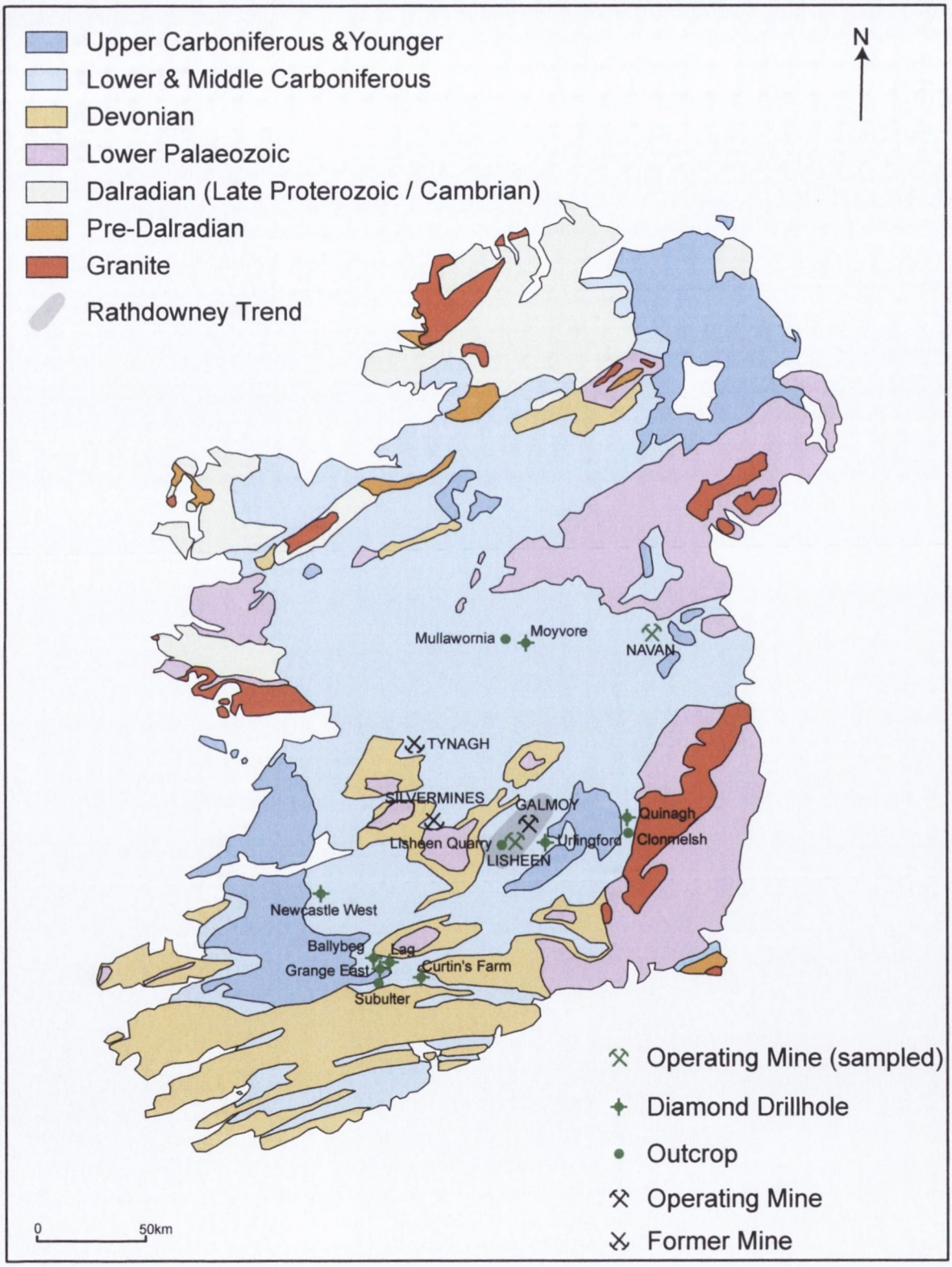

Figure 1.1 Geological map of Ireland showing the location of areas sampled in this study.

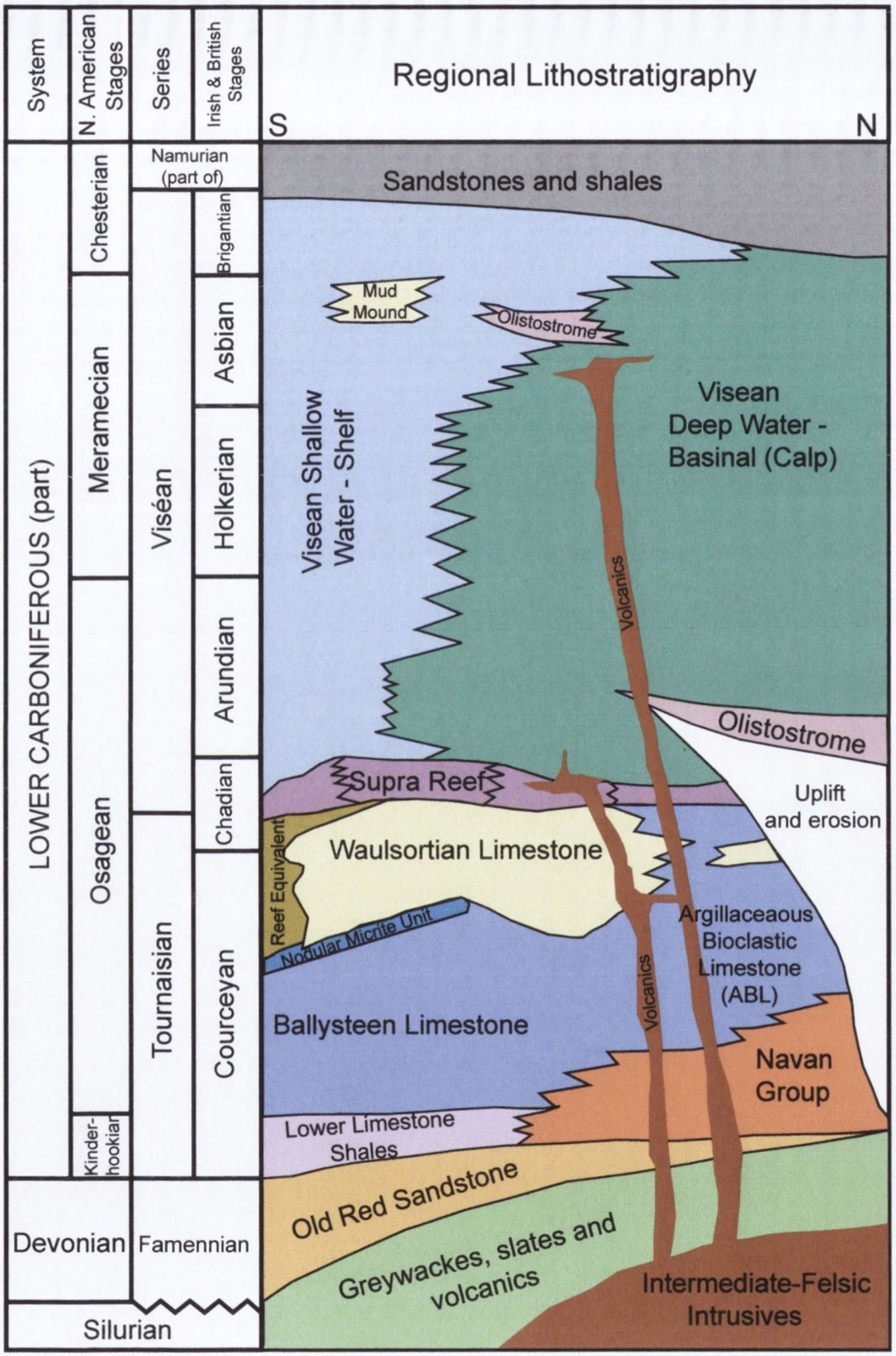

Figure 1.2 Lithostratigraphy and chronostratigraphy used in this study (modified after Hitzman 1992c).

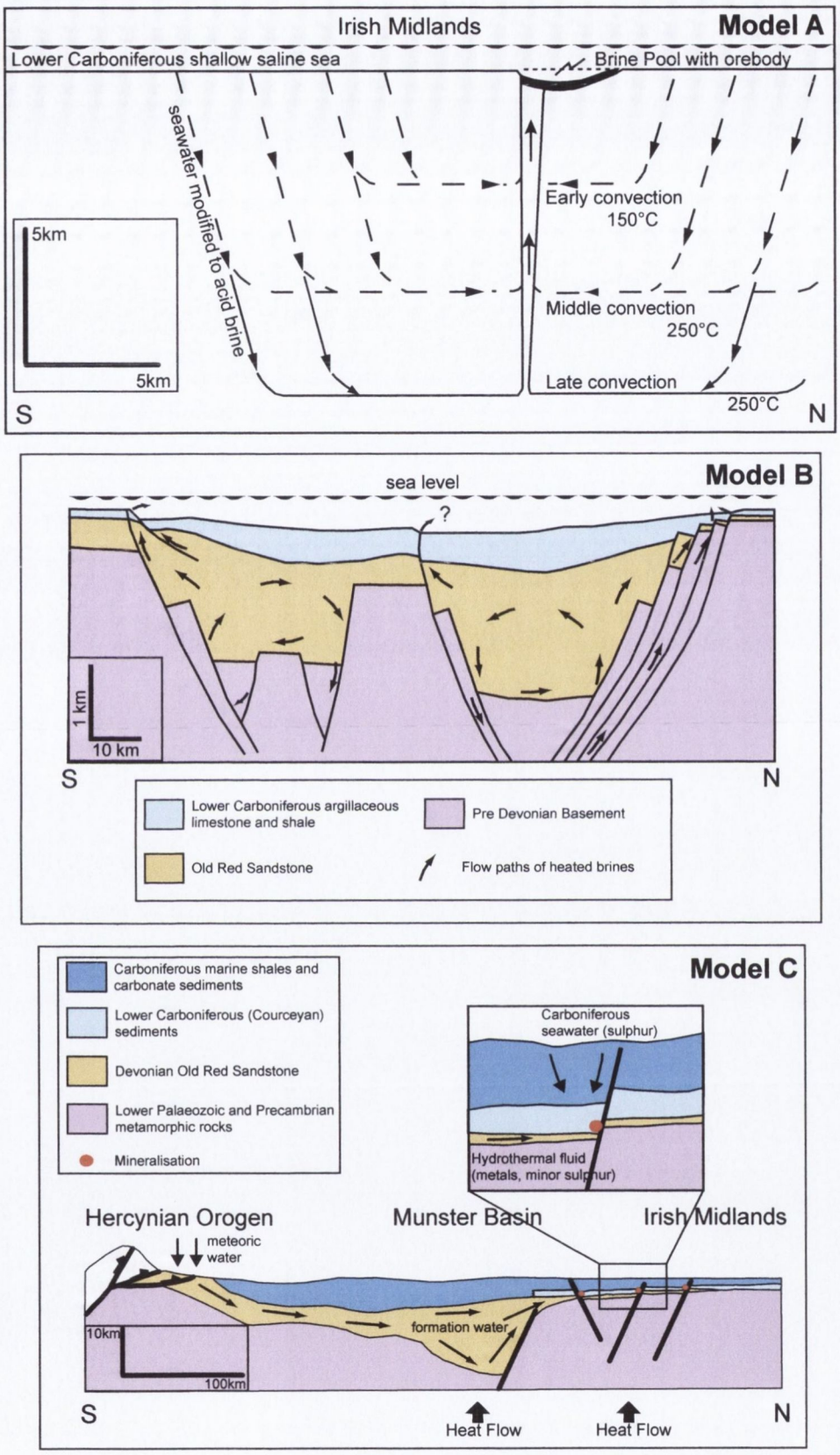

Figure 1.3 Schematic cross sections illustrating the fluid flow models for the formation of the Irish Zn-Pb deposits. Model A. Density-driven convection model (Russell, 1978, 1986). Model B. Basin compaction model (Lydon, 1986). Model C. Topographically driven model (Hitzman and Beaty, 1996).

CHAPTER 2

METHODS AND MATERIALS

2.1 INTRODUCTION

This research project has involved a micro to macro scale investigation, ranging from fluid inclusion analyses (μm) to detailed sampling of drillcore and outcrop (m). The essence of this study has been careful petrographic descriptions in an effort to unravel the paragenesis of the different samples, without which any fluid inclusion or stable isotope data are worthless.

2.2 SAMPLING

Sample areas were chosen from within the main mineralised zone (the Rathdowney Trend) and from areas outside of this trend (Figure 1.1). All of the samples studied were from either exploration boreholes or quarry exposures.

Drillcore from the different study areas was intensively sampled. Where necessary boreholes were logged in detail prior to sampling. Particular attention was paid to samples that provided an opportunity to examine the transition from undolomitised to dolomitised Waulsortian Limestone. Samples containing early calcite cement-filled cavities and their relationship to stylolites and veining, especially possible feeder veins, were also targeted. During sample selection all core was routinely stained with Alizarin red S and Potassium ferricyanide to determine the degree of dolomitisation. 10% HCl acid was also used.

In some instances, outcrop in local working quarries provided an opportunity to study the surface expression of samples obtained from drillcore and where possible orientated samples were taken from these quarry exposures.

2.3 PETROGRAPHY

Routinely all thin sections were stained with both Alizarin red S and Potassium ferricyanide using a modified version of the Dickson (1966) method. The mirror image polished plaquettes were set aside and later used for stable isotope analyses and fluid inclusion wafer preparation. Thin sections were primarily examined using normal transmitted light microscopy and/or reflected light microscopy followed by examination under cathodoluminescence (CL) microscopy.

2.3.1 Transmitted light microscopy

The examination of sections under transmitted light was done principally to obtain petrographic descriptions of the samples. It was also important in scanning for phases within the thin sections that might be favourable for fluid inclusion analyses and in establishing the different fluid inclusion populations before microthermometry could be undertaken.

2.3.2 Reflected light microscopy

Reflected light was used to examine opaque material within the thin sections. It was particularly used for bitumen-bearing samples to identify the mesophase textures that were present and to distinguish between bitumen and opaque sulphide minerals such as pyrite.

2.3.3 Cathodoluminescence (CL) microscopy

Conventional petrographic examination of thin sections makes use of the interaction of light with the mineral or its reflection from a polished surface (Marshall, 1988). CL microscopy is a more specialised petrographic technique. It involves placing the sample in a vacuum and bombarding it with electrons. The sample responds by emitting light of various wavelengths and the minerals present are characterised by the wavelength and intensity of the emission of light. CL petrography was carried out using a Reliotron cold cathode stage, mounted on a Nikon Labophot microscope, with a 12-15kV beam and a current intensity of 0.5mA.

In carbonates the main element that promotes CL (the activator) is Mn^{+2} whereas the main element that diminishes CL (the quencher) is Fe^{+2}. It is the relative proportions of these two elements that determine the CL signature. In many carbonates Mn^{+2} may substitute for Mg^{+2} preferentially over Ca^{+2} resulting in an orange/red luminescence. Low Mg calcites typically have a yellow CL signature whereas high Mg calcites have a more orange/red luminescence. Dolomite usually has a characteristic deep red luminescence and is therefore easily distinguished from calcite.

CL microscopy can highlight overgrowths on minerals and reveal any small solid inclusions that may be present. It also makes it possible to recognise zonation patterns contained in individual crystals. The CL zonation patterns may be considered as being comparable within samples from the same locality, but as they reflect minute changes in

the local pore water chemistry as a result of burial they are not correlatable on a regional scale.

Using the luminescent cement zonation contained within Mississippian limestones from southwestern New Mexico, CL was first applied in reconstructing the local cement stratigraphy (Meyers, 1974, 1978). Meyers (1974) used a mid-Carboniferous aged unconformity as a time-line with which he could date the cements based on whether they were developed above (post-unconformity) or only below (pre-unconformity) the erosion surface. The same underlying principle is applied in this study at Navan (Chapter 9) and Moyvore (Chapter 10) where a major unconformity and volcanic intrusions are the respective datable events with which the local cementation history can be pinned.

2.4 FLUID INCLUSION MICROTHERMOMETRY

Doubly polished 100μm thick fluid inclusion wafers were prepared from the counter parts of the thin sections. All plaquettes were cold mounted on glass slides using Superglue™. The completed wafers were removed from the glass slides by being placed in acetone overnight. In a few cases a second bath of clean acetone was required to remove any excess glue from the polished wafer. A sharp scalpel was used to isolate areas of the wafer for microthermometric analysis. The microthermometric analyses were carried out using a Linkam THMG600 heating-freezing stage mounted on a Nikon Optiphot microscope equipped with x20, x40, x60 and x100 long working distance objectives. Stage calibration was done using the techniques described by Shepherd *et al.* (1985). Accuracy is estimated to be ±0.2°C in the –100 to 30°C range and 0.5°C at higher temperatures. The precision of the measurements, determined from repeated analyses on synthetic inclusions, is 0.1°C. Homogenisation temperatures (Th) and, where possible, first melting temperatures (Tfm), ice melting temperatures (Tm_{ice}) and hydrate melting temperatures (Tm_h) were measured for each inclusion. To limit any error in estimating the salinities they are calculated where possible as combined wt% NaCl and $CaCl_2$ equivalent using a numerical algorithm developed by Naden (1996). This was done because the eutectic temperatures (T_e) of the inclusions are consistent with being part of the $NaCl\text{-}CaCl_2\text{-}H_2O$ ternary system and most of the Tm_{ice} measurements were lower than -21.2°C (Oakes *et al.*, 1990). Where the Tm_{ice} measurements were not less than -21.2°C, the equation of Bodnar (1993) was used to

calculate a wt% NaCl equivalent value. Appendix C contains all of the microthermometric measurements made within this study as well as histograms of the Th data.

2.5 STABLE ISOTOPE GEOCHEMISTRY

The following is only intended to be a brief introduction to stable isotope geochemistry and its applications. For a full background description see Criss (1999), Chacko *et al.* (2001) and Hoefs (2001).

Isotopes are atoms of the same element whose nuclei contain the same number of protons but a different number of neutrons. They can be divided into two fundamental types, stable and unstable (radioactive) isotopes; the discussion here is exclusively restricted to the former. Most naturally occurring elements consist of more than one stable isotope. The isotopic compositions of the elements with a low atomic number (<40) are variable because they can be fractionated on a large scale by natural processes and therefore provide good tracers within low temperature systems. In these elements, it is the light (lower mass number) isotope that has the greatest abundance in nature *i.e.* ^{1}H has a far greater abundance than ^{2}D and similarly ^{16}O is more abundant than ^{18}O. The relative mass difference between the heavy and light isotope is an important control on the magnitude of the fractionation.

2.5.1 Delta Notation

For most geochemical purposes, knowledge of the difference in absolute isotope ratios between two substances is adequate. This difference, termed the 'delta' (δ) value, can be measured much more precisely than the absolute ratios and for this reason is used ubiquitously in the Earth Sciences for reporting isotope abundances and variations. The δ value is the difference in the isotope ratio between a sample and a standard. It is expressed in parts per thousand (‰) and is defined as follows:

$$\delta_A = (R_A - R_{STD})\, R_{STD}^{-1} \times 10^3 \qquad (1)$$

where R_A is $(D/H)_A$, $(O^{18}/O^{16})_A$ etc and R_{STD} is the corresponding ratio in the standard.

2.5.2 Fractionation Factor

The partitioning of isotopes between two substances or two phases of the same substance with different isotope ratios is called isotope fractionation. It is governed by the fractionation factor (α) which is defined as the ratio of the numbers of any two isotopes in one chemical compound A, divided by the corresponding ratio for another chemical compound B such that:

$$\alpha_{A-B} = R_A / R_B \qquad (2)$$

where R_A and R_B are the ratios of the heavy isotope to the light isotope within the two chemical compounds A and B.

In terms of the δ values actually measured in the laboratory, this expression becomes:

$$\alpha_{A-B} = 1000 + \delta_A / 1000 + \delta_B \qquad (3)$$

If the isotopes are randomly distributed over all of the possible sites within the compounds A and B then the fractionation factor can be linked to the equilibrium constant K, by the expression:

$$\alpha = K^{1/n} \qquad (4)$$

where n equals the number of atoms that have been exchanged. For simplicity, isotope exchange reactions are normally written in such a way that only one of a set of exchangeable atoms in each compound takes part. For example, the exchange reaction controlling oxygen isotope fractionation in the CO_2-CO system is as follows:

$$C^{18}O + \tfrac{1}{2}C^{16}O_2 \Leftrightarrow C^{16}O + \tfrac{1}{2}C^{18}O_2$$

Under these circumstances the equilibrium constant is equivalent to the fractionation factor (i.e. $K = \alpha$). Values of α are normally very close to unity and typically vary in the third decimal place. Most values are therefore in the form 1.00X. Usually isotopic fractionations are referred to in terms of their value of X‰ (per mil fractionation). It is a useful

mathematical approximation that 1000ln (1.00X) ~ X. This relationship has the added value that experimental studies have shown that 1000ln α is a smooth and often linear function of $1/T^2$ for mineral-mineral and mineral-fluid pairs. This gives rise to the general relationship for the fractionation factor

$$\mathbf{1000ln\alpha_{mineral\text{-}fluid} = A\ (10^6/T^2) + B} \qquad \mathbf{(5)}$$

where T is in Kelvin and A and B are constants, normally determined by experiment. For example in the case of a quartz-H_2O pair the values for A and B are 3.34 and -3.31 respectively (Matsuhisa *et al.*, 1979) giving the expression

$$\mathbf{1000ln\alpha_{quartz\text{-}water} = 3.34\ (10^6/T^2) + (-3.31)} \qquad \mathbf{(6)}$$

For the two minerals A and B, the δ-values and per mil fractionation (1000ln α) are related by the expression:

$$\mathbf{\delta_A - \delta_B = \Delta_{A\text{-}B} \approx 10^3 \ln \alpha_{A\text{-}B}} \qquad \mathbf{(7)}$$

where $\Delta_{A\text{-}B}$ is the difference between the δ values for two minerals A and B. This approximation works as long as the δ value is less than 10. At δ values greater than 10 the expression given in equation 3 should be used.

2.5.3 Variables affecting the magnitude of fractionation factors

For aqueous fluids the isotopic composition will be determined by firstly, the original composition of the fluid (see Section 2.5.4); and secondly the isotopic partition coefficient between fluid and solid, which in turn will depends on the temperature, pressure, mineral composition and solution composition.

Temperature

In many cases temperature is the single most important variable controlling isotope fractionation. However, at very high temperatures no isotope fractionation occurs. This trend towards zero fractionation does not occur linearly with increasing temperature. Instead, at increasingly higher temperatures, the magnitude of the fractionation factor

firstly decreases, changes sign (called crossover) and increases and then ultimately approaches zero. This crossover phenomenon is due to the complex manner by which thermal excitation of the atoms contribute to the isotope effect (Stern *et al.*, 1968).

Pressure

Below approximately 20kbar the effect of pressure on both carbon and oxygen isotope fractionations is generally assumed to be negligible (Clayton *et al.*, 1975; Chacko *et al.*, 2001). However in some circumstances, particularly in the case of hydrogen isotope fractionation, an increase in pressure can lead to significant changes in the magnitude of the fractionation factors (Driesner, 1997; Horita *et al.*, 1999; Horita *et al.*, 2002).

Mineral composition

It has been suggested that the main compositional controlling factor on oxygen isotope fractionations between carbonates is the mass of the individual cations substituted into the carbonate i.e. those with the smallest mass have the largest fractionation factors. Compositional substitution is also important in the oxygen isotope fractionation behaviour of silicates where, of the common substitution schemes, the plagioclase substitution is known to have the largest isotopic effect (Matsuhisa *et al.*, 1979). The effects of substitution on the hydrogen isotope fractionation are still poorly understood.

Solution composition

The presence of dissolved salts in the fluid phase, known as the isotope 'salt effect' (Γ), can have an important impact on the fractionation factor. The magnitude of the salt effect is usually given by the expression:

$$\Gamma = \alpha_{\text{A-aqueous solution}} / \alpha_{\text{A-pure water}} \qquad (8)$$

where A is a reference phase (water vapour at low temperatures and minerals at high temperatures) with which both pure water and the salt solution are exchanged in separate experiments. The salt effect is therefore a measure of how much the fractionation factor between phase A and an aqueous fluid changes as solutes are dissolved into the fluid. For low temperature (50 to 100°C) single salt solutions the Γ_{Hydrogen} is greater than one for all salt solutions. The magnitudes of the hydrogen isotope effects depend on the dissolved species such that $CaCl_2 \geq MgCl_2 > MgSO_4 > KCl \approx NaCl > Na_2SO_4$ at the same molality

(Horita *et al.*, 1993a). Γ_{Oxygen} at low temperatures in $CaCl_2$ solutions is slightly negative or close to zero whereas in low temperature NaCl solutions there is no noticeable effect. In low temperature mixed salt solutions $\Gamma_{Hydrogen}$ remains positive and Γ_{Oxygen} continues to show negative to zero values (Horita *et al.*, 1993b). For high temperature (up to 350°C) NaCl solutions the Γ_{Oxygen} gradually becomes more negative whereas $\Gamma_{Hydrogen}$ decreases from 10°C to about 150°C and then increases gradually to 350°C (Horita *et al.*, 1995). Only poor data exist for high temperature $CaCl_2$ and mixed salt solutions (J. Horita pers comm. 2003) and therefore the Γ_{Oxygen} in these types of solutions cannot be quantified accurately.

Isotope salt effects will need to be considered when interpreting the isotopic data in this study, because all of the microthermometric data indicate that the fluids involved are high temperature (>100°C) mixed salt solutions (NaCl-$CaCl_2$). Despite not having experimental data to quantify the magnitude of the Γ_{Oxygen} in mixed salt solutions at high temperatures the effect can be approximated. As the majority of brines within the measured fluid inclusions in this study have NaCl > $CaCl_2$ wt% (Appendix C) it can be assumed that the Γ_{Oxygen} will behave similarly to the high temperature NaCl solutions and therefore continue to become more negative with increasing temperature.

2.5.4 Isotopic characteristics of natural waters

Sheppard (1986) and Taylor (1997) both give a detailed description of the isotopic characteristics of the different kinds of water that may be involved in hydrothermal systems. A brief overview is given here and is summarised in Figure 2.1. Values of $\delta^{18}O$ are cited with respect to SMOW (Standard Mean Ocean Water), unless otherwise stated.

Meteoric Water

The isotopic variations of meteoric groundwaters vary systematically on a global scale. They are dependent on certain geographical parameters such as temperature, altitude, latitude, distance from the coasts and intensity of precipitation. In general the values for low temperature meteoric waters become lighter from the equator to the poles and where there has been an increase in elevation. All present day meteoric waters obey the equation (Craig, 1961):

$$\delta D = 8\,\delta^{18}O + 10 \qquad (9)$$

This linear relationship between δD and $\delta^{18}O$ defines what is known as the meteoric water line (MWL).

Seawater

The oxygen and hydrogen isotope compositions of the present-day oceans are comparatively uniform with δD values ranging from +5 to –7‰ and $\delta^{18}O$ values ranging from +0.5 to –1.0‰ (Sheppard, 1986). Deviations from these values can occur in specific circumstances. For instance, at high latitudes seawater may become more depleted in D and ^{18}O than the present day seawater average, whereas in restricted waterways such as the Mediterranean Sea the water can become more enriched. Research on brachiopod shells (Veizer *et al.*, 1999) has shown that there has been a general increase in the $\delta^{18}O$ values of seawater from the Cambrian (-8‰ PDB) to the present day (0‰ PDB). Palaeogeographical reconstructions of Ireland during the Carboniferous suggest that it lay within in tropical latitudes and the $\delta^{18}O$ of the Carboniferous seawater is thought to have been 0 ±1‰.

Organic Waters

Organic waters are waters whose D/H ratio is derived from direct or indirect transformation of organic matter, bitumen, coal, kerogen, petroleum, organic gases, etc. by processes such as dehydration, dehydrogenation, oxidation, and/or exchange. The δD values of organic waters are controlled by the organic source material itself and are typically in the range of –90 to -250‰. $\delta^{18}O$ values are controlled by the reservoir rocks and have values similar to those of formation or metamorphic waters (Figure 2.1).

Sedimentary Pore Fluids

Generally sedimentary pore fluids display a continuous decrease of δ values with depth. The exact reasons for this are not entirely clear but the removal of the heavy $\delta^{18}O$ isotope by the formation of clay rich horizons is thought to play an important role. The $\delta^{18}O$ values of formation waters tend to increase with increasing temperature and salinity. Pore fluids will not only represent the parental fluid composition (seawater or meteoric) but also the signatures of the various lithologies the fluid has passed through (fluid-rock interaction).

Metamorphic Water

The term metamorphic water is a descriptive term referring to water associated with rocks during metamorphism. It is therefore not genetically linked and can include waters of different origins. They can have a wide range of isotopic compositions depending on the rock types involved and the amount of fluid-rock interaction they have undergone, but in general, a range in δD values of –70 to -20‰ and $\delta^{18}O$ values of 5 to 25‰ has been attributed to metamorphic waters.

Magmatic Water

The majority of non-altered igneous rocks have well defined hydrogen and oxygen isotope compositions with a range in δD of –50 to 90‰ and $\delta^{18}O$ of ~ +5.5 to +10‰. These values are often referred to as the 'normal' igneous values. Water in equilibrium with these magmas define the primary magmatic water field with δD = -40 to –80‰ and $\delta^{18}O$ ~ +5.5 to +9.5‰ (Figure 2.1).

Formation Waters (Brines)

Circulating formation waters in sedimentary basins may contain a component of some originally trapped seawater but their isotopic signature is often obscured by the result of mixing with other waters and subsequent water-rock exchange reactions. Many present day formation waters are much more saline than ocean water; this may be the result of the dissolution of evaporite horizons or dehydration reactions. Formation waters show a wide range of $\delta^{18}O$, δD and salinity values. Within a given basin, the $\delta^{18}O$ values of formation waters tend to increase with increases in temperature and salinity.

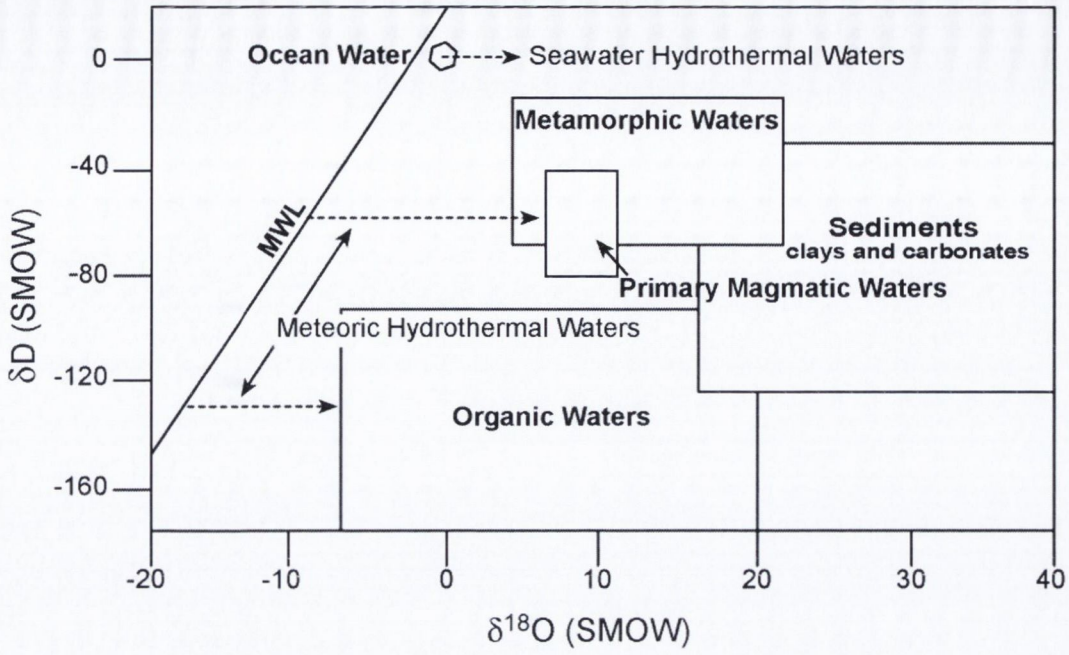

Figure 2.1 Isotopic compositions and fields for the principle water types in the Earth's crust (modified after Sheppard (1986)).

2.5.5 Sample preparation and analysis

Carbonate samples were micro-drilled under a binocular microscope using a hand held slow speed drill. Crown preparation dental drill bits were used (supplied by Tudor Diamonds, U.K.) and were cleaned with deionised water in an ultrasonic bath after each sample was drilled. Polished thin sections were examined under CL to locate the required phase and then the mirror image polished plaqette was drilled. All polished plaquettes were examined under CL both before and after they were drilled to ensure that only the correct phase was sampled. The CO_2 was evolved from individual, helium purged orthophosphoric acid baths and analysed automatically following the method of McCrea (1950) on an Analytical Precision AP2003 mass spectrometer at SUERC with an automatic carbonate preparation system. Reproducibility, based on international and internal laboratory standards analysed during the automatic runs was approximately ± 0.3‰ (1σ) for both C and O isotopes. Samples from Mullawornia (Chapter 8) were analysed on a Thermo Delta^{plus} at TCD with reproducibility based on international and internal laboratory standards being ± 0.1‰ (1σ) for both C and O isotopes.

Quartz and pyrite samples were handpicked from acid insoluble residues of the carbonate host rock using a fine micro-palaeontological brush and washed several times in distilled water. Oxygen isotope analyses of 1-2mg samples of quartz were carried out by laser fluorination with excess ClF_3 (Borthwick & Harmon, 1982) using a CO_2 laser as a heat source (temperature in excess of 1500°C) following Sharp (1990). All fluorinations resulted in 100% release of O_2 from the silica lattice. This O_2 was converted to CO_2 by reaction with hot graphite and then analysed on-line by a VG PRISM III spectrometer. The reproducibility was better than ± 0.3‰ (1σ) based on repeated analyses of the internal laboratory standard. Sulphur isotope measurements were carried out on pyrite following the conventional method of Robinson and Kusakabe (1975), with the evolved SO_2 analysed on a VG Isogas SIRA II mass spectrometer. Repeat analyses of international and laboratory standards, including combustion, gave a 1σ error of reproducibility better than ± 0.2‰. Isotope compositions are given in the delta per mil (‰) notation, versus V-SMOW, V-PDB and V-CDT for $\delta^{18}O$, $\delta^{13}C$ and $\delta^{34}S$ respectively. All isotope analyses (except those from Mullawornia, which were run at Trinity College Dublin) were carried out at SUERC, East Kilbride and the following is a list of the internal laboratory standards used:

Lab Standard:	Mineral:	Element:	Global Standard:
Mab 2b IAEA-CO-1¥	carbonate	carbon & oxygen	Standard Mean Ocean Water (SMOW - $\delta^{18}O$) and Pee Dee Belemnite (PDB - $\delta^{13}C$)
SES	quartz	oxygen	SMOW - $\delta^{18}O$
CP1 NBS123 IAEA-5-5	chalcopyrite sphalerite Ag_2S	sulphur	Canyon Diablo Troilite (CDT - $\delta^{34}S$)

Table 2.1 Internal laboratory standards used at SUERC and TCD¥ and their global equivalents.

2.6 CRUSH-LEACH ION CHROMATOGRAPHY

One of the oldest methods used to reveal the composition of fluid inclusions, first described by Roedder (1958) and Roedder *et al.* (1963), involves opening the inclusion by

crushing the host mineral, leaching the contents of the inclusion and analysing the leached solution. However, the modified technique described by Shepherd *et al.* (1985) and outlined in Section 2.6.1 is much simpler and is currently more commonly used. This bulk sampling method of analysing several fluid inclusion assemblages can be fraught with problems, many of which are outlined in Banks and Yardley (1992). However, major advances in the analytical procedure and instrumental improvements have significantly reduced the sample size needed (70mg), enabling the resolution of the technique to be improved and reducing the likelihood of contamination. Nevertheless the problem of sampling multiple fluid inclusion generations remains an important drawback of this technique.

In this study, crush-leach was used to determine the elementary composition of the fluids enclosed within pre-mineralisation dolomite and associated quartz samples from several sample areas both inside and outside the Rathdowney Trend. The crush-leach analyses were conducted at the University of Alberta, Canada under the supervision of Dr Sarah Gleeson.

2.6.1 Sample preparation and analysis

A minimum of 0.5g of each sample was handpicked under a binocular microscope following acid digestion for the quartz and crushing for the dolomite. The quartz samples were heated (<50°C) in nitric acid overnight and then washed several times in DDIW (doubly distilled deionised water) and allowed to dry in a low temperature oven. Dolomite samples were heated several times in separate baths of DDIW (<50°C) and again allowed to dry in a low temperature oven. Once dry, the samples were ground to a fine powder using an agate mortar and pestle in order to leach the contents of the fluid inclusions. All crushing was done in a laminar flow cabinet contained within a medium level clean laboratory. The powdered samples were then separated with half used for the leaching of the anions and the other half used for the leaching of the cations.

Anions

Between 2-5ml of DDIW was added to the powdered samples in an inert container to re-dissolve the contents of the fluid inclusions. The samples were shaken vigorously and allowed to settle for several hours. The solution was then extracted using a pipette and filtered through a 2μm nylon filter into a new inert container. This removed any solid

contaminants. These samples were then analysed for F^-, Cl^-, Br^- and SO_4^{-2} on a Dionex DX600 ion chromatograph (IC) and Na^+ and K^+ using atomic absorption spectroscopy (AAS). Detection limits for F^-, Cl^-, Br^-, SO_4^{-2}, Na^+ and K^+ were 0.5, 10, 0.5, 10, 30 and 30 ppb respectively.

Cations

Cation analysis can be more problematic as the crushing process creates more reaction sites upon which cations may be adsorbed, creating bias in the results and causing a charge imbalance. This effect is especially significant for polyvalent ions such as Ca^{+2} (Bottrell *et al.*, 1988; Banks & Yardley, 1992). Bottrell *et al.* (1988) suggested that leaching with a solution of 200ppm $LaCl_3$ in 0.15 m HNO_3 instead of DDIW would significantly reduce this effect. These results were further confirmed in a study by Pettke and Diamond (1995), which showed that leaching of synthetic inclusions in DDIW was 93% efficient at releasing the solutes, whereas leaching in a La doped solution was 99.7% efficient. The acidified La solution can be used only for quartz samples, as the nitric acid tends to dissolve carbonate minerals. The powdered quartz samples were mixed with the La doped solution and centrifuged at the maximum speed for 40 minutes. After agitation and settling the solution was transferred using a pipette into a new inert container. The samples were then analysed using inductively coupled plasma-atomic emission spectroscopy and mass spectrometry (ICP-AES and MS). Detection limits for Li^+ using this method were 0.5 ppb.

Results

As Na was determined from all leachate solutions measured by both AAS and ICP it was used to normalise the data to enable the results from each technique to be directly comparable. The analyses were then recalculated to the best estimate of their concentration in the fluid inclusions and are tabulated in Appendix D. The recalculation is based on the mean Cl content of the inclusions which is calculated from the salinity determined by microthermometry and the analysed Cl concentration in the crush-leach solutions such that:

F x elemental crush-leach analyses (ppm) **(10)**

Where F is the microthermometry Cl concentration (ppm)/analysed Cl concentration (ppm) (Banks *et al.*, 2002). There is an error associated with absolute concentrations of the

reported elements mainly due to the determination of salinity by microthermometry and in the assumption that the fluid in the inclusions is part of the H_2O-NaCl binary system. However, as elemental ratios depend only on the accuracy and precision of the analytical equipment, they are more accurate. Maximum error in this study was 5% based on calibration standards and replicate analyses.

In order to assess the quality of the data, a charge balance was performed using the following equation (Shepherd *et al.*, 1985):

$$\Sigma Charge*(C/A)_{cation} / \Sigma Charge*(C/A)_{anion} \quad (11)$$

where C and A represent the concentrations and atomic weights of the cations and anions. The results of the charge balance are also tabulated in Appendix D.

2.6.2 Cl/Br systematics

Halogen ratios, particularly Cl/Br molar ratios are believed to be useful indicators of the source of salinity of a given fluid. The basis of this concept lies in the assumption that both Cl and Br act as conservative elements in solution and provided that there has been no halite recrystallization, are unlikely to be involved in any fluid-rock interactions (Rittenhouse, 1967; Fontes & Matray, 1993a). Their usefulness as salinity source indicators relies on the difference in size of the Br and Cl ionic radii (1.96Å and 1.81Å respectively), as during evaporation and halite precipitation Br, due to its larger size, is thought to remain within the residual brine (also referred to as a bittern brine) rather that being incorporated into the NaCl lattice (Carpenter, 1978; McCaffrey *et al.*, 1987). Fluids with high Br values are assumed to have originated from seawater evaporation whereas fluids with low Br values are interpreted as fluids that have undergone interaction with evaporites. In this way halogen concentrations in extant palaeo-brines can be used to ascertain the origin of the chlorinity in the fluid and in some cases the origin of the fluid itself.

Figure 2.2 is a plot of the Cl versus Br systematics in evaporating systems. The seawater evaporation trajectory (SET) is drawn from data compiled by Carpenter (1978) and represents the evaporation of seawater at surface temperatures. Loss of water from a fluid at high temperatures (100°C) is thought to shift the point of halite saturation to higher

chloride and bromide values meaning that it should be possible to distinguish between sub-aerially evaporated seawater and the concentration of seawater at higher temperatures in the subsurface as a result of hydration reactions (Gleeson, 2003). Also shown are the expected trajectories (Carpenter, 1978) of a seawater-derived brine that has been mixed with meteoric water (in which the data would lie along a 1:1 slope parallel to the SET) and a seawater-derived brine that has been mixed with seawater (in which the data would move in a trend line that would converge on seawater).

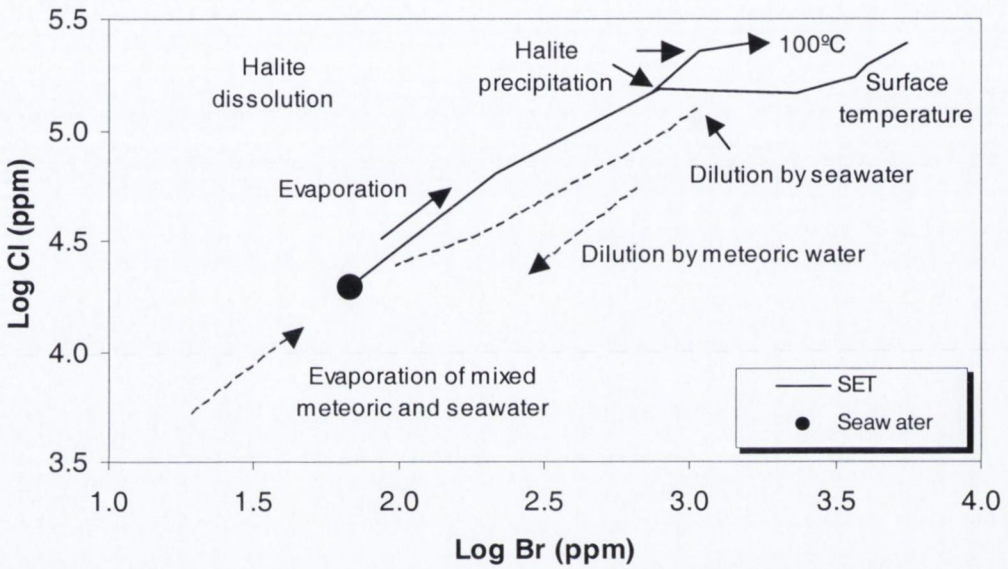

Figure 2.2 Cl and Br systematics in evaporating systems, showing the composition of seawater and the SET (after Carpenter (1978); Gleeson & Yardley (2002).

As absolute concentrations of the solutes cannot be measured directly using the crush-leach technique (as the amount of fluid released by the inclusions is generally unknown) plots of the type used by Kesler (1995; 1996) are useful (Figure 2.3). They utilise the elements normalised to Br, which may be measured using crush-leach and are unaffected by dilution with meteoric water or errors in salinity estimates. Therefore these plots usually provide information on the origin of the solutes rather than the source of the water in the brines (Kesler *et al.*, 1996)

The Na-Cl-Br plot shows that as seawater evaporates the Cl/Br and Na/Br ratios remain constant until halite precipitation occurs (Figure 2.3). At this point Na and Cl are preferentially incorporated into the halite lattice and the ratios decrease resulting in a trend

towards the origin. If any halite dissolution or re-precipitation occurs, the data plot in the field above seawater, as the resulting fluid will be deficient in Br. Na-Ca loss due to exchange reactions can also be identified on a plot such as this.

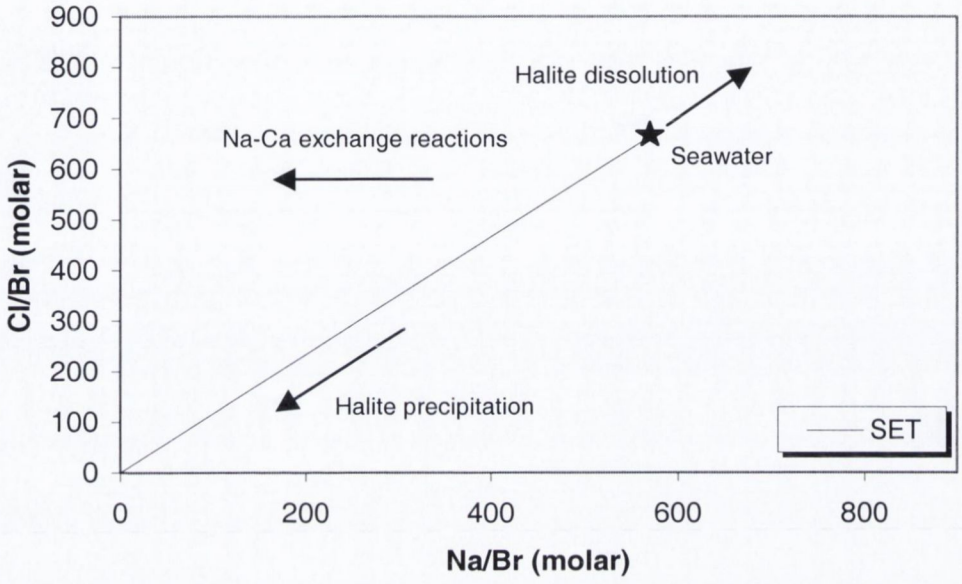

Figure 2.3 Plot of the Na-Cl-Br systematics of formation waters showing the composition of seawater and the SET after Kesler *et al.* (1995).

A halogen geochemistry caveat

Although the use of halogen geochemistry is a widely used technique it is important to be aware that the underlying assumptions regarding the conservativeness of Cl and Br in solution may not be true in some circumstances (Land & Prezbindowski, 1981; Hanor, 1987). For example, work by Collins (1975) has shown that fluids may become enriched in Br by leaching Br-rich organic matter.

2.7 XRD

The method of identifying minerals by x-ray diffraction (XRD) is based on the diffraction of x-rays by a crystal lattice. Minerals have an ordered lattice structure and each mineral has a distinct constant spacing between the lattice planes. X-rays that enter a crystal lattice are reflected by these planes. The condition for maximum reflection is given by the Bragg equation:

$$2d\sin\theta = n\lambda \quad (12)$$

where n is the integer determining the first, second, third..... order peaks, λ is the wavelength of the x-rays, θ is the glancing angle and d is the interplanar spacing of the crystal.

The x-ray diffractometer

The XRD diffractometer used was a Phillips PW1050/25 attached to a Phillips PW1720 generator. It contained a Phillips PW3313/20 Cu k-alpha anode tube that is run with standard conditions of 40kV and 20mA. The machine uses Cu Kα radiation at a constant wavelength of 1.5418Å (representing the Kα peak).

Samples of dolomitised micrite from Lisheen were analysed using XRD in order to determine their stoichiometry. All samples were scanned from 25° to 39° at a speed of 2° 2θ min^{-1}, with a time constant of 1 second and with a scale of $1x10^3$ counts per second (cps). As the peak positions may shift due to natural variations in XRD analysis, quartz was mixed with the samples to normalise the peak positions.

CHAPTER 3

LISHEEN

3.1 INTRODUCTION

The Lisheen orebody is located within the Rathdowney Trend, approximately 10 kilometres northeast of Thurles and 10 kilometres southeast of Templemore (Figure 3.1). This trend is defined by the orebodies at Lisheen and Galmoy as well as several other Zn-Pb prospects including Derrykearn, Tonduff and Durrow. The Lisheen deposit was first discovered in 1990 in a joint venture exploration programme run by Chevron Mineral Corporation of Ireland Ltd. and Ivernia West plc. It is currently owned and operated by Anglo American plc and remains the second largest operating Zn-Pb mine in Ireland with estimated total combined reserves and resources of 17.9 Mt at 11.16 % Zn, 1.72 % Pb (Fusciardi *et al.*, 2003).

3.2 REGIONAL GEOLOGICAL SETTING

3.2.1 Stratigraphy

Hitzman *et al.* (1992), Shearley *et al.* (1996), Redmond (1997) and Hitzman *et al.* (2002) all provide a detailed review of the stratigraphy of the area surrounding the mine at Lisheen. For the purposes of this study a deep (804.5m) stratigraphic drillhole, LK 318, was logged to provide information on the thicknesses of the units and a stratigraphic column was constructed on the basis of this (Figure 3.2). Redmond (1997) provided additional information on the units that occur above the present day erosion surface at the mine which were not intersected by LK 318.

The Tournaisian succession at Lisheen consists of continental red beds (Old Red Sandstone) overlain by shallow water, thinly bedded mudstones, sandstones and limestones, collectively known as the Lower Limestone Shales (it includes the Ballymartin, Ringmoylan Shale, Ballyvergin Shale and Mellon House Formations). Above these lie the three members of the Ballysteen Limestone Formation (Lower Calcareous Member, Lisduff Oolite Member and Upper Calcareous Member). It also has a thin development of nodular chert (Nodular Micrite Unit) at the top, just below the overlying Waulsortian Limestone, the base of which is the main locus for mineralisation. The Waulsortian Limestone is succeeded by the skeletal packstones and grainstones of the Crosspatrick Formation, which in the northern parts of the Rathdowney Trend are overlain by the peloidal limestones and birds-eye micrites of the Aghmacart Formation (Redmond, 1997).

3.2.2 Structure

A number of E-W to WNW-ESE trending, northward dipping, normal faults occur within the mine area (Figure 3.1). The maximum displacement on all of these faults is 220m with the highest grade and thickest developments of ore located at the point of maximum throw (Shearley *et al.*, 1995), or, in rare cases, where the controlling fault changes dip (Cruise, 2000). The overall distribution and geometry of the normal faults has been interpreted as being fundamentally controlled by the reactivation of NE-SW trending Caledonian basement structures (Phillips & Sevastopulo, 1986) due to extension along a N-S axis during the Lower Carboniferous (Johnston *et al.*, 1996).

Compressional structures such as strike-slip faults, folds and thrusts are also found at Lisheen. They are all thought to be attributable to the Late Carboniferous Variscan orogeny, although due to the poor stratigraphic record, a Tertiary age for these structures cannot be ruled out (Carboni *et al.*, 2003). Many thrusts cut the orebodies at Lisheen causing repetition of the mineralised units in the form of a ramp and relay system (M. Cruise pers comm.). These inversion structures therefore provide an upper age limit for the mineralisation at Lisheen, which is generally thought to be at least 10 million years after the deposition of the host rocks (Hitzman *et al.*, 2002), although it may have been substantially younger (Sevastopulo & Redmond, 1999).

3.2.3 Mineralisation and dolomitisation

The bulk of the mineralisation at Lisheen is hosted within a series of flat-lying, stratiform lenses of massive to semi-massive sulphides at, or close to the base of pervasively dolomitised Waulsortian Limestone. Some subordinate mineralisation also occurs within the Lisduff Oolite Member of the underlying Ballysteen Limestone Formation, which itself has only been weakly dolomitised (Hitzman *et al.*, 1992). This close association between pre-mineralisation dolomitisation and ore development is reflected in other deposits in the Rathdowney Trend such as Galmoy (Lowther *et al.*, 1999).

Pre-mineralisation regional dolomitisation

The pre-mineralisation dolomitisation of the Waulsortian Limestone at Lisheen forms part of a more regional scale dolomitisation event(s) in the southeast of Ireland. This so called 'Regional Dolomite' (Hitzman *et al.*, 1992) forms a broad zone that extends westwards from the Leinster Massif and its Lower Palaeozoic envelope to the Lisheen mine area. The

contact between undolomitised Waulsortian Limestone to the west and dolomitised Waulsortian Limestone to the east (Figure 3.3) is straddled at Lisheen and geological mapping indicates that the contact between the two is gradational over a distance of approximately 1 kilometre (Hitzman *et al.*, 1992). The Lisheen mine area therefore provides the ideal location to study the modes and mechanisms of this regional dolomitisation process.

The Regional Dolomite consists of two main components: a buff to pale grey, fine-grained, replacive dolomite; and a texturally later white, coarse-grained dolomite that can be both replacive (Plates 3.1, 3.2) and fill open space (Plate 3.3) produced in the grey replacive dolomite (Hitzman *et al.*, 1998). The grey replacive dolomite is formed of either euhedral or subhedral crystals, averaging 100μm to 500μm in maximum dimension. Their grain size distribution is generally unimodal. The white coarse-grained dolomite has a polymodal crystal size distribution with the euhedral to subhedral grains frequently up to 5mm in size. Many of the crystals have curved faces and exhibit the sweeping extinction indicative of saddle dolomite (Radke & Mathis, 1980). Several of them have highly turbid cores and become increasingly more limpid towards the outer parts of the crystal.

In addition to the grey replacive dolomite and the coarse-grained white dolomite, the Regional Dolomite at Lisheen commonly contains a third dolomite component. This third component is a black, fine-grained dolomite, with an average grain size of approximately 50μm. It has been called 'black tops' or 'dark tops' dolomite by the mine geologists at Lisheen, because it occurs as laterally discontinuous, thin layers (a few millimetres thick at most), which always lie above grey replacive dolomite and below coarse white dolomite (Plate 3.3).

Pre-mineralisation hydrothermal dolomitisation

Within the Waulsortian Limestone at Lisheen the Regional Dolomite is cut by two texturally distinct ore-related hydrothermal dolomites that each form the matrix of two hydrothermal dolomite matrix breccias: the black matrix breccia and the white matrix breccia.

The black matrix breccia (BMB) (Hitzman *et al.*, 1992) is characterised by fine-grained black dolomite that both replaces and infills cavities and veins within the regionally

dolomitised Waulsortian Limestone. It is similar to both the 'rock matrix breccia' (Doyle *et al.*, 1992; Doyle & Bowden, 1995) at Galmoy and the 'dolomite breccia' (Andrew, 1986) at Silvermines. It ranges from clast to matrix supported, with the majority of clasts being Regional Dolomite (containing both the fine-grained and coarse-grained components). Rare clasts of undolomitised Waulsortian Limestone have also been found along with white matrix breccia clasts and clasts of earlier generations of BMB (Hitzman *et al.*, 2002). Hitzman *et al.* (1992) observed that mineralisation cut both the clasts and the matrix, with the matrix being preferentially replaced followed by the clasts. This brecciation by dolomitising geo- or hydrothermal fluids at Lisheen was therefore pre-mineralisation.

White matrix breccia (WMB) (Hitzman *et al.*, 2002) is also restricted to the areas of the Waulsortian Limestone that have been regionally dolomitised. WMB is a stockwork of coarse-grained white dolomite that is seen to cross-cut the Regional Dolomite in the form of veins that expand into zones of brecciation. The clasts within the WMB are mostly Regional Dolomite, although, clasts of earlier generations of WMB and BMB have been identified by Redmond (1997). Although it looks similar to the regionally developed coarse-white dolomite, CL microscopy of the coarse-grained white dolomite of the WMB has shown that it can display a complex zonation pattern whereas the coarse-grained white dolomite component of the Regional Dolomite tends to be poorly zoned. The luminescence signature of both also is usually different with the WMB having a moderate to brightly luminescent signature and the coarse-white dolomite of the Regional Dolomite having a dull to moderate luminescence (Redmond, 1997). In terms of its spatial distribution relative to the BMB, the bulk of the WMB occurs consistently above developments of BMB, although the contact between well-developed examples of the two is rarely observed (Redmond, 1997). There is, therefore, an assumed genetic link between the WMB and BMB with the two differing only in grain size and colour (itself probably a function of grain size). In fact many of the project geologists at Lisheen believe that the WMB is simply a more coarse-grained form of the BMB (J. Güven pers comm.).

A digression on the use of the term 'hydrothermal dolomite'

The use of the term 'hydrothermal dolomite' has come under scrutiny recently (Machel & Lonnee, 2002). Machel and Lonnee (2002) contend that this term should only be applied to dolomitising fluids that are warm or hot relative to the surrounding environment, with no genetic implications regarding the source of the fluid. Under this definition even a

dolomite formed at 40°C may be considered hydrothermal provided that it formed above the ambient temperature. A fluid inclusion study on black dolomite matrix breccias from near Ballinasloe, Co. Galway, which are similar to those found at Lisheen and elsewhere in the Irish orefield (Wilkinson & Earls, 2000), suggests a relatively high temperature hydrothermal origin (Th 150-220°C and 13-20wt% NaCl equivalent) for these breccias. However, as Wilkinson and Earls (2000) make no reference to the ambient temperature, the term hydrothermal dolomite cannot be justifiably used.

Post-mineralisation ferroan dolomite, pink dolomite and calcite veining

Within the Waulsortian Limestone tiny amounts of ferroan dolomite occur within veinlets that cross-cut the Regional Dolomite, BMB and WMB (Redmond, 1997). This late ferroan dolomite has also been observed within the Old Red Sandstone which underlies the carbonate succession at Lisheen and is in fact found throughout many locations in the Irish Midlands irrespective of whether there is a mineral deposit in the vicinity or not (L. Chapman pers comm.). This suggests that late Fe-rich fluids moved through the Old Red Sandstone and up into the overlying carbonate sequence. Whether this fluid movement was the result of lateral flow through the Old Red Sandstone or large convection cells penetrating the underlying basement (or both) is still unclear.

Pink dolomite, which can be either vein hosted or form vug-filling cements, is found at Lisheen. These pink dolomites, referred to by most workers as 'pink plug', are found throughout the Irish Midlands and are not solely restricted to the Lisheen mine area. They are coarse-grained (circa 5mm) and can be associated with tiny grains of pyrite that tend to coat the crystals. Redmond (1997) interpreted the pink dolomite at Lisheen as being a hydrothermal dolomite representing the late stages of the evolution of the Lisheen hydrothermal system. Fluid inclusion data from Eyre (1996) indicate that the fluids from which the pink dolomite precipitated (90-120°C with 25-29wt% NaCl equivalent) were certainly cooler than those that precipitated the WMB (170-230°C with 5-17wt% NaCl equivalent).

Late, coarsely crystalline calcite veins, up to several centimetres in width, cross-cut all rock types at Lisheen. Where observed in this study, these calcites appear to be non-ferroan as they do not stain with Potassium ferricyanide. However, Redmond (1997) reported

examples of ferroan late calcite veins within the Ballysteen Limestone close to major faults.

3.3 PETROGRAPHY

Due to the focus of this project, only the pre-mineralisation regional dolomitisation has been studied in detail. A cursory description of the other dolomite types was given in Section 3.2.3 above, but no detailed petrographic data will be presented. The samples studied came from exploration drillholes (LK 2258-38, LK 3262-18, LK 318, LK 310) as well as a quarry section, referred to in this study as Lisheen quarry (GR 21453 16187), approximately 7 kilometres southwest of the mine (Figure 3.1).

Hand samples

In stained hand samples the selective nature of the replacement by the Regional Dolomite is easily distinguished (Plate 3.1). The replacement of micrite and bryozoans by the fine-grained grey dolomite and the spar-filled cavities by the coarse-grained white dolomite is ubiquitous (Plates 3.1, 3.2). This preferential replacement of the fine-grained material by the grey dolomite occurs prior to the coarse-grained white dolomite and may be a function of the large surface area upon which the dolomitising fluids can act. Within all hand samples from the partially dolomitised zone, areas of cryptofibrous calcite (CFC) cement are not replaced by dolomite (Plate 3.2).

Thin sections

The Waulsortian facies in Ireland has been reviewed in detail by Lees and Miller (1995). Using CL microscopy, the early void filling calcite cements of the Waulsortian Limestone at Lisheen can be separated into four distinct stages (Stages A-D; terminology of Lees and Miller (1995)). Stage A cements are CFC cements, which are interpreted as neomorphosed early marine high Mg calcite cements. Under CL, they have a characteristic patchy/blotchy appearance, partly non-luminescent and partly brightly luminescent (Plate 3.4b). The brightly luminescent parts are micro-veins and partial replacement of the CFC by later early calcite cement generations (Stage C). It is possible however, to find areas of CFC that are non-luminescent. These can therefore be considered as being 'pristine' CFC cements, which can provide uncontaminated samples for stable isotope analysis. Stage B cements are usually non-luminescent (Plate 3.4b), although they may have thin, bright sub-stages

developed within them (the term sub-stage as defined by Gillies (1987) is a localised sub-division of a stage distinguished by distinctive CL characteristics). They were followed by the Stage C cements, which tend to be very bright and Stage D, which usually has a complex zoning pattern with many sub-stages, all of which are generally dully luminescent. At Lisheen the Stage D cements occlude any remaining porosity within the early cavities (Plate 3.4b).

Dolomitisation of the Waulsortian Limestone at Lisheen occurred after the occlusion of all of the primary porosity (Plate 3.4b). As anticipated from what is observed in the hand samples, the fine-grained grey dolomite occurs first and preferentially replaces the micrite and bryozoan fronds (Plates 3.5a, 3.5b). Dolomitisation by the later coarse-grained white dolomite can also be replacive and areas of sparry calcite, such as those found in the centre of large early calcite cavities or fossils, are replaced by sparry dolomite (Plates 3.6a, 3.6b). CFC cements and larger, more robust fossil fragments such as crinoid ossicles remain undolomitised in partially dolomitised samples, indicating that they were amongst the last components to be replaced (Plates 3.7a, 3.7b). In a few cases, the dolomitisation process is not complete and areas of undolomitised calcite remain within the centre of large primary cavities (Plates 3.8a, 3.8b).

The fine-grained and coarse-grained dolomites have similar CL signatures and both tend to be poorly zoned. However, rare examples of the coarse-grained dolomite exhibiting well-developed zonation have been observed (Plate 3.6b). As these zoned coarse-white dolomites come from within partially dolomitised samples, along the so-called 'dolomite front' (Hitzman *et al.*, 1992), they cannot be confused with the zoned coarse-grained white dolomite of the WMB. While dolomitisation by the fine-grained grey dolomite is very selective and broadly retains the shape of the material it is replacing (Plate 3.2), replacement by the coarse-grained dolomite is commonly non-mimetic (Plate 3.9a). Not only are the original fabrics of the limestone destroyed by replacement by the coarse-grained dolomite but also the dolomite crystals themselves tend to be orders of magnitude greater than the calcite crystals they are replacing (Plate 3.9b).

A different type of coarse-grained dolomite is contained exclusively within veins that cross-cut both the fine and coarse-grained dolomites. It differs from the original coarse-grained dolomite only in terms of its CL signature (Plate 3.10b) as it has a darker, more

blood red colour in CL than the moderately luminescent coarse-grained dolomite (herein to be referred to as 2nd coarse dolomite). This dark luminescence may be due to a higher Fe content, but if so it must be slight as the Potassium ferricyanide stain does not highlight it. Evidence for the presence of this second, vein hosted, coarse dolomite was found in only two drillholes, LK 2258-38 (112.44-112.75m) and LK 3262-18 (203-203.62m). It is therefore not thought to be volumetrically significant.

As mentioned above, there is a third component of the Regional Dolomite found at Lisheen, termed the 'black tops' dolomite (Plate 3.3). Its consistent position above fine-grained and below coarse-grained dolomites make it tempting to equate these three dolomite types with common lithologies in undolomitised Waulsortian Limestone. In this interpretation, the fine-grained grey dolomite represents micrite-rich lithologies; the coarse-grained white dolomite represents sparry calcite cements that filled cavities; and the fine 'black tops' dolomite represents geopetal micrite that accumulated on the floor of cavities. The grey dolomite is certainly replacive as it contains tiny relicts of calcite, which are imaged as pits on etched polished surfaces using the SEM in secondary electron emission mode, as bright spots in back scatter mode; and as brightly luminescent spots under CL. However, the pattern of growth of the coarse white dolomite, determined under CL, suggests that it was a space-filling cement (Plates 3.11a, 3.11b). This implies that the 'black tops' dolomite may in fact have nucleated as fine crystals in fluids saturated with respect to dolomite in dissolution cavities and have fallen to the floor to form a geopetal dolomite sediment before the cavities were filled with the white sparry dolomite cement. A problem with this model is the generally slow rate of precipitation of dolomite from supersaturated solutions, although data on the reaction kinetics are mostly from lower temperature fluids than envisaged here. An alternative origin, suggested by Prof Hans Machel (pers comm., 2002), is that the dark geopetal fine-grained dolomite was liberated during solution of partly dolomitised limestone, which led to the creation of the vugs, which were subsequently filled by sparry dolomite. No organic material or sulphide minerals have been identified in the fine-grained 'black tops' dolomite. Its dark colour may be a result of its fine grain size and the presence of fine intercrystal porosity between grains (Plate 3.12) and perhaps the presence of some intragrain porosity also (Plate 3.13). However, it should be noted that the author has been unable to reproduce images of this intragrain porosity and so what is observed in Plate 3.13 may in fact be an artefact.

3.4 PARAGENESIS

The paragenetic sequence inferred at Lisheen is illustrated in Figure 3.4. Pre-ore dolomitisation (regional dolomitisation) occurred after porosity occlusion of the host limestone. The fine-grained component of the Regional Dolomite occurred during the initial stages of dolomitisation followed by the coarse-grained white dolomite component. There was probably some overlap between these two components. Where present the 'black tops' dolomite, if it is geopetal dolomite, must have formed prior to the coarse-grained dolomite. Hydrothermal dolomitisation and brecciation occurred after the regional dolomitisation and prior to the onset of mineralisation. Boyce *et al.* (2003) proposed that these hydrothermal systems must have occurred over an extended time period which they suggested was >7 Ma. Ferroan dolomite, pink dolomite and calcite veining all post-date the mineralisation at Lisheen.

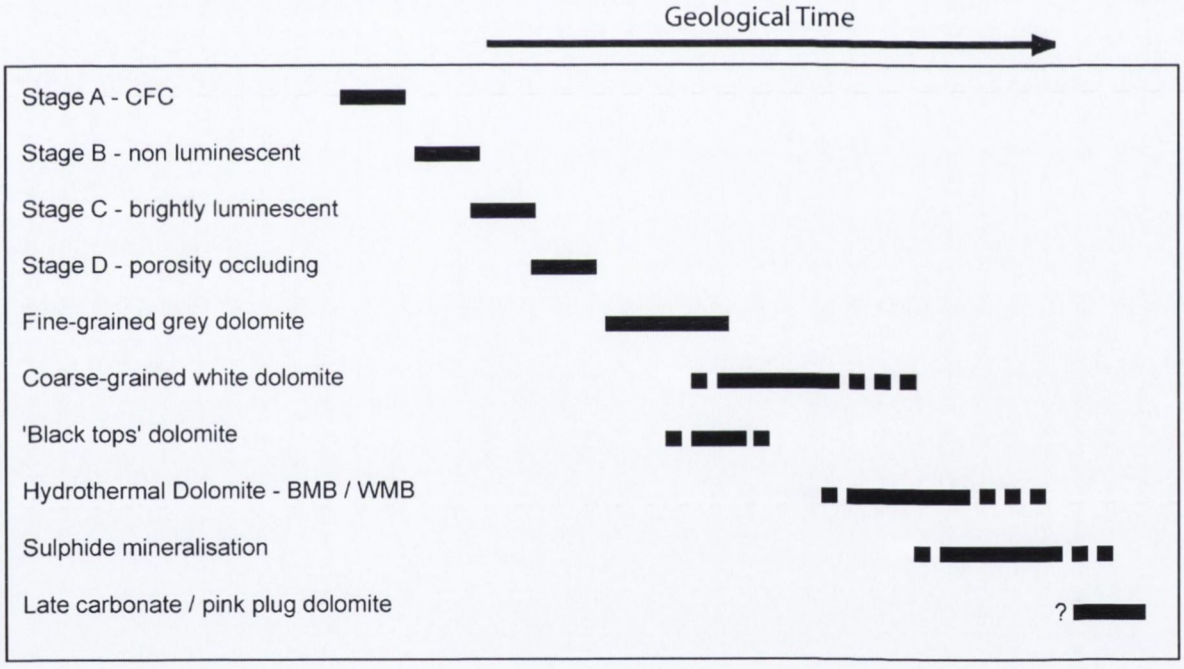

Figure 3.4 Paragenetic sequence as seen at Lisheen based on Redmond (1997), Eyre (1998) and petrographic data from this study.

3.5 XRD ANALYSES OF DOLOMITISED MICRITE

The use of X-ray diffraction (XRD) analysis to determine the stoichiometric composition of dolomite is a well-known technique and is based on calculating the percentage of $CaCO_3$ in a sample using the shift in the d_{104} peak for dolomite (Lumsden, 1979). For example, ideal dolomite, with a stoichiometric composition of Ca_{50}:Mg_{50}, has a d_{104} peak at 2.886Å whereas the d_{104} peak for a dolomite sample with Ca_{55}:Mg_{45} is 2.901Å. This

method has been less widely used in recent years because of concerns over the reliability of the results. Lumsden (1979) noted that the d_{104} peak depends on the Ca excess and at higher $CaCO_3$ contents (>55%) there can be an overestimation of the dolomite content by 10-12%. Also a high Fe content is also known to shift the d_{104} peak to higher angstrom values (Tucker & Wright, 1990). More recent methods to determine the stoichiometry of dolomite have involved the use of the electron microprobe (EMP) to quantify the Ca:Mg ratio. The main limitations of this method are that it is not widely available and it can be costly. A recent study by Jones *et al.* (2001) undertook a comprehensive comparison of results obtained from both the EMP and XRD. They demonstrated that there is strong evidence to suggest that the use of XRD in stoichiometry determination can produce reliable results, comparable with those obtained from the EMP. For this reason it was decided to use XRD to analyse samples of dolomitised micrite from Lisheen and determine their stoichiometry.

Five dolomitised micrite samples from the quarry southwest of Lisheen mine were chosen for analysis, as they were easy to sample and contained negligible amounts of Fe. The powdered samples were mixed with quartz to normalise the peak positions, which may shift due to natural variations in XRD analysis. All were scanned from 25° to 39°2θ, in order to intersect the d_{101} quartz peak at 31.035°2θ, and the d_{110} dolomite peak at 37.391°2θ. Appendix E contains the labelled XRD traces of the samples that were analysed. Using the Lumsden (1979) equation to determine the Ca:Mg ratio it was found that the dolomite samples contained between 48 and 51% Ca and were nearly stoichiometric (Table 3.1).

Sample:	Degrees 2θ:	Angstroms (Å):	% Ca:	Ordering:
A	31.04	2.8811	48.4	0.4
B	30.94	2.890	51.3	0.4
C	30.96	2.8883	50.8	0.5
D	31.04	2.8811	48.4	0.6
E	30.94	2.890	51.3	0.3

Table 3.1 XRD analyses of dolomitised micrite samples from the quarry near Lisheen.

The degree of ordering of the dolomites can be estimated using the method outlined in Hardy & Tucker (1988) that involves looking at the sharpness and relative intensities of the d_{105} and d_{110} dolomite peaks, such that:

degree of ordering = intensity of 015 peak / intensity 110 peak

The intensity of the 015 and 110 peaks were measured for all five samples and the results are also tabulated in Table 3.1. All samples appear to be well ordered, although the correlation between stoichiometry and ordering does not appear to be present as the most stoichiometric dolomite is not the most ordered dolomite. It is theoretically possible for a 50:50 Ca:Mg dolomite to have no ordering reflections if the cation sheets in the dolomite lattice are equal mixtures of Ca and Mg (Tucker & Wright, 1990). As there are a number of factors that can affect the peak intensities, it was concluded that the use of XRD to determine the degree of ordering was probably unreliable.

It was anticipated that the dolomitised micrites from the quarry near Lisheen (and all other dolomite studied in this project) would be nearly stoichiometric. The reason for this is that there is a well-established trend towards increasingly more stoichiometric dolomite in older dolostones probably as a result of dissolution/re-precipitation during diagenesis (Sperber *et al.*, 1984).

3.6 FLUID INCLUSION MICROTHERMOMETRY

Two phases were chosen for fluid inclusion microthermometry analysis: the coarse-grained white dolomite and the Stage D calcite (Appendix C). Both phases were from the same sample (borehole LK 2258-38 at a depth of 121.2-122.23m), which contained a large Stage D filled cavity that was surrounded and partially replaced along the margins by coarse-grained dolomite (dolomitised spar). A detailed petrographic study of the fluid inclusion assemblages in both phases was completed prior to undertaking the microthermometry.

Dolomite fluid inclusion petrography

The coarse-grained dolomite contained a plethora of fluid inclusions but unfortunately the majority were on the sub-micron scale and therefore too small to be useful in terms of obtaining microthermometric data. The dolomite crystals themselves contained highly

turbid cores with visibility towards the outer parts of the crystal increasing such that inclusions could be observed. Workable inclusions, albeit a small number, were located in these outer limpid parts of the dolomite crystals and mapped. These inclusions were two-phase (L+V) inclusions that ranged in size from sub-micron to approximately 8μm with degrees of fill (ψ_{liquid}) of either 0.85 or 0.9. They were subhedral to euhedral in shape and lay in an orientation parallel to the dolomite crystal faces, which were commonly coincident with the CL growth zones. Many of these larger inclusions lay also parallel to the trails of sub-micron sized inclusions.

Dolomite fluid inclusion microthermometry

A total of four fluid inclusions were measured from the coarse-grained dolomite at Lisheen. Their Th values ranged from 173 to 236°C. First melting temperatures indicate that all the inclusions were part of the $NaCl\text{-}CaCl_2\text{-}H_2O$ ternary system (see below). Salinity data for only one inclusion was obtained by sequential freezing (Haynes, 1985) which confirmed with certainty its value of 25.6 combined wt% NaCl and $CaCl_2$ equivalent.

The $NaCl\text{-}CaCl_2\text{-}H_2O$ system

The $NaCl\text{-}CaCl_2\text{-}H_2O$ system is characterised by a eutectic temperature (T_e) of ~-52°C. In the majority of inclusions belonging to this ternary system, the stable solid assemblage below the eutectic temperature is a mixture of ice, hydrohalite ($NaCl.2H_2O$) and antarcticite ($NaCl.6H_2O$) (Yanatieva, 1946; Crawford, 1981). With the exception of very $CaCl_2$-rich solutions, antarcticite will melt at the ternary T_e when heated from frozen, leaving just ice and hydrohalite, whose last melting temperatures are recorded to enable the salinity to be calculated.

During freezing of a two-phase $NaCl\text{-}CaCl_2\text{-}H_2O$ fluid inclusion the liquid freezes at temperatures that can be as low as –100°C. Upon freezing there is a collapse (shrinkage) of the vapour bubble. The vapour bubble may then disappear completely or remain in its shrunken state in the inclusion. Usually when frozen the inclusion has a brown, speckled appearance. As the inclusion is heated it generally darkens in colour and the volume of the vapour bubble decreases further at temperatures between –70 and -50°C. These changes have been attributed by many workers to melting events at metastable eutectics (Vanko *et al.*, 1988; Davis *et al.*, 1990; Spencer *et al.*, 1990). Recent work by Samson and Walker

(2000) has shown that the darkening of the inclusion that occurs between –70 and -50°C coincides with the crystallisation of hydrohalite and antarcticite and that this phase change may be mistaken for the ternary T_e. Using Raman spectroscopy they were able to show that after initial rapid freezing only an ice peak was observed on the spectra and that the presence of hydrate peaks was observed only after the inclusion was warmed and the darkening of the solid phase had occurred (between –70 and -50°C). If the inclusions were cooled rapidly after this phase change was observed, the spectra would then contain hydrate peaks in addition to the ice peaks. Therefore as a caveat in determining the T_e it is important to establish that it is the actual T_e that is being observed and not some phase change due to the crystallisation of hydrates.

Calcite fluid inclusion petrography

There was an abundance of fluid inclusions contained with the Stage D calcite phase at Lisheen. Necking-down and leakage was a common feature within the fluid inclusion assemblage. Trails of tiny secondary inclusions were also present but as the main focus of the fluid inclusion study was to analyse only primary fluid inclusions the secondary inclusions were noted and mapped but not isolated for microthermometry. The remaining inclusions were all two-phase (L+V) inclusions that ranged in size up to a maximum of 22μm with the average being 10μm. Where suitable, potentially non re-equilibrated, primary inclusions were observed they tended to have two completely different ψ_{liquid}, those with ψ_{liquid} of 0.9 and those with ψ_{liquid} of 0.7. This was consistent throughout the sample and each was treated as a separate assemblage while petrographically mapping. No relationship was found between the two assemblages. There was no evidence of one set cross-cutting the other or of their relative timing. In fact, in a few cases along trails, the fluid inclusion ψ_{liquid} were prone to alternate between those with 0.9 and those with 0.7. It was hoped that the two assemblages could be separated by means of their microthermometric data. There was no evidence of heterogeneous trapping (boiling) within the fluid inclusion assemblage as there was no range in the ψ_{liquid} other than those with 0.7 and 0.9. In the case of an assemblage that had undergone boiling, the full spectrum of ψ_{liquid} from 1 to 0 would be visible, with 1 being a pure liquid fluid inclusion and 0 being a pure vapour fluid inclusion (Diamond, 2003).

As growth zones within the Stage D calcite were difficult to determine (except under CL), it was difficult to isolate inclusions that could be considered as being unequivocally primary. The inclusions that were selected for measurement were all isolated inclusions that appeared to be elongated in the direction of growth of the calcite crystal. They strictly should be considered as being indeterminable fluid inclusions (Goldstein, 2003) but they were the best candidates for being primary that could be found within the assemblage.

Calcite fluid inclusion microthermometry

A total of five fluid inclusions from the Stage D calcite were measured. Two of the inclusions had ψ_{liquid} of 0.7 and three had ψ_{liquid} of 0.9. The homogenisation temperatures for the inclusions with the lower ψ_{liquid} (204 and 215°C) were not significantly different from those with the higher ψ_{liquid} (178, 186, 211°C). In fact there is some overlap between the two assemblages. With this limited Th data set it is not possible to establish whether the inclusions are part of a single assemblage. Data on the composition of the inclusions was difficult to obtain. However, the Tfm was observed in three out of five of the inclusions and is consistent with the $NaCl\text{-}CaCl_2\text{-}H_2O$ system. This is very unusual because in the precipitation of the Stage D calcite, $CaCl_2$ would not be expected to be present. Only one Tm_{ice} value was recorded (-3.1°C) but as the Tm_h was not observed for this inclusion, no salinity value could be calculated.

Discussion

The fluids that precipitated the coarse-grained dolomite at Lisheen were moderately hot (173 to 236°C) and very saline (25.6 combined wt% NaCl and $CaCl_2$ equivalent). The measured Th values for fluid inclusions within the Stage D calcite (178 to 215°C) are higher than what would be expected for temperatures obtained directly as a result of burial alone, even if the geothermal gradient was orders of magnitude greater than the present day (22-25°/km). Lees and Miller (1995 p.250 Fig. 46) suggested that cement Stages A-D formed at relatively shallow depths of burial (within approximately 500m of the sea floor). As it is unlikely that the geothermal gradient at the time of precipitation of these cements was high enough to produce such high filling temperatures, re-equilibration must be suspected. The differing ψ_{liquid} and the Tfm data both suggest that the fluid inclusions measured from the Stage D calcite may have equilibrated with a later fluid and that this fluid is likely to have been the regionally dolomitising fluid. This may explain why the

inclusions contained NaCl-$CaCl_2$-H_2O as the most likely Ca-rich brine with which the calcite could have interacted was the dolomitising fluid.

3.7 STABLE ISOTOPE GEOCHEMISTRY

Thirty-seven samples of unaltered Waulsortian Limestone and forty-eight samples of dolomitised Waulsortian Limestone from Lisheen were sampled for stable isotope analysis (Appendix B). A full description of the sampling methods is given in Chapter 2.

3.7.1 Calcite

The phases of the Waulsortian Limestone that were sampled for stable isotope geochemistry were micrite, CFC and Stage D cements (the final porosity occluding cement phase).

The $\delta^{13}C$ values of all three phases of calcite sampled (Figure 3.5) range from 1.94 to 4.19‰ (mean 3.01‰ ± 1.16‰ 2σ; mode 3.2‰) and the $\delta^{18}O$ values range from 22.8 to 27.63‰ (mean 25.36‰ ± 2.62‰ 2σ; mode 26.3‰). These values are similar to those reported by Boast *et al.* (1981a) and Gallagher *et al.* (1992) for undolomitised Waulsortian Limestone at Tynagh and Harberton Bridge respectively and are considered typical for unaltered (i.e. non-mineralised/undolomitised) Waulsortian Limestone.

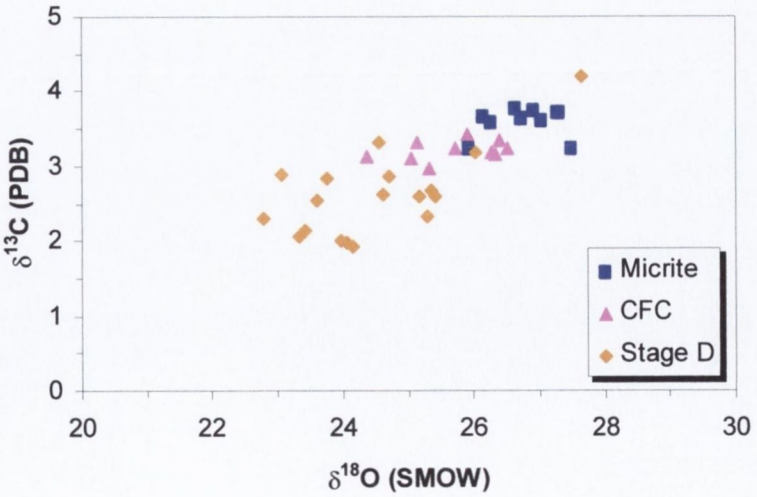

Figure 3.5 Scatter plot of $\delta^{13}C$ and $\delta^{18}O$ values for micrite and early calcite cement phases at Lisheen.

Although the $\delta^{13}C$ values are within the range of carbonates precipitated in equilibrium with Carboniferous seawater (Veizer *et al.*, 1999), the $\delta^{18}O$ values are much lighter. With the exception of one Stage D data point ($\delta^{18}O$ of 27.63‰ and $\delta^{13}C$ of 4.19‰) the calcite data show a progressive shift to lighter values that tracks their paragenesis in that the micrites, have the heaviest $\delta^{18}O$ and $\delta^{13}C$ values and the latest calcite cements, Stage D, have the lightest $\delta^{18}O$ and $\delta^{13}C$ values. Other workers, also sampling individual cement generations, have noted similar trends (Hudson, 1977; Dickson & Coleman, 1980; Moldovanyi & Lohmann, 1984; Given & Lohmann, 1985; Dickson *et al.*, 1990). This shift to lighter $\delta^{18}O$ values in successive cements reflects increasing temperature due to burial and the isotopic evolution of the pore waters (Hoefs, 2001). The minor depletion in $\delta^{13}C$ values may be reflecting the onset of reducing conditions as a result of burial or may be the result of buffering by existing carbonate due to local dissolution and re-precipitation processes (Lees & Miller, 1995).

Upper Palaeozoic seawater

The secondary layer of brachiopod shells, which is thought to precipitate in isotopic equilibrium with seawater, has long been the favoured material upon which the carbon and oxygen composition of Palaeozoic seawater has been based (Veizer *et al.*, 1997; Bruckschen *et al.*, 1999; Veizer *et al.*, 1999). Recent work by Saltzman (2002) suggests that micrite, even after diagenesis, is more reliable than brachiopods at retaining its original carbon isotope values. Based on this, the micrites at Lisheen, which have a very narrow range of $\delta^{13}C$ values (3.23 to 3.77‰, mean of 3.57‰ ± 0.4‰ 2σ), may be considered a reflection of the carbon isotope values at the time of precipitation. These values are also consistent with the published $\delta^{13}C$ values (≤4‰) for Lower Carboniferous (Mississippian) seawater (Brand, 1982; Meyers & Lohmann, 1985; Popp *et al.*, 1986).

In the absence of data from brachiopod shells, micrite has also been used to estimate the original $\delta^{18}O$ composition of marine derived carbonate (Moldovanyi & Lohmann, 1984), although Marshall (1992) suggests that small particles have enhanced solubility due to their high surface area and therefore have greater potential for recrystallisation. Despite this, if the Waulsortian Limestone is assumed to have formed at 25°C, and the median $\delta^{18}O$ value of the micrite is 26.73‰, then the $\delta^{18}O$ of the parental fluid (Friedman & O'Neil, 1977) precipitating the marine carbonate had an isotopic value of –1.65‰. This value is

comparable to the estimation of Meyers and Lohmann (1985), who obtained a $\delta^{18}O$ value of –1.5‰ ± 0.5‰ for early Carboniferous (Tournaisian) seawater from carbonates in New Mexico.

3.7.2 Dolomite

The isotopic data from both the fine-grained and coarse-grained dolomites at Lisheen have been plotted in Figure 3.6. The coarse-grained dolomite values have been broken down into three different types: coarse dolomite, whose calcite precursor is not known with certainty; 2nd coarse dolomite, which is the vein hosted coarse dolomite with the darker red CL signature (Plate 3.10b) and dolomitised sparry calcites. All three coarse dolomite types are petrographically identical and are considered as the one phase.

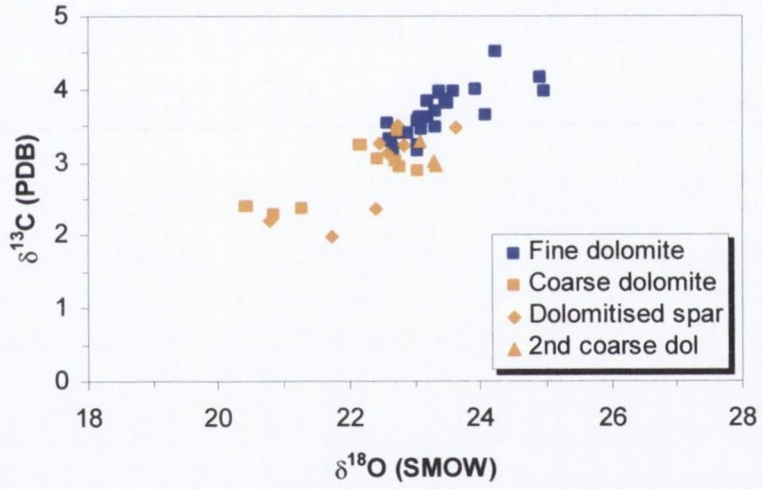

Figure 3.6 Scatter plot of $\delta^{13}C$ and $\delta^{18}O$ values for the dolomites at Lisheen.

The $\delta^{13}C$ values for both the fine and coarse dolomite range from 3.15 to 4.51‰ (mean 3.66‰ ± 0.66‰ 2σ; mode 3.97‰) and 1.99 to 3.52‰ (mean 2.92‰ ± 0.92‰ 2σ; mode 3.0‰) respectively. As carbon isotope compositions are determined by the precursor carbonate (Hoefs, 2001) it is not surprising that the $\delta^{13}C$ values of the dolomites are similar to those of the calcite. Again in accordance with the paragenesis, the dolomitised micrite has the heaviest $\delta^{13}C$ values and the later coarse-grained white dolomite has the lightest $\delta^{13}C$ values.

Dolomitisation of the calcite cements has caused a dramatic shift to lighter $\delta^{18}O$ values. The fine-grained dolomite has $\delta^{18}O$ values that range from 22.58 to 24.96‰ (mean

23.36‰ ± 1.28‰ 2σ; mode 23.1‰). This is a shift of approximately 3‰ from the mean value for undolomitised micrite (range of 25.92 to 27.48‰ and mean of 26.71‰ ± 1.06‰ 2σ; mode 26‰). Likewise the coarse-dolomite values which range from 20.45 to 23.64‰ (mean 22.37‰ ± 1.8‰ 2σ; mode 22.7‰) display a shift of between 2 to 3‰ from the mean Stage D value (mean of 24.5‰ ± 2.38‰ 2σ; mode 24‰) value depending on which type of coarse dolomite is considered.

Discussion

The consistency in the $\delta^{13}C$ values, combined with a shift to lighter $\delta^{18}O$ values upon dolomitisation reflects one of two things: either re-equilibration occurred (due to a temperature increase) of the precursor limestones with a fluid of similar composition to the one that was in equilibrium with them at the time of precipitation; or a later hydrothermal fluid with the same $\delta^{13}C$ values but lower $\delta^{18}O$ values was introduced and re-equilibrated with the precursor limestones. In the latter case the variation would be the result of isotopic exchange between the dolomitising fluid and the precursor limestones, both of which would have had different initial isotopic compositions.

3.8 MODELLING OF PARENTAL FLUIDS

Using the average of the measured $\delta^{18}O$ values for the dolomitised spar (22.47‰) the mineral-water oxygen isotope fractionation curve was constructed using the equation of Land (1983) and is shown in Figure 3.7. The average dolomitised spar value was used, as opposed to the total coarse dolomite average (22.37‰), as the fluid inclusion data came from this phase. The parental fluid composition was calculated using the homogenisation temperature range (rounded to 170 to 240°C). This indicated isotopic values ranging from 9.3 to 13.5‰. This is consistent with a fluid that has undergone a significant amount of fluid-rock interaction.

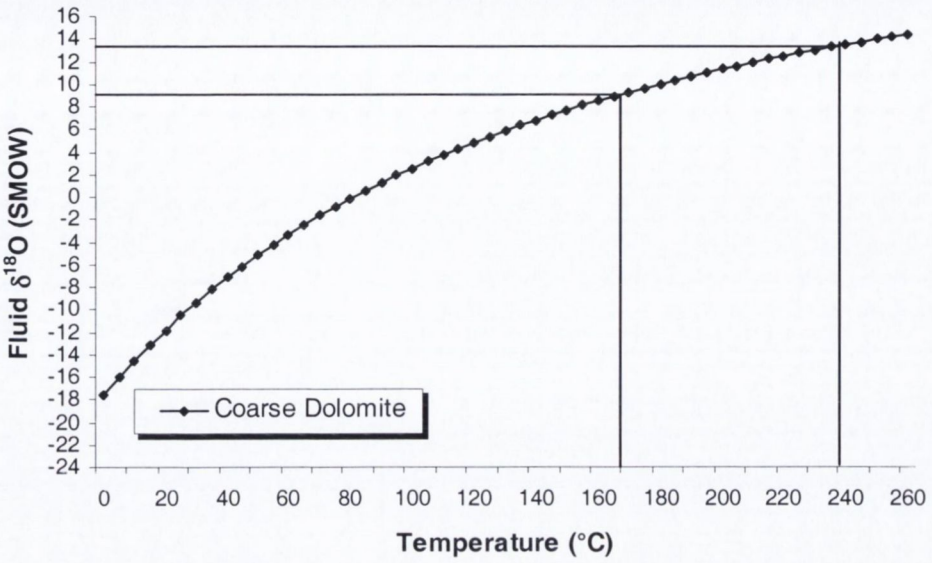

Figure 3.7 Mineral-water oxygen isotope fractionation curve for the dolomitised spar at Lisheen. See text for discussion.

3.9 HALOGEN GEOCHEMISTRY

A sample of coarse dolomite from LK 2258-38 (46.5-46.75m) was prepared for crush-leach analysis using the method outlined in Chapter 2. The data are shown in Appendix D.

Figure 3.8 shows the calculated Cl and Br composition of the fluid within the coarse dolomite fluid inclusions at Lisheen. The data from Lisheen lie directly on the line representing the evaporation of seawater. The positioning of this data indicates that the fluid within these inclusions is residual brine, formed by the evaporation of seawater past the point of halite precipitation.

Also plotted in Figure 3.8 is the composition of a Br-rich fluid in equilibrium with halite precipitated at 100°C, showing that it should be possible to distinguish between seawater evaporated at the surface and the dehydration of seawater at higher temperatures in the subsurface (Gleeson, 2003). The data from the coarse dolomite at Lisheen are more consistent with seawater that had been evaporated at the surface.

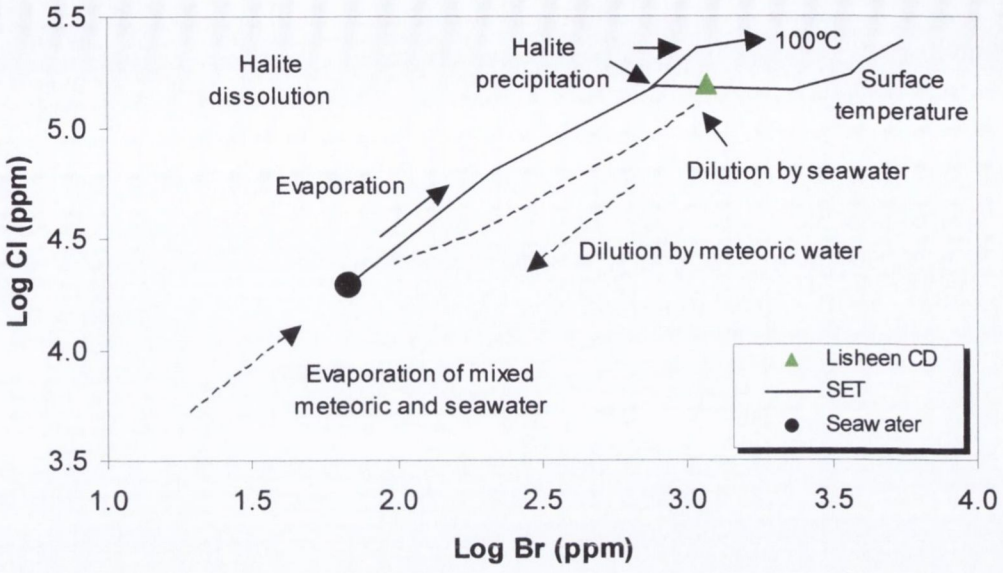

Figure 3.8 Cl and Br systematics of the coarse dolomite at Lisheen. Plot also shows the SET (after Carpenter (1978) and Gleeson & Yardley (2002)).

A plot of the Na-Cl-Br systematics is shown in Figure 3.9. The data from Lisheen lie directly on the SET and have Cl/Br and Na/Br molar ratios (299 and 258 respectively) that are much less than seawater. This is consistent with a seawater-derived fluid evaporated beyond the point of halite precipitation (Cl/Br of 446 and Na/Br of 326 (Fontes & Matray, 1993a)). The data are also consistent with a fluid that was relatively unaffected by exchange reactions involving Na.

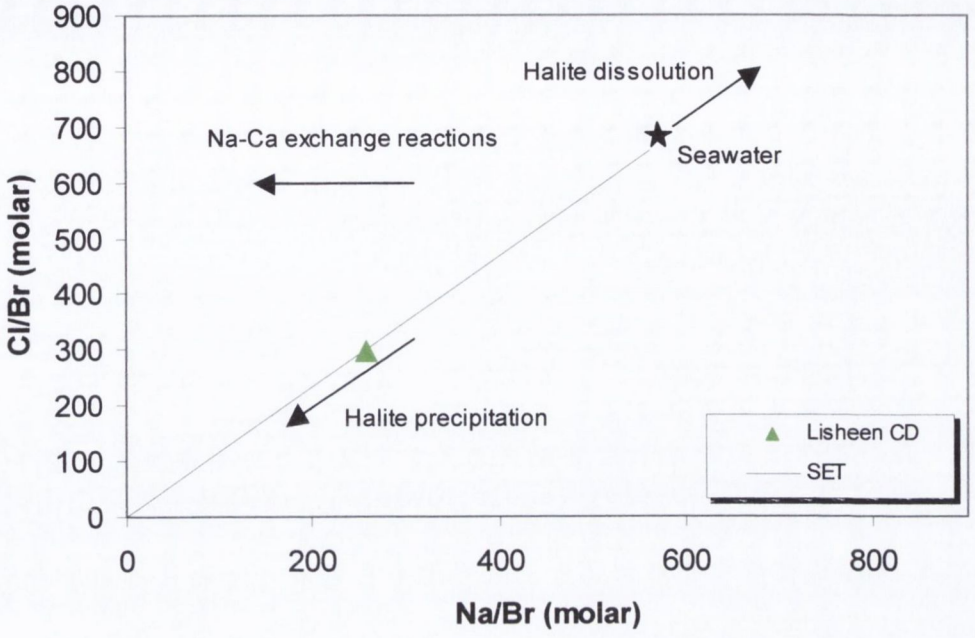

Figure 3.9 Cl-Na-Br systematics for the coarse dolomite from Lisheen. SET after Kesler *et al.* (1995)

Discussion

The halogen data indicate that the fluid that precipitated the coarse-dolomite at Lisheen was residual brine, formed by seawater evaporation past the point of halite precipitation. In relation to the fluids involved in the formation of the Irish base-metal deposits this fluid may be considered as being similar to Fluid 2, the moderately hot, high salinity fluid (see Chapter 1), although the Th data in this study indicate higher temperatures than normally associated with Fluid 2. The data also show that the dolomitising fluid was relatively unaffected by exchange reactions involving Na.

3.10 CONCLUSIONS

- Final porosity occlusion within the Waulsortian Limestone at Lisheen occurred prior to the onset of dolomitisation.

- Fine-grained grey dolomite occurred during the initial stages of dolomitisation and commonly selectively replaced the micrite and bryozoan material. Replacement by this dolomite was generally mimetic. XRD analysis of this dolomite confirms that it is near stoichiometric and well ordered.

- Texturally later coarse-grained white dolomite has a similar luminescence to the fine-grained dolomite and is both a replacive and open space-filling dolomite. Replacement by this dolomite is non-mimetic, with the dolomite crystals being orders of magnitude greater then the precursor calcite phase.

- A third dolomite type occurs at Lisheen, which has been termed 'black tops' dolomite. It occurs as laterally discontinuous, thin layers, which have a consistent polarity relative to the fine-grained and coarse-grained dolomites. Petrographic evidence suggests that it may be a geopetal dolomite.

- Stable isotope data from both the undolomitised and dolomitised Waulsortian Limestone at Lisheen are similar to those obtained by other workers. There is little discernable change in the $\delta^{13}C$ values between undolomitised and dolomitised samples. In contrast the $\delta^{18}O$ values show an average shift of approximately -3‰. Micrite values suggest that a fluid with a $\delta^{18}O$ composition of approximately –1.65‰ was in equilibrium with the limestones during their formation at 25°C. This fluid, or one with a similar composition, probably equilibrated with the limestone as the temperature increased during dolomitisation, causing the shift to lighter $\delta^{18}O$ values.

- Fluid inclusion data from both the coarse-grained white dolomite and the Stage D calcite indicate high temperatures of formation of both (>170°C). However, in contrast to the coarse dolomite data, the Stage D calcite values are is thought to be the product of re-equilibration.

- The coarse-grained dolomite may have attained its high temperatures either by 'deep' burial or by the input of some later hydrothermal fluid. As many of the coarse-grained dolomite crystals have curved faces and exhibit the sweeping extinction indicative of saddle dolomite, a burial origin is inferred. However, a hydrothermal origin cannot be ruled out. Salinity data for the dolomite indicate that very saline fluids were involved in the precipitation of this phase (25.6 combined wt% NaCl and $CaCl_2$ equivalent).

- The range in $\delta^{18}O$ values of the parental fluids (9.3 to 13.5‰) suggests that the fluid had undergone significant amounts of fluid-rock interaction prior to precipitation of the dolomite.

- Halogen geochemistry data indicate that the dolomitising fluids originated as residual brine. In terms of the fluids associated with the Irish Zn-Pb deposits, the fluids within the coarse dolomite fluid inclusions at Lisheen are most similar to Fluid 2.

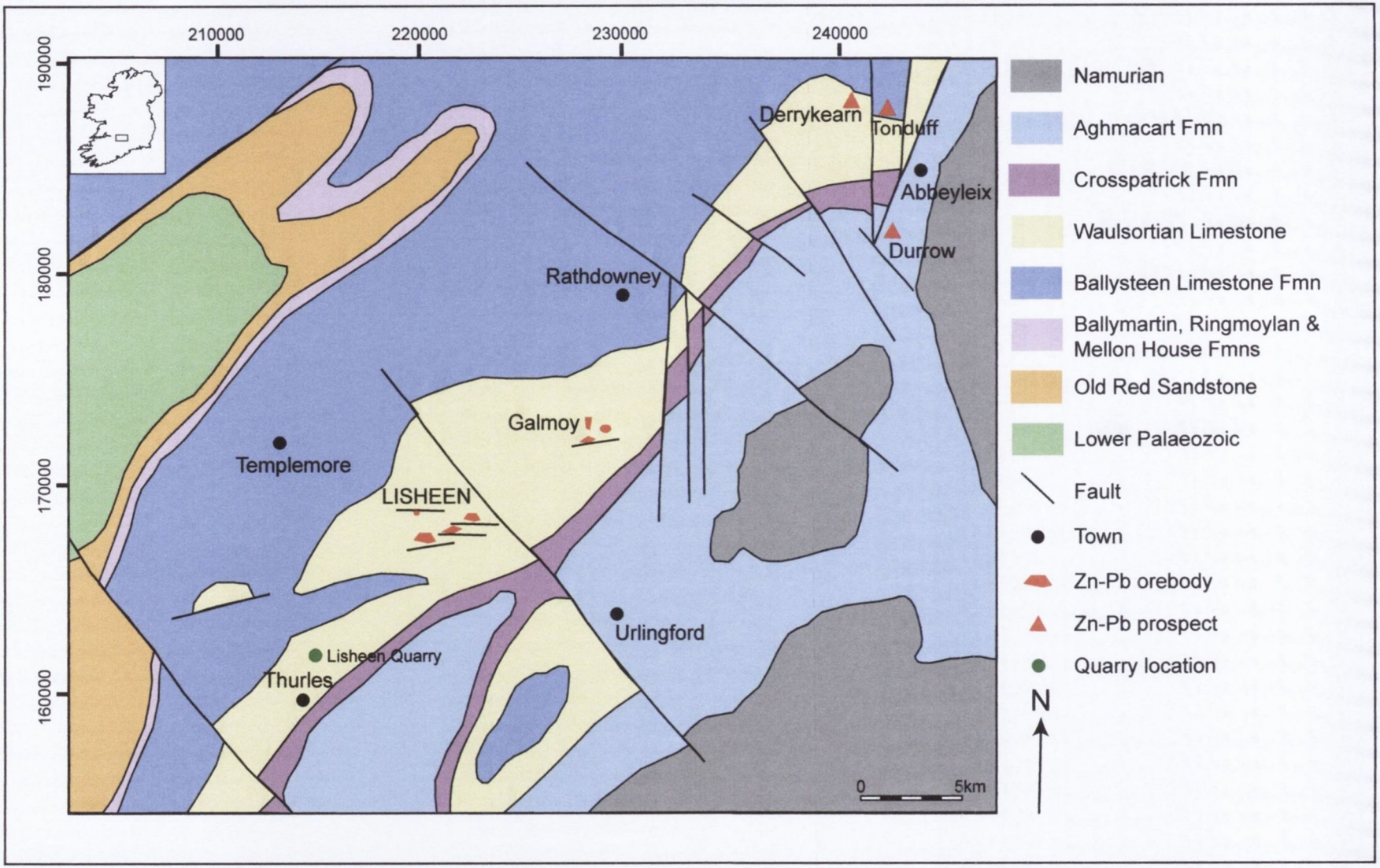

Figure 3.1 Geological map of the Rathdowney Trend showing the location of the Lisheen Zn-Pb deposit (modified after Redmond 1997).

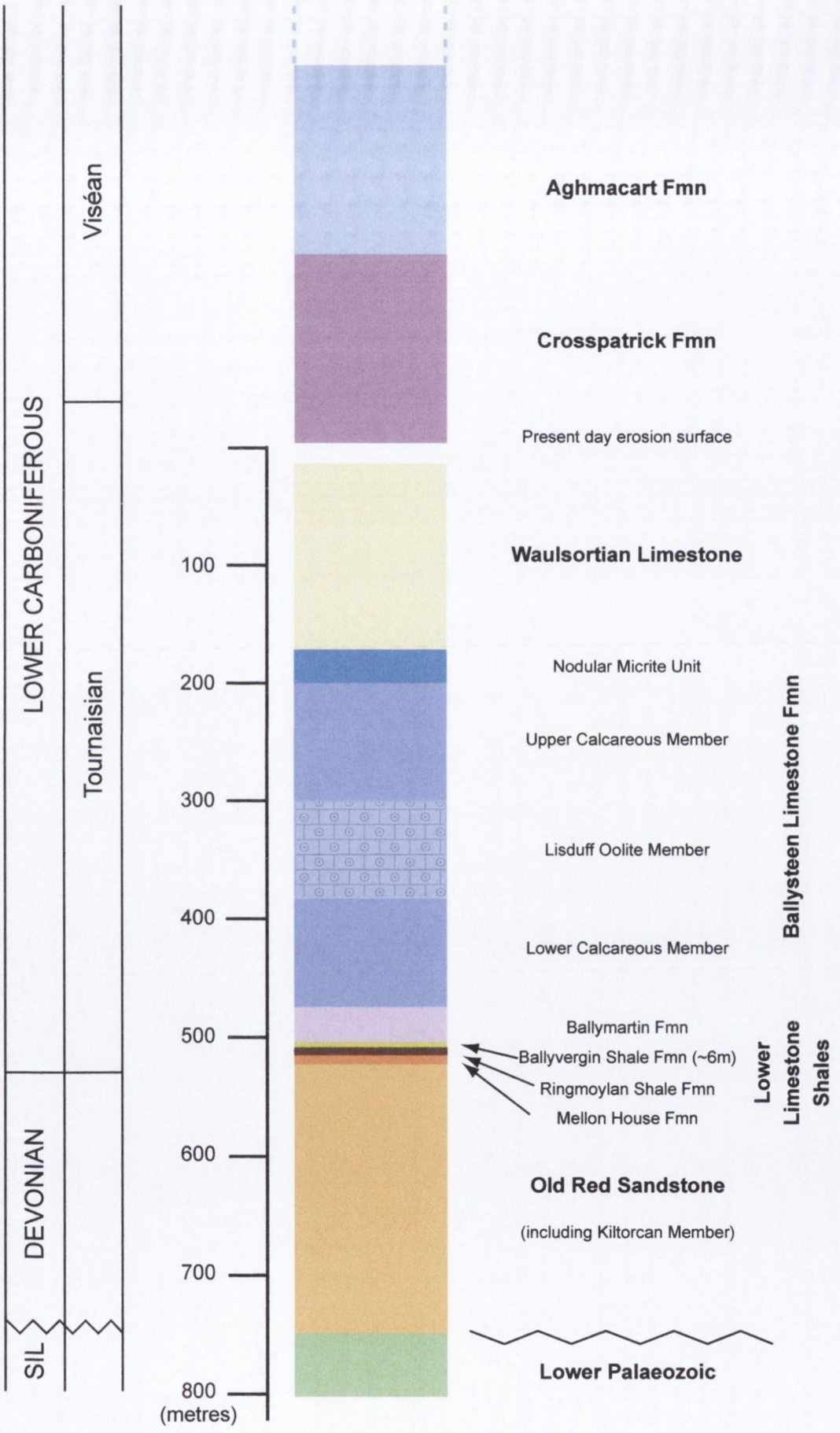

Figure 3.2 Stratigraphic section of the Lisheen mine area based on the LK 318 drillhole and data from Redmond (1997).

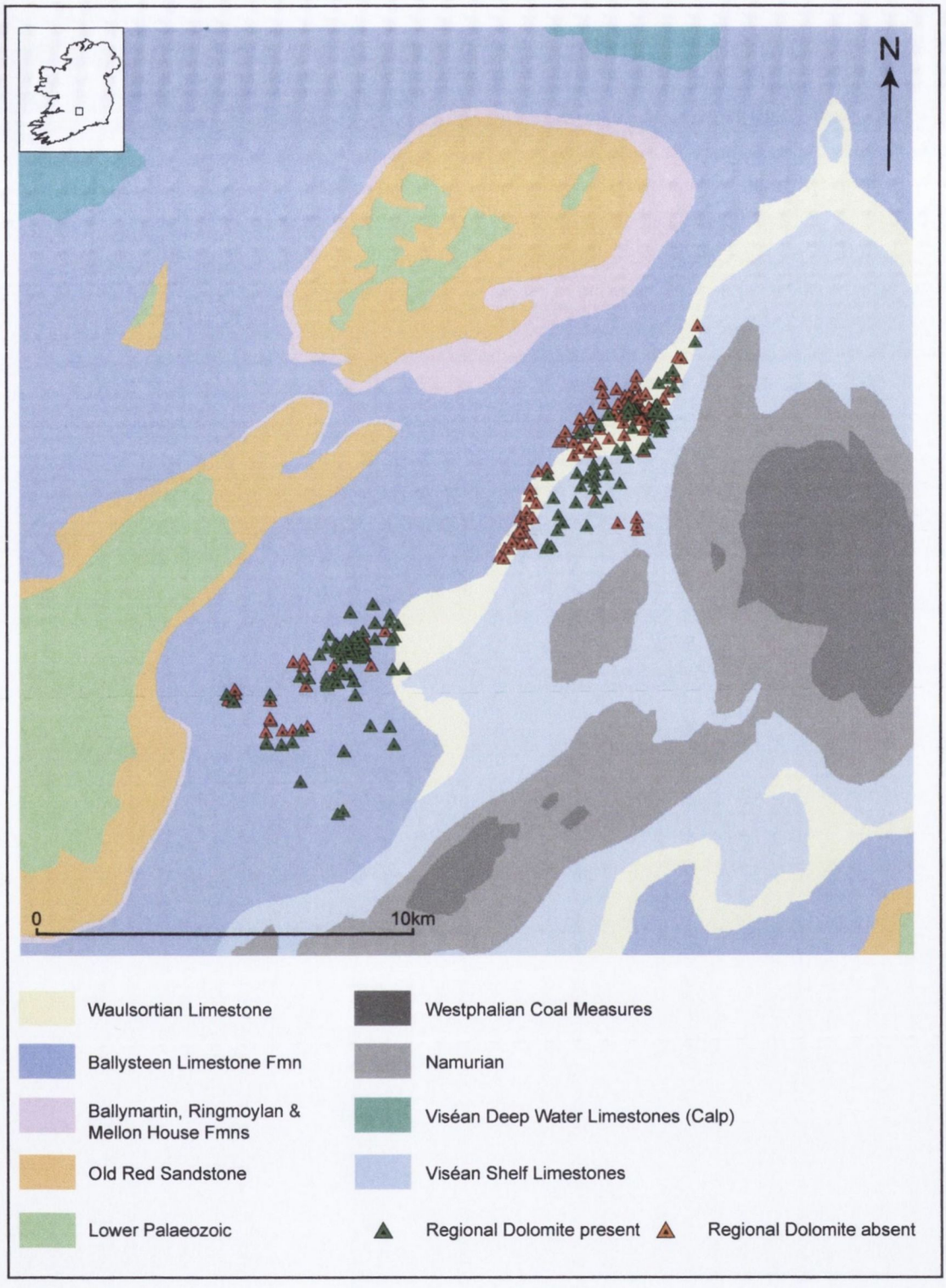

Figure 3.3 Geological map of the Rathdowney Trend and distribution of 'Regional Dolomite' based on all boreholes drilled by Anglo American plc to date (except 26 holes drilled within the mine lease, which for confidentiality reasons cannot be included). Data supplied by K. Henderson and C. Chapman (2003).



Plate 3.1: Stained, partially dolomitised core sample containing an orthoconic nautiloid from LK 2258-38 (183.65-184m). Fine-grained dolomite (FGD) and coarse-grained (CD) dolomite are labelled. Top to the left. Scale bar is 2cm.



Plate 3.2: Stained, partially dolomitised sample from LK 2258-38 (121.2-122.53m) containing selectively dolomitised micrite, bryozoans and coarse-grained dolomite. CFC not replaced. Top to the left. Scale bar is 2cm.

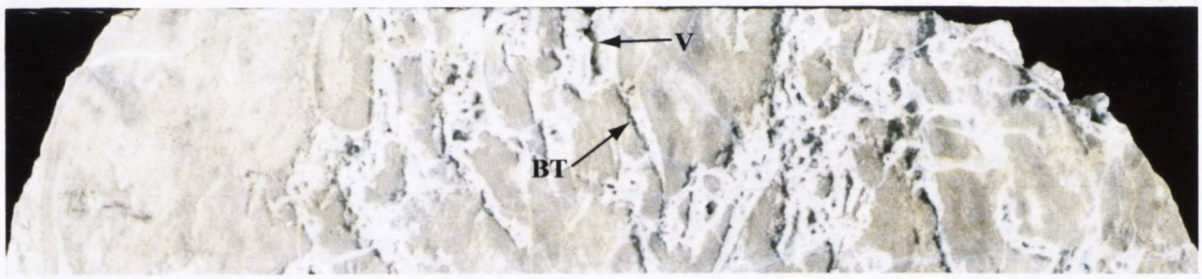

Plate 3.3: Sample of drillcore from LK 555-30 showing the third component of the Regional Dolomite: the black tops (BT). Note the consistent polarity of the black tops, above the fine-grained grey replacive dolomite and below the coarse-grained white open space filling dolomite. A vug into which the coarse-grained white dolomite is growing is also indicated (V). Length of core is 20cm. Top to the right.

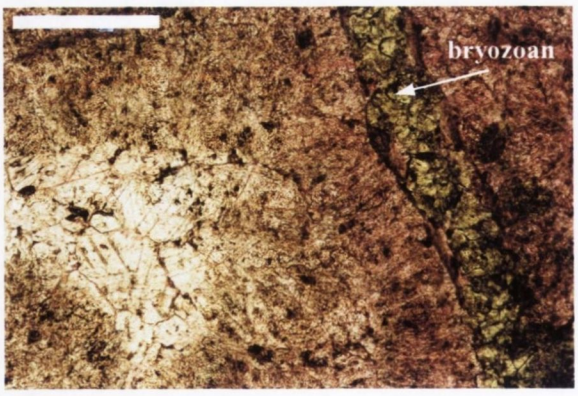

Plate 3.4a: P17500 - LK 2258-38 (249.6-249.8m). PPL view of a stick bryozoan almost completely replaced by dolomite. The area on the left of the photomicrograph is an early calcite-filled cavity. Scale bar is 500µm.

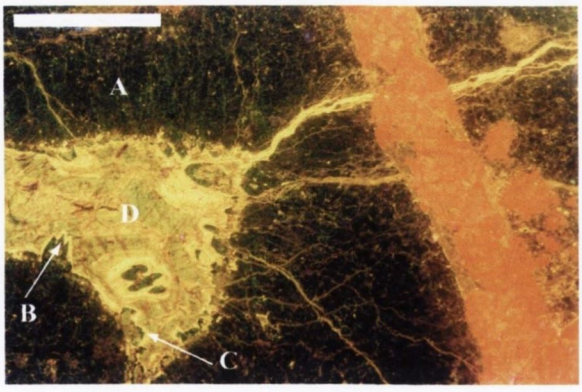

Plate 3.4b: Same view in CL. The early calcite cements (Stages A-D) are labelled. Stage D is the porosity occluding cement. Dolomitisation occurred after precipitation of Stage D and therefore is post porosity occlusion. Scale bar is 500µm.

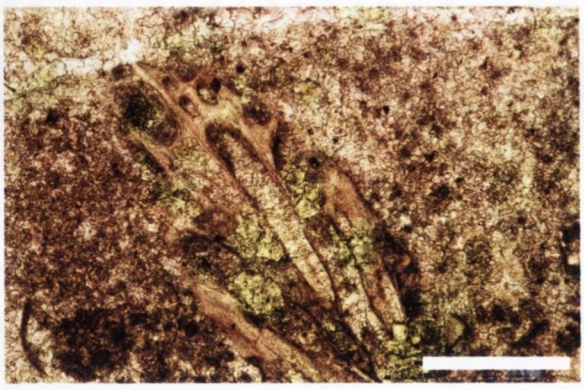

Plate 3.5a: P17500 - LK 2258-38 (249.6-249.8m). PPL view of a fenestrate bryozoan that has been partially dolomitised. Areas within the surrounding micritic matrix have also been dolomitised. Scale bar is 500µm.

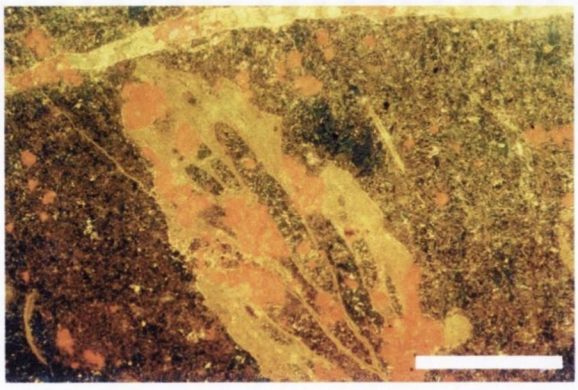

Plate 3.5b: Same view in CL. Note in the upper part of the image a vein filled with the Stage D porosity occluding cement, which can be seen to pre-date the dolomite. Scale bar is 500µm.

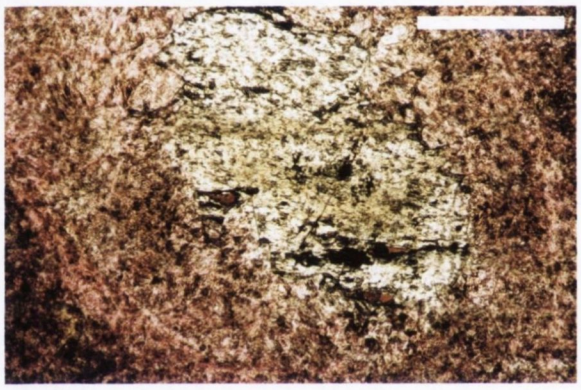

Plate 3.6a: P17500 - LK 2258-38 (249.6-249.8m). PPL view of a brachiopod containing early calcite cements (Stages A-D). The centre of the cavity has been replaced by coarse-grained dolomite. Scale bar is 500µm.

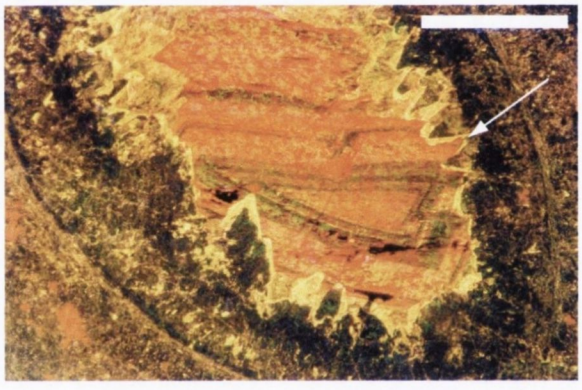

Plate 3.6b: Same view in CL The coarse-grained dolomite is zoned. It has replaced the early calcite cements (arrow). Scale bar is 500µm.

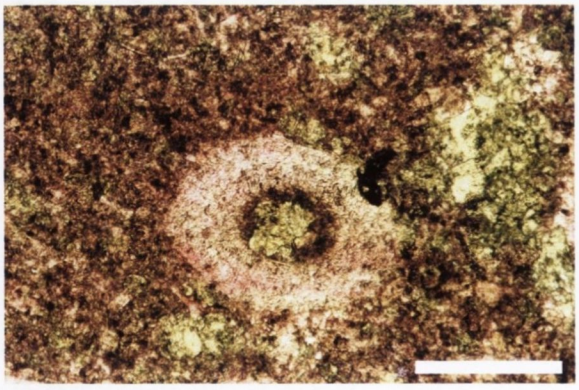

Plate 3.7a: P17500 - LK 2258-38 (249.6-249.8m). PPL view of a crinoid ossicle within a micritic matrix. The surrounding micrite and that within the lumen have been dolomitised but the ossicle itself has not. Scale bar is 500µm.

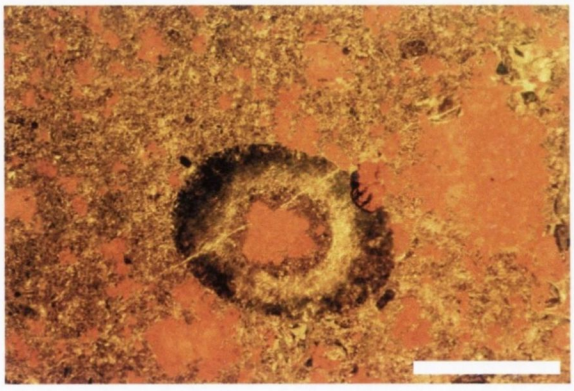

Plate 3.7b: Same view in CL. This suggests that the more robust fossil fragments, such as echinoderms, were amoungst the last components to be replaced by dolomite. Scale bar is 500µm.

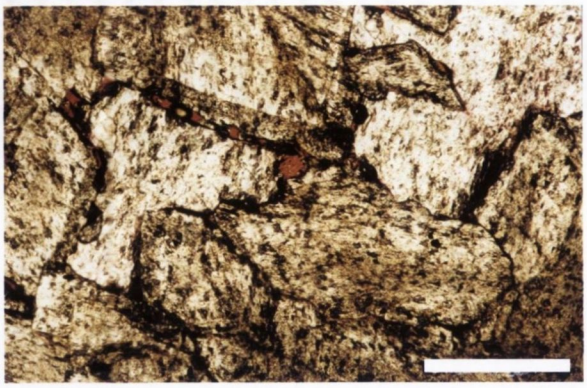

Plate 3.8a: P17502 - LK 2258-38 (121.2-122.53). PPL view of the centre of a large early calcite-filled cavity which, with the exception of some residual calcite that still remains in the centre, has been almost completely replaced by coarse-grained dolomite. Scale bar is 500µm.

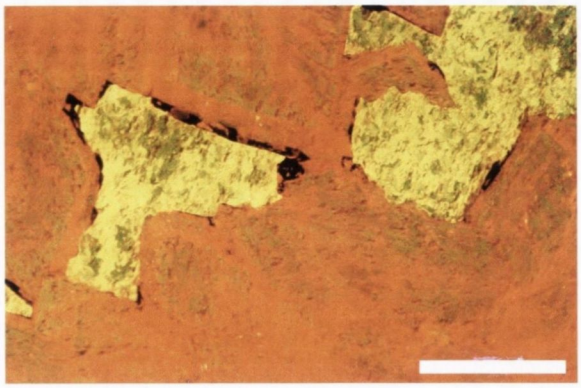

Plate 3.8b: Same view in CL. The coarse-grained dolomite has the same CL signature as the fine-grained dolomite which is seen selectively replacing the micrite and bryozoans. The coarse-grained dolomite is a baroque dolomite. Scale bar is 500µm.

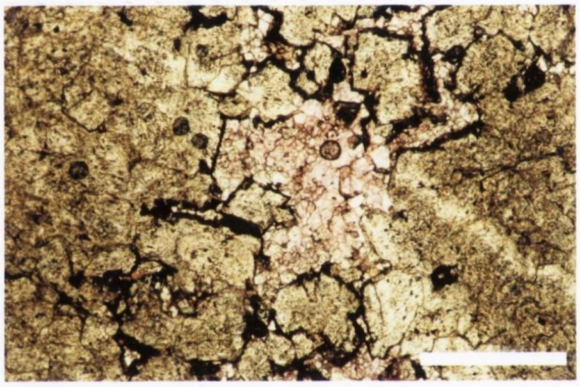

Plate 3.9a: P17505 - LK 2258-38 (112.44-112.75m). PPL view of the non-mimetic replacement of sparry calcite by the coarse-grained dolomite. Scale bar is 500µm.

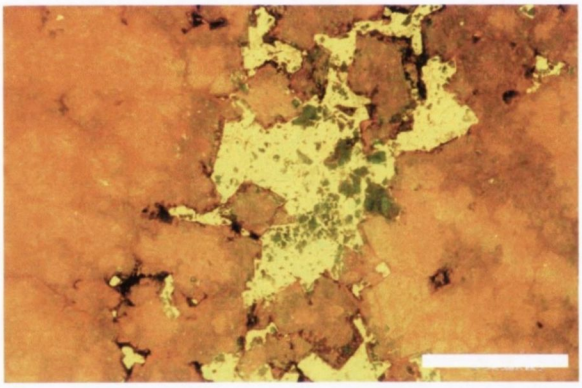

Plate 3.9a: Same view in CL. The dolomite rhombs are an order of magnitude larger than the calcite they are replacing. Scale bar is 500µm.

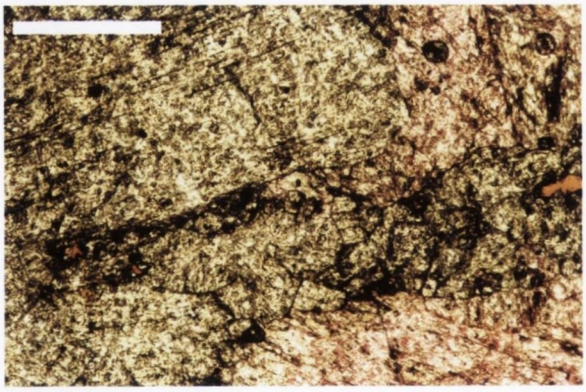

Plate 3.10a: P17504 - LK 2258-38 (112.44-112.75m). PPL view of the coarse-grained dolomite replacing blocky early calcite cement. Scale bar is 500µm.

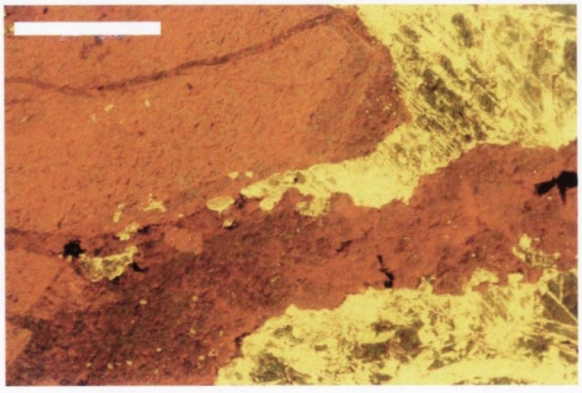

Plate 3.10b: Same view in CL. A second type of coarse-dolomite is visible. It differs from the normal coarse-dolomite in that it has a characteristic blood red colour in CL. Scale bar is 500µm.

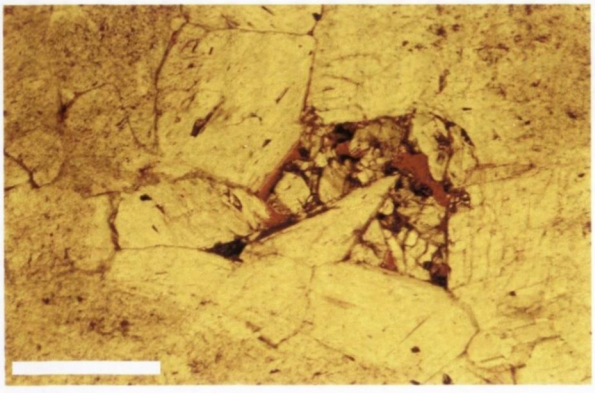

Plate 3.11a: LK 563 (30m). PPL view of coarse-grained white dolomite growing into open space. The red material in the centre is epoxy resin. Scale bar is 500μm.

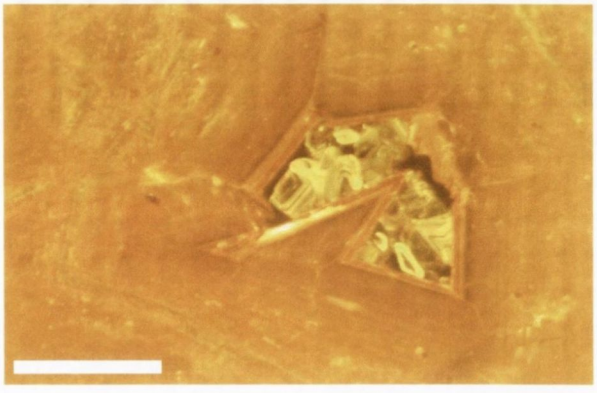

Plate 3.11b: Same view in CL. The brightly luminescent crystals in the centre are calcite. Note the most recent phase of dolomite growth, indicated by the outermost zone growing in towards the cavity. Scale bar is 500μm.



Plate 3.12: LK 563 (30m). SEM image of the black tops dolomite showing large amount of porosity (black) along intergrain boundaries. Scale bar is 30μm.

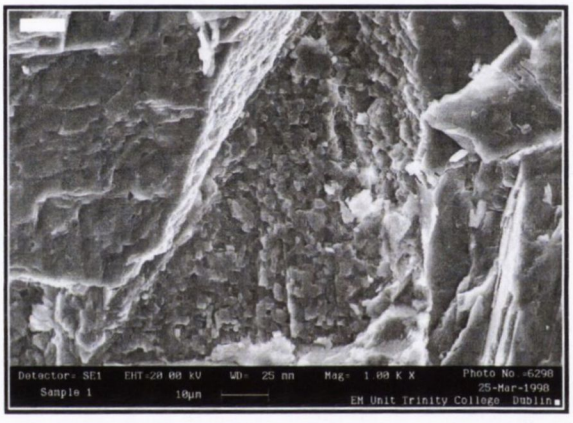

Plate 3.13: SEM image of an individual crystal within the black tops. Not the presence of holes within the crystal itself. Scale bar is 10μm.

CHAPTER 4

URLINGFORD

4.1 INTRODUCTION

The town of Urlingford is located east of the Rathdowney Trend, approximately 10 kilometres north-northeast of Thurles and 20 kilometres southeast of Templemore (Figure 4.1). A borehole (3246-15) drilled by Tara Prospecting Ltd. immediately south of Urlingford was selected for detailed study, as it contained a good intersection of regionally dolomitised Waulsortian Limestone and therefore provided an ideal opportunity to study the Regional Dolomite outside of the mineralised Rathdowney Trend.

4.2 REGIONAL GEOLOGICAL SETTING

4.2.1 Stratigraphy

The stratigraphy of the area surrounding Urlingford is identical to that at Lisheen (Chapter 3) and therefore will not be repeated here.

4.2.2 Structure

Similarly, the structure of the area surrounding Urlingford is identical to the description provided in the discussion on Lisheen (Chapter 3) and will not be replicated here.

4.3 PETROGRAPHY

Hand samples

The Regional Dolomite at Urlingford (Plate 4.1) is identical to that found at Lisheen (Plate 3.3). It contains two main components (Hitzman *et al.*, 1992): the buff to pale grey, fine-grained replacive dolomite; and the texturally later white, coarse-grained open space-filling dolomite. In addition, it contains the third component of the Regional Dolomite that was also observed at Lisheen, the 'black tops' dolomite (Plate 4.1). As at Lisheen, the 'black tops' dolomite at Urlingford occurs in thin, laterally discontinuous layers (a few millimetres thick at most), which always lie above grey replacive dolomite and below coarse white dolomite.

Thin sections

The fine-grained, grey, replacive dolomite is formed in many cases of euhedral or more rarely, of subhedral, non-planar, crystals that average 100μm to 500μm in maximum dimension. Their grain size distribution is generally unimodal (Plate 4.2a). Under CL, the grey replacive dolomite has a dull, homogeneous luminescence (Plate 4.2b). The white

coarse-grained, open space-filling dolomite has a polymodal crystal size distribution with the euhedral to subhedral grains commonly up to 5mm in size (Plate 4.3a). Many of the crystals have curved faces and exhibit the sweeping extinction indicative of saddle dolomite (Radke & Mathis, 1980). Several have highly turbid cores and become increasingly more limpid towards the outer parts of the crystal (Plate 4.3a). Under CL, the coarse-grained white dolomite displays a moderate to bright luminescence and is usually poorly zoned (Plate 4.3b), or not zoned.

The 'black tops' dolomite is a very fine-grained dolomite that has an average grain size of approximately 50μm (Plates 4.4a and 4.5a). It has a dull, homogenous luminescence that is almost identical to that of the fine-grained replacive dolomite (Plate 4.4b). It is readily distinguished from the poorly zoned, coarse-grained, white dolomite (Plate 4.5b). With regard to the origin of the 'black tops' dolomite, a similar hypothesis is invoked here as was suggested at Lisheen (Chapter 3, Section 3.3): it probably represents geopetal dolomite sediment accumulated on the floor of cavities prior to the cavities being filled with the coarse-grained, white dolomite cement.

4.4 PARAGENESIS

The paragenetic sequence at Urlingford is illustrated in Figure 4.2. As only pervasively dolomitised samples were available for study, no early calcite cements were observed in the samples from Urlingford. Therefore the paragenetic sequence at Lisheen (Chapter 3, Section 3.4), which is assumed to be similar, was used to infer the existence and order of precipitation of the pre-dolomite early calcite cements (Stages A-D). In accordance with this, it is assumed that dolomitisation occurred after final porosity occlusion of the host limestone. The fine-grained component of the Regional Dolomite occurred during the initial stages of dolomitisation, followed by the coarse-grained, white dolomite component. There was probably some overlap between these two components. Where present the 'black tops' dolomite, if it is geopetal dolomite, must have formed prior to the coarse-grained dolomite.

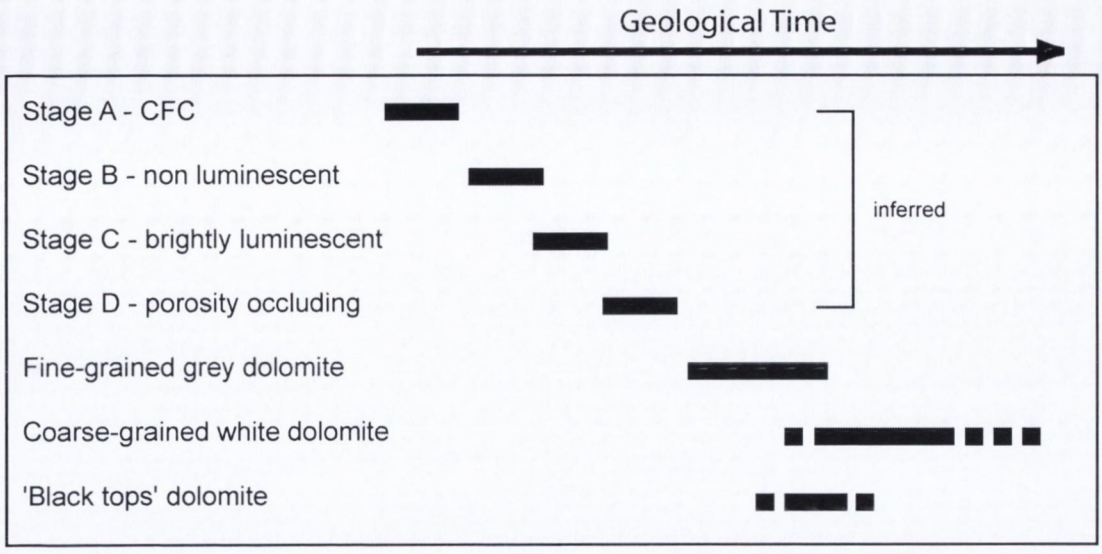

Figure 4.2 Paragenesis of the Waulsortian Limestone at Urlingford. Early calcite cement data is based on information from Lisheen (this study).

4.5 FLUID INCLUSION MICROTHERMOMETRY

Only one phase was isolated for fluid inclusion microthermometry analysis: the coarse-grained white dolomite (Appendix C). The samples came from borehole 3246-15 from a depth of 136.68–136.74m. A detailed petrographic study of the fluid inclusion assemblage was completed prior to undertaking the microthermometry.

Dolomite fluid inclusion petrography

The coarse-grained dolomite contained a large number of fluid inclusions but the majority were less then one micron in diameter and were therefore too small to be useful for obtaining microthermometric data. However, many of the dolomite crystals contained highly turbid cores with visibility towards the outer parts of the crystal increasing such that inclusions could be observed. Workable inclusions, albeit a small number, were located and mapped along both the border between the turbid and limpid parts of the dolomite crystals, as well as within the outer limpid parts of the crystals. These inclusions were all two-phase (L+V) inclusions that ranged in size from less than a micron to approximately 6μm with degrees of fill (ψ_{liquid}) of 0.9. They were mostly subhedral to anhedral (irregular) in shape and formed zones parallel to the dolomite crystal faces, which were commonly coincident with the CL growth zones. Many of the larger inclusions also lay parallel to the trails of sub-micron sized inclusions. In addition to those inclusions that were classified as primary after detailed mapping, several intragranular (Van den Kerkhof & Hein, 2001)

planar arrays of secondary fluid inclusions were observed cutting all of the growth zones within the dolomite crystals. The inclusions contained within these trails were generally minute (1.5μm or less) and commonly proved difficult to observe.

Dolomite fluid inclusion microthermometry

A total of nine fluid inclusions were measured from the coarse-grained dolomite at Urlingford. Of these, six were primary and three were from a trail of secondary fluid inclusions. The primary fluid inclusions had Th values that ranged from 126.2 to 181°C and the secondary fluid inclusions had Th values that ranged from 110 to 110.9°C. The first melting temperatures of the primary fluid inclusions indicate that they were part of the $NaCl\text{-}CaCl_2\text{-}H_2O$ ternary system and Tm_{ice} data indicate a salinity of 20.7 wt% NaCl equivalent (calculated using the equation of Bodnar (1993) as with a Tm_{ice} of –17.6 the numerical algorithm developed by Naden (1996) was not valid). No salinity data were obtained from the secondary fluid inclusions.

Discussion

The fluid that precipitated the coarse-grained white dolomite was moderately hot (126.2 to 181°C) and saline (20.7 wt% NaCl equivalent). The trail of secondary inclusions within the coarse-grained, white dolomite was formed from a slightly lower temperature (~110°C) fluid than the one from which the dolomite precipitated. This fluid may or may not be related to the fluid from which the dolomite precipitated but as no salinity data were obtained for these secondary inclusions, it is difficult to make any inferences.

4.6 STABLE ISOTOPE GEOCHEMISTRY

Twenty-one samples of dolomitised Waulsortian Limestone from Urlingford were sampled for stable isotope analysis. As all the samples from Urlingford were pervasively dolomitised, no early calcite cements were available for sampling. A full description of the sampling methods is given in Chapter 2.

4.6.1 Dolomite

The isotopic data from the fine-grained, coarse-grained and 'black tops' dolomite are plotted in Figure 4.3. The $\delta^{13}C$ values for the three dolomite types range from 3.22 to 4.2‰

(mean 3.8‰ ± 0.58‰ 2σ), 2.36 to 3.92‰ (mean 3.21‰ ± 1.18‰ 2σ) and 3.46 to 3.57‰ (mean 3.52‰ ± 0.16‰ 2σ) respectively.

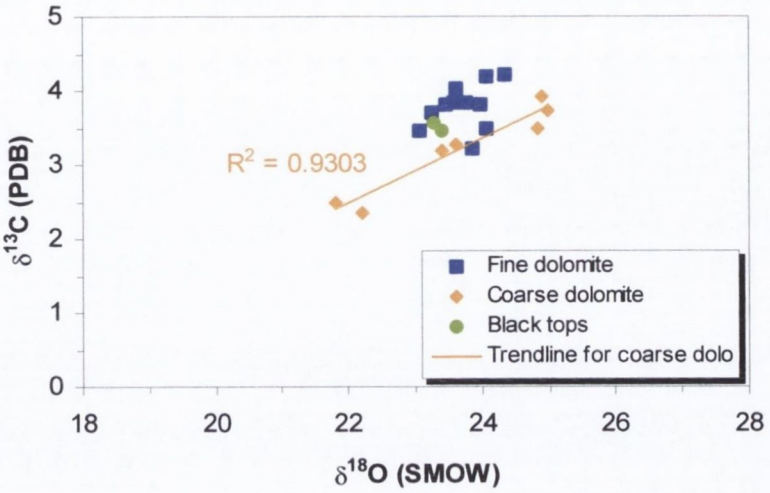

Figure 4.3 Scatter plot of $\delta^{13}C$ and $\delta^{18}O$ values for the dolomites at Urlingford and trendline for $\delta^{13}C$ vs. $\delta^{18}O$ for coarse dolomite.

The $\delta^{18}O$ values for the fine-grained dolomite range from 23.07 to 24.34‰ (mean 23.71‰ ± 0.74‰ 2σ). The $\delta^{18}O$ values for the coarse-grained dolomite range from 21.81 to 24.97 (mean 23.67‰ ± 2.6‰ 2σ; mode 24.8‰) and the $\delta^{18}O$ values for the 'black tops' dolomite range from 23.27 to 23.41‰ (mean 23.34‰ ± 0.18‰ 2σ).

Discussion

The $\delta^{18}O$ values for the fine-grained dolomite are within the range of values obtained for the fine-grained dolomite at Lisheen (22.58 to 24.96‰ Chapter 3, Section 3.7.2) and other areas of Regional Dolomite throughout the Irish Midlands included in the study by Hitzman *et al.* (1998), which also incorporated samples from Urlingford. Similarly the $\delta^{18}O$ values for the coarse-grained dolomite, which are slightly heavier than the range of values obtained for the coarse-grained dolomite at Lisheen (20.45 to 23.64‰ Chapter 3, Section 3.7.2), remain within the range of values obtained by Hitzman *et al.* (1998) for Urlingford and other areas of Regional Dolomite. The $\delta^{18}O$ data from the 'black tops' dolomite is similar to that of both the fine-grained and coarse-grained dolomites, and therefore may have been precipitated by the same (or a similar) fluid.

There is a linear relationship between the $\delta^{13}C$ and $\delta^{18}O$ values of the coarse-grained dolomite (Figure 4.3). This linear relationship may be a mixing line in which the two components are the limestone or fine-grained dolomite (heavy $\delta^{13}C$ and $\delta^{18}O$ values) and a second fluid (see below).

4.7 MODELLING OF PARENTAL FLUIDS

Using the average of the measured $\delta^{18}O$ values for the coarse-grained dolomite (23.67‰) the mineral-water oxygen isotope fractionation curve was constructed using the equation of Land (1983) and is shown in Figure 4.4. The parental fluid composition was calculated using the homogenisation temperature range (rounded to 125-180°C). This indicated water isotopic values ranging from 6.6 to 11.2‰. This suggests that the fluid that precipitated the coarse-grained dolomite had undergone a significant amount of fluid-rock interaction.

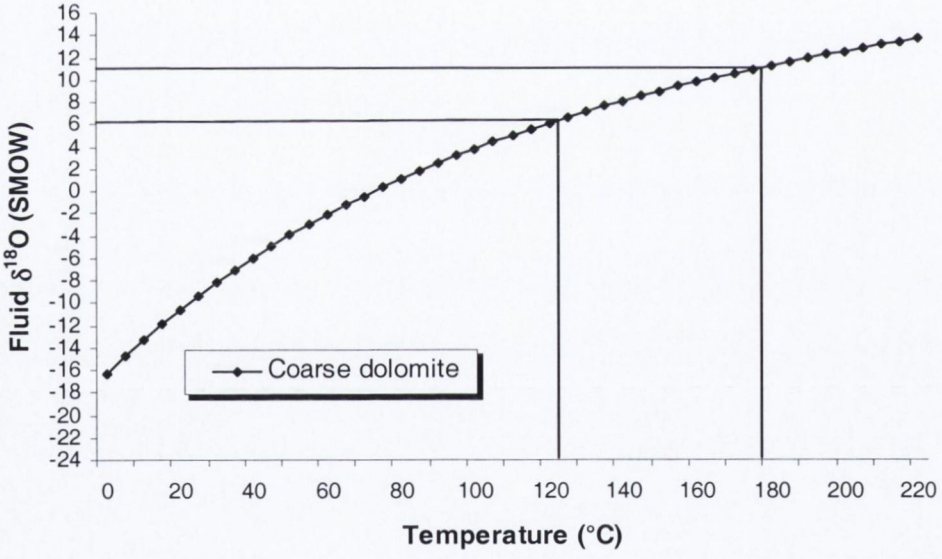

Figure 4.4 Mineral-water oxygen isotope fractionation curve for the coarse dolomite at Urlingford. See text for discussion.

However, as mentioned above, the linear relationship between the $\delta^{13}C$ and $\delta^{18}O$ values of the coarse-grained dolomite may represent a mixing line. If it is assumed that the isotopically lightest coarse dolomite $\delta^{18}O$ value (21.81‰) was precipitated from the second fluid at the highest temperature indicated by the fluid inclusions (180°C), the $\delta^{18}O$

of this fluid can be calculated as being 9.4‰ (Figure 4.5). This provides a limit of the $\delta^{18}O$ value for this second fluid, within the data analysed and assuming that this second fluid represents an uncontaminated end member.

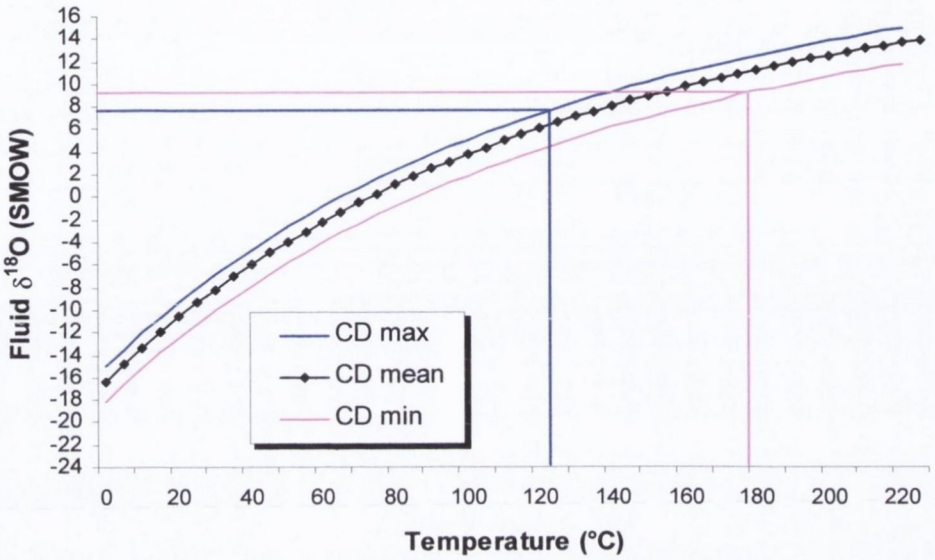

Figure 4.5 Mineral-water oxygen isotope fractionation curves for the minimum, maximum and mean $\delta^{18}O$ values measured for the coarse dolomite at Urlingford. See text for discussion.

4.8 HALOGEN GEOCHEMISTRY

A sample of coarse dolomite from borehole 3246-15 (154m) was prepared for crush-leach analysis using the method outlined in Chapter 2. The data are shown in Appendix D.

Figure 4.6 shows the calculated Cl and Br composition of the fluid within the coarse dolomite fluid inclusions at Urlingford. The sample plots, within analytical uncertainty, on the SET and indicates that the fluid trapped in these inclusions is consistent with having originated as seawater that was evaporated at the surface but not to the point of halite precipitation.

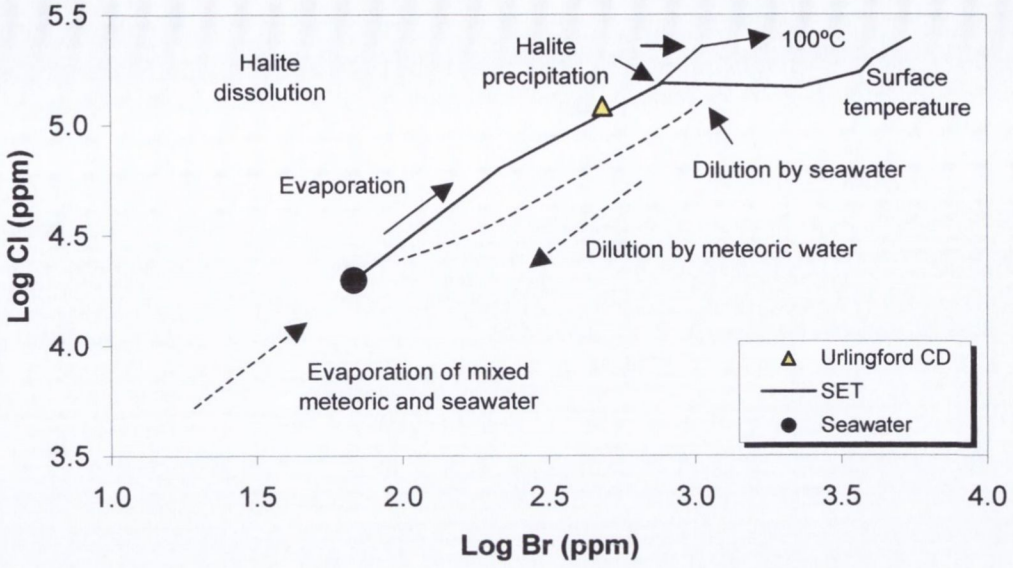

Figure 4.6 Cl and Br systematics of the coarse dolomite at Urlingford. Plot also shows the SET (after Carpenter (1978) and Gleeson & Yardley (2002)).

A plot of the Na-Cl-Br systematics is shown in Figure 4.7. The coarse dolomite data from Urlingford has a Cl/Br ratio of 583 and a Na/Br ratio of 626, which although is less than seawater, is not beyond the point of halite precipitation (Cl/Br of 446 and Na/Br of 326 (Fontes & Matray, 1993a)). The positioning of the data to the right of the SET suggests that the fluid is enriched in Na relative to seawater.

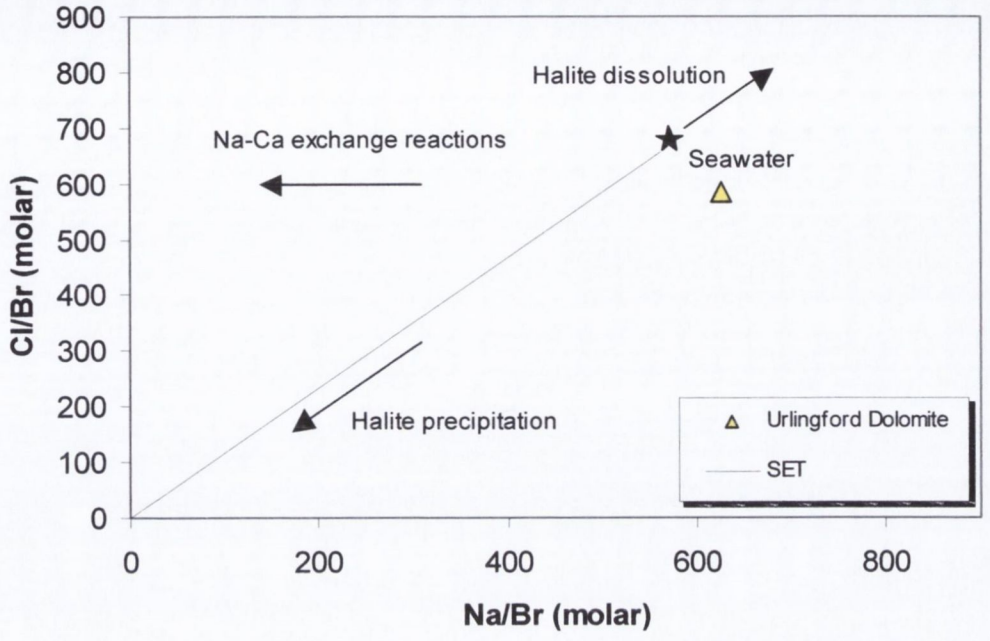

Figure 4.7 Cl-Na-Br systematics for the coarse dolomite from Urlingford. SET data after Kesler *et al.* (1995).

Discussion

The halogen data indicate that the fluid that precipitated the coarse dolomite at Urlingford originated as seawater, which was evaporated at the surface but not to the point of halite precipitation. In relation to the fluids involved in the formation of the Irish base-metal deposits, this fluid may be considered as being similar to Fluid 1, the high temperature, ore-bearing fluid (see Chapter 1). However, the Th data in this study indicate slightly lower temperatures than normally associated with Fluid 1. This fluid appears to be enriched in Na relative to seawater and may suggest that there has been some fluid rock interaction along the fluid flow pathway.

A note on the secondary inclusions in the coarse-grained dolomite

As crush leach ion chromatography provides the average fluid composition, the samples chosen for analyses must be dominated by one population of fluid inclusions only (Gleeson, 2003). During the petrographic examination of the coarse-grained dolomite there was evidence for the existence of secondary fluid inclusions. As no salinity data were obtained from these inclusions the influence they have had on the bulk electrolyte analysis cannot be quantified. The halogen data must therefore be interpreted with caution.

4.9 CONCLUSIONS

- The dolomite at Urlingford is petrographically and isotopically identical to the Regional Dolomite at Lisheen and elsewhere in the Irish Midlands.

- 'Black tops' dolomite, as described at Lisheen, is also present within the pervasively dolomitised samples from Urlingford.

- Fluid inclusion data indicate that the coarse-grained dolomite was precipitated from a moderately hot (126.2 to 181°C), high salinity (20.7 wt% NaCl equivalent) brine.

- Stable isotope data of the dolomite at Urlingford is similar to that obtained from Lisheen and is consistent with the data obtained by other workers.

- However, the modelled parental fluid data from Lisheen (9.3 to 13.5‰) suggest that the fluid that precipitated the coarse-grained dolomite underwent more fluid rock interaction than the one that precipitated the coarse dolomite at Urlingford (6.6 to 11.2‰).

- Halogen data indicate that the fluid that precipitated the coarse-grained dolomite at Urlingford was evaporated seawater that had not reached the point of halite precipitation. In terms of the fluids involved in the formation of the base-metal deposits, this fluid is most similar to Fluid 1, the high temperature, ore-bearing fluid.

- Therefore different fluids were involved in the precipitation of the coarse-grained dolomite at both Lisheen and Urlingford.

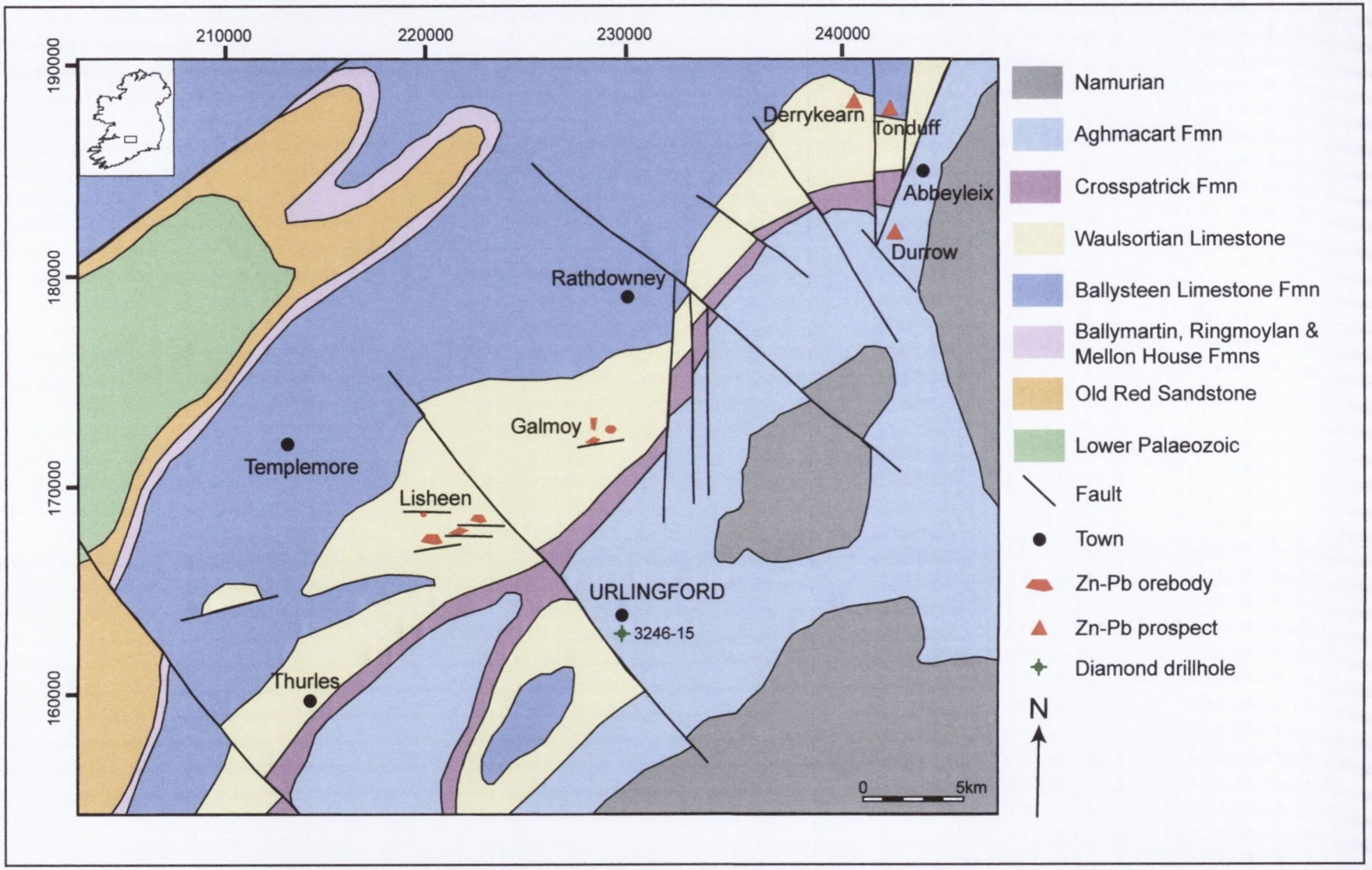

Figure 4.1 Geological map of the Rathdowney Trend showing the location of Urlingford (modified after Redmond 1997).

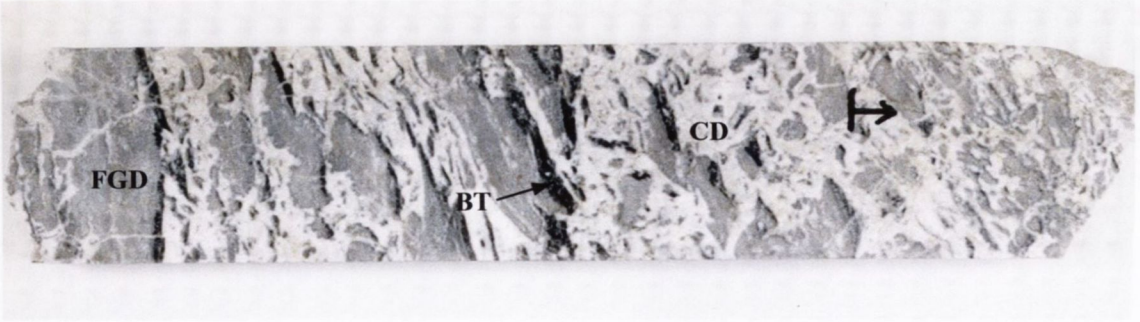

Plate 4.1: Sample of drillcore from 3246-15 (136.5 - 136.74m) showing the Regional Dolomite at Urlingford. The three components, the fine-grained grey dolomite (FGD), the coarse-grained white dolomite (CD) and the black tops (BT) are labelled. Note the consistent polarity of the black tops, above the fine-grained grey replacive dolomite and below the coarse-grained white open space filling dolomite. Length of core is 24cm. Top to the right.

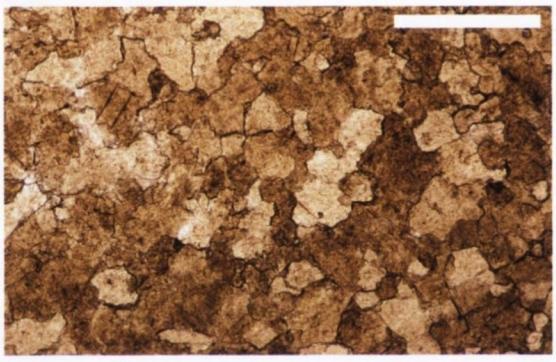

Plate 4.2a: P17556a - 3246-15 (136.55 - 136.58m). PPL view of the unimodal, non-planar, fine-grained grey dolomite at Urlingford. Scale bar is 500µm.

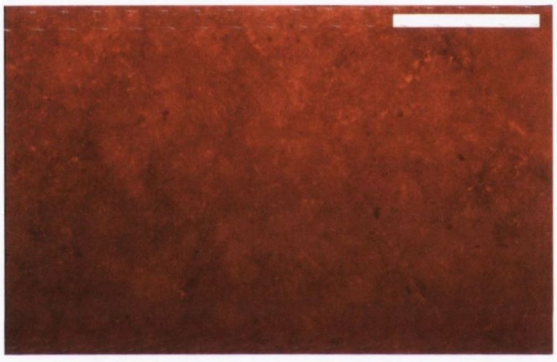

Plate 4.2b: Same view in CL. Note the dull, homogeneous luminescence of the fine-grained grey replacive dolomite. Scale bar is 500µm.

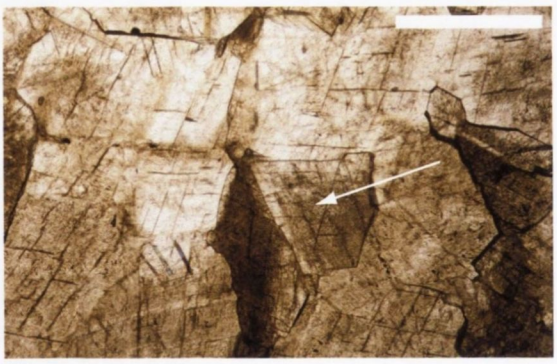

Plate 4.3a: P17557a - 3246-15 (136.58 - 136.62m). PPL view of the coarse-grained white dolomite at Urlingford. Note the turbid cores (arrow) and limpid outer parts of the crystals. Scale bar is 500µm.

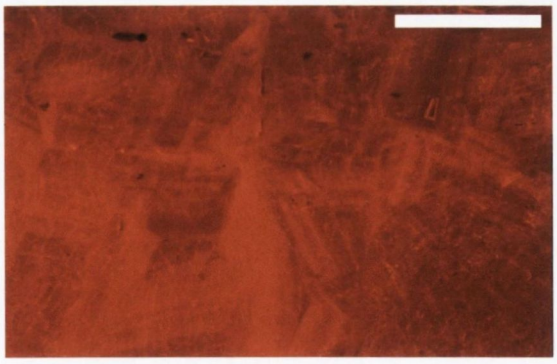

Plate 4.3b: Same view in CL. Note the moderate to bright luminescence of the poorly zoned coarse-grained white dolomite. Scale bar is 500µm.

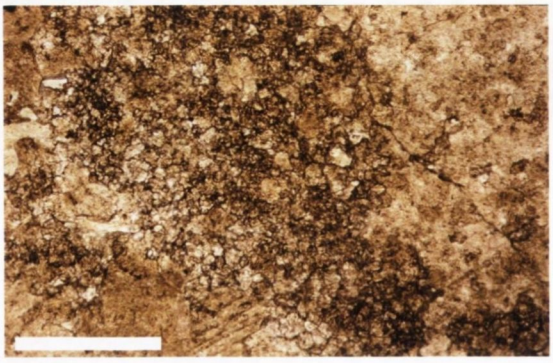

Plate 4.4a: P17636 - 3246-15 (144.7m). PPL view of the black tops dolomite and the fine-grained grey replacive dolomite. Scale bar is 500µm.

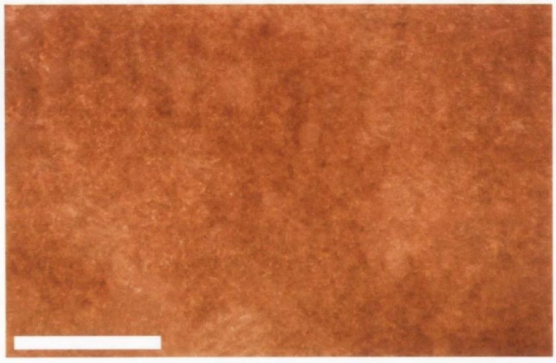

Plate 4.4b: Same view in CL. Note that the black tops dolomite has an almost identical dull, homogeneous luminescence as the fine-grained grey replacive dolomite. Scale bar is 500µm.

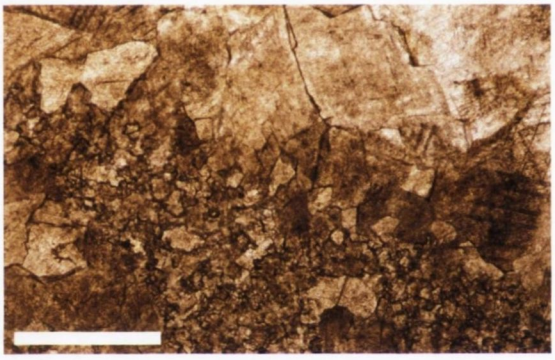

Plate 4.5a: P7556a - 3246-15 (136.58 - 136.62m). PPL view of the black tops dolomite and the coarse-grained white dolomite. Scale bar is 500µm.

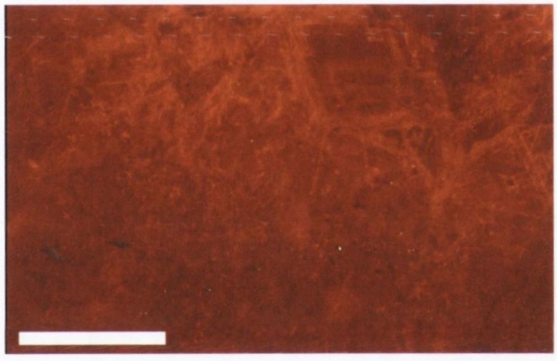

Plate 4.5b: Same view in CL. Note that the poorly zoned coarse-grained white dolomite is readily distinguished from the black tops dolomite developed below. Scale bar is 500µm.

CHAPTER 5

NEWCASTLE WEST

5.1 INTRODUCTION

Newcastle West is located approximately 40 kilometres southwest of Limerick city and 80 kilometres west-southwest of the Rathdowney Trend (Figure 5.1). Drilling on the southwestern outskirts of the town encountered dolomitised Waulsortian Limestone below unconsolidated deposits of Quaternary age. The dolomite is identical in hand sample and petrographically to the Regional Dolomite at Lisheen. The majority of the drill cores contained insignificant amounts of dolomite, most of which was fine-grained, but several cores that define a northeast-southwest trending zone contain long sections of pervasively dolomitised Waulsortian Limestone. This isolated body of dolomite provides an ideal locality to study the dolomitisation process on a smaller scale and away from the main mineralised Rathdowney zone. Samples were selected from two boreholes (OW28 and OW24) at Newcastle West for detailed study.

5.2 REGIONAL GEOLOGICAL SETTING

5.2.1 Stratigraphy

Newcastle West lies in the southern part of the Shannon Basin (Figure 5.1), a long lived, northeast trending downwarp, whose axis lay in the Shannon and Fergus estuaries. Rapid subsidence in the axial part of the basin occurred from the Tournaisian to the early Namurian (Sevastopulo & Wyse Jackson, 2001) and up to 1000m of Waulsortian Limestone may have accumulated near the depocentre in late Tournaisian time. Although the northern margin of the basin is clearly identified by thickness and facies changes, the position and tectonic control of the southern boundary is less clear.

The stratigraphy of parts of County Limerick, adjacent to Newcastle West, was first established by Ashby (1939) and Shephard-Thorn (1963) and later refined by Somerville and Jones (1985), Somerville and Strogen (1992) and Somerville *et al.* (1992). A summary and geological map is given by Sleeman and Pracht (1999) (Figure 5.2). The Upper Palaeozoic succession at Newcastle West consists of fluviatile Old Red Sandstone of late Devonian to early Carboniferous age overlain by Tournaisian marine carbonates and marine Viséan limestones and mudstones. The early Carboniferous marine, carbonate-dominated succession can be divided into three parts: firstly the Tournaisian, which records an overall deepening trend beginning with the Lower Limestone Shales, followed by the Ballysteen Limestone Formation and finally culminating in the deposition of the

Waulsortian Limestone (Figure 5.3); secondly the lower to middle Viséan which is poorly known but is probably represented by deep water calcareous mudrocks; and finally the upper Viséan which consists of shallower water carbonates.

5.2.2 Structure

Faults in the region surrounding Newcastle West display a range of trends (Figure 5.2), most conspicuously north-northwest to northeast and east. Faults have not been mapped in the vicinity of Newcastle West but that is probably a consequence of poor exposure. The drilling on the outskirts of the town was confined to Waulsortian Limestone with the exception of OW24, which also intersected the sub-Waulsortian Limestone. Therefore there is no direct evidence of faulting. However, the disposition of dolomitisation in a steep, approximately NE-SW trending zone suggests the presence of a fault.

5.3 PETROGRAPHY

Hand samples

The Waulsortian Limestone at Newcastle West has typical Waulsortian fabrics, comprising dark grey micrite with numerous stromatactis cavities, which contain coarse-grained early calcite cements. In hand sample the transition between undolomitised Waulsortian Limestone and dolomitised Waulsortian commonly appears to be abrupt (Plate 5.1). However, examination in thin section reveals that what appears macroscopically to be undolomitised limestone often contains a significant amount of fine-grained dolomite.

An enigmatic feature of the Waulsortian Limestone at Newcastle West is the occurrence of a large number of quartz crystals (Plate 5.1). They occur almost exclusively in micritic limestone and increase in both size and abundance towards the limestone/dolomite contact. They are mostly euhedral (prisms with pyramidal terminations) and range in size up to a maximum of 5mm in length. Minor amounts of sulphide mineralisation are developed at the base of the Waulsortian Limestone (Plate 5.2). Pyrite is the dominant sulphide, with rare occurrences of sphalerite and galena also.

Thin sections

The early calcite cavity-filling cements (Stages A-D) are well-developed within the Waulsortian Limestone (Plate 5.3). As seen at Lisheen, it is the Stage D cement that is the final porosity occluding cement. In some cases there is a thin, non-luminescent sub-stage developed at the beginning of the Stage D (Plate 5.4). This sub-stage, which using the nomenclature of Gillies (1987) is referred to here as Da, appears to be very localised. A fifth early calcite stage is developed at Newcastle West, which is referred to here as Stage *E* (this is not the Stage E cement described by Lees and Miller (1995)). It is brightly luminescent and is found within veinlets that cross-cut Stage D cements (Plates 5.5a, 5.5b).

As at Lisheen, dolomitisation at Newcastle West occurred after porosity occlusion (Plate 5.6). The fine-grained components (micrite and bryozoans) were the first to be dolomitised (Plate 5.7). Again this replacement was commonly mimetic. The occurrence of small dolomite rhombs along dissolution seams that cross-cut the early calcite cements, implies that at least during the earliest stages of dolomitisation, the magnesium-bearing fluids exploited these structures as conduits (Plates 5.8a, 5.8b). The coarse white dolomite typically infills veins (Plate 5.1) and lines open vugs. It commonly has the curved crystal faces typical of saddle dolomite (Plates 5.9a, 5.9b). The development of the coarse dolomite is usually pervasive with evidence for what it has replaced often absent. This is in contrast to what is found within the partially dolomitised zone at Lisheen where the partial replacement of calcite spar (Stage D) by the coarse-grained white dolomite (Chapter 3, Plate 3.8b) is common. The luminescence signature of both the coarse-grained dolomite and the fine-grained dolomite at Newcastle West is similar. In some cases the coarse-grained dolomite is weakly zoned with slight changes in CL signature between sub-stages corresponding to areas of high turbidity in plane-polarised light (Plates 5.10a, 5.10b).

The authigenic quartz crystals within the micrite commonly have well-developed pyramidal terminations (Plate 5.11a). Acicular forms, with slightly curved margins that taper to a point, have also been observed but these are thought to be the moulds of sponge spicules (Plate 5.11a). The absence of the central canal within the spicules suggests that the present infill of silica is not the original siliceous material. The occurrence of large (hyalosteliid) sponge spicules shows that the Waulsortian Limestone at Newcastle West is Phase B, C or D (Lees *et al.*, 1985). This corresponds to deposition in water depths of

280m or less ((Lees *et al.*, 1985), p.153 Fig. 11). Both the authigenic quartz crystals and the silica fills of sponge spicule moulds are non-luminescent in CL (Plate 5.11b). Stage D veins commonly circumvent the sponge spicules (Plate 5.11b). As all the authigenic idiomorphic quartz crystals post-date the Stage D cements, this supports the hypothesis that these acicular tapering forms are moulds of sponge spicules. CL petrography indicates that the idiomorphic quartz crystals pre-dated (or were contemporaneous with) dolomitisation (Plate 5.11b).

The relationship between the Stage *E* calcite and the quartz crystals is unclear. There is evidence for quartz crystals post-dating (Plates 5.12a, 5.12b) and pre-dating (Plates 5.13a, 5.13b) the development of the Stage *E* calcite. This suggests that there are either two episodes of Stage *E* calcite veining, or two episodes of quartz precipitation, or perhaps the near-contemporaneous formation of both.

5.4 PARAGENESIS

The interpreted paragenetic sequence at Newcastle West is illustrated in Figure 5.4. The early calcite cements, Stages A-D, occur within the centres of large early cavities. Stage D is the porosity occluding cement. A development of a fifth calcite cement phase, referred to here as Stage *E*, is found within veinlets that cross-cut the Stage D cements and so post-dated the porosity occlusion. Dissolution seams that cross-cut early cement filled cavities that contain Stages A-D also occur and are later than the occlusion of porosity in these limestones. Tiny dolomite rhombs occur along the length of these dissolution seams which probably acted as conduits for the dolomitising fluids, at least during the initial stages of dolomitisation. Quartz precipitation pre-dated or may have been contemporaneous with dolomite precipitation. Stage *E* cements are found within veins both pre- and post-dating the quartz precipitation and therefore may suggest that there were either two episodes of Stage *E* veining or two stages of quartz precipitation or more probably, the near-contemporaneous formation of both. Sulphide mineralisation post-dated dolomitisation and was the last event to have occurred.

However, it should be noted that Reed and Wallace (2001) proposed that Zn-Pb mineralisation at Courtbrown, approximately 25 kilometres NNE of Newcastle West, was

contemporaneous with the development of the Stage D porosity occluding cements and that dolomitisation pre-dated their formation.

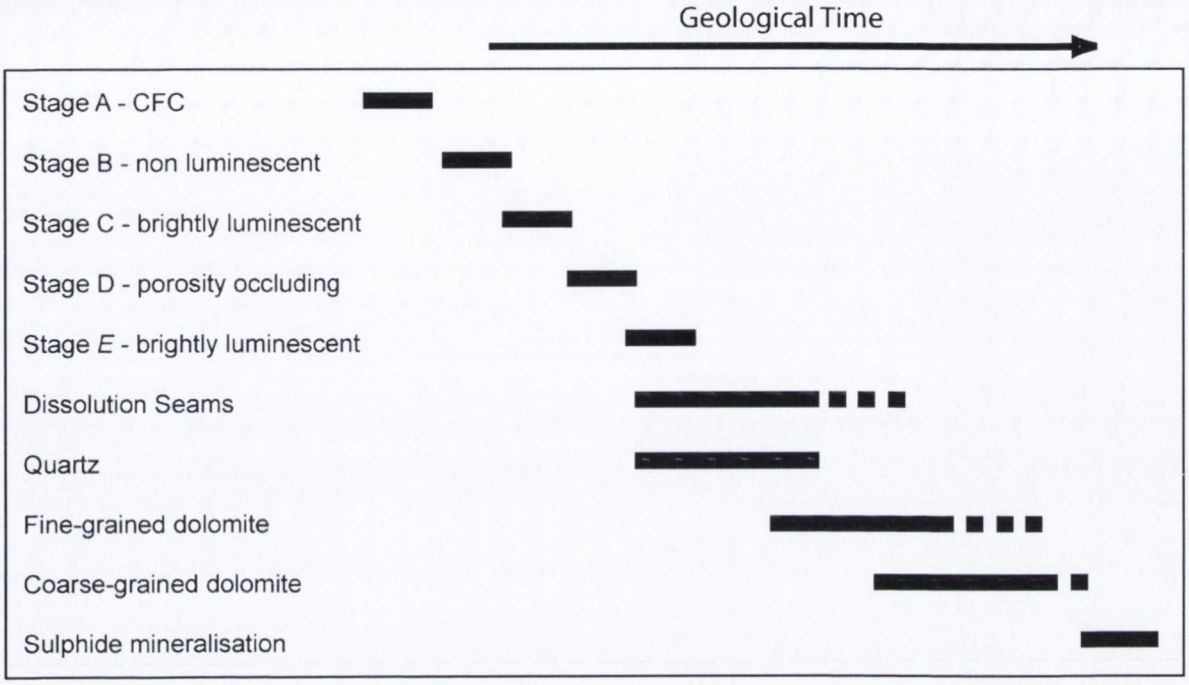

Figure 5.4 Paragenesis and cement stratigraphy of Waulsortian Limestone and dolomite at Newcastle West.

5.5 FLUID INCLUSION MICROTHERMOMETRY

Two mineral phases were isolated for fluid inclusion microthermometry analysis: the coarse-grained white dolomite and the quartz (Appendix C). The samples selected were from both OW24 and OW28. A detailed petrographic study of the fluid inclusion assemblages in both phases was completed prior to undertaking the microthermometry.

Dolomite fluid inclusion petrography

The coarse-grained, white dolomite crystals at Newcastle West contain large numbers of fluid inclusions, the majority of which were less than one micron. Several fluid inclusions that were large enough to be measured were found within the turbid cores of the coarse-dolomite crystals, as well as in the clearer outer rims (Plate 5.14). They were all two-phase (L+V) inclusions that ranged in size from 2 to 20μm with a ψ_{liquid} of either 0.85 or 0.9. They were subhedral to euhedral in shape and commonly lay in an orientation parallel to the dolomite crystal faces, which were generally coincident with the CL growth fronts. Many of the larger inclusions also lay parallel to the trails of sub-micron sized inclusions.

Dolomite fluid inclusion microthermometry

A total of seventeen fluid inclusions were measured from the coarse-grained dolomite at Newcastle West. Their Th values ranged from 125 to 199°C. First melting temperatures indicate that all the fluids were part of the $NaCl\text{-}CaCl_2\text{-}H_2O$ ternary system. The salinity data indicate an average of 25.3 combined wt% NaCl and $CaCl_2$ equivalent for the dolomite in OW28 and 24.5 combined wt% NaCl and $CaCl_2$ for the dolomite in OW24 (see Appendix C).

Quartz fluid inclusion petrography

Fluid inclusions within the quartz in Newcastle West are rare. Numerous quartz crystals were carefully scanned but only approximately 5% of them contained fluid inclusions. However, those quartz crystals that did contain an inclusion usually contained more than one. The inclusions in the quartz were all two-phase (L+V). In comparison to the size of the inclusions within the coarse-grained white dolomite, those within the quartz crystals were minute (Plate 5.15). They ranged in size from 3 to 5μm and had ψ_{liquid} of either 0.85 or 0.9 (except for one with a ψ_{liquid} of 0.95). Their shape was commonly subhedral with the majority being rounded. Classifying the inclusions in terms of primary, pseudosecondary and secondary was difficult. No zoning was visible within the quartz crystals from which the fluid inclusions selected for measurement came as they had generally been cut parallel to the c-axis.

Quartz fluid inclusion microthermometry

A total of sixteen fluid inclusions were measured from the quartz at Newcastle West. Their Th values ranged from 131 to 187°C. First melting temperatures indicate that all the inclusions were part of the $NaCl\text{-}CaCl_2\text{-}H_2O$ ternary system. The salinity data indicate an average of 24.8 combined NaCl and $CaCl_2$ wt% equivalents for the quartz in OW28 and 25.5 combined NaCl and $CaCl_2$ wt% equivalents for the quartz in OW24.

Implications for the Th of the fine-grained dolomite

No fluid inclusion data were obtained from the fine-grained dolomite, as the crystals were too small and turbid. Despite this, the paragenetic relationship between the dolomite and the quartz can be used to infer the temperature of formation of the fine-grained dolomite. As the fine-grained dolomite was precipitated after (or during) quartz precipitation and

before coarse white dolomite precipitation, it can be assumed that the homogenisation temperature of the fine-grained dolomite lies between that of the quartz and the coarse dolomite and therefore is above 131°C. This moderately high temperature of formation for the fine-grained dolomite at Newcastle West implies that dolomitisation may have occurred at depth or been the product of a high temperature, hydrothermal fluid. This is in contrast to the model of low temperature (<50°C), early diagenetic dolomitisation by seawater interpreted by Wright *et al.* (2000) and Gregg *et al.* (2001) for the fine-grained dolomite (their pk1 cement) found in the Irish Midlands and Dublin Basin.

Discussion

The fluid that precipitated the coarse-grained white dolomite at Newcastle West was moderately hot (125 to 199°C) and very saline (25.2 combined wt% NaCl and $CaCl_2$ equivalent). Likewise, the fluid that precipitated the quartz was moderately hot (131 to 187°C) and also very saline (an average of 25.4 combined wt% NaCl and $CaCl_2$ equivalent for both boreholes). The close spatial association between the dolomite and the quartz and the overlap in the homogenisation temperature and salinity data suggests that both minerals precipitated from the same fluid (but see Section 5.8 below).

5.6 STABLE ISOTOPE GEOCHEMISTRY

Forty-four samples of unaltered Waulsortian Limestone and thirty-four samples of dolomitised Waulsortian Limestone from Newcastle West were sampled for stable isotope analysis. Individual quartz crystals and pyrite were also sampled and their isotopic compositions determined (Appendix B). A full description of the sampling methods is given in Chapter 2.

5.6.1 Calcite

Micrite, CFC and Stage D calcite (the final porosity occluding cement phase) were sampled for stable isotope geochemistry.

The range in $\delta^{13}C$ values (Figure 5.5) for micrite is 3.2 to 4.36‰ (mean 3.83‰ ± 0.84‰ 2σ); for the CFC cements is 3.83 to 4.57‰ (mean 4.14‰ ± 0.48‰ 2σ); and for the Stage D cements is 2.13 to 4.69‰ (mean 3.29‰ ± 1.46‰ 2σ). These values are within the range of the $\delta^{13}C$ values for micrite and early calcite cements in the Waulsortian Limestone at

Lisheen (Chapter 3, Figure 3.4) and elsewhere in the Irish Midlands (Boast *et al.*, 1981a; Gallagher *et al.*, 1992).

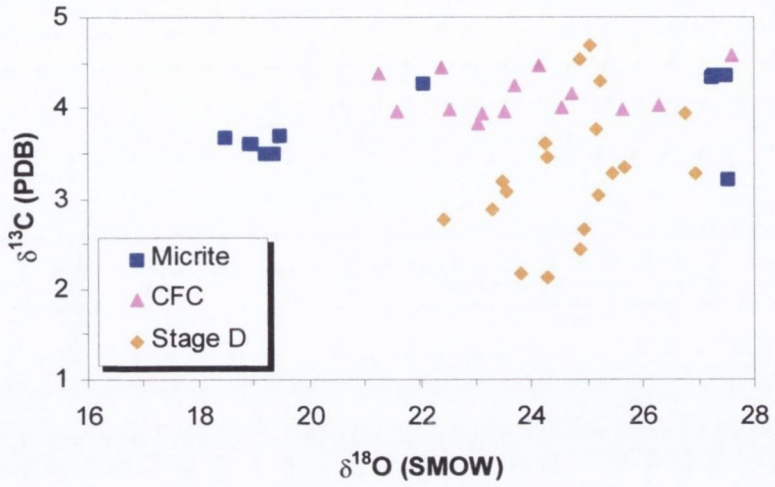

Figure 5.5 Scatter plot of $\delta^{13}C$ and $\delta^{18}O$ values for micrite and early calcite cement phases at Newcastle West.

However, the $\delta^{18}O$ values of the early calcite cements have a much broader range than those reported from Lisheen (Chapter 3 this study; Eyre (1998)) or in isotopic studies undertaken elsewhere in the Irish Midlands (Boast *et al.*, 1981a; Gallagher *et al.*, 1992). In order to simplify the $\delta^{18}O$ data from the early calcite cements from Newcastle West, data from each borehole are plotted separately.

Figure 5.6 shows the data from the micrite and calcite cements from OW28. A conspicuous feature of this plot is the cluster of light values (around 19‰) from samples of micrite. These values are much lighter than would be expected from micrite precipitated directly from seawater at geologically reasonable temperatures. The data from the CFC from OW28 have a broad spread and range from 21.6 to 26.3‰ (mean 23.69‰ ± 3.68‰ 2σ; mode 23‰). Due to the pervasive nature of the dolomitisation in borehole OW28 no pristine Phase D cement could be sampled and therefore no isotopic data were obtained.

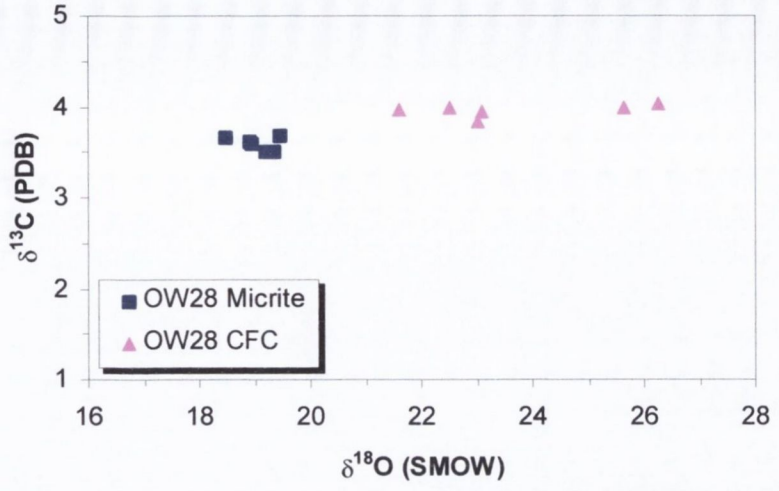

Figure 5.6 Scatter plot of $\delta^{13}C$ and $\delta^{18}O$ values for the micrite and early calcite phases in borehole OW28.

The data from the micrite and early calcite cements from OW24 are shown in Figure 5.7. Apart from one micrite data point at 22.1‰ the other micrite samples have $\delta^{18}O$ values that cluster around 27‰. Consistent with the results from OW28, the CFC $\delta^{18}O$ data from OW24 display a broad spread, ranging from 21.2 to 27.6‰ (mean 23.97‰ ± 3.72‰ 2σ; mode 24‰). The Stage D $\delta^{18}O$ data also have a broad spread, with values ranging from 22.4 to 26.9‰ (mean 24.71‰ ± 2.26‰ 2σ; mode 24.9‰). In addition they have a slightly wider range of $\delta^{13}C$ values than either the micrite or the CFC, but still remain within the typical Waulsortian Limestone range.

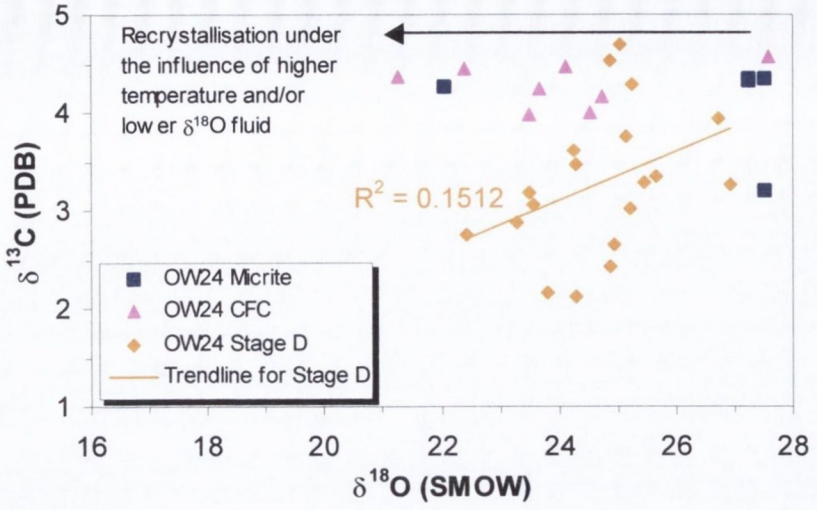

Figure 5.7 Scatter plot of $\delta^{13}C$ and $\delta^{18}O$ values for the micrite and early calcite phases in borehole OW24.

Discussion

In view of the rigorous sampling protocol outlined in Chapter 2, the samples analysed are unlikely to have been contaminated significantly by later phases and the data obtained are considered to reflect the isotopic values of the phases identified. The light $\delta^{18}O$ values for the micrite in OW28 are unusual and may indicate either a) 'recrystallisation' under the influence of a fluid with the same isotopic composition but at a higher temperature, or b) 'recrystallisation' by a fluid with a different isotopic composition (Figure 5.7). The spread in the CFC $\delta^{18}O$ data may also reflect one of the two possibilities outlined above but perhaps due to their larger crystal size, each individual CFC cement crystal may not have equilibrated to the same extent and therefore the spread in the $\delta^{18}O$ may be indicating varying degrees of equilibration.

The $\delta^{18}O$ data for the micrite in OW24, with their bimodal distribution, are difficult to interpret. The values that cluster around 27‰ probably reflect normal seawater values at the time of precipitation. The only low $\delta^{18}O$ value (22.1‰) comes from a shallower sample interval than the other four (see Appendix B). As this light micrite value is only one data point it is speculative to invoke the presence of another fluid to explain its $\delta^{18}O$ value. More $\delta^{18}O$ data from the micrite in OW24 are needed to establish if this one data point represents an outlier in a bigger dataset that clusters around 27‰ or if there is a

range in $\delta^{18}O$ values that extends from 27‰ down to 22‰; the latter seems more probable (see below).

The simplest model to explain the range in $\delta^{18}O$ values of the micrite and CFC is that both have equilibrated to a varying degree with a later fluid, which may or may not have had a higher temperature and/or lower $\delta^{18}O$ value than Carboniferous seawater. The Stage D cements show a broad trend towards lighter $\delta^{18}O$ and $\delta^{13}C$ values (Figure 5.7) as seen at Lisheen. To what extent the $\delta^{18}O$ values are lighter than anticipated from a simple model of cement growth during burial is not known.

5.6.2 Dolomite

The isotopic data from both the fine-grained and coarse-grained dolomites at Newcastle West have been plotted in Figure 5.8. The fine-grained dolomite has a broad range of $\delta^{18}O$ values (20.6 to 24.9‰ with a mean of 22.91‰ ± 2.44‰ 2σ; mode 23.3‰) and a narrow range of $\delta^{13}C$ values (3.8 to 4.6‰ with a mean of 4.07‰ ± 0.38‰ 2σ). Similarly the coarse-grained dolomite has a broad range in $\delta^{18}O$ values of 16.75 to 22.33‰ (mean of 18.76‰ ± 3.64‰ 2σ; mode 17.4‰) and a range in $\delta^{13}C$ values of 2.80 to 3.82‰ (mean of 3.28‰ ± 0.68‰ 2σ).

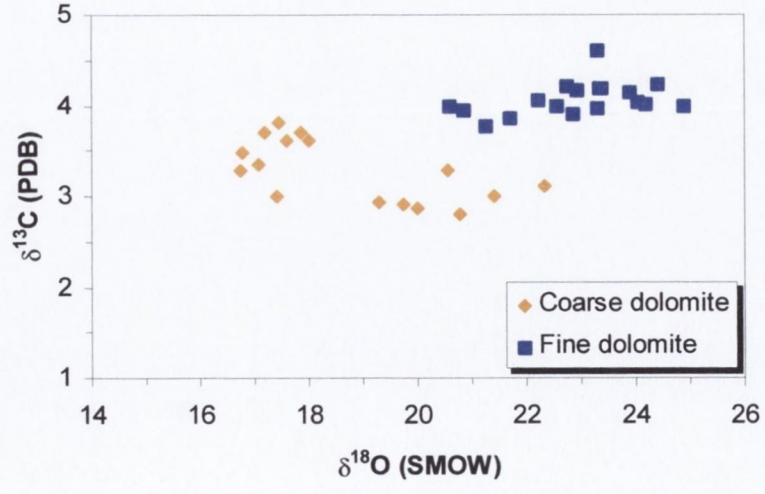

Figure 5.8 Scatter plot of $\delta^{13}C$ and $\delta^{18}O$ values for the dolomite at Newcastle West.

Again, in order to interpret the isotopic data for the dolomite at Newcastle West it is useful to plot the data from each borehole separately (Figure 5.9).

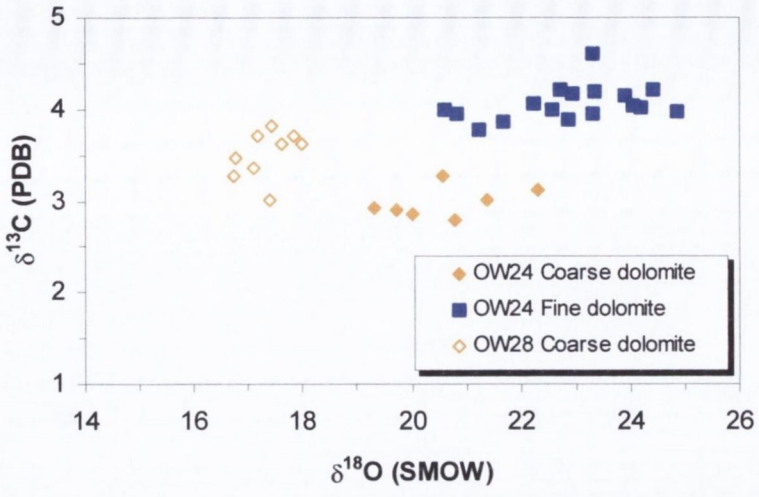

Figure 5.9 Scatter plot of $\delta^{13}C$ and $\delta^{18}O$ values for the dolomite at Newcastle West, with data from each borehole plotted separately.

The $\delta^{18}O$ values of the coarse dolomite from OW28 are all exceedingly light and cluster around 17‰. Unfortunately due to the pervasive nature of the coarse-grained dolomite no areas of fine-grained dolomite were sufficiently developed within OW28 to enable pristine samples to be isolated. Therefore, all of the fine dolomite data analysed came from OW24. The coarse dolomite from OW24 ranges from 19.31 to 21.39‰ (mean of 20.59 ± 1.03‰ 1σ).

Discussion

The coarse dolomite data from OW28, which clusters around 17‰, have the lightest $\delta^{18}O$ values in the entire dolomite dataset from Newcastle West. These light coarse dolomite values coupled with the light micrite values seen in Figure 5.6 may be consistent with OW28 being located in the vicinity of a fault. This would have enabled fluids to exploit the fault as a conduit and allowed any fluid expelled to alter the isotopic signatures of the rocks closest to it. Regrettably no isotopic data from the Stage D calcite from OW28 was obtained. If this fault hypothesis is correct then any $\delta^{18}O$ values of the Stage D cements would be expected to cluster around 20‰. This would facilitate a shift to lighter values of about 3‰ upon dolomitisation and thus explain the coarse-grained dolomite values around 17‰. The CFC $\delta^{18}O$ data in OW28 come from the same sample interval as the micrite $\delta^{18}O$ data (see Appendix B). It is thought that perhaps due to its larger crystal size not all of the CFC may have equilibrated with any incoming fluids to the same extent as the fine-

grained micrite. This could therefore explain the broad spread in the $\delta^{18}O$ values of the CFC and the tight cluster of light $\delta^{18}O$ values for the fine-grained micrite.

The spread in the $\delta^{18}O$ of the fine-grained dolomite from OW24 may represent one of three things. Firstly, that the samples analysed were not pristine; secondly there was a variation in fluid temperature at the time of precipitation; or thirdly precipitation occurred within a closed system and therefore the fluid $\delta^{18}O$ composition varied as the system evolved.

With regards to the first possibility, the rigorous sampling protocol ensured that any sample with evidence of contamination was discarded. It is conceded that the possibility remains that some calcite may have remained within the dolomite and was a sufficiently small amount to avoid detection using CL.

Secondly, a variation in the fluid temperature at the time of deposition may be a possibility. However, taking the heaviest (24.9‰) and lightest (20.6‰) $\delta^{18}O$ value for the dolomitised micrite and modelling their parental fluid compositions over a range of temperatures of precipitation (Land, 1983), implies that the range in temperature over which the dolomitised micrite formed was between approximately 65 and 90°C. Likewise doing the same for the coarse dolomite implies the range in temperature over which it precipitated was 80 to 105°C. These temperatures are lower than the measured homogenisation temperatures for the coarse dolomite and the minimum temperature estimated for the fine dolomite (125-199°C and 131°C respectively). Therefore, based on these isotopic measurements, a variation in the temperature of the fluid at the time of dolomitisation is considered unlikely.

The third suggestion is that the trend in the dolomitised micrite data seen in Figure 5.8 is evidence for a fluid precipitating within a closed system, resulting in a shift to progressively heavier values as the lighter isotope is fractionated out. This trend has been previously noted by Gregg *et al.* (2001) and has been used as evidence to argue that the heavy $\delta^{18}O$ values of the fine-grained dolomite represent their precipitation from modified Lower Carboniferous seawater at low temperatures (<50°C). The evidence from the fluid inclusion data in this study indicates that the fine-grained dolomite was likely to have

formed at high temperatures (>131°C) and so the spread in the $\delta^{18}O$ values of the fine-grained dolomite represents a change in the $\delta^{18}O$ of the fluid and not a change in the temperature. This supports the suggestion that the $\delta^{18}O$ values of the fine-grained dolomite may represent evidence of precipitation within a closed system.

5.6.3 Quartz

Individual quartz crystals from both OW28 (n=14) and OW24 (n=15) were extracted and analysed using laser fluorination to obtain their $\delta^{18}O$ values (see Appendix B). The quartz from OW28 has a range of $\delta^{18}O$ values of 18.4 to 19.5‰ (mean of 19.23‰ ± 0.56‰ 2σ) and the quartz from OW24 has a range of 18.3 to 19.8‰ (mean of 19.08‰ ± 0.88‰ 2σ). A 'difference of two means' test was performed on the means of these two quartz populations to test the hypothesis that they are part of the one population. It was decided before the test was performed that a probability value above 10% was not significant, meaning that the two means could be considered the same. A probability value of 28.8% was obtained. Therefore, there is enough confidence within the data to say that the two means are the same and that they are part of the same population.

5.6.4 Pyrite

Six samples of pyrite from OW24 were analysed. Five had well-developed cubic crystal forms and one (sample 4) was of pyritised micrite that still had the bedding within the micrite clearly discernable. All of the pyrite samples had isotopically heavy $\delta^{34}S$ values ranging from 2.1 to 9.2‰ (mean 7.4‰ ± 5.2‰ 2σ; mode 8.3‰). Sample 4 had a value that was slightly isotopically lighter than the other five samples (2.14‰). When this sample was re-run an almost identical $\delta^{34}S$ value was obtained (2.35‰) and so rather then taking an average of the two measured $\delta^{34}S$ values, the former value was retained (see Appendix B).

Discussion

All of the pyrite samples analysed from Newcastle West had isotopically heavy $\delta^{34}S$ values and are consistent with a deep-seated, hydrothermal, source for the sulphur (Fluid 1). There is no evidence for the isotopically light, bacteriogenic sulphur component (Fluid 2) as described in several major Irish Zn-Pb deposits (Hitzman & Beaty, 1996; Fallick *et al.*, 2001; Blakeman *et al.*, 2002). This may therefore explain the absence of any major

mineralisation at Newcastle West. Similar observations have been made in many of the prospects of the Kildare District (Gallagher *et al.*, 1992; Hitzman & Beaty, 1996), where the absence of the bacteriogenic sulphur component has been noted and has been suggested as a possible reason why these prospects never became major deposits.

5.7 MODELLING OF PARENTAL FLUIDS

Mineral-water oxygen isotope fractionation curves were constructed using an average of the measured $\delta^{18}O$ values for both the coarse dolomite (Land, 1983) and the quartz (Matsuhisa *et al.*, 1979) (Figure 5.10). Fluid compositions were calculated for the coarse dolomite and the quartz using the homogenisation temperature ranges (125 to 200°C and 130 to 190°C respectively), which represent minimum entrapment temperatures. The modelled isotopic values of the fluids from which dolomite and quartz precipitated range from 1.7 to 7.6‰ for the coarse dolomite and 2 to 6.9‰ for the quartz. Therefore the $\delta^{18}O$ of the parental fluid that precipitated the dolomite and quartz had isotopic values ranging from 1.7 to 7.6‰ and are consistent with a fluid(s) that has undergone a moderate amount of fluid rock interaction.

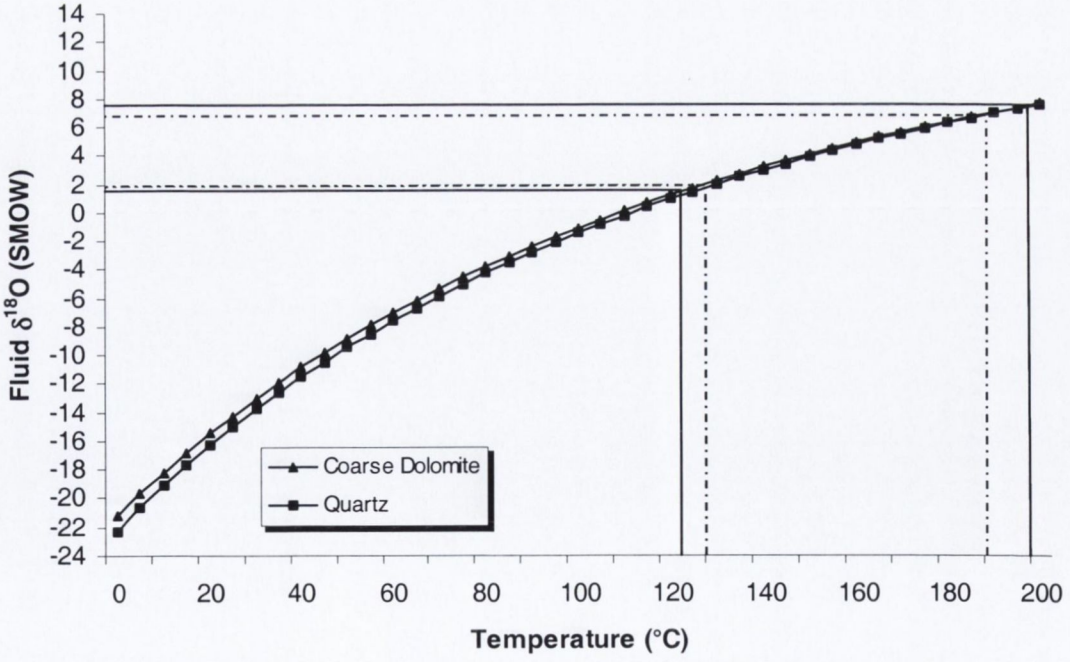

Figure 5.10 Mineral-water oxygen isotope fractionation curves for coarse dolomite and quartz at Newcastle West. See text for discussion.

5.7.1 A note on silica solubility

In order to establish the physico-chemical parameters of a fluid that precipitates both dolomite and quartz, it is necessary to know both the solubility of silica and the factors that may influence it.

Equilibrium between a solid silica polymorph, $SiO_{2(s)}$, and an aqueous solution can be described by the following reaction:

$$\mathbf{SiO_{2\,(s)} \Leftrightarrow SiO_{2\,(aq)}}$$

The equilibrium constant (K) for the above reaction can be expressed as:

$$\mathbf{K = aSiO_{2(aq)} = mSiO_{2(aq)}\ \gamma SiO_{2(aq)}}$$

where $aSiO_{2(aq)}$ is the activity of aqueous silica, $mSiO_{2(aq)}$ is the silica concentration of aqueous silica and $\gamma SiO_{2(aq)}$ is the activity coefficient of aqueous silica.

Effect of temperature and pressure

The solubility of quartz increases with increasing temperature and increasing pressure (Fournier & Potter, 1982). The only exception to this is for a small region around the critical point of water (374°C, 221 bars) where solubility is observed to decrease with increasing temperature (Fournier *et al.*, 1982). A reduction in temperature is known to produce the largest amount of precipitation for solutions at both high temperatures and pressures. Reductions in pressure are not thought to be as important as temperature reductions except under conditions of fracturing (Rimstidt, 1997b). Under these circumstances, where the pressure may change suddenly from lithostatic to hydrostatic, the pressure drop can cause a rapid decrease in the solubility of quartz.

Effect of pH

The solubility of silica is independent of pH over the range expected for most natural hydrothermal solutions, but silica solubility is known to increase with increasing pH in alkaline solutions (Fleming & Crerar, 1982). This is due to the fact that H_4SiO_4 is a weak acid and can dissociate appreciably at high pH to $H_3SiO_4^-$ and H^+. Such high pH values

(>8) are uncommon in hydrothermal environments with the exceptions of low silica environments like carbonatites and serpentinites (Rimstidt, 1997b).

Effect of electrolytes in solution

In dilute fluids it is generally assumed that $aSiO_{2(aq)} = mSiO_{2(aq)}$. However, dissolved electrolytes can affect the solubility by reacting with $SiO_{2(aq)}$ to form complexes and/or interacting with water molecules, thereby altering the hydration energy of $SiO_{2(aq)}$ (Dove & Rimstidt, 1994). In concentrated solutions, $aSiO_{2(aq)}$ differs significantly from $mSiO_{2(aq)}$ and must therefore be known precisely for accurate thermodynamic calculations. At constant pressure, the solubility of silica at low temperatures generally decreases with increasing concentration of inorganic electrolytes (Azaroual *et al.*, 1997). This 'salting-out' effect, which is the decrease in solubility with the addition of salt, has been shown to be essentially cation dependent with silica solubility greatly decreasing with the addition of $MgCl_2$ and $CaCl_2$ to pure water (Marshall & Warakomski, 1980). Fournier (1983) has shown that the 'salting-out' effect decreases, and thus the solubility of silica increases, with increasing salinity ('salting-in') in hydrothermal solutions. This switch from 'salting-out' to 'salting-in' can be explained by the fact that strong electrolytes (those that decrease water activity by ionic hydration and almost complete dissociation) become weak electrolytes (which form ion association but have little effect on the activity of water) due to the decrease in the dielectric constant of water (Helgeson *et al.*, 1981). Although Fournier (1983) investigated quartz solubilities only in aqueous NaCl solutions, Marshall and Chen (1982) examined mixed electrolyte solutions and showed that silica solubilities in multicomponent electrolyte solutions can be estimated from the solubilities in single salt solutions.

Discussion

The fluid that precipitated the quartz and the dolomite at Newcastle West was both moderately hot and very saline. Fluid inclusion data confirm that the electrolyte species contained within these fluids included NaCl and $CaCl_2$. However, the high salinities, which may have induced a 'salting-out' effect at low temperatures, were possibly counterbalanced by the moderately high temperatures of the fluid and so enabled quartz to be carried in solution. If temperature is therefore assumed to be the controlling factor in the solubility of the quartz at Newcastle West then the close spatial association between the quartz precipitation and the proximity to the 'dolomite front' may be taken as further

evidence to support this. As the 'dolomite front' probably represents the interface between this moderately high temperature, high salinity fluid and the surrounding limestone lithosome, a decrease in temperature is likely to have occurred along this surface, forcing quartz precipitation to occur.

5.8 HALOGEN GEOCHEMISTRY

Coarse-grained dolomite and quartz separates from both OW28 (269.1 and 297.45m respectively) and OW24 (506.95 and 506.75m respectively) were prepared for crush-leach analysis using the method outlined in Chapter 2. The results are tabulated in Appendix D.

The calculated Cl and Br composition of the fluids within the inclusions of quartz and coarse dolomite are shown in Figure 5.11. The quartz data lie to the left of the SET and indicate that the fluids within these inclusions may be a mixture of evaporated seawater and a fluid, which has acquired some Cl from the dissolution of halite. The dolomite data lie, within analytical uncertainty, on the SET and indicate that the fluid within these inclusions is residual brine. Therefore, contrary to the petrographic and isotopic data, the halogen geochemistry data indicate that two different fluids precipitated the quartz and dolomite at Newcastle West.

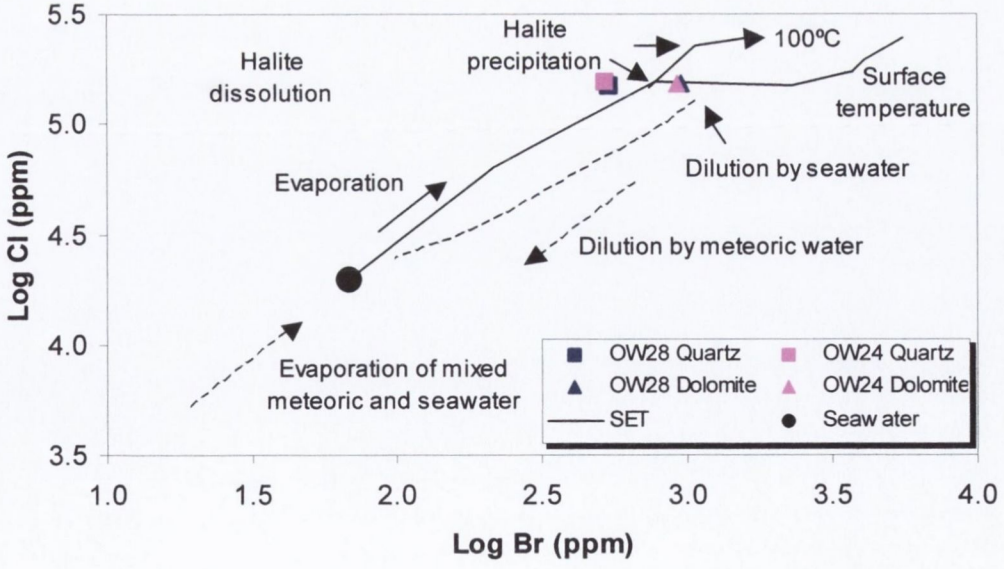

Figure 5.11 Cl and Br systematics of the coarse dolomite and quartz at Newcastle West. Plot also shows the SET (after Carpenter (1978) and Gleeson & Yardley (2002)).

A plot of the Na-Cl-Br systematics is shown in Figure 5.12. The quartz samples from OW24 and OW28 have Cl/Br ratios that are similar to seawater (675 and 634 respectively) but Na/Br ratios (426 and 408 respectively) that are lower than the values expected for seawater. These high Cl/Br values can be explained in one of two ways: either analytical error; or the addition of a minor amount of Cl from another source.

The data are unlikely to be due to analytical error as, in order to eliminate any error directly associated with the samples themselves or the analyses, a second set of samples (both quartz and dolomite) were analysed and yielded similar results. Therefore the high Cl/Br ratios of the quartz from Newcastle West are likely to be the result of the addition of Cl (and probably Na as well) from another source, perhaps a component of halite dissolution. The fluids within the inclusions in the quartz at Newcastle West are therefore thought to be a mixture of residual brine (i.e. seawater evaporated beyond the point of halite dissolution) and a minor amount of a fluid, which has acquired some Cl from the dissolution of halite

The dolomite samples from OW24 and OW28 have Cl/Br ratios (361 and 364 respectively) and Na/Br ratios (409 and 250 respectively) that are less than the values expected for seawater and are consistent with the evaporation of seawater beyond the point of halite precipitation. The positioning of the dolomite data to the right and left of the SET indicate that the fluids within these inclusions have Na concentrations that are different from those expected for seawater. The dolomite data, which plots to the left, may indicate that there has been some Na-Ca exchange due to fluid rock interaction. The dolomite data, which plots to the right, indicates that these fluids are enriched in Na relative to seawater.

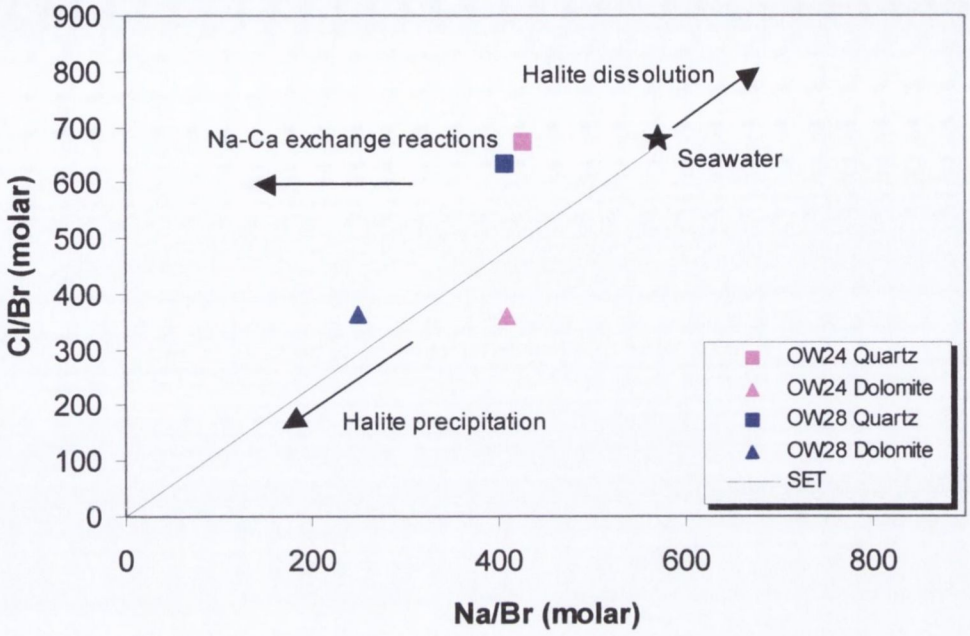

Figure 5.12 Cl-Na-Br systematics for the coarse dolomite and quartz from Newcastle West. SET data after Kesler *et al.* (1995).

Discussion

The fluid inclusion microthermometric data and the overlap in the $\delta^{18}O$ of the modelled parental fluids strongly suggested that the same fluid precipitated both the quartz and the coarse dolomite. This was further supported by the petrographic evidence, which implied that, due to their close spatial association, both the quartz and the dolomite were genetically linked. However, the crush-leach data do not support the hypothesis that both the quartz and the dolomite precipitated from a single fluid.

The halogen data from the quartz indicate that the fluids within these inclusions probably contain a mixture of residual brine and a fluid, which has acquired some Cl from the dissolution of halite. The halogen data from the dolomite suggest that the fluid within these inclusions is residual brine. The Na concentrations of the dolomitising fluids vary from those expected for seawater, with the data from the dolomite from OW28 indicating some Na-Ca exchange and the dolomite from OW24 indicating an enrichment in Na.

In terms of the fluids involved in the formation of the Irish Zn-Pb deposits, the quartz and dolomite from Newcastle West may be considered as being similar to Fluid 2, the low

temperature, residual brine. However, the measured $\delta^{34}S$ values for the pyrite indicate a deep-seated, hydrothermal source for this sulphur, which is normally associated with the ore-bearing Fluid 1. These data indicate that there is evidence for elements of both fluids within the Newcastle West samples.

5.9 CONCLUSIONS

- In terms of its CL signature and its gross morphology in hand sample, the dolomite at Newcastle West is identical to the Regional Dolomite found at Lisheen and elsewhere throughout the Irish Midlands.

- Dolomitisation occurred after all of the primary porosity within the limestone lithosome had been occluded.

- At least during the initial stages of dolomitisation, dissolution seams may have been exploited as conduits, enabling the Mg bearing fluids to move through the well-cemented limestone.

- Quartz crystals occur within the micrite of the limestone and increase in both size and abundance towards the limestone/dolomite contact. This close spatial association between the quartz and the dolomite implies that these two phases are genetically linked.

- Fluid inclusion data indicate that moderately hot (>125°C), high salinity (~25 combined wt% NaCl and $CaCl_2$) fluids precipitated both the coarse-grained dolomite and the quartz.

- In the absence of fluid inclusion data for the fine-grained dolomite, the paragenetic relationship between the dolomite and the quartz can be used to infer the homogenisation temperature data of the fine-grained dolomite. This suggests that the fine-grained dolomite formed at temperatures >131°C.

- This temperature is substantially hotter than the <50°C suggested by other workers (Wright *et al.*, 2000; Gregg *et al.*, 2001) for the fine-grained dolomite found in the Irish

Midlands and the Dublin Basin and indicates that dolomitisation could not have occurred by the circulation of seawater during early diagenesis.

- There is an overlap in the range of $\delta^{18}O$ values of the parental fluids for both the quartz (1.7 to 7.6‰) and the dolomite (2 to 6.9‰). These data indicate that the fluid(s) that precipitated these phases had undergone a moderate amount of fluid rock interaction.

- All of the pyrite analysed had isotopically heavy $\delta^{34}S$ values and are consistent with a deep-seated, hydrothermal, source for the sulphur (Fluid 1).

- The halogen data contradict the petrographic, fluid inclusion and modelled parental fluid data, which all indicate that the same fluid precipitated both the coarse dolomite and the quartz at Newcastle West.

- The fluids within the quartz inclusions are probably a mixture of residual brine and a fluid, which has acquired some Cl from the dissolution of halite, whereas the fluids within the dolomite inclusions are likely to be residual brine.

- In terms of the fluids associated with the Irish Zn-Pb deposits both the quartz-bearing fluid and the dolomitising fluid are consistent with Fluid 2, the residual brine.

- The heavy $\delta^{34}S$ data (Fluid 1) and the halogen data (Fluid 2) suggest that there is evidence for elements of both fluids within the Newcastle West samples.

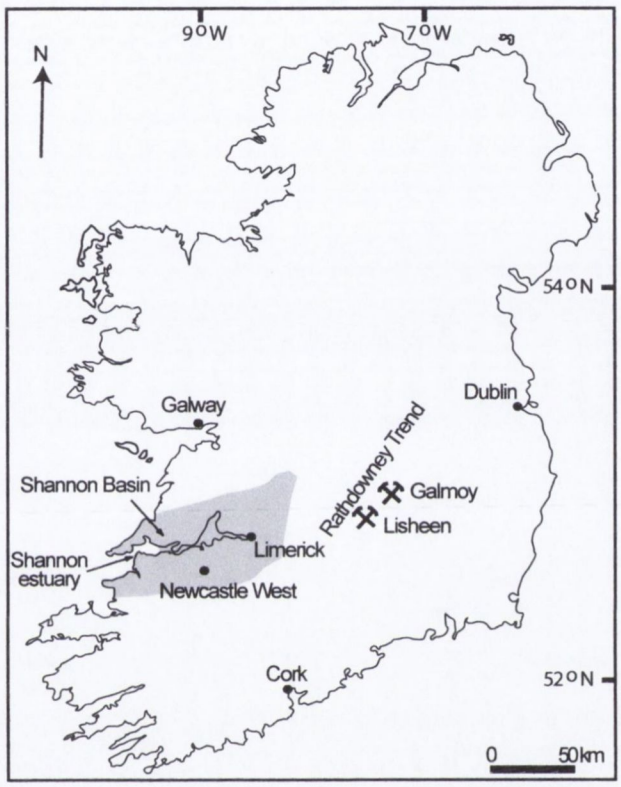

Figure 5.1 A map of Ireland outlining the location of Newcastle West in relation to the Rathdowney Trend, which includes the mines at Lisheen and Galmoy. The outline of the Shannon Basin (shaded) is taken from Strogen *et al.* (1996).

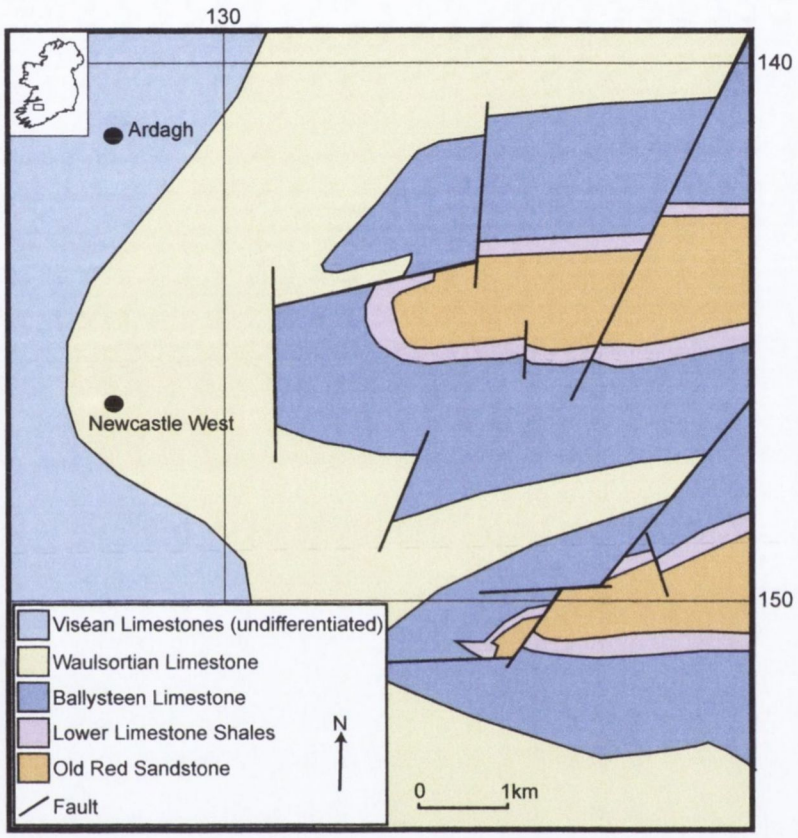

Figure 5.2 A simplified geological map of the area surrounding Newcastle West, Co. Limerick. Grid lines refer to the Ordnance Survey of Ireland National Grid. Modified after Sleeman and Pracht (1999).

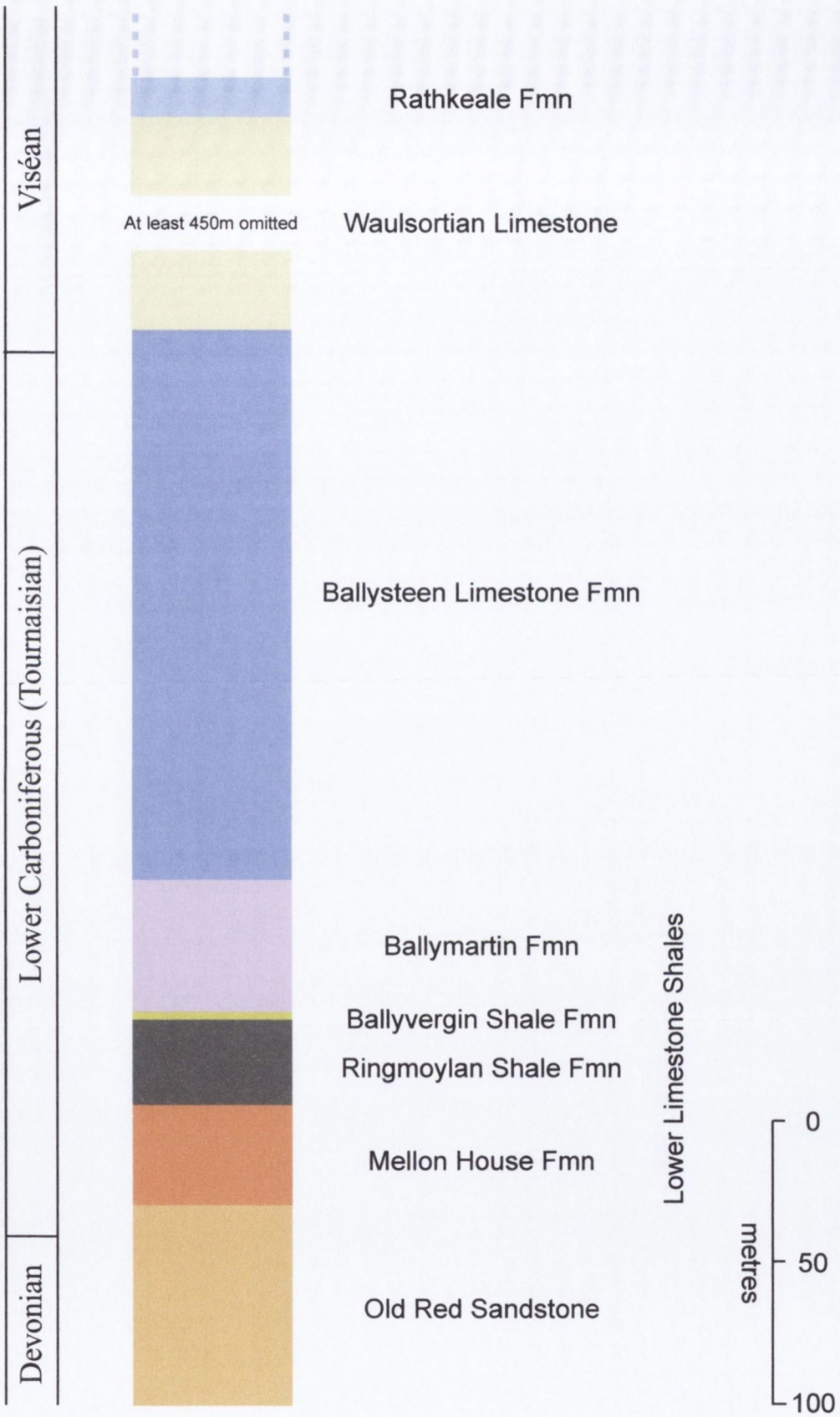

Figure 5.3 Stratigraphic section of the Newcastle West area. Thicknesses are based on the Pallaskenry Borehole after Somerville and Jones (1985).



Plate 5.1: Stained core sample from the dolomite front in OW28/67 (297.45-297.5m). Microscopically the front is not as abrupt as it appears. Note the presence of quartz crystals within the micrite (arrowed). They increase in both size and abundance towards the limestone/dolomite contact. Veins of coarse-grained dolomite are also present along the front. Top to the left.

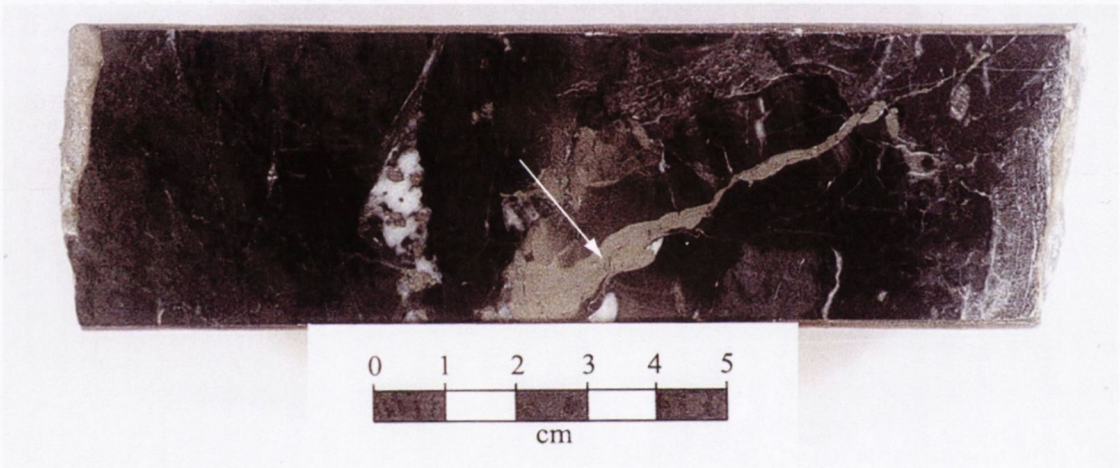

Plate 5.2: Drillcore sample from the base of the Waulsortian Limestone in OW24 (506.6 - 506.75m) which contains minor amounts of pyrite (arrowed). Top to the left.

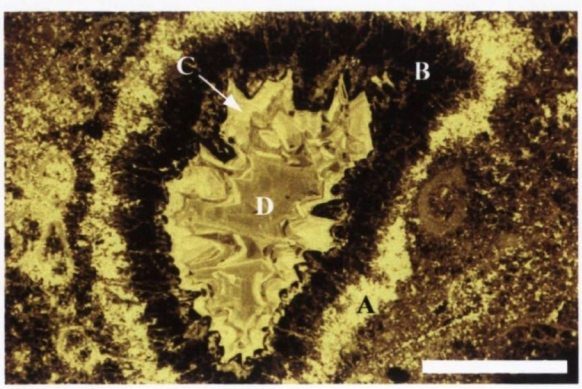

Plate 5.3: P16777 - OW28/67 (297.71 - 297.75m). CL view of an early calcite-filled cavity with Stages A-D labelled. As seen in the samples from Lisheen, Stage D is the porosity occluding cement. Scale bar is 500µm.

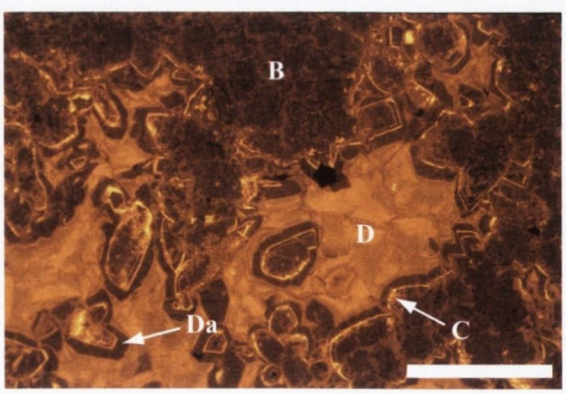

Plate 5.4: P16777 - CL view of an early calcite cavity with cement stages B-D labelled. Note the development of a non-luminescent sub-stage (Da) at the beginning of Stage D. Scale bar is 500µm.

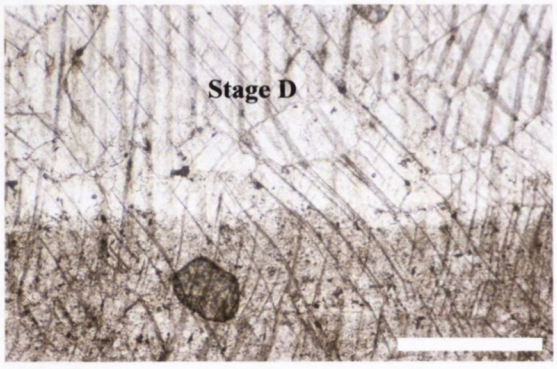

Plate 5.5a: P16777 - OW28/67 (297.71 - 297.75m). PPL view of the edge of a thick vein which is filled with Stage D calcite cement (labelled). Scale bar is 500µm.

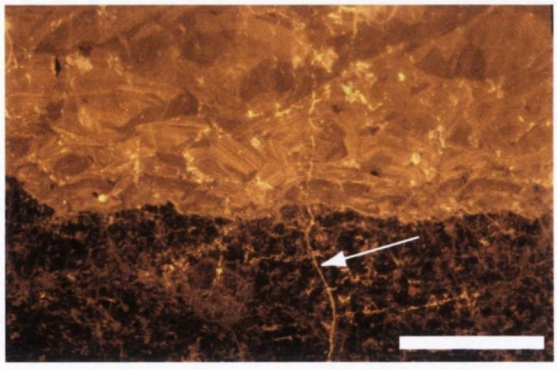

Plate 5.5b: Same view in CL. Thin vein of a later calcite cement - Stage *E* (arrow) cross-cutting the thick vein of Stage D. Scale bar is 500µm.

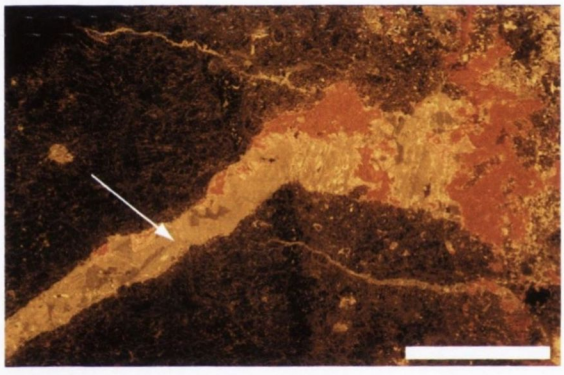

Plate 5.6: P16778 - OW28/67 (297.61 - 297.63m). CL view of a vein of Stage D calcite that is partially replaced by dolomite (arrow). Dolomitisation is post the Stage D calcite and hence post porosity occlusion. Scale bar is 500µm.

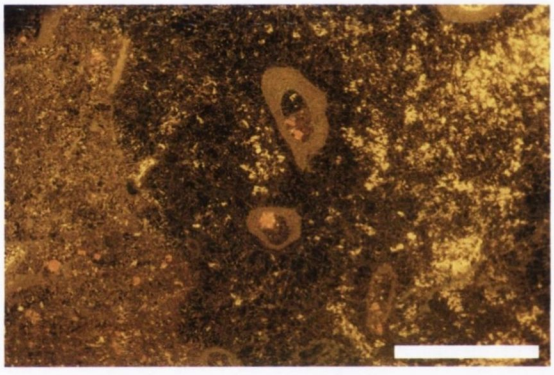

Plate 5.7: P16777 - OW28/67 (297.71 - 297.75m). CL view of the selective replacement of the micrite and bryozoans by fine-grained dolomite. Scale bar is 500µm.

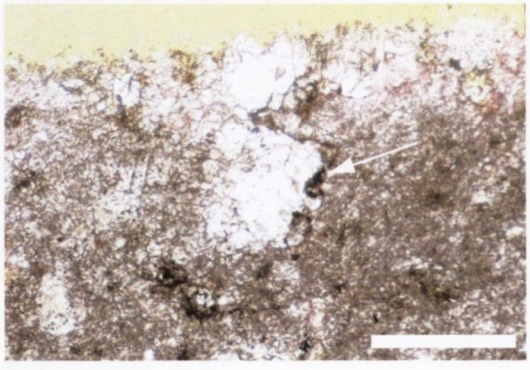

Plate 5.8a: P16778 - OW28/67 (297.61 - 297.63m). PPL view of a small cement-filled cavity which is cut by a dissolution seam (arrow). The yellow substance at the top of the image is epoxy resin. Scale bar is 500µm.

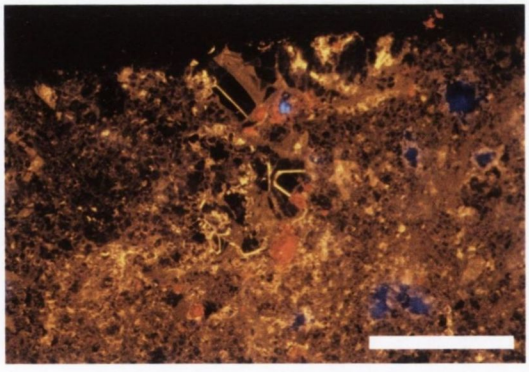

Plate 5.8b: Same view in CL. The dissolution seam post-dates the early calcite cements. Dolomite rhombs occur along the seam implying that it was exploited as a conduit. Scale bar is 500µm.



Plate 5.9a: P16782 - OW28/67 (297.42 - 297.45m). PPL view of the coarse dolomite growing into a large vug. Note the curved crystal shapes typical of saddle dolomite. Scale bar is 500µm.

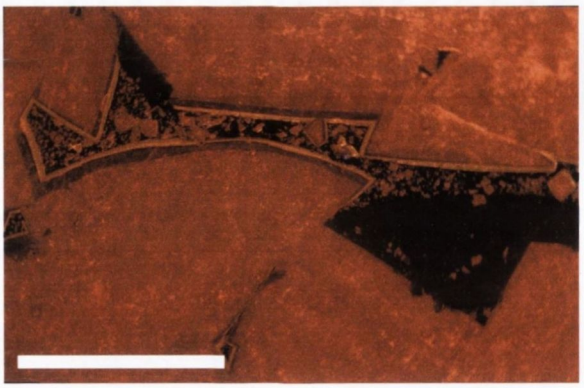

Plate 5.9b: Same view in CL. The thin outer zones of the coarse dolomite clearly show that this dolomite is growing into open space. Scale bar is 500µm.

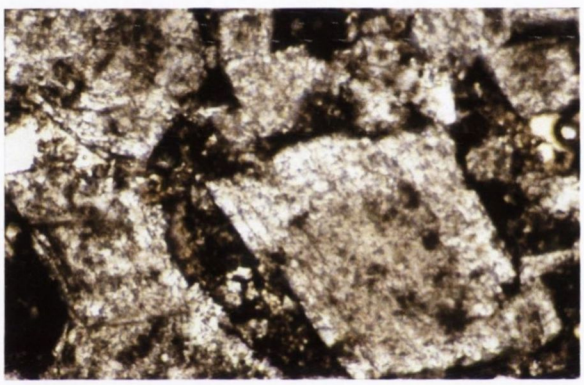

Plate 5.10a: P16782 - OW28/67 (297.42 - 297.45m). PPL view of the zonation within the coarse dolomite. Note the turbid inner cores and lighter outer parts. Scale bar is 500µm.

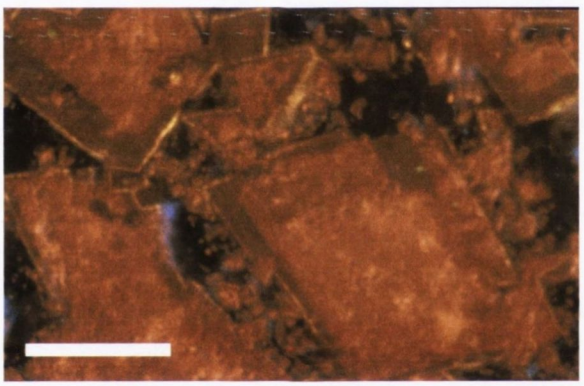

Plate 5.10b: Same view in CL. The zonation seen in PPL is highlighted under CL. Scale bar is 500µm.

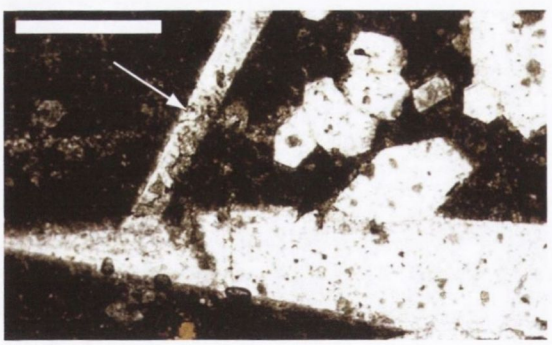

Plate 5.11a: P16780 - OW28/67 (297.5 - 297.54m). PPL view of the authigenic quartz crystals and a sponge spicule (arrow) within the micrite. Scale bar is 500µm.

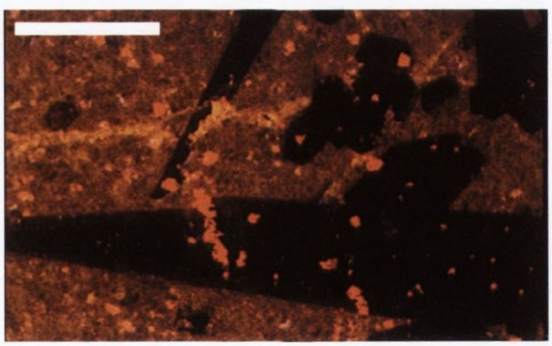

Plate 5.11b: Same view in CL. Dolomite crystals clearly post-date the quartz. Vein of Stage D spreads sideways at the spicule which confirms that the spicule pre-dates the vein. Scale bar is 500µm.

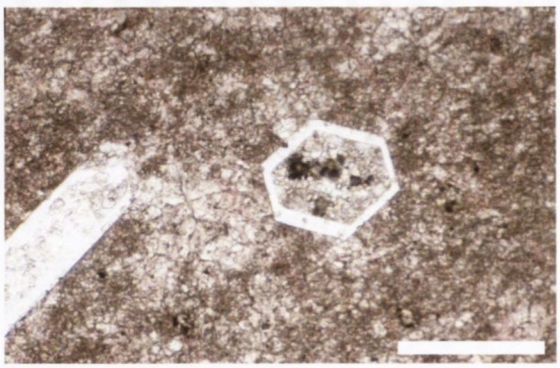

Plate 5.12a: P16779 - OW28/67 (297.54 - 297.58m). PPL view of quartz crystals within the micrite. Note the turbid cores of the quartz crystals. Scale bar is 500µm.

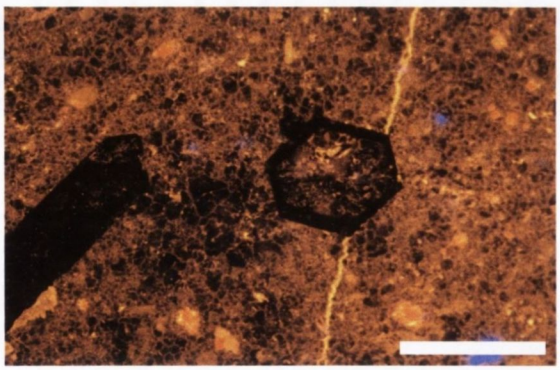

Plate 5.12b: Same view in CL. The euhedral quartz crystal post-dates a vein of the Stage *E* cement. The blue in the image is resin. Scale bar is 500µm.

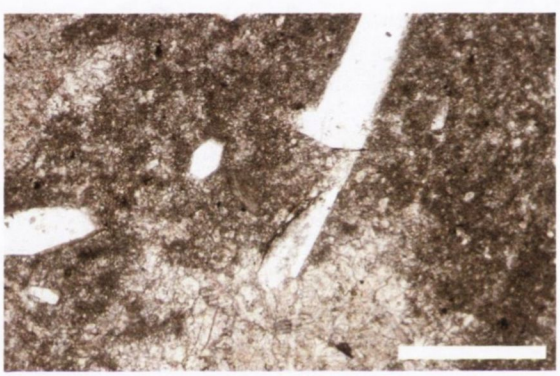

Plate 5.13a: P16779 - OW28/67 (297.54 - 297.58m). PPL view of quartz crystals in the micrite. Scale bar is 500µm.

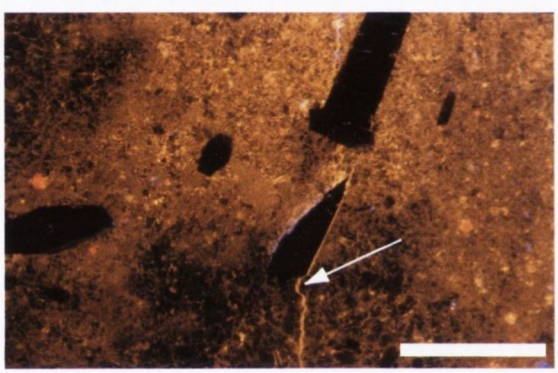

Plate 5.13b: Same view in CL. A vein of the Stage *E* calcite cement (arrow) has been deflected by the quartz crystal. Scale bar is 500µm.

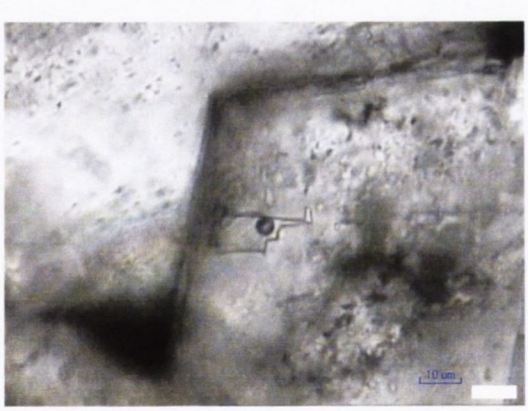

Plate 5.14: Image of the 5.1.1 two-phase fluid inclusion from the coarse-grained dolomite in OW28 (297.45 - 297.5m). Note its negative shape. Scale bar is 10µm.



Plate 5.15: Image of the 1.5.7 two-phase fluid inclusion in quartz (arrow) from OW28 (297.5 - 297.54m). Scale bar is 10µm.

CHAPTER 6

NORTH CO. CORK

6.1 INTRODUCTION

A number of borehole cores drilled by Anglo American plc in north Co. Cork include good intersections of partially dolomitised Waulsortian Limestone. Drilling at the time of sampling (July, 2001) was concentrated in the area south of Buttevant and north of Fermoy (Figure 6.1). A quarry at Subulter (GR 1443 1042), approximately 14 kilometres northwest of Mallow and 14 kilometres southwest of Buttevant, also provided samples of dolomitised Waulsortian Limestone. The samples from Subulter were notably vuggy and were of pervasively dolomitised Waulsortian with little or no original limestone preserved. The study of the Regional Dolomite by Hitzman *et al.* (1998) included the quarry at Subulter. They inferred a south to north trend in the isotopic values of the Regional Dolomite, largely because the dolomite at Subulter had slightly lighter $\delta^{18}O$ values than those found elsewhere in the Irish Midlands. A detailed examination of the dolomites from north Co. Cork was therefore undertaken in order to determine their petrographic, geochemical and isotopic characteristics.

6.2 REGIONAL GEOLOGICAL SETTING

6.2.1 Stratigraphy

The area surrounding and to the west of Buttevant has been intensively studied (Hudson & Philcox, 1965; Campbell, 1988; Gallagher & Somerville, 1997). A summary of the geology is given by Pracht (1997); the area further east surrounding Fermoy has been described by Sleeman and McConnell (1995). The stratigraphic succession includes the Ballysteen Limestone overlain by Waulsortian Limestone of Tournaisian to early Viséan age, which is succeeded in the area surrounding Buttevant by what has been termed in this study the Suprareef Limestones (the Copstown, Hazelwood, Ballyclough and Liscarroll Limestone Formations). Basic pyroclastic volcanics of the Subulter Volcanic Formation (Hudson & Philcox, 1965) (Figure 6.2) interdigitate with the lower parts the Copstown Limestone Formation and are thought to be Arundian in age (Sevastopulo & Wyse Jackson, 2001). Extensive developments of Namurian sandstones and shales occur in the areas directly to the north and south of Buttevant and to the north of Fermoy (Figure 6.1) but are not shown on the stratigraphic section in Figure 6.2.

6.2.2 Structure

The north Co. Cork area has been intensively folded and faulted as a result of the Variscan Orogeny. The fold axes have an approximate east-west trend and plunge in a westerly direction (Philcox, 1964). They are cut by many strike-slip faults that have either a northeast-southwest or a northwest-southeast trend (Figure 6.1). This has led to discontinuities of structures along strike, which has been referred to by Philcox (1964) as 'compartment deformation'. A number of thrust faults also occur throughout the North Cork area. According to Ford (1987) Variscan shortening in this area was on the order of 50%.

6.3 PETROGRAPHY

Hand samples

Drillholes south of Buttevant from the townlands of Ballybeg (3536-06), Grange East (3536-07) and Lag (3537-04) as well as two from Curtin's Farm (3626-01 and 3626-02), approximately 2 kilometres north of Fermoy, were selected for detailed study (Figure 6.1). They all contain long sections of partially dolomitised Waulsortian Limestone. In addition, the quarry at Subulter provided samples of pervasively dolomitised Waulsortian Limestone.

The samples from Subulter are notably vuggy (Plate 6.1). The vugs range in size up to a maximum of 3cm in diameter and in some cases are aligned within the host dolostone (Plate 6.2). They are lined with large quartz crystals (Plate 6.3) up to 10mm in length that commonly have well-developed euhedral shapes. The quartz crystals are ubiquitous within the vugs throughout all of the samples and clearly post-date the dolomite at Subulter.

A few of the vugs at Subulter are filled with 'pink plug' dolomite (Plate 6.4), identical to the pink dolomite described at Lisheen (Chapter 3, Section 3.2.3) and elsewhere in the Irish Midlands. The pink dolomite clearly also post-dates the formation of the matrix dolomite at Subulter. Unfortunately it has not been found in association with the post-dolomite quartz and so its relationship to the quartz is unknown.

En échelon veins filled by pink plug dolomite are found in the northern end of the quarry (Plate 6.5). Some of the veins with a similar orientation to the veins containing pink

dolomite also contain coarse white dolomite. The veins filled by coarse white dolomite have a strike of 320° and a dip of 60° to the east (Plate 6.6). These correspond to the V_4 vein set of de Brit (1988), which has been interpreted as being possibly Mesozoic in age. This raises the possibility that some of the dolomitisation at Subulter was younger than previously thought.

Thin sections

Early calcite cements are rare in the thin sections from the partially dolomitised Waulsortian Limestone samples from north Co. Cork. Whether this is purely a function of bias in the sample selection or reflects a cavity-poor facies of the Waulsortian Limestone in this part of southern Ireland is not clear. However, examples were observed where the Stages B-D were present (Plates 6.7a and 6.7b). As at Lisheen and Newcastle West, Stage D cement is the final porosity occluding cement (Plate 6.7b).

Large numbers of euhedral quartz crystals occur within both the micrite and CFC cement (Plates 6.8a and 6.8b) components of the undolomitised Waulsortian Limestone at Mallow. They are very small, up to a maximum of 5mm long. As they clearly pre-date dolomitisation they are referred to as the pre-dolomite quartz generation. When dissolved out from pervasively dolomitised samples by digestion in HCl, the crystals generally have very ragged outlines making them easily distinguishable from the post-dolomite quartz generation whose pristine crystals line the vugs.

The dolomites from north Co. Cork are petrographically very similar to the Regional Dolomite found throughout the Rathdowney Trend. The style of replacement of the Waulsortian Limestone is indistinguishable from that at Lisheen or Newcastle West: the fine-grained components such as the micrite (Plates 6.9a and 6.9b) and the bryozoans are replaced first followed by the other cement phases. However, in north Co. Cork the intermediate stage between partial dolomitisation and pervasive dolomitisation has been preserved. In some samples fine-grained dolomite is found partially replacing the CFC cements (Figure 6.9b). At Lisheen and Newcastle West the CFC cements were either untouched or completely replaced by dolomite. The coarse-grained dolomite, which is commonly found replacing the Stage D cements (Plate 6.10a), has a similar luminescence signature to that of the fine-grained dolomite (Plate 6.10b). Most of the coarse dolomite crystals have turbid inner cores and more limpid outer zones (Plates 6.10a and 6.12a).

Within pervasively dolomitised samples from Subulter, isolated relict crystals of the pre-dolomite quartz generation can be observed (Plate 6.11a). They are difficult to locate in PPL and are more easily observed under CL (Plate 6.11b). As mentioned above, when extracted from pervasively dolomitised samples, they generally have ragged outlines. This implies that the dolomitisation of these limestones involved some dissolution or replacement of silica because in the partially dolomitised samples these quartz crystals have euhedral outlines (Plate 6.8a). The abundant post-dolomite quartz crystals have well-developed planar crystals faces; they commonly infill the vugs contained within the dolostone (Plates 6.12a and 6.12b).

6.4 PARAGENESIS

The paragenetic sequence seen in Mallow and Fermoy is illustrated in Figure 6.3. The early calcite cements, Stages A-D, occur within the centres of early cavities. Stage D is the final porosity occluding cement. A generation of quartz that pre-dates the precipitation of dolomite and post-dates at least the CFC cements is found within partially dolomitised samples from Mallow but not from Fermoy. Dolomitisation occurred after all of the porosity was occluded within these rocks. During the initial stages of dolomitisation the fine-grained dolomite selectively replaced the micrite and the bryozoans within all samples and within certain samples some CFC cements also. This was followed by replacement by the coarse-grained dolomite, although some overlap in the replacement by these two dolomite components may have occurred. Large quartz crystals occur growing into vugs that were probably created by the dolomitisation process. These are referred to as the post-dolomite quartz. Late pink plug dolomite is also found infilling vugs created by dolomitisation. Samples containing both the post-dolomite quartz generation and the pink plug dolomite were not observed and so their relationship was not determined.

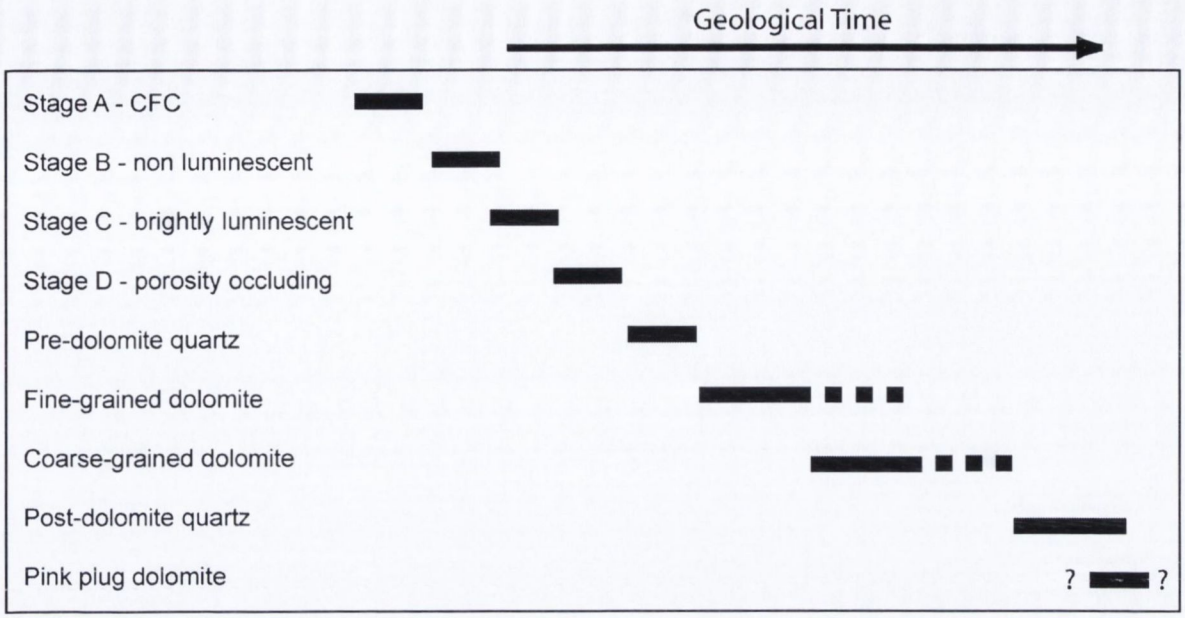

Figure 6.3 The paragenetic sequence as seen in the samples from Mallow and Fermoy.

6.5 FLUID INCLUSION MICROTHERMOMETRY

Three phases were isolated for fluid inclusion microthermometry analysis: the pre-dolomite quartz, the coarse-grained dolomite and the post-dolomite quartz (Appendix C). All of the fluid inclusion data from north Co. Cork were obtained from the Subulter quarry samples. Wafers were made from many of the partially dolomitised drillcore samples from Fermoy and Buttevant but none yielded workable fluid inclusions.

Pre-dolomite quartz fluid inclusion petrography

The analysis of fluid inclusions within the pre-dolomite quartz generation at Subulter was difficult because of the scarcity of the quartz crystals. Wafers commonly contained only a few quartz crystals and in many cases none included fluid inclusions. Where found, the inclusions measured were all two-phase (L+V) inclusions that homogenised into the liquid phase. They ranged in size from 1 to 22μm, with an average of 7μm and had a ψ_{liquid} of mostly either 0.85 or 0.9 (except for one inclusion with a ψ_{liquid} of 0.8). Their shape was commonly subhedral, with the majority being elongate. In terms of classification, many of the fluid inclusions contained within the pre-dolomite quartz at Subulter, lay parallel to growth zones still visible within the quartz crystals and so a primary origin was assumed. One six-sided fluid inclusion (negative crystal) was also observed within the samples (Plate 6.13). This was also taken as evidence to suggest entrapment during the growth of these quartz crystals.

Pre-dolomite quartz fluid inclusion microthermometry

A total of eleven fluid inclusions were measured from the pre-dolomite quartz at Subulter. Their Th values ranged from 105 to 149°C. First melting temperatures indicate that all the inclusions were part of the NaCl-$CaCl_2$-H_2O ternary system. The Tm_{ice} and Tm_h data indicate a salinity of 25 combined wt% NaCl and $CaCl_2$ equivalent.

Dolomite fluid inclusion petrography

The coarse-grained, white dolomite crystals at Subulter contained large numbers of fluid inclusions, the majority of sub-micron size. Most of the workable fluid inclusions were found within the inner turbid cores of the coarse dolomite crystals (Plate 6.14) but some were also found in the clearer outer rims. All were two-phase (L+V) inclusions that ranged in size from 1.5 to 20μm (mean of 7μm) and had a ψ_{liquid} of either 0.8 or 0.9 (with three inclusions having a ψ_{liquid} of 0.85). They were mostly subhedral or euhedral (negative) in shape and commonly lay in an orientation parallel to the dolomite crystal faces, which were also coincident with the CL growth zones. Many of the larger inclusions also lay parallel to the trails of sub-micron sized inclusions.

Dolomite fluid inclusion microthermometry

A total of thirty fluid inclusions were measured from the coarse-grained dolomite at Subulter. Their Th values ranged from 109.2 to 160.1°C. First melting temperatures indicate that all the inclusions were part of the NaCl-$CaCl_2$-H_2O ternary system. The salinity data indicate an average of 23.8 combined wt% NaCl and $CaCl_2$ equivalent.

Post-dolomite quartz fluid inclusion petrography

Despite the abundance of the post-dolomite quartz, the number of quartz crystals that contained fluid inclusions was small. Where observed, all were two-phase (L+V) inclusions that ranged in size from 6 to 35μm (mean of 15μm) and had a consistent ψ_{liquid} of 0.9. They were mostly subhedral in shape with two of the inclusions having well-developed euhedral (negative crystal with six sides) shapes. Classifying the fluid inclusions within the post-dolomite quartz was made difficult as the host quartz crystals were large (up to 10mm in length) and the numbers of inclusions contained therein were few. The use of negative crystal shapes as a criterion for the identification of primary inclusions is not advisable (Goldstein, 2003). However, as some of the inclusions with negative crystal

shapes were also six-sided (Plate 6.15) it was concluded that these crystals were likely to have been trapped during the growth of the quartz crystals and so were probably primary. One trail of petrographically later fluid inclusions (secondary) was observed within the assemblage and measured. These inclusions were all 4μm in size with ψ_{liquid} of 0.9.

Post-dolomite quartz fluid inclusion microthermometry

A total of ten fluid inclusions were measured from the post-dolomite quartz at Subulter. Of these, six were primary fluid inclusions and four were part of a trail of secondary fluid inclusions. The primary fluid inclusions had Th values that ranged from 78 to 87.4°C and the secondary fluid inclusions had Th values that ranged from 103.1 to 140.5°C. The first melting temperatures of the primary fluid inclusions indicate that they were part of the $NaCl\text{-}CaCl_2\text{-}H_2O$ ternary system and Tm_{ice} and Tm_h data indicate a salinity of 19.2 combined wt% NaCl and $CaCl_2$ equivalent. No salinity data were obtained from the secondary fluid inclusions.

Implications for the Th of the fine-grained dolomite

No fluid inclusion data were obtained from the fine-grained dolomite, as the crystals were too small and turbid. Despite this, the paragenetic relationship between the dolomite and the pre-dolomite quartz can be used to infer the temperature of formation of the fine-grained dolomite. As the fine-grained dolomite was precipitated after the pre-dolomite quartz generation and before the coarse white dolomite, it can be assumed that the homogenisation temperature of the fine-grained dolomite lies between that of the pre-dolomite quartz and the coarse dolomite and therefore is above 105°C. This moderately high temperature of formation for the fine-grained dolomite at Subulter is similar to that inferred for Newcastle West (>131°C) and implies that dolomitisation may have occurred at depth or been the product of a high temperature, hydrothermal fluid.

A note on the behaviour of the fluid inclusions from Subulter

The behaviour of many of the fluid inclusions from Subulter as they proceeded towards homogenisation was slightly different from what had been observed in other areas in this study. Normally when an inclusion is heated the bubble remains in constant motion within the vacuole. This is probably due to extremely rapid flow at the bubble's surface due to contrasts in surface tension caused by infinitesimally small thermal gradients (Roedder, 1984). However, what was observed in many of the fluid inclusions measured from

Subulter (independent of the host mineral) was that the bubble remained stationary within the same part of the vacuole and decreased in size as the temperature increased. This made obtaining Th measurements, especially from small inclusions, more difficult. Therefore, in order to determine the Th of such inclusions the cycling technique outlined in Goldstein and Reynolds (1994) was employed. This proved successful as all of the inclusions measured were high salinity inclusions which, according to Goldstein and Reynolds (1994), usually only require a few degrees of under-cooling for the bubble to reappear.

Discussion

The fluid that precipitated the pre-dolomite quartz at Subulter was moderately hot (105 to 149°C) and very saline (25 combined wt% NaCl and $CaCl_2$ equivalent). The fluid that precipitated the coarse-grained white dolomite was also moderately hot (109.2 to 160.1°C) and very saline (23.8 combined wt% NaCl and $CaCl_2$ equivalent). These similar fluid inclusion data may be coincidence or may perhaps suggest that these two phases are genetically linked. Stable isotope data and halogen geochemistry are likely to determine whether there is any link between these two phases and are discussed in Sections 6.6 and 6.8 below.

The post-dolomite quartz generation was precipitated from a low temperature (78 to 87.4°C), high salinity (19.2 combined wt% NaCl and $CaCl_2$ equivalent) fluid. As this quartz generation clearly post-dates the formation of the dolomite there are no constraints on its age. It may therefore have been precipitated by a post-Variscan, perhaps Mesozoic, fluid.

The lower Th of post-dolomite quartz generation in relation to the other phases could be explained in more then one way. One explanation is that the post-dolomite quartz generation was precipitated during the waning phase of a hydrothermal (*sensu* Machel and Lonnee (2002)) cycle whose previously higher temperature history included the precipitation of the pre-dolomite quartz and the coarse dolomite. If this were the case the parental fluid from which the post-dolomite quartz precipitated would be expected to have an isotopic composition only slightly modified from that of the parental fluid of the coarse dolomite.

An alternative explanation is that the fluids responsible for precipitating the pre-dolomite quartz, coarse dolomite and post-dolomite quartz were geothermal (*sensu* Machel and Lonnee (2002)). In that case, the post-dolomite quartz would have formed at a shallower depth than the coarse dolomite. It is known that peak temperatures attained by Carboniferous rocks in the Mallow area correspond to a Conodont Alteration Index (CAI) of 5 or >5 and a vitrinite reflectance of 5% (Clayton *et al.*, 1989), that is around 300°C (Merriman & Kemp, 1997). There is no evidence in the local stratigraphy of the intra Carboniferous uplift of the several hundred metres that would be required to account for the difference of several 10's of degrees Celsius between the coarse dolomite and the post-dolomite quartz. Therefore it follows that either the pre-dolomite quartz and the coarse dolomite formed before Variscan inversion and the post-dolomite quartz after Variscan inversion, or all three phases were post inversion.

This is supported by looking at the cumulative thickness of the Carboniferous rocks (both on and offshore) that would have lain above the point of post-dolomite quartz precipitation (~3.8km) and comparing this value to the calculated thickness based on a 10°C surface temperature and a conservative geothermal gradient of 25°C/km (~2.8km). This 1km difference between the measured and the calculated thicknesses may be accounted for by uplift and erosion associated with Variscan inversion (latest Carboniferous to early Permian (Graham, 2001)) and suggests that these quartz crystals may have formed from a fluid that was Mesozoic in age. If this hypothesis is correct then it is likely that the source of the salinity within the post-dolomite quartz fluid inclusions may have come from the dissolution of Mesozoic evaporites and the halogen geochemistry data from the fluid inclusions within the post-dolomite quartz should highlight this.

The trail of secondary inclusions within the post-dolomite quartz, were formed from a higher temperature fluid (103.1 to 140.5°C) than the one that precipitated the quartz. This fluid is therefore probably not related to the low temperature parental fluid that precipitated the quartz and may be evidence of a later heating event.

6.6 STABLE ISOTOPE GEOCHEMISTRY

Twenty-three samples of unaltered Waulsortian Limestone and thirty-one samples of dolomitised Waulsortian Limestone from both Mallow (Buttevant and Subulter) and

Fermoy were sampled for stable isotope analysis. Individual pre-dolomite and post-dolomite quartz crystals were also sampled from Subulter and their isotopic compositions determined (Appendix B). A full description of the sampling methods is given in Chapter 2.

6.6.1 Calcite

The phases of the Waulsortian Limestone that were sampled for stable isotope geochemistry were micrite, CFC and Stage D cements (the final porosity occluding cement phase). Nowhere in the samples that were available was the bright yellow luminescent cement Stage C sufficiently developed to enable pristine samples to be isolated.

The $\delta^{13}C$ values of all three phases of calcite sampled from Mallow (Figure 6.4) range from 2.69 to 4.09‰ (mean 3.39‰ ± 1.02‰ 2σ; mode 3‰) and the $\delta^{18}O$ values range from 24.1 to 26.99‰ (mean 26.04‰ ± 1.88‰ 2σ; mode 26‰).

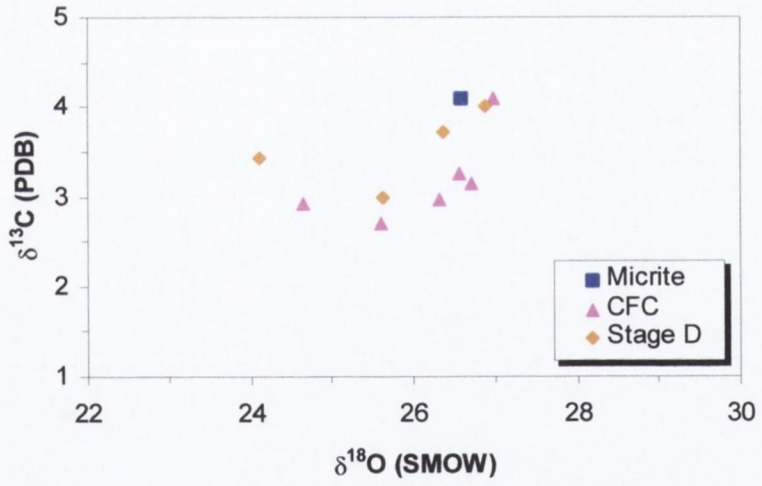

Figure 6.4 Scatter plot of $\delta^{13}C$ and $\delta^{18}O$ values for micrite and early calcite cement phases at Mallow.

The $\delta^{13}C$ values of all three phases of calcite sampled from Fermoy (Figure 6.5) range from 2.74 to 4.06‰ (mean 3.61‰ ± 0.8‰ 2σ) and the $\delta^{18}O$ values range from 24.71 to 28.66‰ (mean 27.14‰ ± 2.56‰ 2σ with modes of 26.6‰ and 28.7‰).

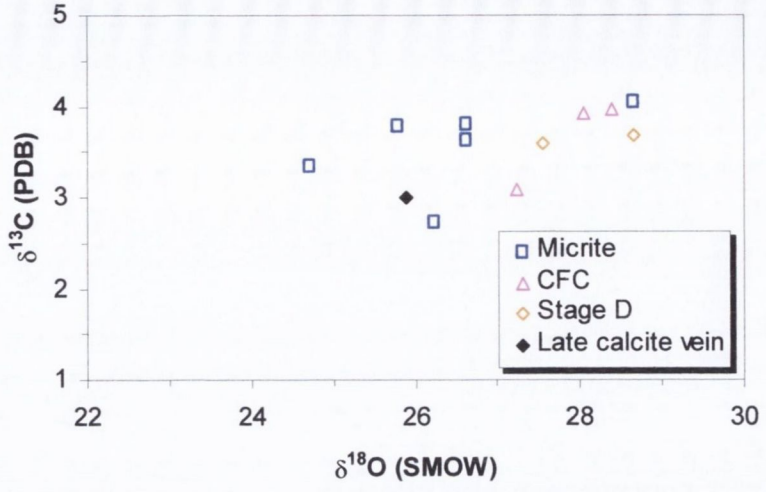

Figure 6.5 Scatter plot of $\delta^{13}C$ and $\delta^{18}O$ values for micrite and early calcite cement phases at Fermoy.

The range in isotopic values from both Mallow and Fermoy is similar to the Waulsortian Limestone micrite and early calcite cements at Lisheen (Chapter 3, Figure 3.4) and elsewhere in the Irish Midlands (Boast *et al.*, 1981a; Gallagher *et al.*, 1992). One sample of late calcite within a vein that cross-cut all cement phases at Fermoy was also sampled. It had a $\delta^{13}C$ value of 3‰ and a $\delta^{18}O$ value of 25.89‰ (Figure 6.5).

Discussion

The samples of Waulsortian Limestone from Fermoy were generally more micritic than those from Mallow. This meant that the number of micrites sampled from Mallow (n=1) was less than those sampled from Fermoy (n=6). In general the $\delta^{18}O$ data for the early calcite cements from Fermoy are isotopically heavier than those from Mallow but still remain within the normal range for Waulsortian Limestone. The single late calcite data point from Fermoy is consistent with the $\delta^{18}O$ data for the micrite but is slightly lighter than the early calcite $\delta^{18}O$ values. As this phase is only represented by one data point it is impossible to interpret this observation.

6.6.2 Dolomite

The isotopic data from both the fine-grained and coarse-grained dolomites at Mallow have been plotted in Figure 6.6. The $\delta^{13}C$ values for both the fine and coarse dolomite range from 3.64 to 4.64‰ (mean 4.21‰ ± 0.7‰ 2σ) and 2.97 to 4.61‰ (mean 3.5‰ ± 1.2‰

2σ; mode 3.1‰) respectively. The $\delta^{18}O$ values for the fine dolomite ranges from 21.91 to 24.57‰ (mean 23.52‰ ± 1.9‰ 2σ; mode 24.2‰) and the $\delta^{18}O$ values for the coarse dolomite ranges from 22.3 to 24.89 (mean 23.96‰ ± 1.86‰ 2σ; mode 24‰). Four pink plug dolomite samples were also analysed. Their $\delta^{13}C$ values range from 4.15 to 4.58‰ (mean 4.42‰ ± 0.42‰ 2σ) and their $\delta^{18}O$ values from 22.95 to 24.98‰ (mean 24.19‰ ± 1.74‰ 2σ; mode 24‰). These $\delta^{18}O$ data are similar to those obtained for pink plug dolomite at Lisheen by Eyre (1998) but the $\delta^{13}C$ data are heavier (Figure 6.6).

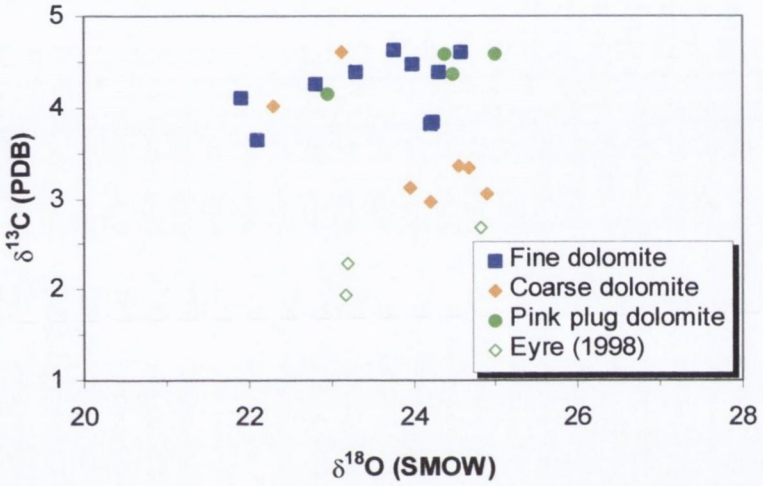

Figure 6.6 Scatter plot of $\delta^{13}C$ and $\delta^{18}O$ values for the dolomites at Mallow, which includes data from Eyre (1998) for the pink plug dolomite at Lisheen.

The isotopic data from both the fine-grained and coarse-grained dolomites at Fermoy have been plotted in Figure 6.7. The $\delta^{13}C$ values for both the fine and coarse dolomite range from 2.99 to 4.11‰ (mean 3.66‰ ± 0.96‰ 2σ) and 3.58 to 4.03‰ (mean 3.76‰ ± 0.4‰ 2σ) respectively. The $\delta^{18}O$ values for the fine dolomite ranges from 24.52 to 26.32‰ (mean 25.54‰ ± 1.7‰ 2σ and a mode 26‰) and the $\delta^{18}O$ values for the coarse dolomite ranges from 21.3 to 23.72 (mean 22.93‰ ± 1.72‰ 2σ; mode 23‰).

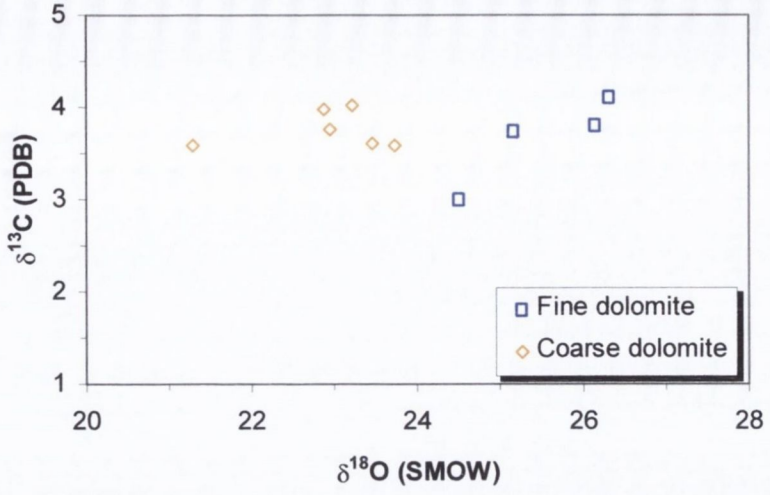

Figure 6.7 Scatter plot of $\delta^{13}C$ and $\delta^{18}O$ values for the dolomites at Fermoy.

Discussion

The micrite and early calcite data from Mallow show a consistent shift to lighter $\delta^{18}O$ values upon dolomitisation. This shift is in the order of -2‰ for both the Stage D cements and the micrite. In contrast the $\delta^{18}O$ data for the samples from Fermoy are not as straightforward. There is overlap between the $\delta^{18}O$ values of the micrite and the fine dolomite, which suggests that either the dolomitised micrite was not fully dolomitised and some residual micrite remained or that the micrite itself contained some dolomite that was not detected under CL. The $\delta^{18}O$ values of the coarse-grained dolomite from Fermoy are consistent with what has been observed in other areas of Regional Dolomite (Hitzman *et al.*, 1998), although when compared to the $\delta^{18}O$ values of early calcite cements, they represent a large shift to lighter values. This large shift, which is on the order of 5-6‰, may have been biased by the small number of early calcite samples for which $\delta^{18}O$ data was obtained.

Is there a geographical trend in the dolomite $\delta^{18}O$ data?

As stated above, the quarry at Subulter played a pivotal role in the argument put forward by Hitzman *et al.* (1998) that there was a south to north trend in the $\delta^{18}O$ values of the two components of the Regional Dolomite (dolomitised micrite and coarse dolomite). They used this as evidence in support of a model involving topographically driven, northward moving, fluid flow to explain the origin of the Regional Dolomite and the associated Zn-Pb mineralisation. The $\delta^{18}O$ values Hitzman *et al.* (1998) obtained from Subulter were lighter

than those found elsewhere in the Irish Midlands. However, data from this study does not support these findings. Hitzman *et al.* (1998) also inferred temperatures of formation of the Regional Dolomite at Subulter by assuming the isotopic composition of the parental fluid. Fluid inclusion analyses from this study show that the temperature of formation of the coarse dolomite is generally higher than that calculated by Hitzman *et al.* (1998). However, the lower end of the measured temperature range in this study for both the pre-dolomite quartz and the dolomite are similar to that estimated by Hitzman *et al.* (1998).

Figure 6.8 shows a plot of the $\delta^{18}O$ values for the dolomitised micrite (Figure 6.8a) and coarse dolomite (Figure 6.8b) components of the Regional Dolomite versus distance from Mallow (Subulter) for four of the localities from the Hitzman *et al.* (1998) study. Also shown are the $\delta^{18}O$ values for the dolomitised micrite (Figure 6.8c) and coarse dolomite (Figure 6.8d) obtained from Mallow (Subulter), Fermoy, Lisheen and Urlingford in this study.

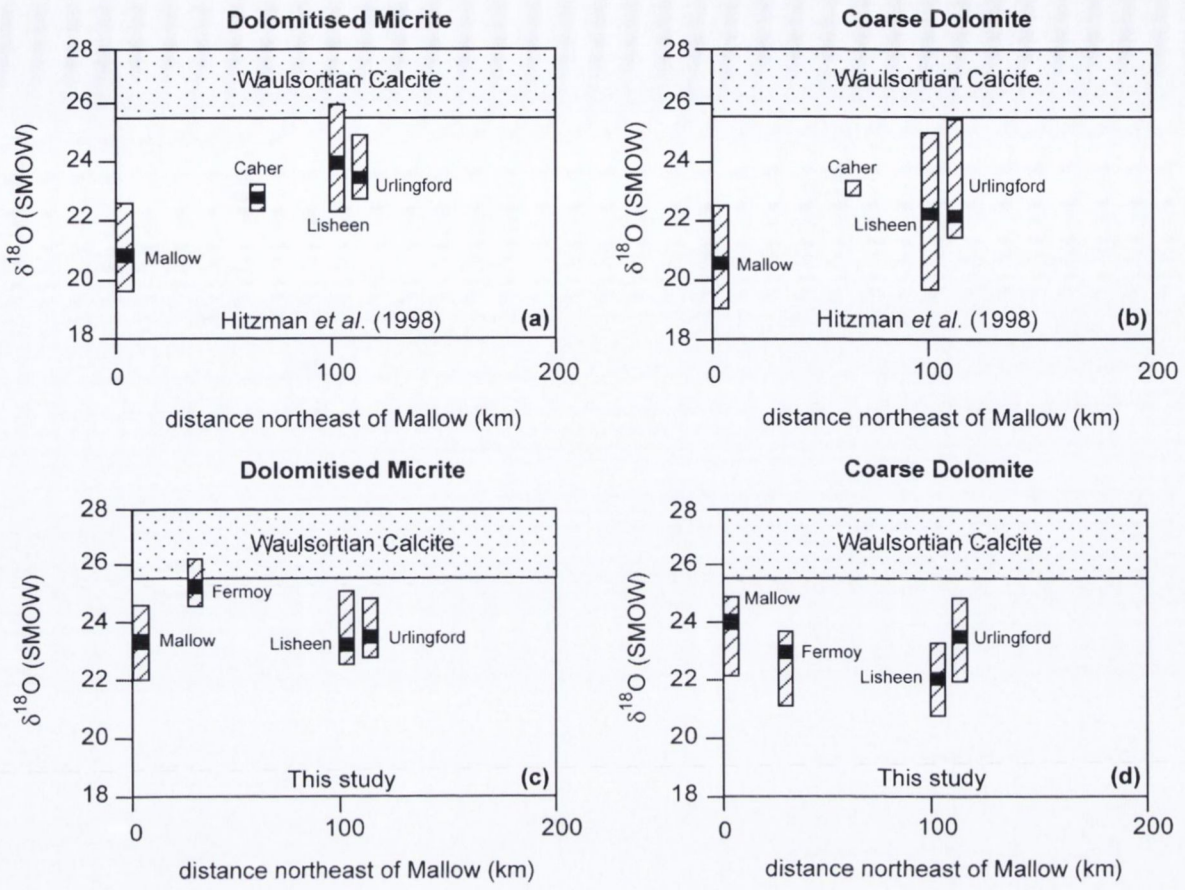

Figure 6.8 Plots of $\delta^{18}O$ values versus distance from Mallow (Subulter) for the (a) dolomitised micrite and (b) coarse dolomite from the Hitzman *et al.* (1998) study and the (c) dolomitised micrite and (d) coarse dolomite from this study.

The data from this study do not support the south to north trend shown in Figures 6.8a and 6.8b (Hitzman *et al.*, 1998). Figure 6.8c shows that there is little difference in the $\delta^{18}O$ data from the dolomitised micrite at Urlingford, Lisheen and Subulter and that no south to north trend exists. Surprisingly Figure 6.8d (with the exception of the Urlingford data) displays an inverse trend in the $\delta^{18}O$ values of the coarse dolomite as the mean values appear to become lighter from south to north. There is therefore no validity in the suggestion that there is a systematic regional variation in the isotopic signatures of the components of the Regional Dolomite.

6.6.3 Pre-dolomite quartz

Six individual pre-dolomite quartz crystals from Subulter were extracted and analysed using laser fluorination to obtain their $\delta^{18}O$ values. The $\delta^{18}O$ values ranged from 17.14 to

19.08‰ (mean of 17.93‰ ± 1.42‰ 2σ). One sample (sample 4) was slightly heavier than the other samples (19.08‰). It is possible, based on these data, that this is a post-dolomite quartz crystal although during sample selection this crystal did not look like a post-dolomite quartz crystal. If this sample were to be removed from the dataset there would be no significant change in the overall mean value (17.7‰) and the standard deviation would decrease only slightly (± 0.94‰ 2σ). As removing this data point does not produce any changes within the dataset that are likely to alter the overall interpretation of the $\delta^{18}O$ values of the pre-dolomite quartz it was decided not to consider it an outlier and to retain it within the dataset.

6.6.4 Post-dolomite quartz

Eighteen individual post-dolomite quartz crystals from Subulter were extracted and analysed using laser fluorination to obtain their $\delta^{18}O$ values. They had $\delta^{18}O$ values that ranged from 19.56 to 21.7‰ (mean of 20.72‰ ± 1.2‰ 2σ).

6.7 MODELLING OF PARENTAL FLUIDS

Using the equations of Land (1983) for dolomite and Matsuhisa *et al.* (1979) for quartz an average of the measured isotope values for the pre-dolomite quartz, coarse dolomite and post-dolomite quartz from Mallow was used to model their parental fluid compositions over a range of temperatures of precipitation (Figure 6.9). The standard deviations of the isotopic measurements of all three phases (0.7, 0.9 and 0.6 respectively) were thought to be within acceptable limits to justify the use of the average of these measurements in these equations. Using the homogenisation temperature ranges (105 to 150°C, 110 to 160°C and 80°C respectively), fluid compositions were calculated for all three phases.

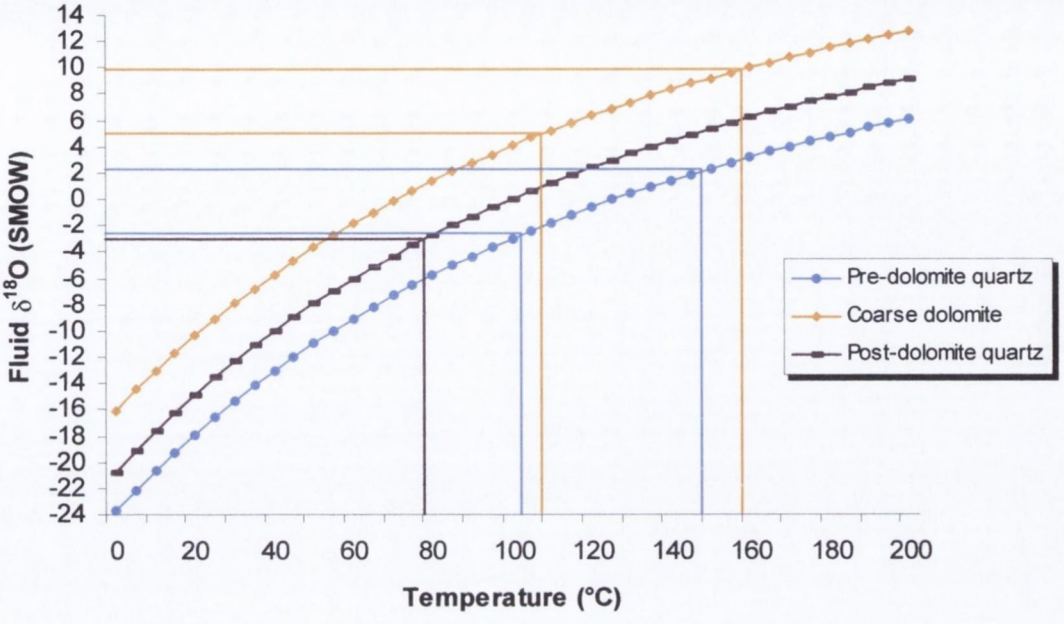

Figure 6.9 Mineral-water oxygen isotope fractionation curves for the pre-dolomite quartz, coarse dolomite and post-dolomite quartz at Mallow. See text for discussion.

Discussion

The pre-dolomite quartz has a modelled parental fluid with $\delta^{18}O$ values that range from –2.3 to 2.4‰. These values are thought to reflect pore waters of nearly unmodified Carboniferous seawater at the time of precipitation (0 ±1‰). The coarse dolomite values appear to suggest precipitation from a more modified parental fluid whose modelled $\delta^{18}O$ value ranges from 5.2 to 10‰. This suggests a fluid that has undergone a significant amount of fluid-rock interaction. The modelled parental fluid for the post-dolomite quartz has a $\delta^{18}O$ value of –2.8‰. This value is consistent with the range of –2 and –2.5‰, obtained by other workers for precipitation of marine carbonate during the Lower Cretaceous (Scholle & Arthur, 1980; Czerniakowski *et al.*, 1984; Moldovanyi & Lohmann, 1984).

6.8 HALOGEN GEOCHEMISTRY

Samples of pre-dolomite quartz, coarse dolomite and post-dolomite quartz from Subulter were prepared for crush-leach analysis using the method outlined in Chapter 2. The data are shown in Appendix D.

Figure 6.10 shows the calculated Cl and Br composition of the fluids within the pre-dolomite quartz and the coarse dolomite fluid inclusions. The post-dolomite quartz data are also plotted. However, as the levels of Br within the post-dolomite quartz fluid inclusions were below detection limits (<0.005mg/L), this data point represents a maximum possible Br value. Therefore the post-dolomite quartz may lie further to the left of where it has been plotted i.e. lower Br values but the same Cl values.

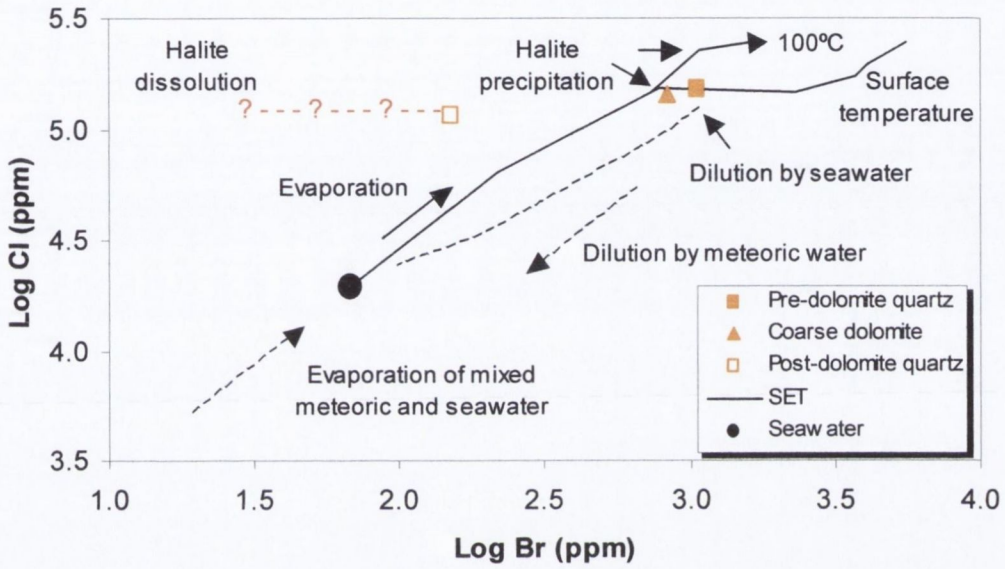

Figure 6.10 Cl and Br systematics of the pre-dolomite quartz, coarse-dolomite and post-dolomite quartz at Subulter. Plot also shows the SET (after Carpenter (1978) and Gleeson & Yardley (2002)).

The pre-dolomite quartz and coarse dolomite samples lie, within analytical uncertainty, on the SET and indicate that the fluids within these inclusions are residual brine, formed by the evaporation of seawater past the point of halite precipitation. The post-dolomite quartz has much lower Br values and slightly depleted Cl values relative to the other two samples. As mentioned above (Section 6.5) the post-dolomite quartz samples formed from a low temperature, saline brine that may have been Mesozoic in age. The Cl-Br data indicate that the fluid that precipitated the post-dolomite quartz was a Br-poor fluid, which may further support a Mesozoic age for this fluid, as the data are consistent with the possible dissolution of evaporites. If the Br values for the fluid inclusions within the post-dolomite quartz are substantially lower than the detection limits of the analysis, the data could plot within the halite dissolution field indicated in Figure 6.10.

A plot of the Na-Cl-Br systematics is shown in Figure 6.11. The Cl/Br and Na/Br molar ratios of the pre-dolomite quartz (325 and 203 respectively) and coarse dolomite (390 and 259 respectively) are consistent with a seawater-derived fluid, evaporated beyond the point of halite precipitation (Cl/Br of 446 and Na/Br of 326 (Fontes & Matray, 1993a)). The data also lie to the left of the SET and indicate that both fluids are slightly depleted in Na relative to seawater.

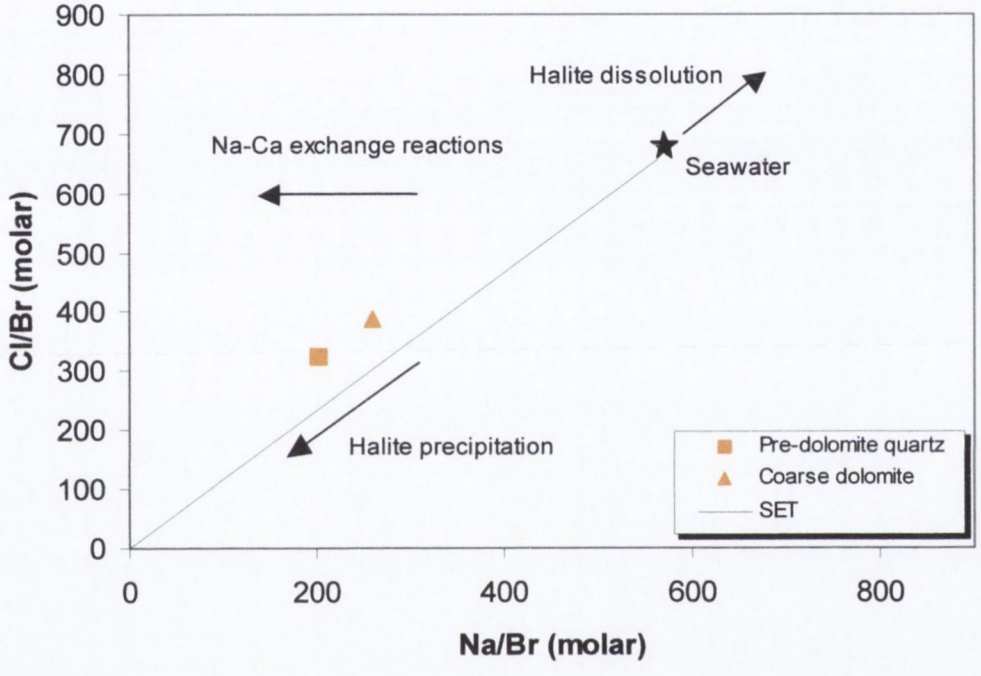

Figure 6.11 Cl-Na-Br systematics for pre-dolomite quartz and coarse dolomite fluid inclusions from Subulter. SET data after Kesler *et al.* (1995).

The post-dolomite quartz data are not plotted on Figure 6.11 because the Br values within the fluid inclusions were below the detection limits. However, were the lowest detectable limits (0.005mg/L) used to calculate the Na-Cl-Br molar ratios for the post-dolomite quartz a Cl/Br molar ratio of 1754 and a Na/Br molar ratio of 1572 would be obtained (Appendix D). These data would plot off the scale of Figure 6.11 but well into the halite dissolution field. This would again be consistent with the solutes within this brine having originated from the dissolution of evaporites.

Discussion

The halogen data indicate that the fluids, which precipitated both the pre-dolomite quartz and the coarse dolomite at Subulter, were probably residual brines, formed by the evaporation of seawater beyond the point of halite precipitation. In terms of the fluids associated with the Irish Zn-Pb deposits, the dolomitising and quartz-bearing fluids at Subulter are probably equivalent to Fluid 2. The microthermometric data from this study are also consistent with what is normally observed for Fluid 2.

The low Br values from the post-dolomite quartz generation suggest that these fluids may have been involved in halite dissolution. As extensive evaporite deposits are known to have formed during the Upper Permian and Lower Triassic in Ireland (Wilson *et al.*, 2001) this is further support for the hypothesis that the fluid, which precipitated the post-dolomite quartz crystals, may be Mesozoic in age.

The Cl/Br and Na/Br ratios indicate that the fluids, which precipitated both the pre-dolomite quartz and the coarse dolomite, were slightly depleted in Na relative to seawater. This may suggest that there has been a degree of Na-Ca exchange along the fluid flow pathway.

A note on the secondary inclusions in the post-dolomite quartz

As crush leach ion chromatography is a bulk fluid analysis it provides the average fluid composition of a given sample. Ideally, the sample concerned must be dominated by only one population of fluid inclusions (Gleeson, 2003). During microthermometry the post-dolomite quartz crystals showed evidence of some secondary inclusions. No salinity data was obtained from these inclusions and therefore the influence that these inclusions may have had on the bulk electrolyte analysis cannot be quantified. However, only one isolated trail of secondary inclusions was found within all of the post-dolomite quartz crystals examined. It is therefore assumed that these secondary inclusions are not volumetrically significant enough to effect the overall average fluid composition.

6.9 CONCLUSIONS

- The dolomite from North Cork is identical to the Regional Dolomite from Lisheen and elsewhere in the Rathdowney trend.

- Dolomitisation occurred after all the porosity within the Waulsortian Limestone lithosome had been occluded.

- The intermediate stage between partial dolomitisation and pervasive dolomitisation was observed in the North Cork samples as fine-grained dolomite was observed replacing CFC cements.

- A generation of quartz that pre-dated the onset of dolomitisation and post-dated the formation of at least the CFC cements was observed in both the partially dolomitised samples and as surviving relicts within pervasively dolomitised samples.

- A generation of quartz that post-dated the dolomitisation also occurred within the samples from North Cork. These quartz crystals are much larger and more lucid than the pre-dolomite quartz generation and therefore the two cannot be confused.

- Fluid inclusion data from both the pre-dolomite quartz and the coarse dolomite are broadly similar (105 to 149°C with 25 combined wt% NaCl and $CaCl_2$ equivalent and 109.2 to 160.1°C with 23.8 combined wt% NaCl and $CaCl_2$ equivalent respectively).

- In the absence of fluid inclusion data for the fine-grained dolomite, the paragenetic relationship between the dolomite and the quartz can be used to infer the homogenisation temperature data of the fine-grained dolomite. This suggests that the fine-grained dolomite formed at temperatures >105°C, which is substantially hotter than the <50°C suggested by other workers (Wright *et al.*, 2000; Gregg *et al.*, 2001) for the fine-grained dolomite found in the Irish Midlands and the Dublin Basin. This indicates that dolomitisation could not have occurred by the circulation of seawater during early diagenesis.

- Th and salinity data from the post-dolomite quartz indicate that this quartz generation was precipitated from a low temperature (78 to 87.4°C), saline (19.2 combined wt% NaCl and $CaCl_2$ equivalent) brine.

- Stable isotope data from both the undolomitised and dolomitised Waulsortian Limestone from North Cork are similar to other areas in this study and to those obtained by other workers. Data from this study suggest that there is no south to north trend in the $\delta^{18}O$ values of the dolomite.

- Isotopic data from the coarse-grained dolomite indicated a range in parental fluid $\delta^{18}O$ values of 5.2 to 10‰ and suggests that these dolomitising fluids underwent significant fluid rock interaction.

- Isotopic data from both the pre-dolomite quartz and post-dolomite quartz was obtained and indicated a range in the $\delta^{18}O$ values of the parental fluid of –2.3 to 2.4‰ for the pre-dolomite quartz and a value of –2.8‰ for the post-dolomite quartz. The pre-dolomite quartz values are broadly consistent with Carboniferous seawater values (0 ±1‰) at the time of precipitation. The post-dolomite quartz values are similar to estimates of Lower Cretaceous seawater.

- Halogen geochemistry data indicate that the fluids that precipitated both the pre-dolomite quartz and the coarse dolomite were originally seawater that had been evaporated at the surface beyond the point of halite precipitation (Fluid 2). The solutes within the fluid inclusions in the post-dolomite quartz originated from the dissolution of evaporites. This further supports the hypothesis that these quartz crystals formed from a low temperature, saline brine that was probably Mesozoic in age.

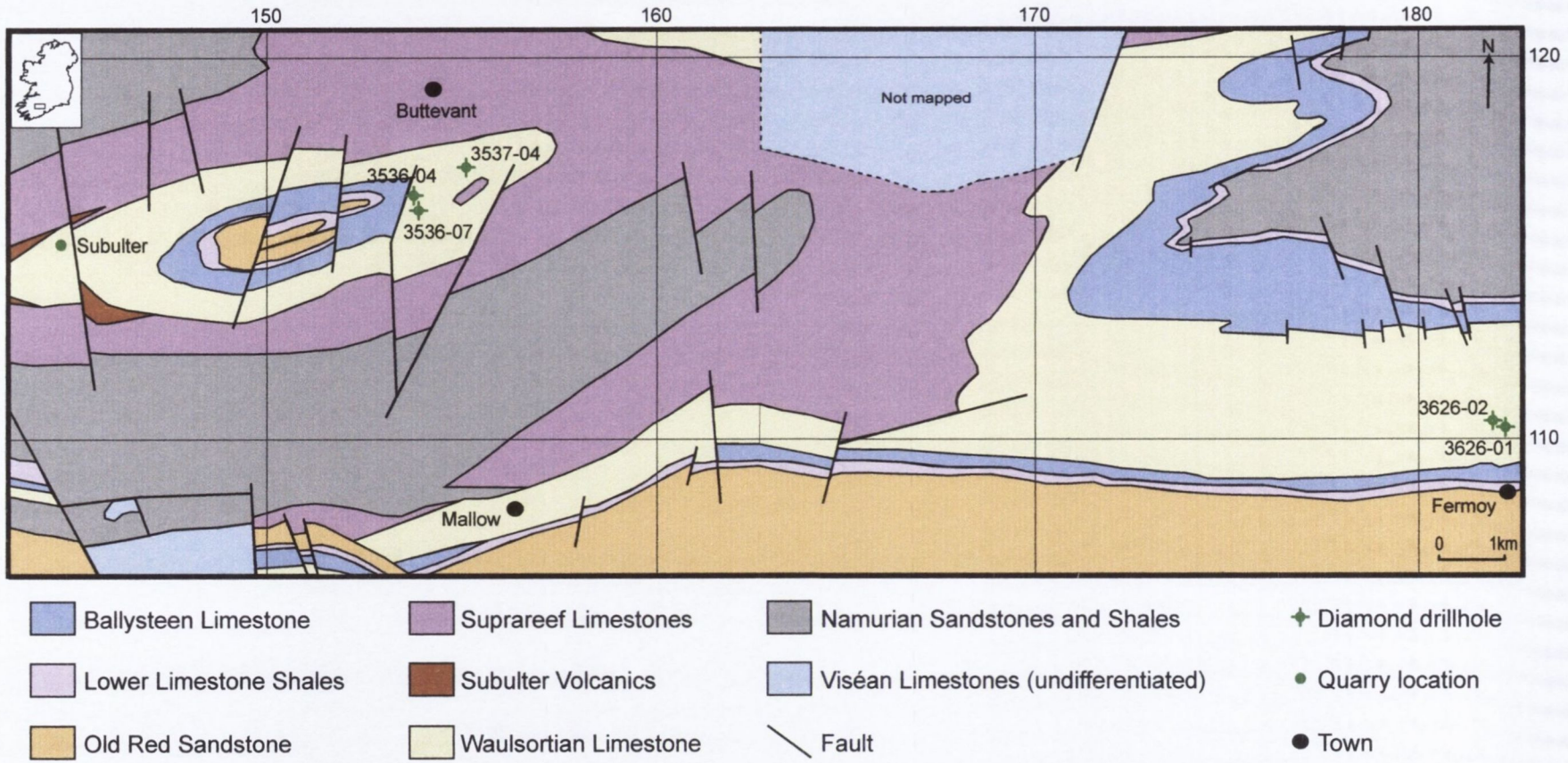

Figure 6.1 A simplified geological map of north Co. Cork showing the locations of Subulter quarry and the drillholes studied. Grid lines refer to the Ordnance Survey of Ireland National Grid. Modified after Sleeman and McConnell (1995) and Pracht (1997).

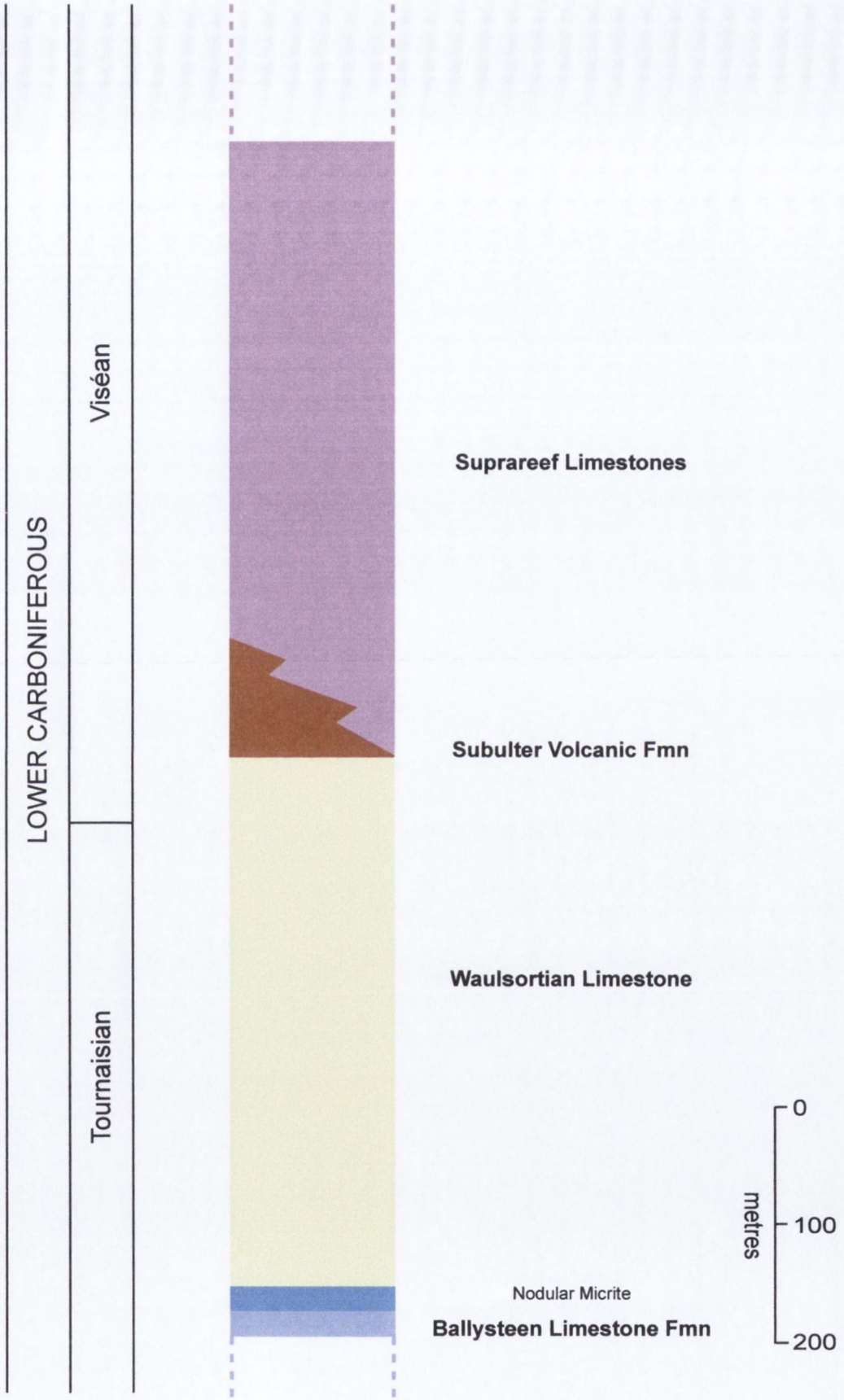

Figure 6.2 Stratigraphic section of the Buttevant area based on data from Hudson and Philcox (1965), Campbell (1988), Gallagher and Somerville (1997) and the 3536-04 drillhole from this study.



Plate 6.1: Vuggy dolomite sample from Subulter Quarry. Co. Cork. The vugs are lined with large quartz crystals that post-date the dolomite. Size of coin is 22mm.



Plate 6.2: Some of the vugs appear aligned in bands within the dolostone. Lens cap is 52mm in diameter.



Plate 6.3: Euhedral quartz crystals that post-date the dolomite and occur ubiquitously within all of the vugs. Note the limpid nature of the crystals. Scale bar is 250mm.



Plate 6.4: View of the pink plug dolomite that is contained within some of the vugs at Subulter. Lens cap is 52mm in diameter.

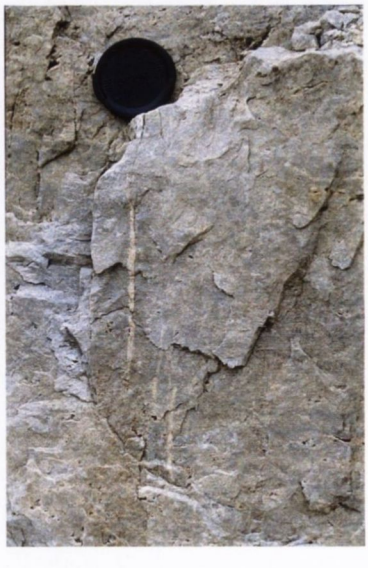

Plate 6.5: View of a vertical en échelon vein set that has been infilled with pink plug dolomite. Lens cap is 52mm in diameter.



Plate 6.6: View of an en échelon vein set filled by coarse white dolomite. The set is orientated 340/60°E. The arrows on the image highlight the array as it continues to step eastwards.

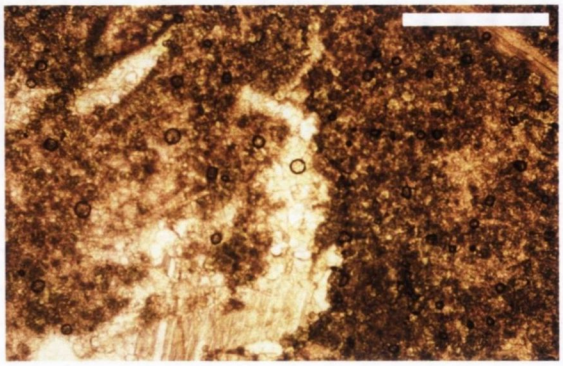

Plate 6.7a: P17549 - Lag 3537-04 (71.7 - 71.88m). PPL view of an early calcite-filled cavity partially replaced by fine dolomite. Scale bar is 500µm.

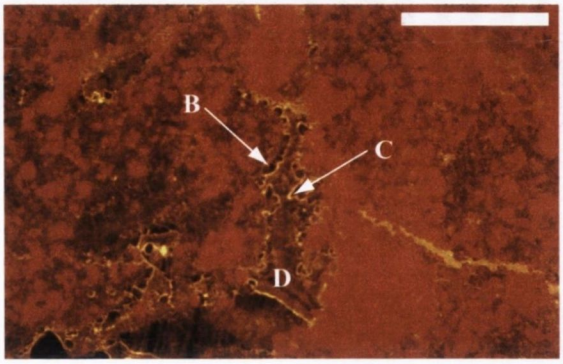

Plate 6.7b: Same view in CL. Stages B-C are labelled. Stage D is the final porosity occluding cement. Dolomitisation occurred after the precipitation of Stage D and is therefore post porosity occlusion. Scale bar is 500µm.

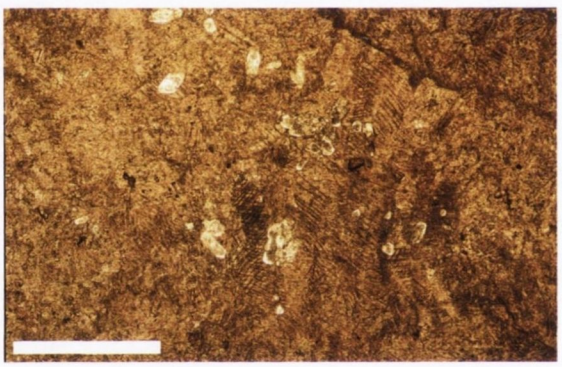

Plate 6.8a: P17549 - Lag 3537-04 (71.7 - 71.88m). PPL view of euhedral quartz crystals contained with the CFC cements. These are the pre-dolomite quartz generation. Scale bar is 500µm.

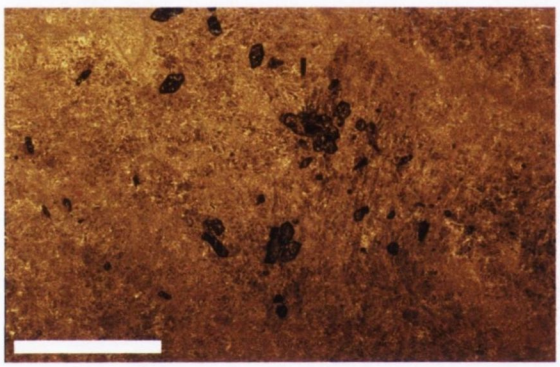

Plate 6.8b: Same view in CL. All of the quartz crystals are non-luminescent under CL. These quartz crystals can be up to a maximum of 5mm in length. Scale bar is 500µm.

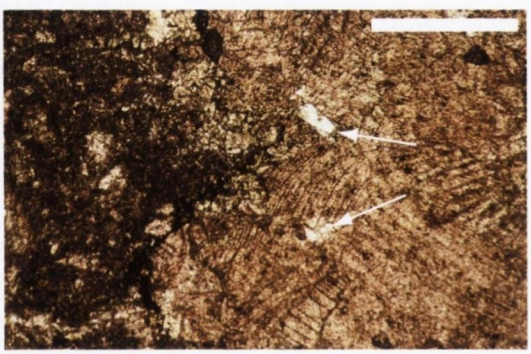

Plate 6.9a: P17549 - Lag 3537-04 (71.7 - 71.88m). PPL view of the pre-dolomite quartz (arrowed) within CFC and the fine-grained dolomite replacing the CFC. Scale bar is 500µm.

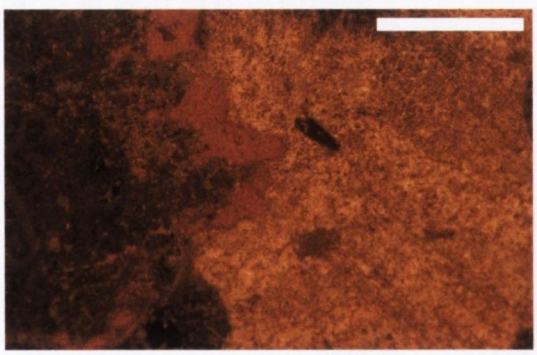

Plate 6.9b: Same view in CL. CFC is partially replaced by dolomite. Scale bar is 500µm.

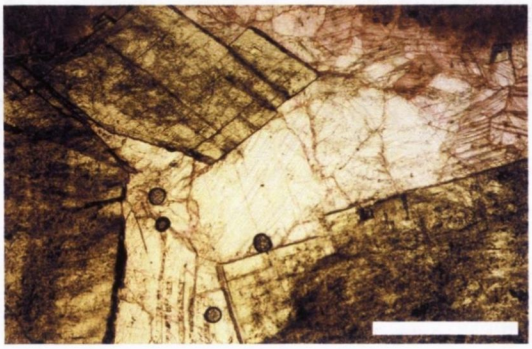

Plate 6.10a: P17545 - Curtin's Farm 3626-02 (54 - 54.1m). PPL view of the coarse dolomite replacing Stage D calcite. Scale bar is 500µm.

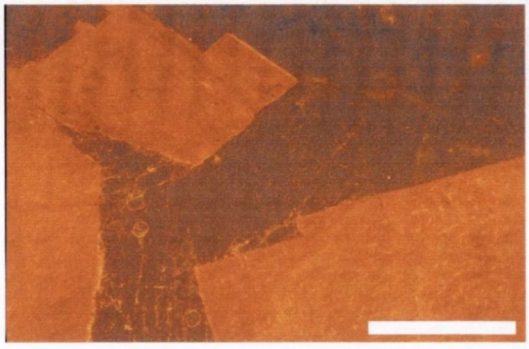

Plate 6.10b: Same view in CL. Note the homogeneous luminescence of the coarse dolomite crystals which is similar to that of the fine dolomite. Scale bar is 500µm.

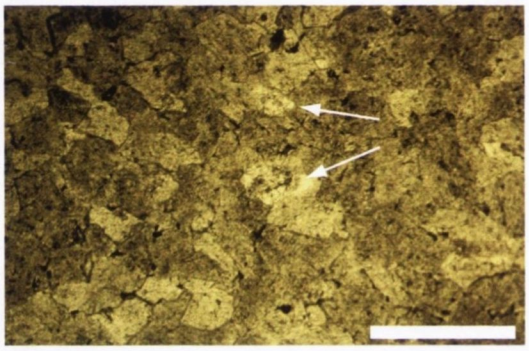

Plate 6.11a: P17533 - Subulter Quarry. PPL view of the pre-dolomite quartz (arrowed). Note how the dolomitisation is almost complete making the quartz difficult to see. Scale bar is 500µm.

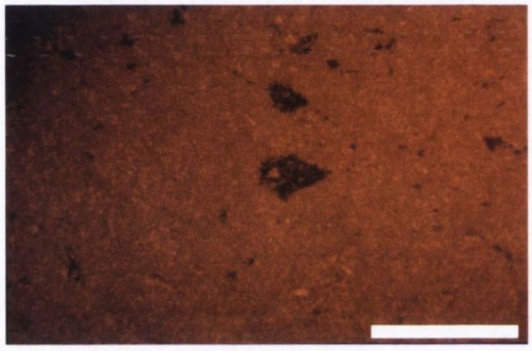

Plate 6.11b: Same view in CL. Note how the pre-dolomite quartz generation is easier to locate under CL. Scale bar is 500µm.

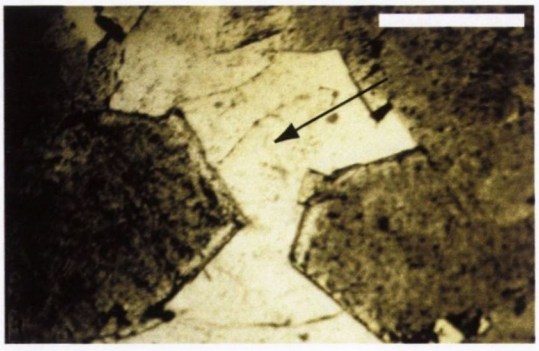

Plate 6.12a: P17533 - Subulter Quarry. PPL view of the post-dolomite quartz (arrow) that is found growing into vugs. Scale bar is 500µm.

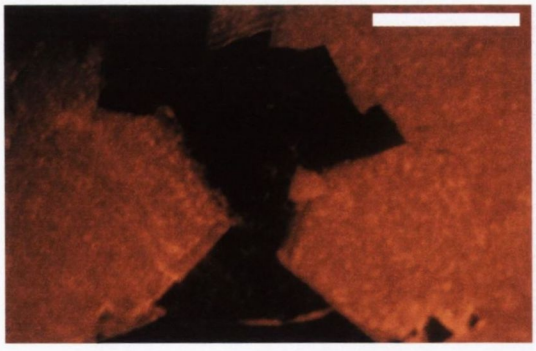

Plate 6.12b: Same view in CL. The quartz crystals can be 10mm in length and have well-developed euhedral shapes. Scale bar is 500µm.

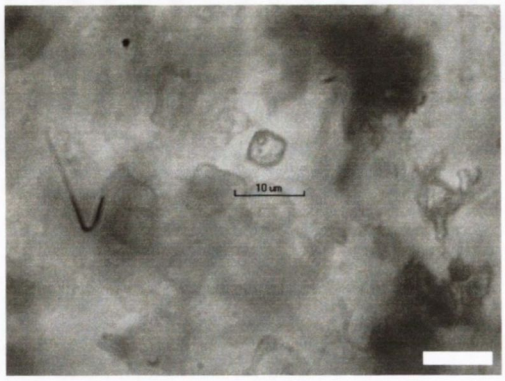

Plate 6.13: Image of the F.A.3 fluid inclusion contained within the pre-dolomite quartz. Note the negative shape of the inclusion and that it has six sides. Scale bar is 10μm.

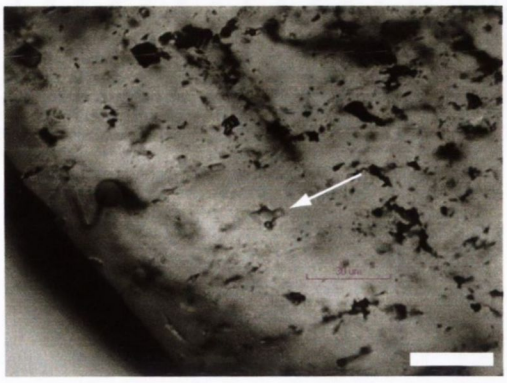

Plate 6.14: Image of the G.4.1 fluid inclusion contained within the inner zone of a coarse dolomite crystal (arrow). Note the negative shape of the inclusion. Scale bar is 30μm.

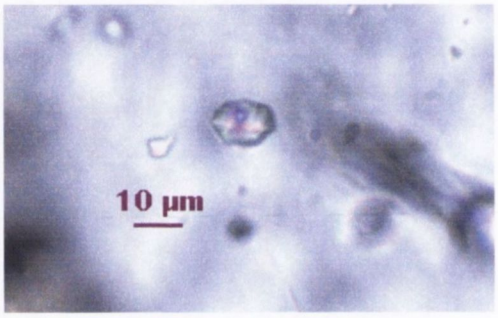

Plate 6.15: Image of the A.1.2 fluid inclusion contained within the post-dolomite quartz. Note the negative shape of the inclusion and that it has six sides. Scale bar is 10μm.

CHAPTER 7

CO. CARLOW

7.1 INTRODUCTION

Along the edge of the Leinster Granite the fossiliferous packstones and grainstones of the Ballysteen Limestone, which is in part stratigraphically equivalent to and in part older than the Waulsortian Limestone, have been pervasively dolomitised. A notable feature of the dolomite is the occurrence of large vugs similar to those found in dolomitised Waulsortian Limestone in the Rathdowney Trend. Some commentators have maintained that the latter represent the amplification of pre-existing stromatactis cavities within the Waulsortian Limestone. As the Ballysteen Limestone does not contain large primary cavities this explanation for the formation of the vugs is not tenable. A detailed examination of the dolomitisation of the Ballysteen Limestone was undertaken in order to understand the genesis of the large vugs and their link to dolomitisation. Petrographic studies have been based on a borehole drilled by the Geological Survey of Ireland in the townland of Quinagh (GR 2732 1744), approximately 2 kilometres southeast of Carlow town and an extensive quarry section at Clonmelsh (GR 2724 1702), approximately 5 kilometres northeast of Leighlinbridge (Figure 7.1).

7.2 REGIONAL GEOLOGICAL SETTING

7.2.1 Stratigraphy

The Leinster Granite batholith (Figure 7.1), the largest body of granite in Ireland, was emplaced during the early Devonian (405 ± 2 Ma; O'Connor *et al.* (1989)), towards the end of the Caledonian Orogeny. It is a two-mica peraluminous granite that is composed of several large plutons that are each distinguished by their mineralogy and texture. Lying unconformably above this granite are shallow marine mudstones and sandstones of the Porter's Gate Formation (Figure 7.2) whose basal beds, which are probably equivalent to the Ringmoylan Shale Formation (Sevastopulo & Wyse Jackson, 2001), include weathered granite clasts. The interbedded dark grey muddy limestones and calcareous shaley mudstones of the Ballymartin Formation overlie the Porter's Gate Formation, which are themselves overlain by the Ballysteen Limestone Formation. Late Viséan and Upper Carboniferous rocks outcrop to the west of Carlow town. These include Namurian sandstones and shales and Westphalian rocks of Langsettian (Westphalian A) age (Sevastopulo, 2001), which contain the paralic coal deposits that form the Leinster coalfield (Figure 7.1).

7.2.2 Structure

The Lower Carboniferous succession in the Carlow area is cut by a number of northwest-southeast trending faults (Figure 7.1). These faults also cut the Upper Carboniferous Leinster Coalfield to the west, which is known to be an elevated basin elongated in a north-south direction as a result of east-west compression (Tietzsch-Tyler & Sleeman, 1994). The whole Carboniferous succession in the Carlow area was folded into a series of very broad, shallow folds during the Variscan orogeny.

7.2.3 Dolomitisation

Dolomitisation of the Ballysteen limestone in the Carlow area has been pervasive. This is best illustrated in the quarry exposure at Clonmelsh. However, the Quinagh borehole preserves the transition from partially dolomitised to pervasively dolomitised Ballysteen Limestone and therefore provides an opportunity to observe the limestone lithosome and its cementation prior to and during the onset of dolomitisation.

7.3 PETROGRAPHY

Hand samples

The most striking feature of the pervasively dolomitised Ballysteen Limestone at both Quinagh and Clonmelsh is the occurrence of large vugs similar to those found in dolomitised Waulsortian Limestone throughout the Rathdowney Trend. They range in size from less than a centimetre to about 20 centimetres at maximum dimension and appear to be preferentially developed within particular beds (Plate 7.1). The vugs are rimmed, or less commonly completely infilled, by coarse-grained white dolomite, which is clearly later than the dark grey dolomite that makes up the bulk of the rock. In the majority of vugs, euhedral quartz crystals, some as large as 40mm in length, have grown from the surface of the coarse-grained, white dolomite into the open space remaining in the centre (Plate 7.2).

The coarse-grained, white dolomite also fills veins that are both parallel and normal to bedding; in many cases they can be seen to connect to the dolomite in the vugs (Plate 7.3). The veins also form the matrix of breccias that contain fragments of the dark grey dolomite (Plate 7.3). These breccias commonly display refittable fabrics and are likely to be the product of hydraulic fracturing (Plate 7.4). This style of brecciation is very similar to the

white matrix breccia described from the Lisheen deposit (Chapter 3, Section 3.2.3, (Hitzman *et al.*, 2002)).

In close spatial association with the coarse-grained, white dolomite is a development of coarse-grained, pink dolomite (Plate 7.5), similar to the 'pink plug' described from Lisheen (Chapter 3, Section 3.2.3) and North Co. Cork (Chapter 6, Section 6.3). The crystals of pink dolomite are up to 2mm in maximum dimension and clearly post-date the coarse-grained white dolomite (Plate 7.5).

Some samples from the Quinagh borehole contain rare crystals of fluorite (Plate 7.6). The largest of these is approximately 5mm in maximum dimension and all have a slight purple tinge. It is thought that the development of this fluorite may be directly related to fluid flow through the underlying granite.

Thin sections

As mentioned above, due to the pervasive nature of the dolomitisation process, occurrences of undolomitised Ballysteen Limestone at Clonmelsh were not observed. The discussion of the partially dolomitised Ballysteen Limestone is therefore restricted to the samples from the borehole at Quinagh.

Within the partially dolomitised samples from Quinagh there is little evidence of fragmentation of the bioclastic material. Long brachiopod shells, some up to 2mm in length, remain intact. This suggests that breakage due to compaction may have been prevented to some degree by early cementation. Stylolites and dissolution surfaces are common, especially in the more argillaceous parts of the succession.

The most notable feature of these partially dolomitised samples is the abundance of silicified fossils (Plates 7.7a and 7.7b). Brachiopods and echinoderm fragments are the most abundant and many have been partially replaced by length-slow fibrous quartz. Length-slow chalcedonic quartz is commonly associated with former evaporitic sulphate beds (Folk & Pittman, 1971). However, length-slow chalcedony is also known to occur within silicified fossils within non-evaporitic rocks (Jacka, 1974; Meyers, 1977).

Silicification of fossils by length-slow fibrous quartz has been used as one line of evidence to suggest the existence of extensive evaporite deposits adjacent to the Leinster Massif during the Viséan (Nagy *et al.*, 2002). Nagy *et al.* (2001) have suggested that the postulated evaporite deposits are the source of the excess chlorinity in the mineralising brines in the Irish orefield (Banks *et al.*, 2002). They have also invoked the reflux of the dense evaporitic seawater that would have arisen from these evaporites as the driving mechanism for the fluid(s) involved in the regional dolomitisation and base-metal mineralisation (Nagy *et al.*, 2002).

Developments of the earliest calcite cements within the partially dolomitised samples from Quinagh are rare and volumetrically minor. Where found they clearly pre-date the compaction and breakage of skeletal grains. The majority of the early calcite cement post-dates compaction and occludes all, or almost all, of the primary porosity within the limestones (Plates 7.8a and 7.8b). In accordance with what is seen in partially dolomitised Waulsortian Limestone samples throughout the Rathdowney Trend, dolomitisation within the Ballysteen Limestone clearly post-dates final porosity occlusion (Plate 7.8b). However, unlike the Regional Dolomite, the dolomite at Quinagh appears to replace the early calcite cements preferentially and to leave the bioclastic material untouched.

In thin section, the dark grey dolomite is a medium-grained planar dolomite that has a polymodal crystal size distribution. Euhedral to subhedral crystals normally range in size from 50 to 250μm and their replacement of the host limestone is usually non-mimetic (Plate 7.8a). In CL the dolomite crystals are conspicuously zoned (Plate 7.7b) with up to five conformable alternating dark and light zones (Plate 7.8b). From the core of the crystal to the rim these zones are as follows: zone 1 is a mottled medium to dully luminescent zone; zone 2 is a series of thin alternating dull and bright red subzones; zone 3 is poorly luminescent to non-luminescent; zone 4 has a bright yellow/orange luminescence; and zone 5 is non-luminescent and unlike zones 1-4 tends not to be isopachous (Plate 7.8b). Neither of the non-luminescent zones (zones 3 and 5) are ferroan as they do not stain with Potassium ferricyanide (Plate 7.8a).

The zonation in the medium-grained dark grey dolomite at Quinagh is almost identical to the description given by Wright *et al.* (2001) for what they termed CL package 2 (pk2) cement. Wright *et al.* (2001) also report a pk1 cement package that pre-dated the pk2

cement package but no evidence of this earlier dolomite package was found within any of the partially dolomitised samples from Quinagh.

In pervasively dolomitised samples ghosts of former bioclasts are clearly visible (Plate 7.9a). This fabric preservation is probably the product of insoluble material within the fossils and is not mimetic replacement by dolomite. The CL zonation sequence (zones 1-5) within partially dolomitised samples as described above is no longer discernable within pervasively dolomitised samples (Plate 7.9b). Some zonation is present however, but the contrast between the different zones is not as distinct as seen in Plate 7.8b. Three zones within the pervasively dolomitised Ballysteen Limestone have been identified (Plate 7.9b). From the core of the crystal to the rim these zones include: zone 1, a mottled medium to dully luminescent zone that may or may not contain a moderately luminescent red band towards the edge; zone 2, a dark red dully luminescent zone; and zone 3, a thin brightly luminescent zone. These conformable zones (zones 1-3) do not correspond directly to any of the zones within the dolomite from the partially dolomitised samples (zones 1-5). It is possible however, that recrystallisation/neomorphism of the medium-grained dark grey dolomite, observed in partially dolomitised samples (Plate 7.8b), may have led to the fabrics seen in pervasively dolomitised samples (Plate 7.9b).

A second dark grey dolomite occurs within samples from both Clonmelsh and Quinagh. This second dolomite contains a large amount of intercrystal organic material (Plate 7.10a) making it easily distinguishable from the original dark grey dolomite (Plates 7.11a and 7.11b). It is moderately luminescent with no apparent zoning within the individual dolomite crystals (Plate 7.10b). This dolomite type, which is referred to as the grey organic dolomite, occurs consistently above the dark grey replacive dolomite (Plates 7.11a and 7.11b) and below the coarse white open space-filling dolomite (Plates 7.12a and 7.12b). It is therefore probably geopetal dolomite, similar to the 'dark tops' dolomite described from Lisheen (Chapter 3, Section 3.3) and Urlingford (Chapter 4, Section 4.3). Contained within it are large numbers of tiny quartz crystals (Plate 7.10a), which are referred to as the pre-dolomite quartz generation because they pre-date the precipitation of the coarse-grained, white dolomite. These quartz crystals range in size up to a maximum of 1mm and all are non-luminescent in CL (Plate 7.10b).

The brightly luminescent, coarse-grained, white dolomite is sufficiently different from the grey organic dolomite that occurs below it that the two are easily distinguished in both PPL (Plate 7.12a) and CL (Plate 7.12b). The coarse-grained white dolomite shows evidence of being a space-filling cement (Plates 7.12b and 7.14b). This was already observed in hand sample where the centre of the vugs rimmed by coarse-grained white dolomite remained as open space (Plate 7.2). Zoning is present within the coarse white dolomite crystals (Plates 7.12b and 7.13b) but is more commonly restricted to the outer parts of the crystals (Plate 7.14b).

The post-dolomite quartz generation (Plates 7.2 and 7.13a) is easily distinguished from the pre-dolomite quartz generation, as crystals of the former are orders of magnitude larger than the latter. In CL, the post-dolomite quartz generation is non-luminescent (Plate 7.13b).

In view of the work by Nagy *et al.* (2001; 2002), it is tempting to equate the vugs with quartz geodes formed by the silicification of anhydrite nodules (Chowns & Elkins, 1974; Maliva, 1986). However, the vugs in this study lack the distinctive cauliflower shape associated with quartz geodes and contain no microcrystalline silica rind or evidence of replacement of former evaporite minerals.

7.4 PARAGENESIS

The paragenetic sequence of the Ballysteen Limestone reconstructed from the Carlow area is illustrated in Figure 7.3. The earliest calcite cements that were developed are volumetrically minor and occurred during the initial stages of diagenesis and prevented the fragmentation of the bioclastic material during compaction. Silicification of the bioclasts by length-slow fibrous silica is ubiquitous. The majority of early calcite cements post-date compaction and occlude all remaining porosity. Dolomitisation by the dark grey dolomite occurred after the porosity occlusion within the host limestone, silicification of bioclasts and many of the stylolites and dissolution seams. This medium-grained replacive planar dolomite occurred during the initial stages of dolomitisation and under CL is highly zoned. This zoned dolomite probably underwent subsequent recrystallisation as less well-zoned examples of it are found within pervasively dolomitised samples.

The vugs, which developed after calcite cementation, may have been contemporaneous with, or post-dated the formation of the dark grey dolomite. Their formation preceded the hydraulic fracturing and brecciation of the dark grey dolomite and emplacement of the coarse-grained white dolomite. Where present the grey organic dolomite, if it is geopetal dolomite, must have formed prior to the coarse-grained, white dolomite and after the formation of the dark grey dolomite. The pre-dolomite quartz generation probably formed contemporaneously with, or after the formation of the grey organic dolomite, but certainly prior to the formation of the coarse-grained white dolomite.

The post-dolomite quartz generation formed after the open space-filling, coarse white dolomite was precipitated. Coarse-grained, pink dolomite, fluorite, late calcite and pyrite were the last phases to form.

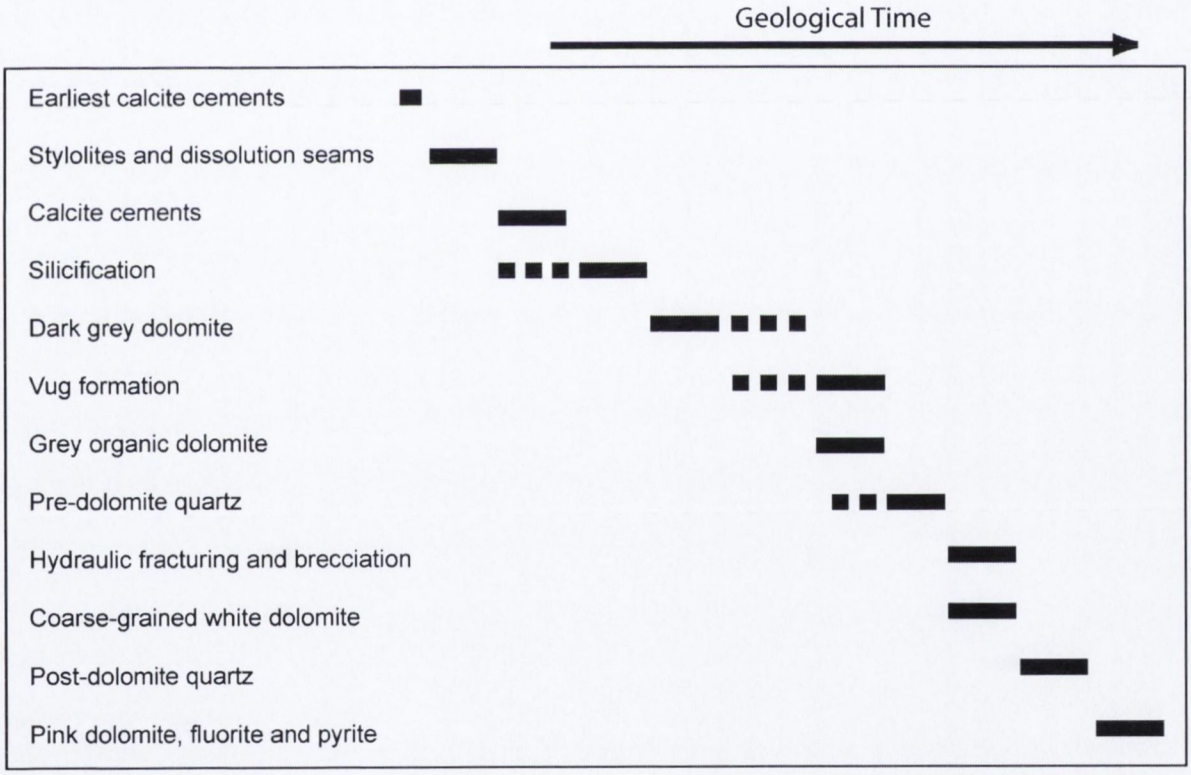

Figure 7.3 Paragenesis of the Ballysteen Limestone and dolomite in Carlow.

7.5 FLUID INCLUSION MICROTHERMOMETRY

Three mineral phases were isolated for fluid inclusion microthermometry analysis: the pre-dolomite quartz, the coarse-grained dolomite and the post-dolomite quartz (Appendix C). All of the samples selected came from the borehole at Quinagh. A detailed petrographic

study of the fluid inclusion assemblages in each phase was completed prior to undertaking the microthermometry.

Pre-dolomite quartz fluid inclusion petrography

Not all of the pre-dolomite quartz crystals examined contained fluid inclusions. However, those quartz crystals that did contain an inclusion; usually contained more than one. The inclusions measured were all two-phase (L+V) inclusions that homogenised into the liquid phase. They ranged in size from 5 to 25μm, with an average of 13μm and had a ψ_{liquid} of mostly either 0.85 or 0.9. Their shapes were commonly rounded or elongate (Plate 7.17a). Classification of the fluid inclusions contained within the pre-dolomite quartz at Quinagh was difficult as no growth zones were visible within the quartz crystals. However, as many of the inclusions appeared to be aligned in poorly-developed random trails within the quartz crystals, it is assumed that they were trapped after the growth of the quartz crystals and are therefore secondary.

Pre-dolomite quartz fluid inclusion microthermometry

A total of nine fluid inclusions were measured from the pre-dolomite quartz at Quinagh and although the freezing temperature data for all inclusions were collected after the heating work was completed, it will be discussed first. Upon cooling, all of the pre-dolomite quartz fluid inclusions nucleated an unexpected second bubble (Plate 7.17b). This second bubble consistently appeared at around 5°C and continued to increase in size, becoming larger than the original bubble, as the inclusions were cooled (Plate 7.17c). The original bubble in all of the inclusions collapsed at around -108°C and no other changes occurred down to the boiling point of liquid N_2 (-196°C). As the inclusions were heated from frozen, the original bubble reappeared and a fourth phase simultaneously nucleated (~107°C). This fourth phase dissolved as a liquid at an average of –85.8°C (Tm1) and, at the same temperature, the solid in the liquid part of the vacuole melted. This implies that there is no aqueous component within the vacuoles and that these inclusions are probably hydrocarbon (C_xH_y) inclusions. As the inclusion continued to be heated the bubble that appeared on cooling continued to become smaller (Plate 7.17d) and finally homogenised (Plate 7.17e) at between 14.4 and 45.9°C (Th1). The second bubble homogenised before the original bubble in all of the inclusions measured. The original bubble, upon further heating, homogenised (Plate 7.17f) between 49.7 and 119.1°C (Th2).

The phenomenon of nucleating one or more bubbles during cooling has been documented by other workers investigating petroleum-bearing inclusions (Kelly & Nishioka, 1985) and organic liquid-bearing inclusions (Kvenvolden & Roedder, 1971) and so it is likely that the inclusions within the pre-dolomite quartz at Quinagh are indeed hydrocarbon-bearing inclusions. As low temperature solid-liquid-vapour phase behaviour is difficult to observe, and equally difficult to interpret, only qualitative interpretations can be given on the content of these hydrocarbon inclusions. The critical point of pure methane is –82.5°C (above this temperature only $CH_{4(l)}$ or $CH_{4(v)}$ exist). This temperature is similar to the Tm1 measurements, which had an average of –85.8°C. However, no solid nucleated down at the boiling point of liquid nitrogen, where $CH_{4(s)}$ should be easily observed (Burruss, 2003), but as it was very difficult to maintain the freezing stage at such low temperatures and visibility was very much reduced, it is possible that $CH_{4(s)}$ was present but not observed. This would imply that the solid that melts at –85.8°C is $CO_{2(s)}$, which has had its triple point (-56.6°C) lowered due to the presence of CH_4. This would suggest that the inclusions within the pre-dolomite quartz are C_xH_y-CH_4-CO_2–bearing inclusions.

In order to try and determine additional compositional information based on fluorescence behaviour (Munz, 2001; Burruss, 2003) the inclusions were observed under a UV microscope. This was firstly done at Trinity College Dublin on a standard UV microscope. None of the inclusions fluoresced. It was thought that perhaps the second bubble, which appears on cooling may fluoresce and so it was attempted again on a UV microscope mounted with a cooling stage at the University of Leuven, Belgium. The inclusions still did not fluoresce. A possible reason for non-fluorescence may be that the petroleum present within the inclusions contains less than ten carbon atoms and therefore the fluorescence wavelengths are not visible by a typical commercially available fluorescence microscope (Burruss, 1991; Stasiuk & Snowden, 1997).

Dolomite fluid inclusion petrography

The coarse-grained white dolomite crystals from Quinagh contained large numbers of fluid inclusions, the majority of which were less than one micron in maximum dimension. Several fluid inclusions that were large enough to be measured were found within the turbid cores of the coarse-dolomite crystals (Plate 7.15), as well as in the clearer outer rims. They were all two-phase (L+V) inclusions that ranged in size from 2 to 10μm with an average of 4μm and had a ψ_{liquid} of 0.80 (except for two with a ψ_{liquid} of 0.85 and one with

a ψ_{liquid} of 0.75). They were mostly rounded or irregular in shape and commonly lay in an orientation parallel to the dolomite crystal faces, which were generally coincident with the CL growth fronts. Many of the larger inclusions also lay parallel to the trails of sub-micron sized inclusions.

Dolomite fluid inclusion microthermometry

A total of twenty-seven fluid inclusions were measured from the coarse-grained dolomite at Quinagh. Their Th values ranged from 192.7 to 267°C. First melting temperatures indicate that all the fluids were part of the NaCl-$CaCl_2$-H_2O ternary system. The salinity data indicate an average of 17.7 combined wt% NaCl and $CaCl_2$ equivalent.

Post-dolomite quartz fluid inclusion petrography

Despite the abundance of the post-dolomite quartz, the number of quartz crystals that contained fluid inclusions was small. Where observed, all of the inclusions were two-phase (L+V) inclusions that ranged in size from 10 to 50μm, with an average of 25μm. They had a ψ_{liquid} of either 0.85 or 0.9 (with one inclusion having a ψ_{liquid} of 0.8) and were commonly elongate in shape (Plate 7.16). The large size and the lack of growth zoning within the post-dolomite quartz crystals rendered classifying the fluid inclusions difficult.

Post-dolomite quartz fluid inclusion microthermometry

A total of twelve fluid inclusions were measured from the post dolomite quartz at Quinagh. Their Th values ranged from 174 to 214.7°C (with one outlier at 275°C). First melting temperatures indicate that all the inclusions were part of the NaCl-$CaCl_2$-H_2O ternary system. The salinity data, obtained by sequential freezing (Haynes, 1985), indicate an average of 25.4 combined wt% NaCl and $CaCl_2$ equivalent.

Discussion

As the behaviour of the inclusions within the pre-dolomite quartz is so distinctive and therefore easily recognisable they are useful in terms of determining the timing of hydrocarbon migration. Although classified as secondary, these inclusions are not found within the coarse-grained white dolomite or the post-dolomite quartz and so their formation is bracketed between the time of pre-dolomite quartz precipitation (which would mean that they are primary or pseudosecondary) and coarse-grained white dolomite

precipitation. In terms of a likely source for these hydrocarbon inclusions, the most obvious one is the intercrystal organic material in the grey organic dolomite within which the pre-dolomite quartz crystals occur. However, if not sourced locally other possible sources could have been from stratigraphically above the Ballysteen Limestone where the oldest potential source rocks are Upper Carboniferous black shales.

The fluid that precipitated the coarse-grained white dolomite was a high temperature (192.7 to 267°C), moderately saline brine (17.7 combined wt% NaCl and $CaCl_2$ equivalent). Similarly, the fluid that precipitated the post-dolomite quartz was a high temperature (174 to 214.7°C), high salinity (25.4 combined wt% NaCl and $CaCl_2$ equivalent) fluid. Despite the overlap in Th data, the salinity data indicate that two different fluids precipitated the coarse dolomite and post-dolomite quartz at Quinagh.

7.6 STABLE ISOTOPE GEOCHEMISTRY

Twenty-two samples of dolomitised Ballysteen Limestone from both Quinagh and Clonmelsh were sampled for stable isotope analysis. Nowhere in the samples that were available were early calcite cements sufficiently developed to enable pristine samples to be isolated. Individual pre-dolomite and post-dolomite quartz crystals were also sampled from Quinagh and their isotopic compositions determined (Appendix B). A full description of the sampling methods is given in Chapter 2.

7.6.1 Dolomite

The isotopic data from both the medium-grained dark grey dolomite and the coarse-grained white dolomite at Quinagh and Clonmelsh have been plotted in Figure 7.4. The $\delta^{13}C$ values for the medium and coarse dolomite range from 2.5 to 2.66‰ (mean 2.56‰ ± 0.10‰ 2σ) and 0.15 to 3.16‰ (mean 1.58‰ ± 1.9‰ 2σ; mode 1.8‰) respectively. The $\delta^{18}O$ values for the medium dolomite ranges from 23.84 to 27.79‰ (mean 25.15‰ ± 3.34‰ 2σ; mode 24‰) and the $\delta^{18}O$ values for the coarse dolomite ranges from 20.13 to 22.4 (mean 20.8‰ ± 1.32‰ 2σ; mode 20.2‰). Three coarse-grained pink dolomite samples were also analysed. Their $\delta^{13}C$ values range from 1.37to 1.47‰ (mean 1.41‰ ± 0.10‰ 2σ) and their $\delta^{18}O$ values from 15.87 to 16.08‰ (mean 16.0‰ ± 0.22‰ 2σ). The pink dolomite data are very different from those obtained from the pink dolomite in North Co. Cork

(Chapter 6, Section 6.6.2) and from 'pink plug' dolomite at Lisheen by Eyre (1998), which are also plotted in Figure 7.4 to serve as a comparison.

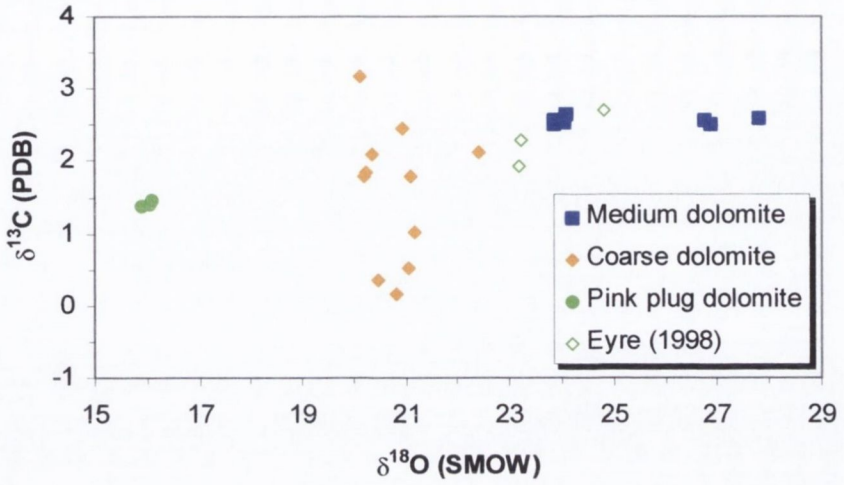

Figure 7.4 Scatter plot of $\delta^{13}C$ and $\delta^{18}O$ values for the dolomites at Clonmelsh and Quinagh, which includes data from Eyre (1998) for the pink dolomite at Lisheen.

Discussion

The medium-grained, dark grey dolomite has $\delta^{13}C$ values that are within the range of carbonates precipitated in equilibrium with Carboniferous seawater (Veizer *et al.*, 1999). The $\delta^{18}O$ values, which are the heaviest $\delta^{18}O$ values in the entire dolomite dataset, have a bimodal distribution with modal values of 24‰ and 27‰. These values are heavier than those from the fine-grained component of the Regional Dolomite at any other of the sample areas studied. However, since all of the medium-grained, dark grey dolomite samples came from pervasively dolomitised samples and there is evidence that there was extensive recrystallisation post dolomitisation, it is possible that the dolomite before recrystallisation was light and that it has equilibrated with a later fluid.

In contrast, the coarse-grained dolomite has a narrow range of $\delta^{18}O$ values that cluster around 21‰, slightly lighter than the values obtained for the coarse-grained white dolomite component of the Regional Dolomite. The most noticeable feature of the coarse dolomite data is the broad spread in the $\delta^{13}C$ data (0.15 to 3.16‰). These light $\delta^{13}C$ values may suggest the presence of organic carbon within the system (Hoefs, 2001). This is already indicated by the presence of the grey organic dolomite and the hydrocarbon-

bearing inclusions contained within the pre-dolomite quartz crystals. As both the grey organic dolomite and the hydrocarbon-bearing inclusions pre-date the formation of the coarse-grained white dolomite, this suggests that either the coarse-grained dolomite-bearing fluid interacted with these organic rich reservoirs and had their $\delta^{13}C$ values shifted to lighter values, or the breakdown of C-bearing long chain molecules was still ongoing during the precipitation of the coarse-grained dolomite.

The coarse pink dolomite samples have both lighter $\delta^{13}C$ and $\delta^{18}O$ values than those obtained by Eyre (1998) for the pink dolomite at Lisheen. This suggests that the late diagenetic fluids involved in the precipitation of the 'pink plug' dolomites in Carlow were more evolved than those at Lisheen (and also in North Co. Cork) and so the 'pink-plug' dolomite found throughout the Irish Midlands may not necessarily have formed from the same fluid.

7.6.2 Pre-dolomite quartz

Several individual minute pre-dolomite quartz crystals from Quinagh were extracted for analysis using laser fluorination to obtain their $\delta^{18}O$ values. However, only four were large enough to yield enough oxygen to be detected and measured by the mass spectrometer. They yielded $\delta^{18}O$ values that ranged from 19.37 to 21.15‰ (mean of 20.16‰ ± 1.54‰ 2σ; mode 19‰).

7.6.3 Post-dolomite quartz

Eight individual post-dolomite quartz crystals from Quinagh were extracted and analysed using laser fluorination to obtain their $\delta^{18}O$ values. They had $\delta^{18}O$ values that ranged from 18.93 to 21.49‰ (mean of 20.28‰ ± 1.9‰ 2σ; mode 21‰).

7.7 MODELLING OF PARENTAL FLUIDS

Using the equations of Matsuhisa *et al.* (1979) for quartz and Land (1983) for dolomite an average of the measured isotope values for the pre-dolomite quartz, post-dolomite quartz and coarse dolomite from Quinagh was used to model their parental fluid compositions over a range of temperatures of precipitation. The standard deviations of the isotopic measurements of all three phases (0.77, 0.95 and 0.72 respectively) were thought to be within acceptable limits to justify the use of the average of these measurements in these

equations. Using the homogenisation temperature ranges (50 to 120°C, 175 to 215°C and 190 to 270°C respectively), fluid compositions were calculated for all three phases. The quartz data were plotted separately (Figure 7.5) from the dolomite data (Figure 7.6), as plotting them together would overcrowd the plot and render it difficult to read.

Calculated fluid compositions for the pre-dolomite quartz using the range in homogenisation temperatures indicates isotopic values of the parental fluid within the range –8.5 to 1.9‰. Similarly, calculated compositions of the parental fluid for the post-dolomite quartz using the range in homogenisation temperatures indicates water isotopic values in the range from 7 to 9.6‰.

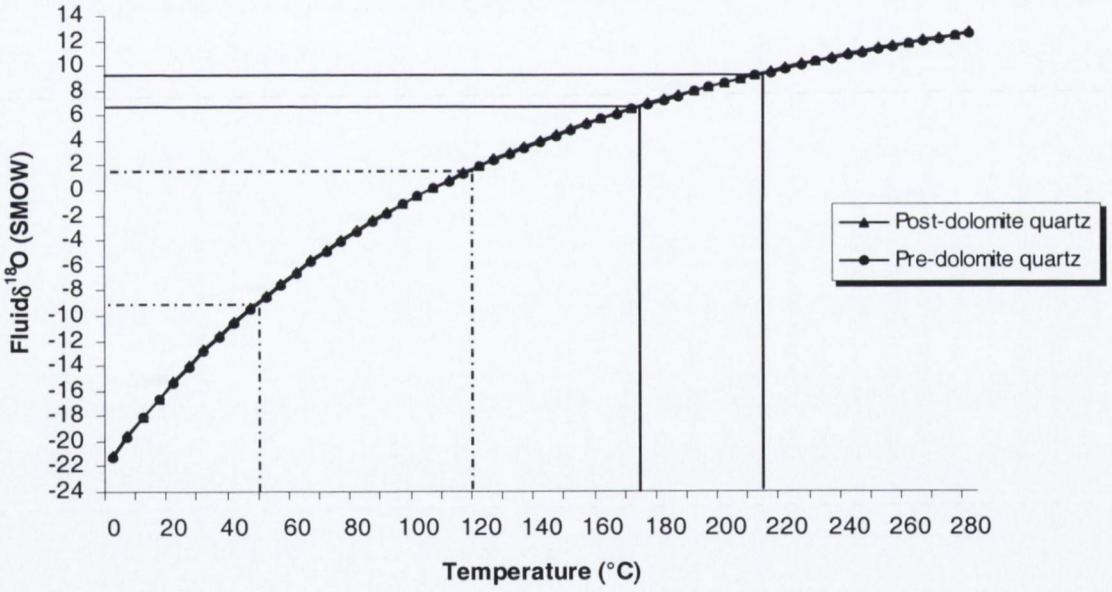

Figure 7.5 Mineral-water oxygen isotope fractionation curves for the pre-dolomite and post-dolomite quartz at Quinagh. See text for discussion.

Calculated fluid compositions for the coarse white dolomite using the range in homogenisation temperatures indicate $\delta^{18}O$ values of the parental fluid ranging from 9.2 to 13.3‰. It should be noted that an average of the coarse white dolomite values from Quinagh (20.99‰) was used to construct this plot and not the mean of all coarse white dolomite values from both Quinagh and Clonmelsh (20.8‰).

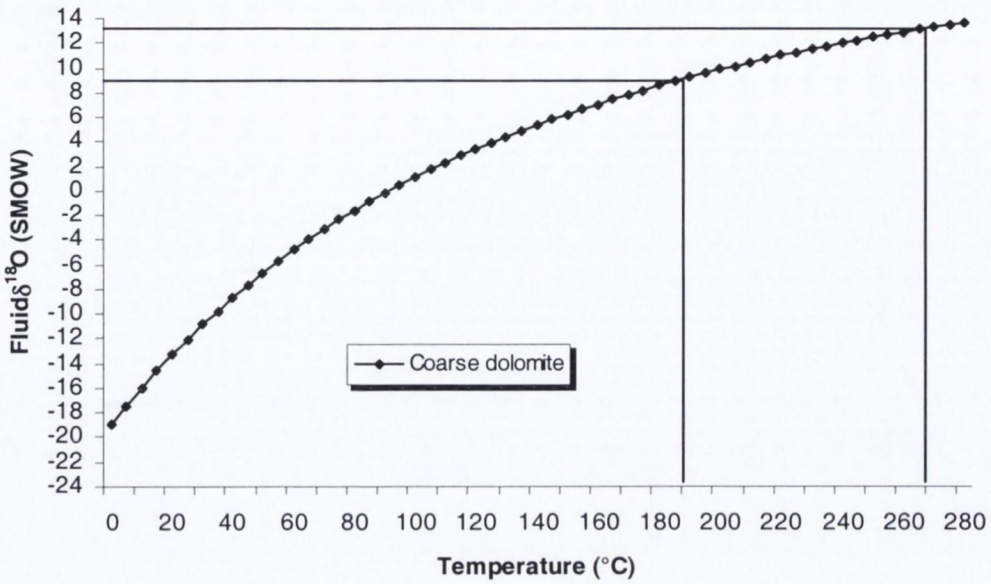

Figure 7.6 Mineral-water oxygen isotope fractionation curve for the coarse dolomite at Quinagh. See text for discussion.

Discussion

The pre-dolomite quartz, with a modelled parental fluid $\delta^{18}O$ that ranges from –8.5 to 1.9‰, may suggest some input from meteoric water. However, as the oxidation of organic matter may have been another important process underway during the precipitation of these quartz crystals, it is more likely that the modelled parental fluid values are highlighting this influence. The usual isotopic signature associated with this process is a shift towards lighter $\delta^{13}C$ values (Hoefs, 2001). Unfortunately no isotopic data was obtained from the grey organic dolomite, within which the pre-dolomite quartz crystals occur. However, light $\delta^{13}C$ values are associated with the coarse white dolomite, which directly post-dates the grey organic dolomite. This suggests that the breakdown of C-bearing long chain molecules may have been in progress during the precipitation of this coarse-grained white dolomite, or that, perhaps, the Mg-bearing fluid interacted with this organic-rich reservoir. The hydrocarbon-bearing fluid inclusions contained within the pre-dolomite quartz further support the influence of organic matter.

The modelled parental fluids for the post-dolomite quartz and the coarse dolomite have $\delta^{18}O$ values that range from 7 to 9.6‰ and 9.2 to 13.3‰ respectively. This suggests that these fluids have undergone significant amounts of fluid-rock interaction.

7.8 HALOGEN GEOCHEMISTRY

Samples of coarse dolomite and post-dolomite quartz from both Quinagh and Clonmelsh were prepared for crush-leach analysis using the method outlined in Chapter 2. The data are shown in Appendix D. However, because microthermometric data was obtained only for the samples from Quinagh, calculations based on the salinity for the Clonmelsh samples were made using the average of the data obtained from the Quinagh samples.

Figure 7.7 shows the calculated Cl and Br composition of the fluids within the coarse dolomite and post-dolomite quartz fluid inclusions at both Quinagh and Clonmelsh. The post-dolomite quartz data from Clonmelsh indicate that the fluid within these inclusions is residual brine, formed by the evaporation of seawater beyond the point of halite precipitation. The post-dolomite quartz data from Quinagh, which lie to the left of the SET, indicate that the fluid within these inclusions is probably a mixture of evaporated seawater and a fluid, which has acquired some Cl from the dissolution of halite.

The dolomite data from both Clonmelsh and Quinagh, which lie to the left of the SET, suggest that the fluids within these inclusions may contain a mixture of residual brine and a low salinity fluid (meteoric water or seawater).

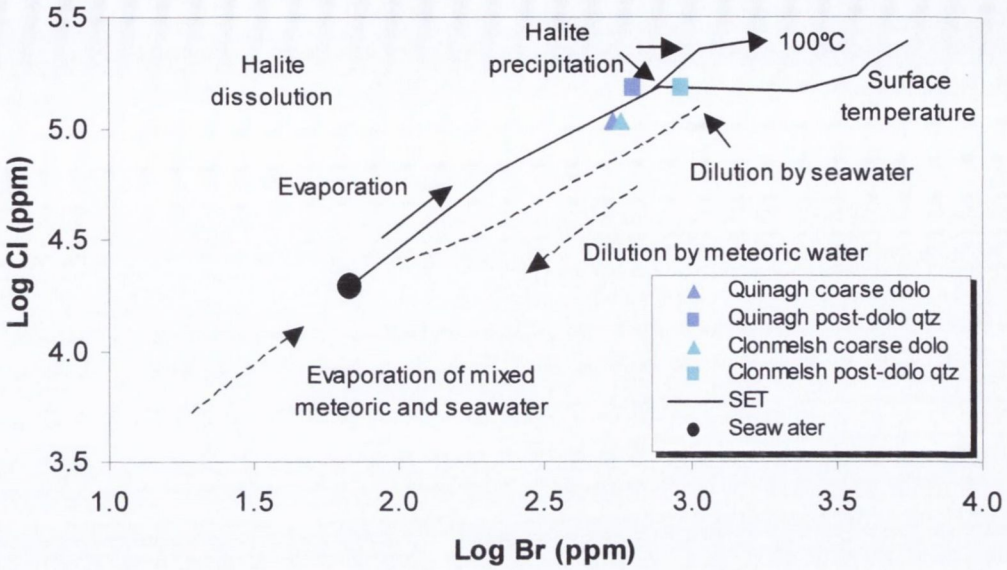

Figure 7.7 Cl and Br systematics of the coarse dolomite and post-dolomite quartz at both Quinagh and Clonmelsh. Plot also shows the SET (after Carpenter (1978) and Gleeson & Yardley (2002)).

A plot of the Na-Cl-Br systematics is shown in Figure 7.8. The Cl/Br ratios of the quartz and dolomite samples from both Clonmelsh and Quinagh are broadly similar in that they are all less than seawater and with the exception of the post-dolomite quartz from Quinagh, plot in the region expected for the composition of a brine evaporated beyond the point of halite precipitation (Fluid 2).

The post-dolomite quartz from Quinagh has a significantly higher Na/Br ratio (664) than seawater (562). This may be due to analytical error (supported by a poor charge balance, which indicates an excess of cations, see Appendix D) or the result of the addition of a small amount of Na from another source. If the interpretation of the fluid within the post dolomite quartz inclusions is correct, and it does contain a mixture of residual brine and a component of halite dissolution, then this would provide a source for the Na and elevated Cl as shown in Figure 7.7. The post-dolomite quartz data from Clonmelsh are consistent with a fluid that was relatively unaffected by exchange reactions involving Na. However, the dolomite data from both Clonmelsh and Quinagh indicate that the fluids within these inclusions are enriched in Na relative to the values expected for seawater. As these dolomitising fluids probably contain a mixture of residual brine and a dilute fluid it is not

possible to determine whether this increase in the Na/Br ratios is a result of the original composition of the dilute fluid or fluid-rock interactions along the fluid flow pathway.

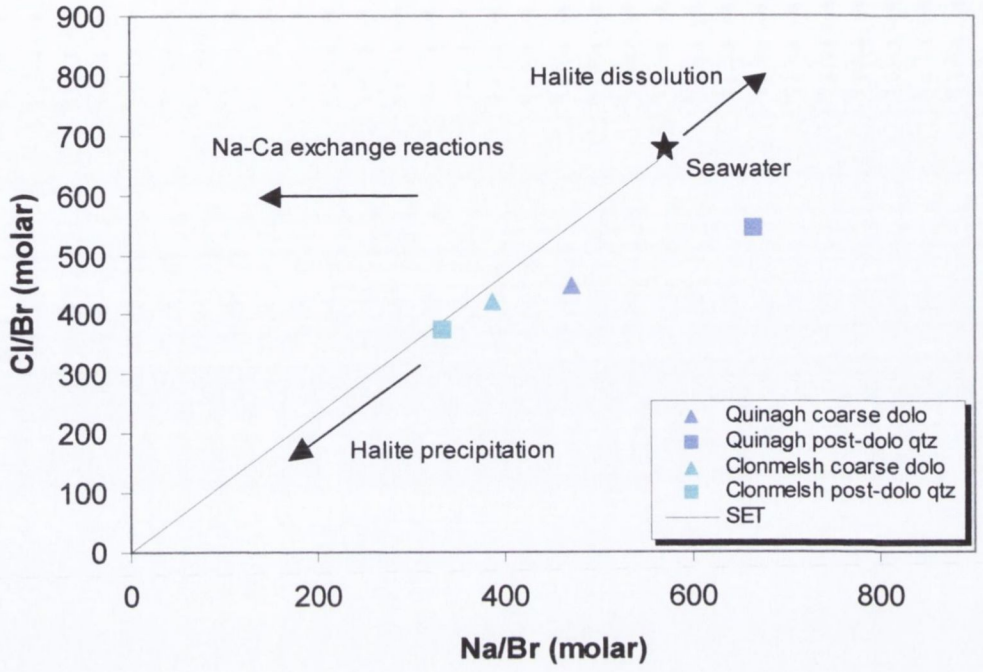

Figure 7.8 Cl-Na-Br systematics for the coarse dolomite and post-dolomite quartz from both Quinagh and Clonmelsh. SET data after Kesler *et al.* (1995).

Discussion

The fluids within the post-dolomite quartz from Clonmelsh are probably residual brine, formed by the evaporation of seawater beyond the point of halite precipitation. The fluids within the dolomite inclusions from both Clonmelsh and Quinagh are probably a mixture of residual brine and a component of a low salinity fluid (meteoric water or seawater). The fluids within the post-dolomite quartz inclusions from Quinagh may be a mixture of evaporated seawater and a fluid, which has acquired some Cl from the dissolution of halite. However, as the charge balance for the Quinagh quartz was poor this data must be treated with caution.

In terms of the fluids involved in the formation of the Irish Zn-Pb deposits, the Clonmelsh data and the dolomite from Quinagh may be considered as being similar to Fluid 2.

7.9 CONCLUSIONS

- Dolomitisation within the Ballysteen Limestone occurred after all of the primary porosity within the limestone lithosome had been occluded.

- Silicification of fossils by length-slow fibrous quartz is common and has been used as evidence for the existence of extensive evaporite deposits adjacent to the Leinster Massif (Nagy *et al.*, 2002).

- Large vugs occur within pervasively dolomitised Ballysteen Limestone samples and are not the amplification by dolomitisation of pre-existing calcite-filled cavities within the limestone lithosome, as in contrast to the situation in the Waulsortian Limestone, there are no 'stromatactis-like' cavities within the Ballysteen Limestone.

- These vugs are not thought to be quartz geodes formed by the silicification of anhydrite nodules as they lack the distinctive cauliflower shape associated with quartz geodes and contain no microcrystalline silica rind or evidence of replacement of former evaporite minerals.

- The timing of formation of the vugs was probably contemporaneous with, or post, the dark grey dolomite and pre the hydraulic fracturing and brecciation of the dark grey dolomite and emplacement of the coarse-grained white dolomite.

- The depth of burial at which the vugs formed can be bracketed between the depth of formation of the dark grey dolomite and that of the coarse-grained white dolomite. The former was probably at a minimum of least several hundred metres, in view of the degree of compaction and stylolitization; the latter is likely to have been substantial based on the evidence of the minimum temperatures at which both the coarse white dolomite and later quartz precipitated (193 and 174°C respectively).

- Isotopically light $\delta^{13}C$ data for the coarse white dolomite indicate that the breakdown of C-bearing long chain molecules may have been underway during the precipitation of this phase or that the dolomite-bearing fluid interacted with organic-rich reservoirs.

- Hydrocarbon-bearing inclusions contained within the pre-dolomite quartz further support the influence of organic matter.

- The coarse pink dolomite from Carlow is isotopically different from that studied from Lisheen or North Co. Cork. This suggests that not all of the pink dolomite found throughout the Irish Midlands is the same or indeed that it formed from the same fluid.

- The halogen data indicate that fluid that precipitated the post-dolomite quartz at Clonmelsh was residual brine, formed by the evaporation of seawater beyond the point of halite precipitation. Similarly, the fluids that precipitated the dolomite at both Quinagh and Clonmelsh were probably a mixture of residual brine and a low salinity fluid. In terms of the fluids involved in the formation of the Irish base-metal deposits, these fluids are most similar to Fluid 2.

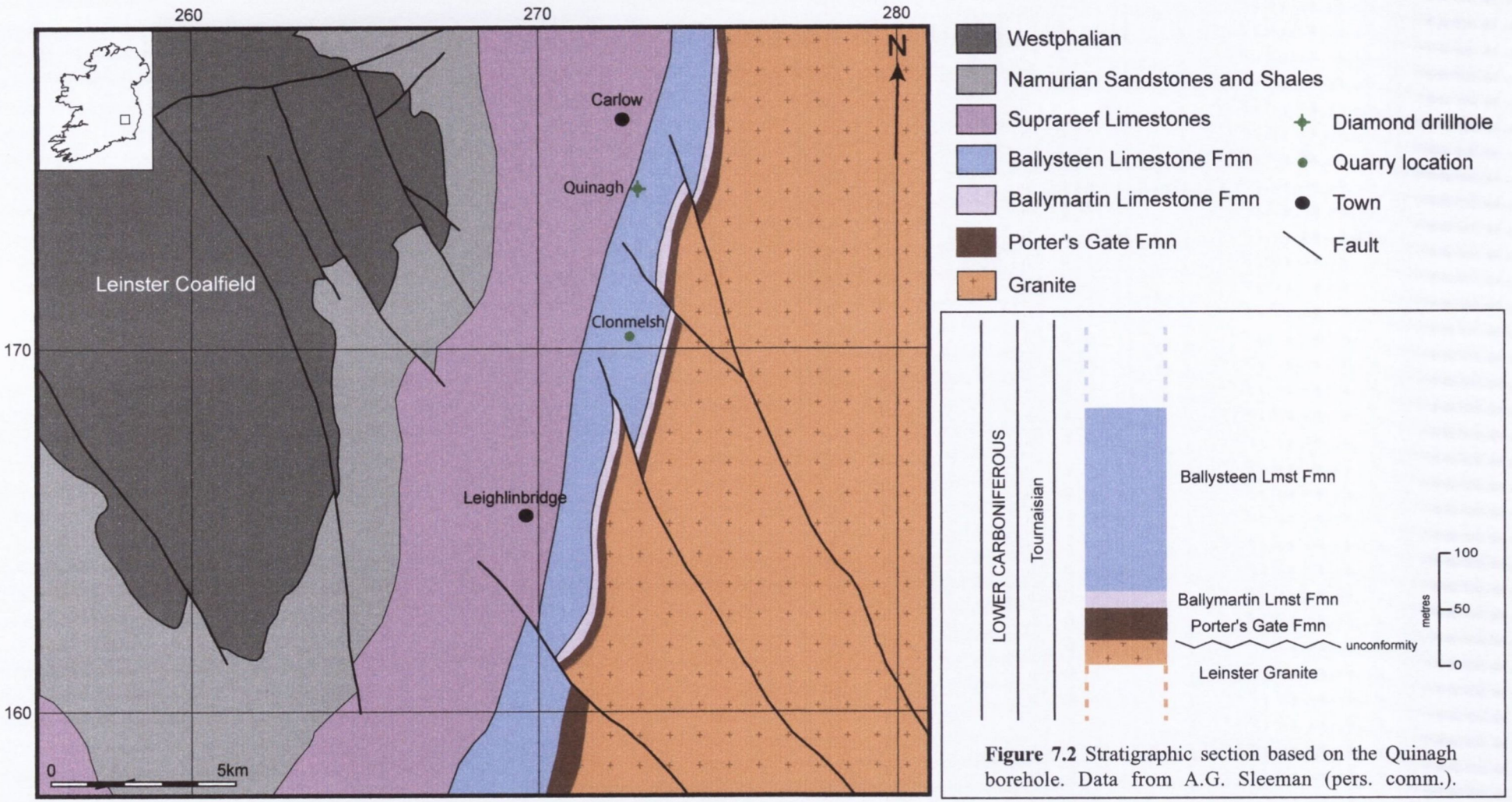

Figure 7.2 Stratigraphic section based on the Quinagh borehole. Data from A.G. Sleeman (pers. comm.).

Figure 7.1 A simplified geological map of the Carlow area showing the locations of the Quinagh borehole and the quarry at Clonmelsh. Grid lines refer to the Ordnance Survey of Ireland National Grid. Modified after Tietzsch-Tyler and Sleeman (1994).

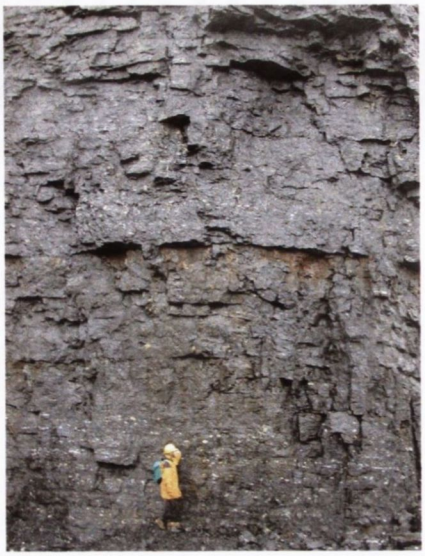

Plate 7.1: Distribution of vugs along the north quarry face at Clonmelsh. Note that the vugs are preferentially developed within certain beds. The vugs are rimmed or, less commonly, totally infilled by coarse-grained white dolomite.



Plate 7.2: Detail of a vug within the dark grey dolomite from the quarry at Clonmelsh. It is lined by coarse white dolomite and contains a single euhedral quartz crystal growing into the open space within the centre of the vug. Size of coin is 22mm.



Plate 7.3: Vug from the quarry at Clonmelsh almost totally filled with coarse white dolomite that has been fed by bed parallel veins. Note that the veins also form the matrix of minor breccias containing fragments of the dark grey dolomite (arrowed).



Plate 7.4: Hand sample from Clonmelsh quarry illustrating the crackle breccia of dark grey dolomite cemented by coarse-grained white dolomite. Size of coin is 22mm.



Plate 7.5: Hand sample from Clonmelsh quarry showing the coarse pink dolomite contained within the centre of a vug. Note that it clearly post-dates the coarse white dolomite. Size of coin is 22mm.



Plate 7.6: Cube of fluorite (arrowed), surrounded by coarse white dolomite, contained within a vug within the Quinagh borehole (77.28 - 77.38m). Its presence may be related to fluid flow upwards from the underlying granite. Scale bar is 5mm.

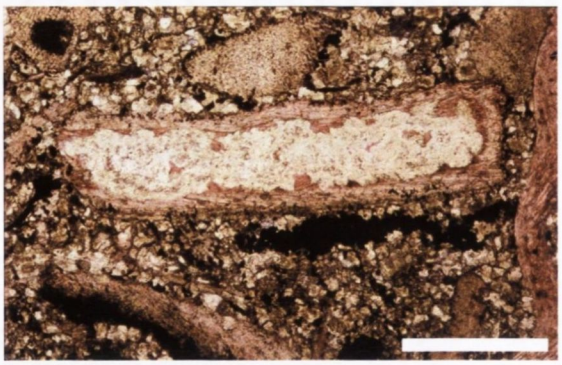

Plate 7.7a: P17632 - Quinagh borehole (158.5m). PPL view of a preferentially silicified bioclast - probably a brachiopod. Scale bar is 500μm.

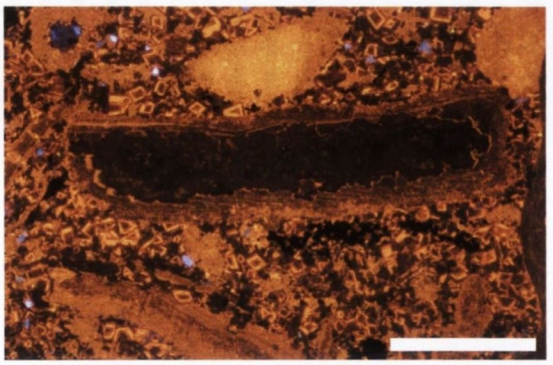

Plate 7.7b: Same view in CL. Note the abundant highly zoned dolomite rhombs surrounding the bioclastic material. Scale bar is 500μm.

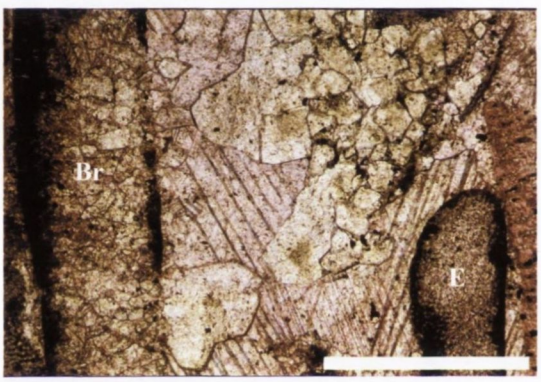

Plate 7.8a: P17633 - Quinagh borehole (152.5m). PPL view of a brachiopod (Br) and an echinoderm fragment (E) surrounded by early calcite cements which are being replaced by dolomite. Scale bar is 500μm.

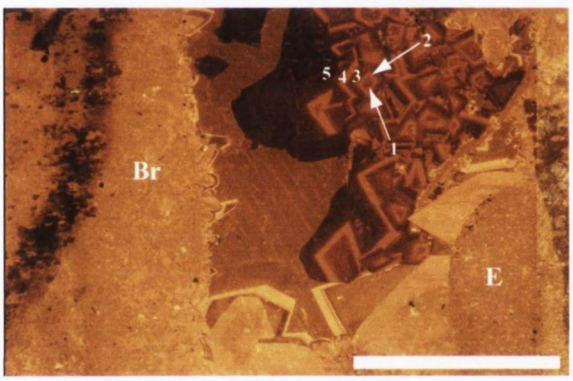

Plate 7.8b: Same view in CL. The early calcite cements occlude all remaining porosity prior to dolomitisation. The dolomite is a medium-grained, highly zoned dolomite that contains up to five different zones (labelled). Scale bar is 500μm.

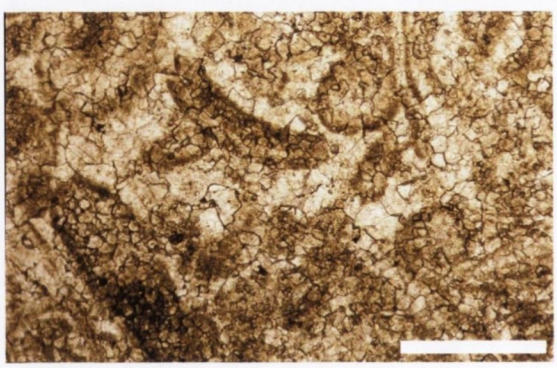

Plate 7.9a: P17634 - Quinagh borehole (98.5m). PPL view of a pervasively dolomitised sample containing numerous ghosts of former fossils. Scale bar is 500μm.

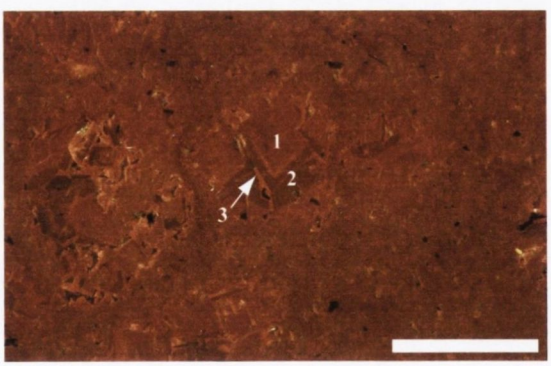

Plate 7.9b: Same view in CL. Note that the dolomite is very different from that in Plate 7.8b. Three zones are visible within this dolomite (labelled). Scale bar is 500μm.

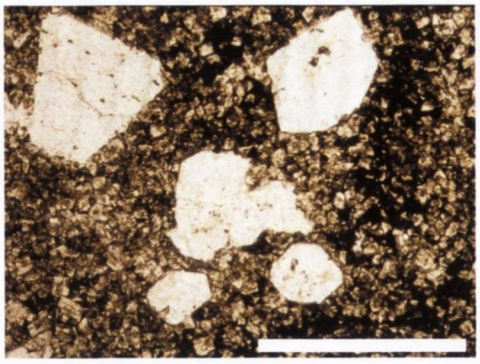

Plate 7.10a: P17635 - Quinagh Borehole (36.8 - 37m). PPL view of the pre-dolomite quartz crystals contained within the grey organic dolomite. Note the organic material that is contained between the individual dolomite grains. Scale bar is 500µm.

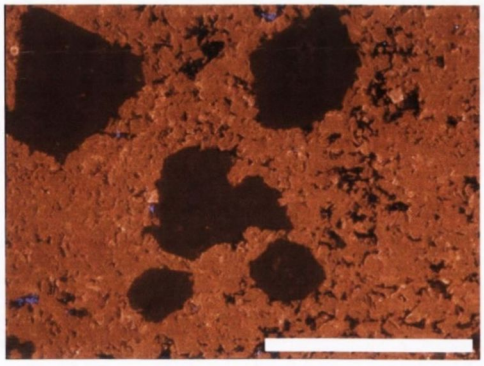

Plate 7.10b: Same view in CL The pre-dolomite quartz crystals are all non-luminescent in CL. The grey organic dolomite has a moderate luminescence. The organic material between the dolomite grains remains dark. Scale bar is 500µm.

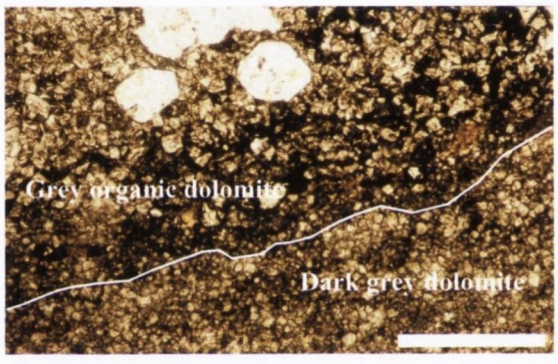

Plate 7.11a: P17635 - Quinagh Borehole (36.8 - 37m). PPL view of the contact (outlined) between the grey organic dolomite and the dark grey dolomite below. Scale bar is 500µm.

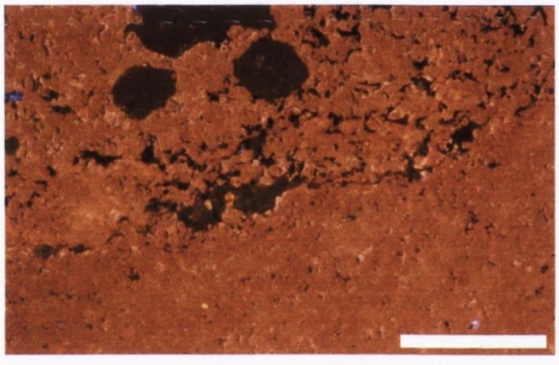

Plate 7.11b: Same view in CL. Note that grey organic dolomite and the dark grey dolomite have a similar luminescence but the non-luminescent organic material within the grey organic dolomite makes it easy to distinguish. Scale bar is 500µm.

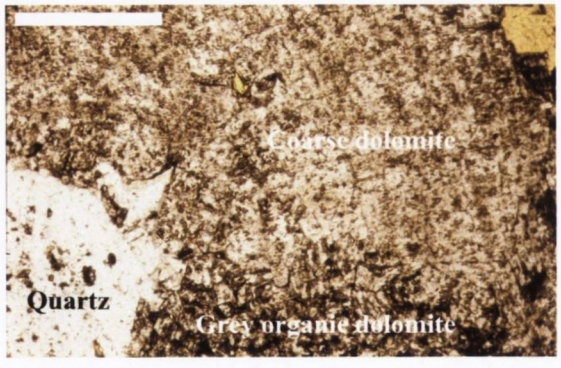

Plate 7.12a: P17635 - Quinagh Borehole (36.8 - 37m). PPL view of a pre-dolomite quartz crystal within the grey organic dolomite which lies below the coarse dolomite. The yellow substance in the image is epoxy resin. Scale bar is 500µm.

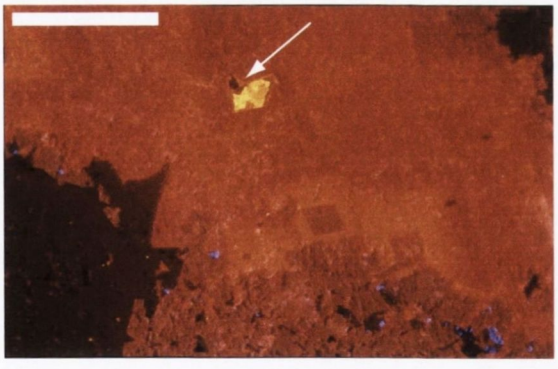

Plate 7.12b: Same view in CL. The coarse dolomite has a different luminescence than the grey organic dolomite. Note the thin outer zone of the coarse dolomite (arrow) that is surrounding a late calcite-filled vug. This clearly indicates that this dolomite was growing into open space. Scale bar is 500µm.

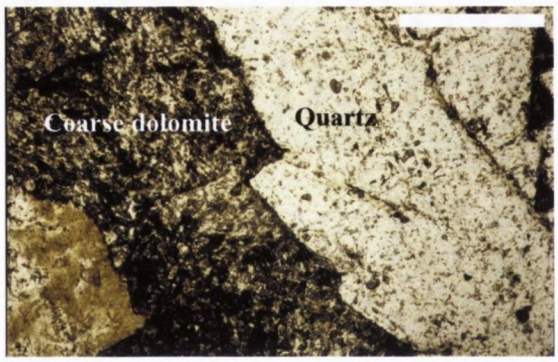

Plate 7.13a: P17635 - Quinagh Borehole (36.8 - 37m). PPL view of the coarse dolomite and post-dolomite quartz (labelled). Scale bar is 500µm.

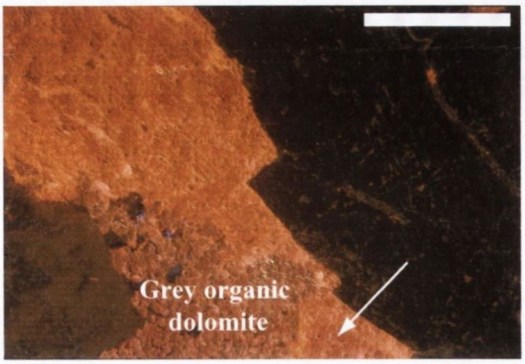

Plate 7.13b: Same view in CL. The quartz is non-luminescent and the coarse-grained dolomite is weakly zoned (arrow). Note that an area of grey organic dolomite, barely visible in PPL, is highlighted under CL. Scale bar is 500µm.

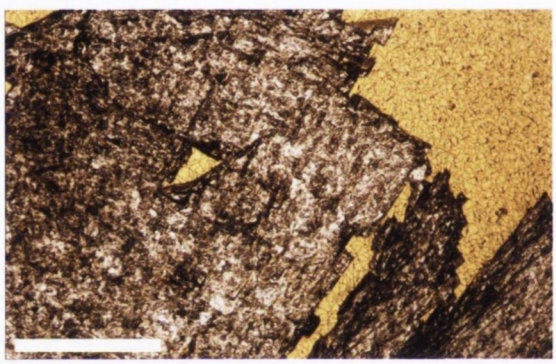

Plate 7.14a: P17635 - Quinagh Borehole (36.8 - 37m). PPL view of the coarse dolomite growing into the open space within a vug. Yellow substance in the image is epoxy resin. Scale bar is 500µm.

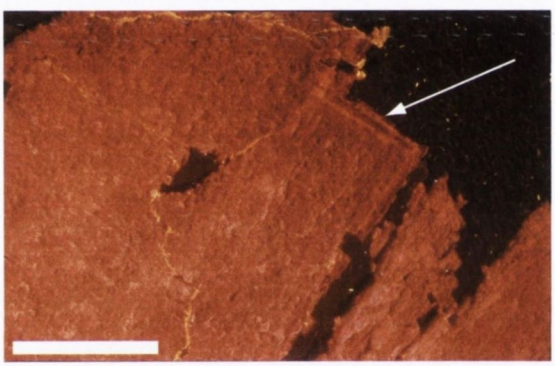

Plate 7.14b: Same view in CL. Note the same outer zone on the coarse dolomite crystals (arrow) that was observed in Plate 7.12b. This is further evidence that the coarse dolomite is an open space filling dolomite. Scale bar is 500µm.

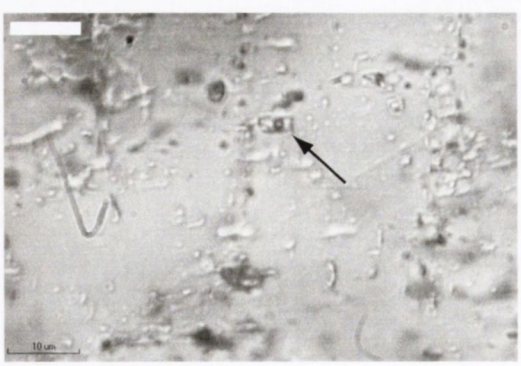

Plate 7.15: Image of the E4.1 two phase fluid inclusion (arrow) from within the coarse-grained white dolomite at Quinagh. Scale bar is 10µm.

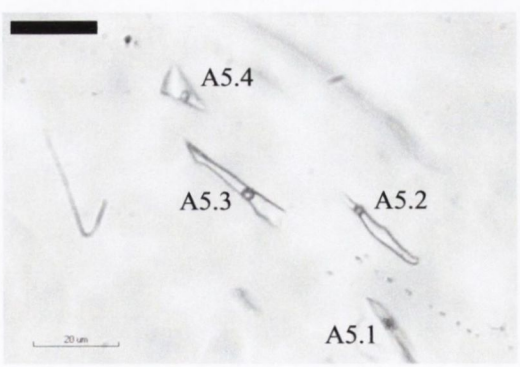

Plate 7.16: Image of four of the two phase fluid inclusions measured from within the post-dolomite quartz generation at Quinagh. Scale bar is 20µm.



Plate 7.17a: View of the elongate OI CA1 fluid inclusion (arrowed) contained within the pre-dolomite quartz at Quinagh. Image captured at room temperature (20°C). Scale bar is 20µm.

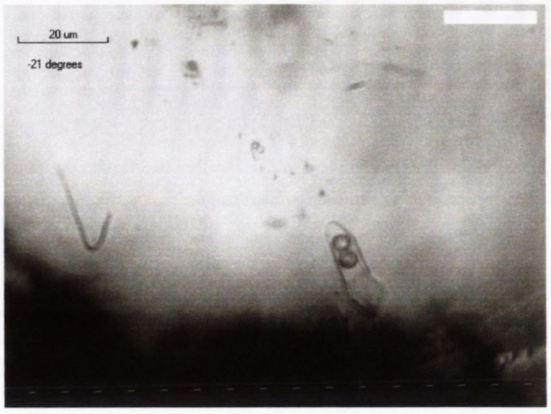

Plate 7.17b: Upon cooling the two-phase inclusion develops a second bubble which continues to increase in size as the inclusion is cooled. Image captured at -21°C. Scale bar is 20µm.

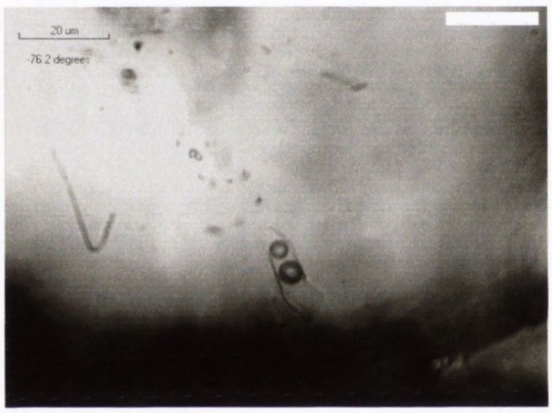

Plate 7.17c: With continued cooling the second bubble increases in size and becomes larger than original bubble until the original bubble eventually collapses at around -108°C. Image captured at -76.2°C. Scale bar is 20µm.



Plate 7.17d: With continued heating the second bubble becomes progressively smaller. Image captured at 18.6°C. Scale bar is 20µm.



Plate 7.17e: Second bubble homogenises between 14-46°C (Th2) leaving only the original bubble. Image captured at 23.5°C. Scale bar is 20µm.

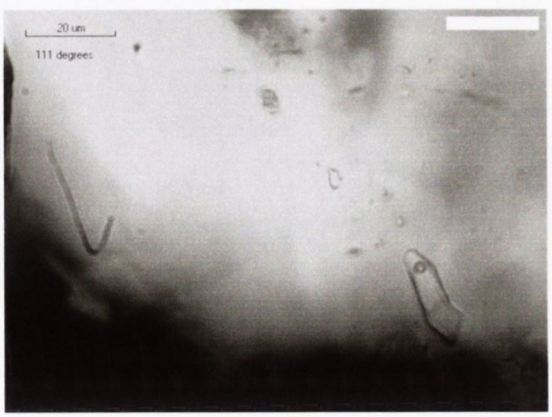

Plate 7.17f: The original bubble finally homogenises between 50-120°C (Th1). Image captured at 111°C. Scale bar is 20µm.

CHAPTER 8

MULLAWORNIA

8.1 INTRODUCTION

A disused quarry located at Mullawornia (GR 2130 2590), 3 kilometres northwest of Ballymahon Co. Longford, provides a good section of Waulsortian Limestone (Figure 8.1). Substantial amounts of solid hydrocarbons (bitumen) are contained within veins and large secondary cavities throughout the quarry. Petrographic examination of the bitumen indicates that it was emplaced as a liquid after the host limestone was cemented. This has implications for the porosity and permeability evolution of the limestone, as conduits must have been available within the well-cemented host to enable the hydrocarbons to be emplaced. Also, thermal maturity indicators such as reflectance and optical anisotropy under white reflected light suggest that the bitumen probably experienced high temperatures. This has implications for the thermal history of the limestones. A detailed examination of the Waulsortian Limestone and its associated bitumen at Mullawornia was therefore undertaken to investigate the porosity and permeability evolution of the limestones and to reconstruct their thermal history.

8.2 REGIONAL GEOLOGICAL SETTING

8.2.1 Stratigraphy

The area surrounding the quarry at Mullawornia was first mapped by Foot and O'Kelly (1865). More recently, Nevill (1958), Lees (1964), King (1984) and Lord (1999) have provided overviews, which have concentrated on the Waulsortian Limestone in the area.

Borehole data from both Keel, approximately 9 kilometres northeast of Mullawornia and Moyvore, approximately 13 kilometres to the southeast of Mullawornia (Figure 8.1) has shown that the upper part of the Old Red Sandstone, the Basal Sandstones, are present in the area (Philcox, 1984). These are known to lie unconformably upon Lower Palaeozoic rocks and are Lower Carboniferous in age. Above the Basal Sandstones, the Navan Group is followed by the Argillaceous Bioclastic Limestones (ABL) and the Waulsortian Limestone. To the south and directly to the northwest of the quarry at Mullawornia, basinal Viséan limestones (Calp) overlie the Waulsortian Limestone (Figure 8.1).

The thickness of the Waulsortian Limestone in the area surrounding Mullawornia is poorly constrained. Borehole data from Keel (Crean, 1987) gives a local thickness of 132 metres. However, work by Jones and Brand (1986) has demonstrated that the thickness of the

Waulsortian Limestone in the north Midlands can be variable over relatively short distances. Allowing for this, Lord (1999) has estimated the thickness of the present day exposure in the vicinity of Mullawornia to be on the order of 100 to 200 metres.

8.2.2 Structure

The area surrounding Mullawornia lies on the northwestern margin of the Dublin Basin. The basin is known to have covered most of the Irish Midlands during the Viséan (Sevastopulo & Wyse Jackson, 2001) with basement structures invoked as a control on sedimentation (MacDermot & Sevastopulo, 1972; Nolan, 1986, 1989; Pickard *et al.*, 1992; Pickard *et al.*, 1994). The basin and its margins have been most intensively studied in north Co. Dublin and in Co. Meath (Nolan, 1986, 1989; Pickard *et al.*, 1992; Pickard *et al.*, 1994), but many of the controlling structures in the western parts of the basin have not been identified. A number of northwest-southeast trending faults occur in the area surrounding Mullawornia (Figure 8.1) and are probably related to Variscan deformation. The northeast-southwest trending structures (Figure 8.1), which are re-activated Caledonian structures, may have been active during the Dinantian.

8.3 PETROGRAPHY

Hand samples

One of the most striking features of the Waulsortian Limestone at Mullawornia is the occurrence of large cavities (Plate 8.1). These are up to 10cm in diameter and commonly contain geopetal sediment along their base with coarse-grained calcite spar developed above. They have irregular shapes and do not resemble the typical stromatactis cavities described by Lees and Miller (1995). Many of them are oblique to sheet spar developments.

They are commonly rimmed by CFC cements, whose thickness is not always isopachous (Plate 8.1). Towards their base, large saddle-shaped crystals of dolomite occur above the geopetal sediment but below the calcite spar (Plate 8.1). The geopetal sediment is typically dolomitised.

Bitumen occurs ubiquitously within the cavities (Plate 8.1) and its development appears intimately associated with the occurrence of the calcite spar (herein referred to as the

bitumen-related calcite). It usually occurs within the lower parts of the cavities and commonly forms globular shapes that are usually 1mm or less (Plate 8.1). There is evidence throughout the quarry for it being vein-fed (Plate 8.1). Pyrite also occurs within these cavities and appears to post-date the bitumen.

The cavities are not thought to be the early calcite cavities usually found within the Waulsortian Limestone, as their shapes are too irregular. They are probably secondary cavities, formed as a result of a solution event that occurred after the Waulsortian Limestone was cemented.

Thin sections

The early calcite cavity-filling cements (Stages A-D) are well-developed within the Waulsortian Limestone at Mullawornia (Plates 8.2a and 8.2b). However, Stage C, which is usually a brightly luminescent stage, appears to have a duller luminescence in the samples from Mullawornia than those studied elsewhere. Stage D is the final porosity occluding cement (Plate 8.2b).

All of the early calcite cavities found throughout the Waulsortian Limestone at Mullawornia are identical in that they contain Stages A-D and have had their porosity occluded by the Stage D cements. It is therefore likely that the solution event that created the irregularly-shaped cavities occurred after the Waulsortian Limestone was cemented and had its final porosity occluded.

During or shortly after the formation of the secondary cavities, a second generation of CFC was developed which formed a rim around the cavities (Plates 8.1 and 8.3a). At the beginning of this study this second generation of CFC was confused with the Stage A CFC cements found with the early calcite cavities. However, this secondary generation of CFC (herein referred to as CFC2) is not followed by a conformable zone of Stage B cements as seen in the early calcite cavities, but by a thin development of geopetal sediment (Plate 8.3a). Although commonly completely replaced by fine-grained dolomite, partially dolomitised samples of the geopetal sediment are also found (Plate 8.3b). Thin brightly luminescent veins that cross-cut the CFC2 cements are observed feeding the relict calcite found within the geopetal sediment. This confirms that the geopetal sediment formed after the precipitation of the CFC2. Other thin, more dully luminescent, veins cross-cut the

CFC2 cements and relict calcite in the geopetal sediment (Plate 8.3b). However, these appear to be related to some dully luminescent zones, which occur in the later coarse-grained dolomite.

Coarse-grained dolomite occurs above the geopetal sediment (Plate 8.1). It is restricted to the floor of the cavities, which may suggest that it formed as a geopetal dolomite. It was certainly an open space-filling dolomite as growth zoning within the dolomite indicates that it grew into the available space created within the secondary cavities rather than being replacive (Plates 8.4a and 8.4b). Under CL, the coarse-grained dolomite crystals are conspicuously zoned with up to five conformable, alternating dark and light zones (Plates 8.4b). From the core of the crystal to the rim, the zones are as follows: zone 1 is a mottled dully luminescent zone; zone 2 is a thin, moderately luminescent zone; zone 3 is a thick non-luminescent, ferroan zone that stains dark blue with Potassium ferricyanide (Plates 8.4a and 8.5a); zone 4 has a bright red luminescence and may have thin sub-zones developed towards the outer parts of the zone; and zone 5 is dully luminescent and has a blood red colour. Commonly the coarse-grained dolomite crystals display the curved crystal faces (Plates 8.4a and 8.5a) and sweeping extinction indicative of saddle dolomite.

The bitumen-related calcite followed the precipitation of the coarse-grained dolomite and filled all of the remaining open space within the secondary cavities (Plate 8.1). In CL, the bitumen-related calcite (Plate 8.6b) has a similar luminescence to the Stage D, final porosity occluding cement (Plate 8.2b). However, its intimate association with the bitumen (Plates 8.6a and 8.6b) enables it to be differentiated from the Stage D cement.

The bitumen has a spherical or globular shape and is usually found along the base of the secondary cavities, near the tips of the saddle dolomite (Plates 8.6a and 8.7a). This implies that bitumen formation may have occurred during the early stages of precipitation of the bitumen-related calcite. Beneath the underside of many of the globules of bitumen a meniscus of the bitumen-related calcite appears to have formed (Plates 8.6a and 8.6b). Since cement menisci usually form in the vadose zone, and these cements almost certainly formed well into the phreatic zone, it is not clear how the menisci formed.

In reflected light the bitumen displays strong optical anisotropy (Plates 8.7b and 8.8b). This has been termed mesophase texture based on an analogy with coke (Gize, 1986). A

mesophase texture represents the 'liquid crystal' state intermediate between a solid and a liquid exhibited by some organic compounds. This state has crystallographic structure but also allows flow like a liquid. It is achieved by heating and therefore indicates growth at elevated temperatures. The experimental production of mesophase textures requires temperatures of at least 350°C (White, 1976), although mesophase bitumens have also been recorded in geological settings where palaeotemperatures are unlikely to have exceeded 200°C (Gize, 1986). The mesophase texture in the bitumens at Mullawornia consists of anisotropic spheres, which have grown and merged to a coke-like texture of coalesced domains and radial textures around the bitumen rims (Plate 8.7b). Some of the bitumens show evidence of brittle failure in the form of cracks (Plate 8.8b). This may be directly related to the thin sectioning process although it may also be a function of the response of the bitumen to stress (most likely burial induced).

In terms of the mechanisms for bitumen emplacement, feeder veins to the secondary cavities that are filled with bitumen-related calcite appear to been also exploited by the bitumen-bearing fluids (Plate 8.1).

Pyrite is present within the majority of samples and clearly post-dates the precipitation of the bitumen (Plates 8.9a and 8.9b). Evidence of pyrite pre-dating the precipitation of the bitumen was documented in previous studies of samples from Mullawornia (G. Sevastopulo and M. Cruise pers. comm.) but no evidence for this was found in this study.

8.4 PARAGENESIS

The paragenetic sequence seen at Mullawornia is illustrated in Figure 8.2. The formation of the secondary cavities occurred during a solution event that took place at some time after final porosity occlusion of the Waulsortian Limestone. A second generation of CFC cement (CFC2) formed either contemporaneously with or just after cavity formation and rimmed the outside of the cavities. Geopetal sediment was then precipitated and lined the base of the cavities before being replaced by fine-grained dolomite. Coarse-grained saddle dolomite was precipitated and grew into the open space available within the cavities. This was followed by the coarse-grained bitumen-related calcite, which filled all of the remaining open space within the cavities. Bitumen was precipitated contemporaneously with the bitumen-related calcite, probably during the early stages. Pyrite post-dated the

bitumen in all of the samples examined in this study. However, evidence for pyrite pre-dating the bitumen has been documented in other studies (G. Sevastopulo pers. comm.).

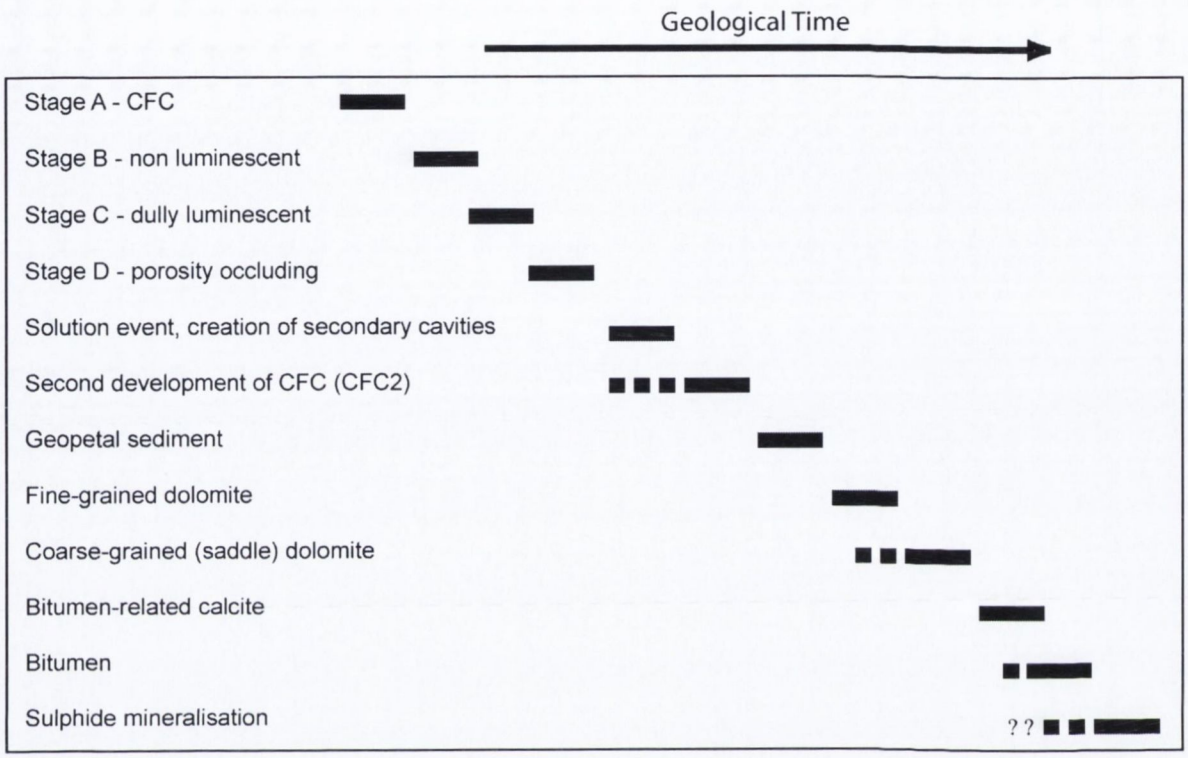

Figure 8.2 Paragenetic sequence inferred at Mullawornia based on petrographic data from this study.

8.5 FLUID INCLUSION MICROTHERMOMETRY

One phase was isolated for fluid inclusion microthermometry analysis: the coarse-grained white dolomite (Appendix C). The sample that was prepared came from the mirror image polished plaquette of the hand samples shown in Plate 8.1. A detailed petrographic study of the fluid inclusion assemblage was completed prior to undertaking the microthermometry.

Dolomite fluid inclusion petrography

The coarse-grained dolomite contained a large number of fluid inclusions, but as the majority were less then one micron in diameter they were too small to be useful for obtaining microthermometric data. Workable inclusions, albeit a small number, were located and mapped within both the Fe-bearing zone (zone 3, Plate 8.10) and along the border between the Fe-bearing and bright red luminescent zone (zone 4). These inclusions were all two-phase (L+V) inclusions that ranged in size from less than a micron to

approximately 5μm with degrees of fill (ψ_{liquid}) of 0.9. They were mostly euhedral (rectangular) to subhedral (rounded) in shape and formed zones parallel to the dolomite crystal faces, which were coincident with the CL growth zones. Many of the larger inclusions also lay parallel to the trails of sub-micron sized inclusions.

Dolomite fluid inclusion microthermometry

A total of six fluid inclusions were measured from the coarse-grained dolomite at Mullawornia. Their Th values ranged from 146 to 182.9°C. Due to the small size of the inclusions, no first melting temperatures were obtained. However, one reproducible Tm_{ice} measurement was made at -5°C. As the final phase to melt was ice and assuming that the inclusion is part of the H_2O-NaCl binary system, the equation of Bodnar (1993) can be used to convert the Tm_{ice} to a salinity value of 7.9 wt% NaCl equivalent.

Discussion

The fluid that precipitated the coarse-grained dolomite at Mullawornia was moderately hot (146 to 183°C) and moderately dilute (7.9 wt% NaCl equivalent). These data are similar to those reported for unmineralised, cross-cutting quartz-calcite-fluorite veins from Fulmort quarry (Gleeson & Yardley, 2002), approximately 25 kilometres east-northeast of the quarry at Mullawornia. Gleeson and Yardley (2002) reported evidence for the mixing of two fluids: a high temperature, low salinity fluid (Fluid 1) and a low temperature, high salinity fluid (Fluid 2). The data from Mullawornia suggest the presence of only Fluid 1. However, as the microthermometric data from Mullawornia is very much preliminary data, it is possible that with further work, evidence for the lower temperature, high salinity Fluid 2 will be found.

A note on the inclusions in the bitumen-related calcite

The bitumen-related calcite contains large numbers of fluid inclusions. They are all two-phase (L+V) inclusions and range in size up to about 12μm with degrees of fill (ψ_{liquid}) that range from 0.9 to 0.7. The assemblage is complex and clearly contains several different generations of fluid inclusions with most appearing to be secondary. Necking-down and leakage is a common feature within the assemblage. As the host phase is intimately associated with bitumen it can be assumed that there will be some petroleum-bearing inclusions within the assemblage. This was confirmed by observing thin sections of the bitumen-related calcite under the UV microscope. Several of the fluid inclusion trails

exhibit a green fluorescence while others appear not to fluoresce at all or have a dull reddish/brown fluorescence. This may indicate that there is a range of oils trapped in these inclusions. It is possible that these inclusions could be used to constrain the temperatures of petroleum migration and perhaps indicate if there has been multiple generations or pulses of hydrocarbons.

8.6 STABLE ISOTOPE GEOCHEMISTRY

Eleven samples of unaltered Waulsortian Limestone and eight samples of dolomitised Waulsortian Limestone from Mullawornia quarry were sampled for stable isotope analysis (Appendix B). A full description of the sampling methods is given in Chapter 2.

8.6.1 Calcite

The phases of the Waulsortian Limestone that were sampled for stable isotope geochemistry were micrite and the bitumen-related calcite. Nowhere in the samples that were available was the final porosity occluding cement phase, Stage D, sufficiently developed to enable pristine samples to be isolated.

The $\delta^{13}C$ values for the micrite and the bitumen-related calcite range from 3.77 to 4.39‰ (mean 4.1‰ ± 0.42‰ 2σ) and 1.58 to 3.38‰ (mean 2.47‰ ± 1.78‰ 2σ) respectively (Figure 8.3). The $\delta^{18}O$ values for the micrite range from 26.88 to 28.83‰ (mean 27.91‰ ± 1.4‰ 2σ; mode of 27.5‰) and 27.9 to 28.56‰ (mean 28.3‰ ± 0.6‰ 2σ) for the bitumen-related calcite.

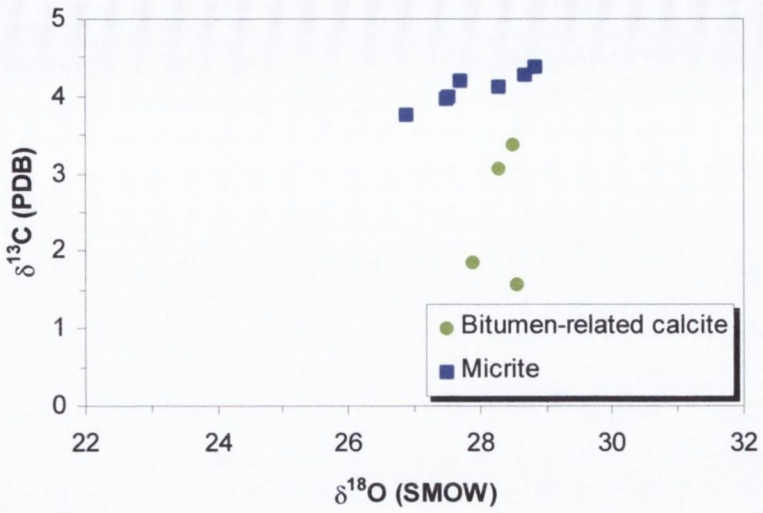

Figure 8.3 Scatter plot of $\delta^{13}C$ and $\delta^{18}O$ values for micrite and bitumen-related calcite phases at Mullawornia.

Discussion

The range in $\delta^{13}C$ values for the micrite is similar to that measured in other areas in this study and elsewhere in the Irish Midlands (Boast *et al.*, 1981a; Gallagher *et al.*, 1992). The bitumen-related calcite has $\delta^{13}C$ values that are slightly lower than Waulsortian Limestone cements, and may reflect the presence of an organic carbon component in the bicarbonate from which the $CaCO_3$ was precipitated.

The $\delta^{18}O$ values of both phases are slightly heavier than those measured in other areas throughout this study. As discussed in Chapter 3 (Lisheen), since brachiopods with a secondary layer were unavailable, micrite has been used to estimate the original $\delta^{18}O$ composition of marine derived carbonate (Moldovanyi & Lohmann, 1984). Mullawornia provides a better sampling site than Lisheen to estimate the $\delta^{18}O$ of Lower Carboniferous seawater as it is well outside the main mineralised zone. This reduces the possibility of alteration of the $\delta^{18}O$ signature by the multistage fluid flow associated with both regional dolomitisation and mineralisation. However, it is conceded that the hydrocarbon-bearing fluid may also alter the $\delta^{18}O$ signature. To minimise any possible effects on the $\delta^{18}O$ values of the micrite, samples were taken from areas where little or no bitumen was developed.

Using the median value of the micrite (27.5‰) and assuming that the Waulsortian Limestone formed at 25°C, the calculated $\delta^{18}O$ of the parental fluid (Friedman & O'Neil, 1977) precipitating the marine carbonate was –0.88‰. This value is comparable to the estimation of Meyers and Lohmann (1985), who obtained a $\delta^{18}O$ value of –1.5‰ ± 0.5‰ for early Carboniferous (Tournaisian) seawater from carbonates in New Mexico. It is also similar to the $\delta^{18}O$ value of –0.9‰ suggested by Gallagher *et al.* (1992) for unmineralised Waulsortian Limestone at Harberton Bridge, approximately 60 kilometres southeast of Mullawornia.

8.6.2 Dolomite

As the crystal size of the coarse-grained dolomite was commonly quite large, it was possible to sample individual zones within the dolomite. Two zones were isolated: zone 3, the thick non-luminescent, ferroan zone; and zone 4, the brightly luminescent zone (Plate 8.4a). The isotopic data for both zones are plotted in Figure 8.4.

The $\delta^{13}C$ values of both zones range from –0.19 to 4.28‰ (mean 3.61‰ ± 3.08‰ 2σ; mode of 4.2‰) and the $\delta^{18}O$ values range from 25.26 to 27.68‰ (mean 26.45‰ ± 2.2‰ 2σ; modes of 25‰ and 27‰).

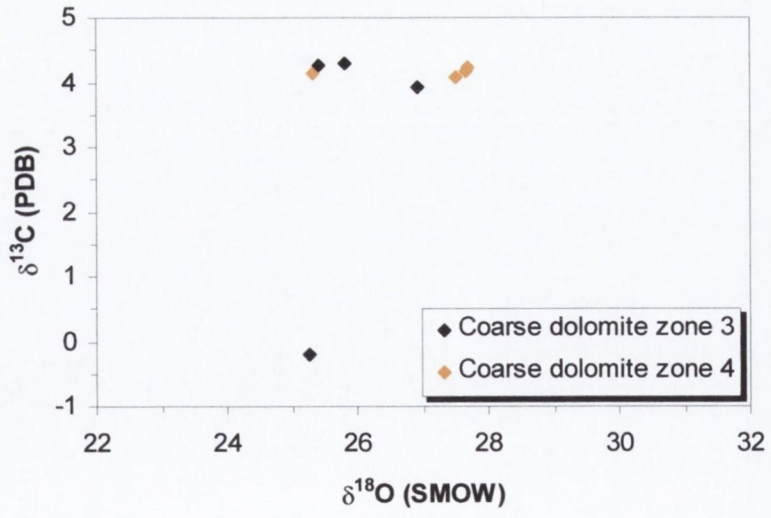

Figure 8.4 Scatter plot of $\delta^{13}C$ and $\delta^{18}O$ values for the coarse dolomites at Mullawornia.

Discussion

The $\delta^{13}C$ values of both dolomite zones (with the exception of one value at –0.19‰) are within the range of $\delta^{13}C$ values for Lower Carboniferous seawater (Brand, 1982; Meyers & Lohmann, 1985; Popp *et al.*, 1986). The one light $\delta^{13}C$ value at –0.19‰ may reflect the influence of the surrounding bitumen.

The $\delta^{18}O$ values of the coarse-grained dolomite at Mullawornia are much heavier than any of the dolomites sampled in the other areas in this study. With one exception, the bimodal distribution of the $\delta^{18}O$ data for the coarse-grained dolomite appears to mimic the sampled zone, in that the lightest $\delta^{18}O$ values are from zone 3 and the heaviest $\delta^{18}O$ values are from zone 4. It may be possible that had zones 1 and 2 been sampled they would have had lighter $\delta^{18}O$ values than either zones 3 or 4, with zone 1 being lighter than zone 2.

8.7 MODELLING OF PARENTAL FLUIDS

Due to the bimodal distribution in the $\delta^{18}O$ values of the coarse-grained dolomite it was not possible to construct a mineral-water oxygen isotope fractionation curve based on the mean of all of the measured $\delta^{18}O$ values. However, separate mineral-water oxygen isotope fractionation curves were constructed for both zone 3 and 4 using the equation of Land (1983) and are shown in Figures 8.5 and 8.6. The curves for the minimum, maximum and mean measured $\delta^{18}O$ values are shown in both.

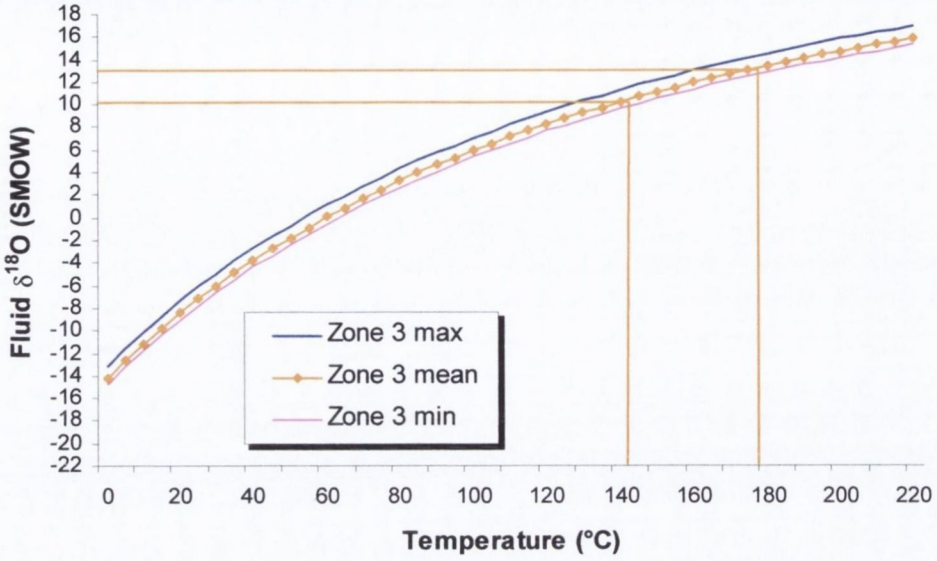

Figure 8.5 Mineral-water oxygen isotope fractionation curves for the minimum, maximum and mean $\delta^{18}O$ values measured for zone 3 of the coarse dolomite at Mullawornia. See text for discussion.

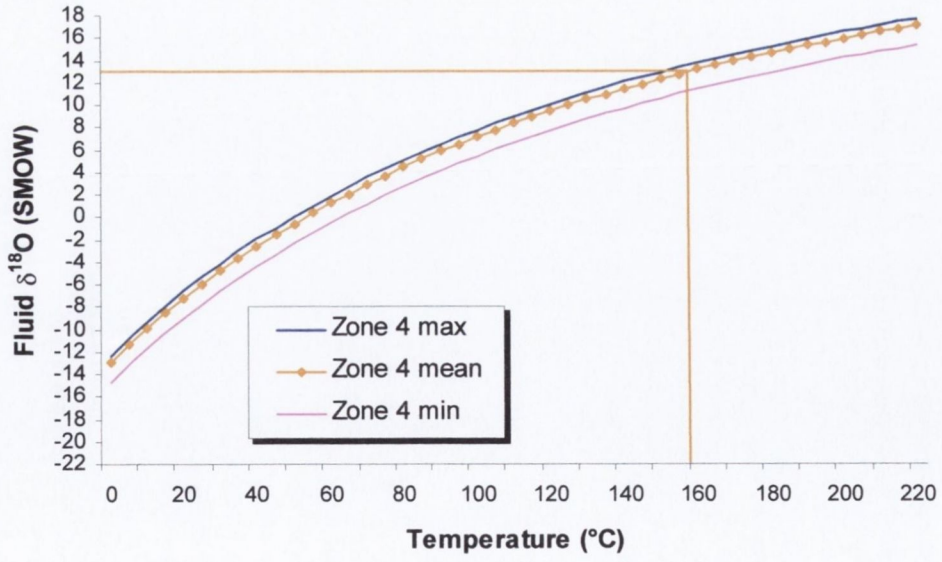

Figure 8.6 Mineral-water oxygen isotope fractionation curves for the minimum, maximum and mean $\delta^{18}O$ values measured for zone 4 of the coarse dolomite at Mullawornia. See text for discussion.

Discussion

The composition of the parental fluid of the zone 3 dolomite (using the curve constructed with the mean value) was calculated using the homogenisation temperature range (rounded to 145-180°C). This indicated isotopic values ranging from 10.7 to 13.5‰. The composition of the parental fluid of the zone 4 dolomite (again using the curve constructed with the mean value) was calculated using the homogenisation temperature range (rounded to 160°C). This indicated an isotopic value of 13.1‰.

Using the curves constructed from the minimum and maximum values for both zone 3 and 4 would alter these water isotopic values to 10.1 to 14.5‰ and 11.4 to 13.8‰ respectively. This suggests that whether the mean of the measured $\delta^{18}O$ values for each zone is used, or the minimum and maximum values, the $\delta^{18}O$ values inferred for the parental fluid still indicate that if seawater was the precursor it underwent a significant amount of fluid-rock interaction.

8.8 THERMAL HISTORY

The thermal maturity of the limestones at Mullawornia has been determined previously using Condont Alteration Indices (CAI) and bitumen reflectance, which in the absence of vitrinite can been used as an estimate of the thermal maturity (Parnell *et al.*, 1996).

Clayton *et al.* (1989) recorded a CAI value of 4.5, which corresponds to a vitrinite reflectance value of approximately 3.5% and a temperature of ~250°C (Merriman & Kemp, 1997). Parnell *et al.* (1996) recorded a mean bitumen reflectance value of 3.1%, which appears broadly consistent with the CAI data. The closest localities yielding vitrinite reflectance data are some 22 kilometres to the northeast at Ballinalack. The value recorded is 3.68% (Clayton *et al.*, 1989).

The occurrence of a large quantity of bitumen exhibiting mesophase texture at Mullawornia raises two questions: the origin of the liquid hydrocarbons that were the progenitors of the solid bitumens and inferences of thermal history and timing of emplacement to be drawn from this; and the thermal regime under which the mesophase textures formed.

In relation to the origin of the hydrocarbons, the sub-Waulsortian succession in the Irish Midlands is poor in terms of its source rock potential, whereas the supra-Waulsortian basinal sequences contain substantial intervals where the total organic carbon (TOC) is >1% (G. Sevastopulo pers. comm.) Therefore, the rocks above the Waulsortian Limestone, in particular the Calp (Figure 8.1), are most likely to have provided the ultimate source of the bitumen.

Vitrinite reflectance data from a 2km deep stratigraphic borehole drilled at Athboy, Co.Meath, approximately 60 kilometres northeast of Mullawornia, indicate that the geothermal gradient at peak burial in that area was ~51°C km^{-1} (Corcoran & Clayton, 2001). Given that the bitumen was clearly emplaced as a liquid, its progenitor must have been generated within the oil window (~70-110°C). This implies that the amount of cover needed above the bitumen source rocks was >1km. If the Calp is assumed to have been the original source of these solid hydrocarbons, this amount of cover (>1km) would not have been attained until the Asbian at the oldest (Strogen *et al.*, 1990).

As mentioned above, the mesophase textures within the bitumens have generally been interpreted as evidence of high temperatures (~350°C) of formation for these solid hydrocarbons. It this is true, their presence implies either: very substantial burial at 'normal' geothermal gradients or a high geothermal gradient perhaps linked to high heat flow associated with the Variscan orogeny; or a local hydrothermal (*sensu* Machel and Lonnee (2002)) event.

Taking the geothermal gradient from Corcoran and Clayton ((2001) p.75 Fig. 10) and projecting it to a vitrinite reflectance value of ~0.2% (the value for lignite) suggests that 1300m has been removed above the succession preserved in the Athboy borehole. Under this amount of cover, the suggested temperatures needed to generate the mesophase textures at Mullawornia, by burial alone, would not be attained.

Therefore it seems more likely that the mesophase textures exhibited by the bitumens at Mullawornia did not form at temperatures as high as 350°C, but were generated at temperatures ~250°C. This would be consistent with the CAI, vitrinite reflectance and fluid inclusion data.

In summary, it is thought that the bitumen was generated in basinal Calp Limestones no earlier than the Asbian. It migrated up dip to the basin margin and was trapped in secondary cavities, which were sealed by calcite. During peak burial in the late Carboniferous, geothermal temperatures reached ~250°C, which produced the mesophase texture.

8.9 CONCLUSIONS

- Large cavities occur within the Waulsortian Limestone at Mullawornia, which are probably secondary solution cavities that originated after porosity occlusion within the host limestone.

- Saddle dolomite is found growing into the open space within these secondary cavities. This dolomite appears restricted to the floor of the cavities, which may suggest that it formed as a geopetal dolomite.

- Th data indicate that these dolomites formed at temperatures >145°C. A single reproducible Tm_{ice} indicates that the dolomitising fluid was moderately saline (7.9 wt% NaCl equivalent).

- In relation to the fluids involved in the formation of the Irish base-metal deposits these microthermometric data imply that the dolomitising fluids may be considered as being equivalent to Fluid 1, the high temperature, moderate salinity, ore-bearing fluid.

- Bitumens exhibiting mesophase textures, supposedly indicative of formation at very high temperatures, also occur within these cavities. Veins filled with bitumen-related calcite, which pre-dates or is contemporaneous with the bitumen, appear to have been exploited by the bitumen-bearing fluids as a means of emplacement.

- The mesophase textures exhibited by the bitumens at Mullawornia probably formed at temperatures much lower than those derived by experiment (350°C). They are more likely to have developed at peak Variscan burial (~250°C).



Figure 8.1 A simplified geological map of the area surrounding Mullawornia. Grid lines refer to the Ordnance Survey of Ireland National Grid. Modified after Hitzman (1992c).

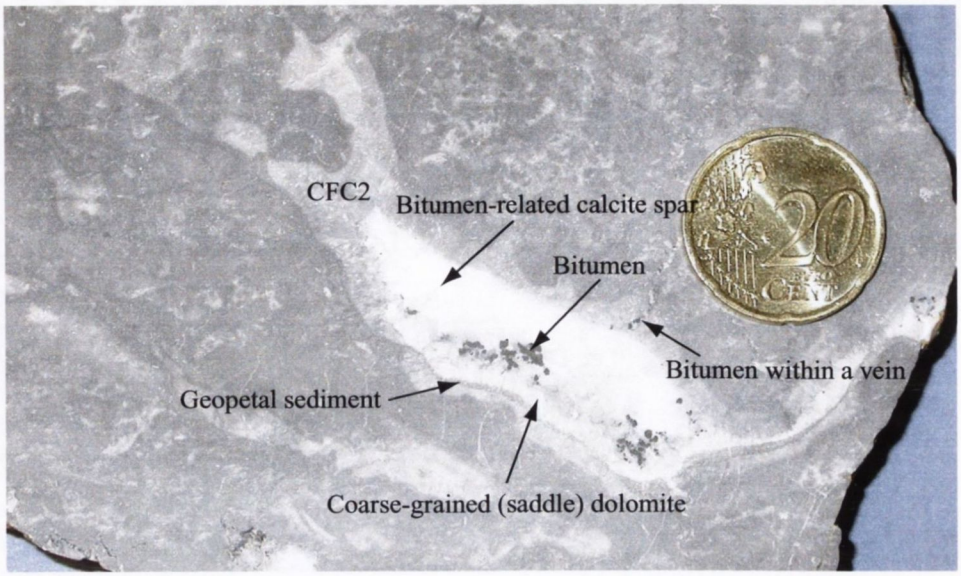

Plate 8.1: View of one of the large irregularly-shaped cavities found within the Waulsortian Limestone at Mullawornia Quarry. The main features of the cavity are labelled. Size of coin is 22mm.

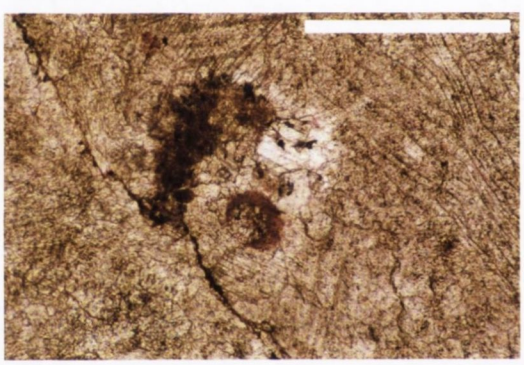

Plate 8.2a: P17639 - Mullawornia Quarry. PPL view of an early calcite-filled cavity. Scale bar is 500µm.

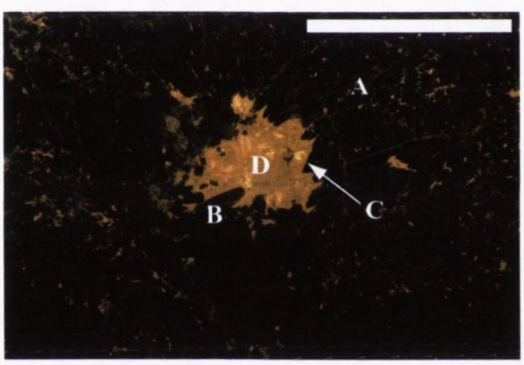

Plate 8.2b: Same view in CL. The early calcite cements (Stages A-D) are labelled. Stage D is the porosity occluding cement. Scale bar is 500µm.

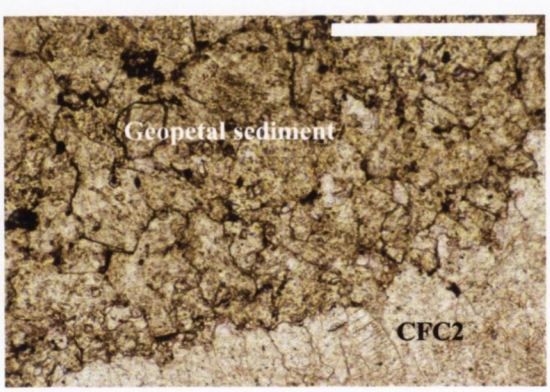

Plate 8.3a: P17637 - Mullawornia Quarry. PPL view of the base of the cavity shown in Plate 8.1. The second development of CFC (CFC2) and the overlying geopetal sediment are indicated. Scale bar is 500µm.

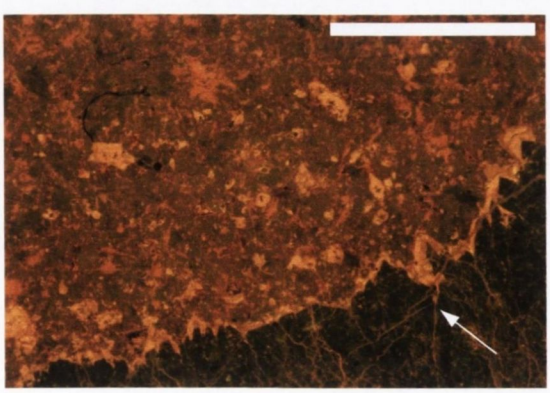

Plate 8.3b: Same view in CL. The geopetal sediment has been partially replaced by fine-grained dolomite. Thin veins that cross-cut the CFC2 (arrow) appear to feed the relict calcite within the geopetal sediment. Scale bar is 500µm.

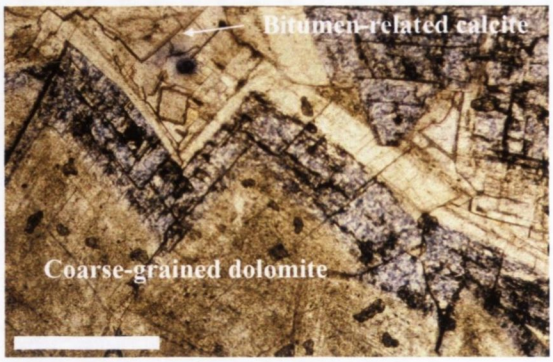

Plate 8.4a: P17637 - Mullawornia Quarry. PPL view of the coarse-grained dolomite and the bitumen-related calcite. Note that the turbidity and the stain highlights the zoning within the dolomite crystals. Scale bar is 500µm.

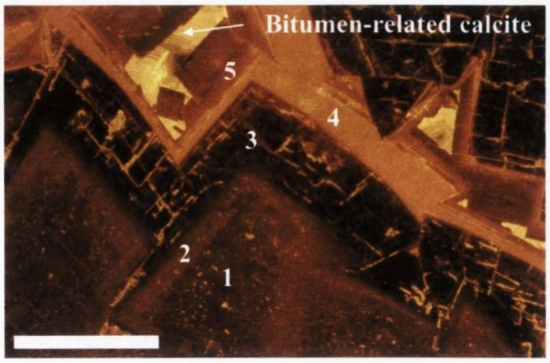

Plate 8.4b: Same view in CL. Note that the coarse-grained dolomite contains up to five different zones (labelled). Scale bar is 500µm.

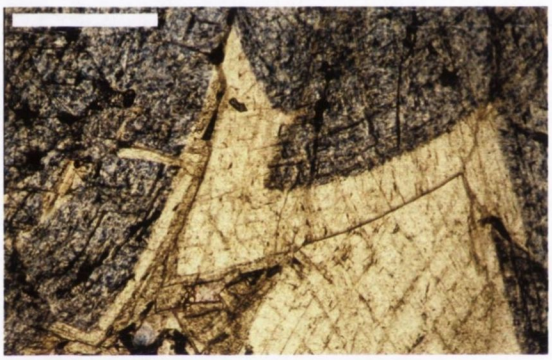

Plate 8.5a: P17637 - Mullawornia Quarry. PPL view of the saddle crystal shapes of the coarse-grained dolomite. Scale bar is 500µm.

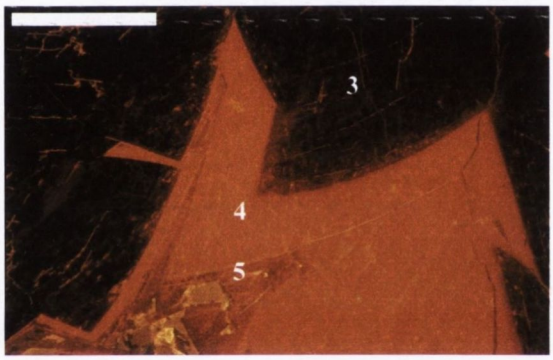

Plate 8.5b: Same view in CL. Note that only the last 3 zones are present in the image (labelled) but zones 1 and 2 also display saddle shapes. Scale bar is 500µm.

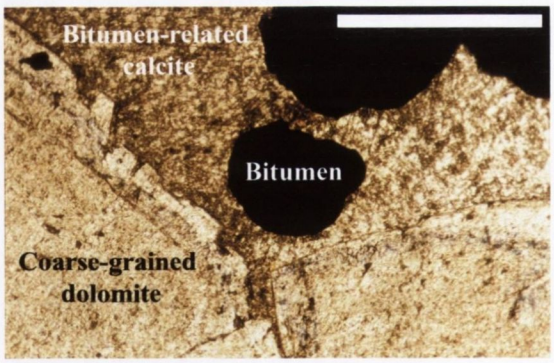

Plate 8.6a: P17637 - Mullawornia Quarry. PPL view of the coarse-grained dolomite, bitumen-related calcite and bitumen. Scale bar is 500µm.

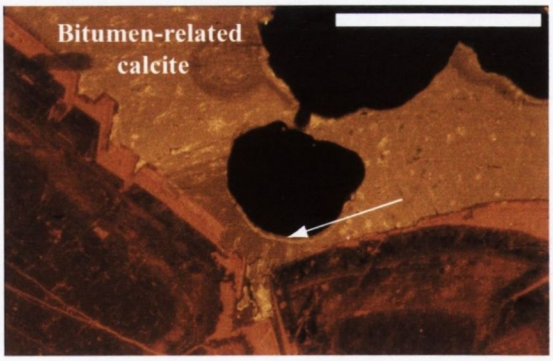

Plate 8.6b: Same view in CL. The bitumen-related calcite has a similar luminescence to the Stage D calcite. Note the development of a cement meniscus at the base of the bitumen (arrowed). Scale bar is 500µm.

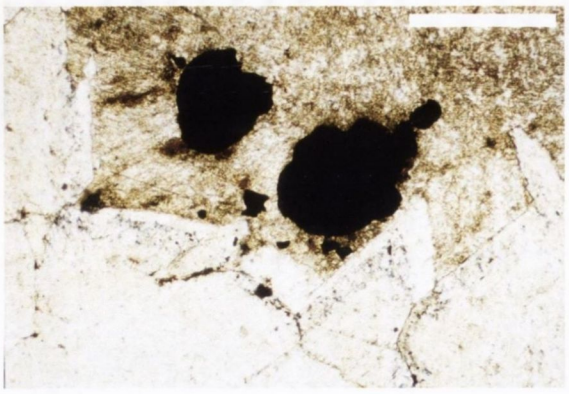

Plate 8.7a: P17637 - Mullawornia Quarry. PPL view of bitumen contained within the bitumen-related calcite. Scale bar is 500µm.

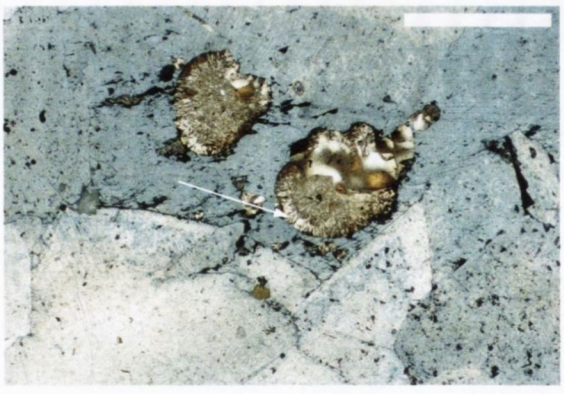

Plate 8.7b: Same view in reflected light, with cross polars. Note the mesophase textures, which consist of anisotropic spheres and a radial texture around the rim (arrow). This suggests formation at elevated temperatures. Scale bar is 500µm.



Plate 8.8a: P17637 - Mullawornia Quarry. PPL view of bitumen contained within the bitumen-related calcite. Scale bar is 500µm.



Plate 8.8b: Same view in reflected light, with cross polars. Mesophase textures again visible but also a crack (C) in the bitumen indicating brittle failure. Scale bar is 500µm.

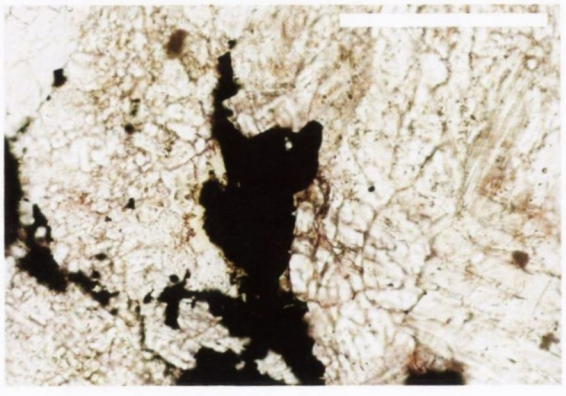

Plate 8.9a: P17637 - Mullawornia Quarry. PPL view of bitumen contained within the bitumen-related calcite. Scale bar is 500µm.

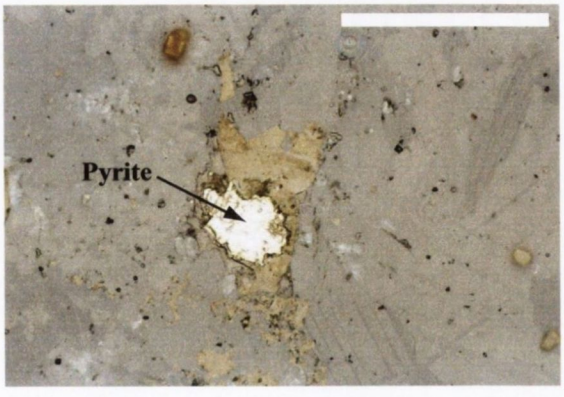

Plate 8.9b: Same view in reflected light. Note that pyrite is also present and only becomes visible under reflected light. The pyrite post-dates the bitumen. Scale bar is 500µm.

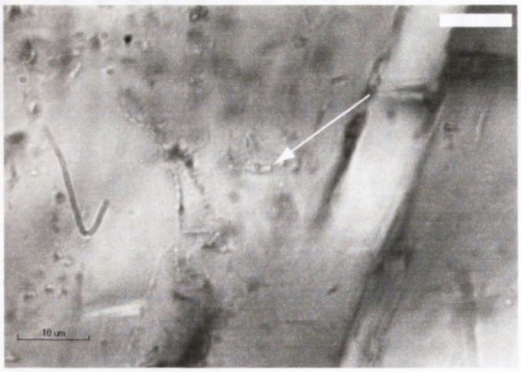

Plate 8.10: Image of the A1 fluid inclusion contained within the Fe-rich zone 3 of a coarse dolomite crystal (arrow). Scale bar is 10μm.

CHAPTER 9

STRATIGRAPHICAL AGE OF CEMENTATON: NAVAN

9.1 INTRODUCTION

The dolomite in the occurrences described in previous chapters has been shown to have been emplaced after all of the calcite cements, that occluded porosity in the host limestones, had formed. However, in the south of the country there is no direct method of stratigraphically dating the last, porosity occluding calcite cement stage in these limestones. In the Midlands, there are several localities where the cements can be dated stratigraphically. The majority of these are stratigraphically dated conglomerates containing clasts that had been cemented before they were incorporated; a few are volcanic breccias that have entrained sedimentary clasts. One example of each type is described in this and the following chapter.

The Navan Zn-Pb orebody is located just outside the town of Navan, Co. Meath, approximately 50 kilometres northwest of Dublin (Figure 9.1). The deposit was discovered in 1970 by Tara Exploration and Development Ltd. and remains the largest Zn-Pb deposit in Europe. Initial reserves amounted to 69.9 Mt (Andrew & Ashton, 1985; Ashton *et al.*, 1986) but the recent acquisition of the Bula orebody to the northwest of the main mine and the discovery of the South West Extension (SWEX; Ashton *et al.* (2003)) probably raises present day reserves closer to 100 Mt. Until recently the mine was owned and operated by Outokumpu but has now been sold to Boliden.

In the Navan area there is an early Viséan (late Chadian) unconformity, below which substantial parts of the Lower Carboniferous succession have been removed. A polymict conglomerate termed the Boulder Conglomerate lies above the unconformity. This erosion surface can be used to determine the porosity of the underlying limestones at the time in the early Viséan when they were incorporated as clasts in the Boulder Conglomerate. A similar approach was used by Meyers (1974), when he used a mid-Carboniferous aged unconformity in New Mexico to date cements, based on whether they were developed above (post-unconformity) or only below (pre-unconformity) the erosion surface.

9.2 REGIONAL GEOLOGICAL SETTING

9.2.1 Stratigraphy

Work by Philcox (1984; 1989) provided the first detailed descriptions of the stratigraphy at Navan and the surrounding area. Andrew and Ashton (1985), Ashton *et al.* (1986), Strogen

et al. (1990), Rizzi (1993), Ford (1996), Anderson *et al.* (1998), Peace (1999), Peace *et al.* (2003) and Ashton *et al.* (2003) all have provided overviews of the geology and mineralisation of the Navan deposit.

In the Navan area, Lower Carboniferous red sandstones, termed the Red Beds (Figure 9.2), overlie the Lower Palaeozoic rocks. They are analogous to the Old Red Sandstone developed further south. They are overlain by the marginal marine Laminated Beds followed by the Muddy Limestone, which to the west of the mine contains channels that cut down into the Laminated Beds sequence. The succeeding Pale Beds are shallow water limestones, dolomites and sandstones and are the major host rocks to the Zn-Pb mineralisation at Navan. The basal unit of the Pale Beds, termed the Micrite Unit, is a pale grey, micritic limestone containing oncolites and bird's eye textures. Many distinctive marker horizons occur within the Pale Beds and serve to subdivide the various ore lenses and are valuable tools in the structural interpretation of the orebody. The overlying Shaley Pales are thinly bedded, calcareous sandstones and shales and are included with the underlying succession to make up the Navan Group (Figure 9.2). Above the Shaley Pales, deeper water crinoidal limestones, termed the Argillaceous Bioclastic Limestone (ABL), are followed by a laterally impersistent development of Waulsortian Limestone. In the mine area proper, both the ABL and Waulsortian Limestone have been removed below the erosion surface (see below). No significant mineralisation has been documented from the Waulsortian Limestone in the Navan area despite its role as the dominant host at other Zn-Pb deposits throughout the Irish Midlands (Hitzman, 1995a). As the Waulsortian Limestone mudbanks are often interdigitated with the ABL they have both been informally assigned to the ABL Group in the Navan area (Figure 9.2).

Substantial parts of the Lower Carboniferous succession in the area surrounding the mine have been removed below a major unconformity, termed the 'Erosion Surface' by Philcox (1989) (Figures 9.1 and 9.2). The unconformity has been interpreted by Boyce *et al.* (1983b) and Ashton *et al.* (1986) as being the expression of large-scale submarine slumping and sliding caused by growth faulting, as a result of extension in the Navan area during the early Viséan. A breccia-conglomerate, termed the Boulder Conglomerate and interpreted as a debris flow, overlies the unconformity. It varies in thickness from <1m to ~50m and consists of chaotically distributed clasts of Pale Beds (mineralised and unmineralised), Shaley Pales and Waulsortian Limestone enclosed in a dark argillaceous

matrix. The clasts are up to a maximum of 8m in diameter and are mostly sub-angular to angular in shape. Clasts of Lower Palaeozoic rocks occur in the Boulder Conglomerate to the south of the orebody (Ashton, 1995) where the erosion surface has removed almost the entire Lower Carboniferous section (Figure 9.2).

The Boulder Conglomerate is overlain by a thick sequence of well-bedded limestones, interpreted as calciturbidites, known as the Upper Dark Limestones (UDL). The basal contact between the UDL and the Boulder Conglomerate varies, being sharp in some locations and more gradational in others. In the east of the mine, the contact is gradational, with the presence of alternating layers of mudstone and thin pebble conglomerates. These are succeeded by a unit of thinly bedded mudstone and limestone termed the Thin Bedded Unit (Figure 9.2).

Above the Thin Bedded Unit, but below the AA marker, are further horizons of conglomerate (Figure 9.2), termed the 'Conglomerate Complex' (Philcox, 1989). These are also chaotic, coarse conglomerates, approximately 20m thick. The 'Conglomerate Complex' represents further major debris flows, but is probably more proximal in aspect than the Boulder Conglomerate because large rafts of the Shaley Pales commonly remain intact within it (Philcox, 1989). Boulders of Waulsortian Limestone and bird's eye micrites (Pale Beds) have also been found within this conglomerate. Microfaunal dating by G. Sevastopulo (pers. comm.) has shown that the Thin Bedded Unit and a few metres of overlying beds are of early Viséan (pre-Arundian) age. The 'Conglomerate Complex' is therefore probably Arundian in age (G. Sevastopulo pers. comm.).

9.2.2 Structure

The structure at Navan (Figure 9.1) is dominated by a complex, faulted, broadly antiformal structure, which plunges gently to the southwest (Ashton, 1995; Anderson *et al.*, 1998). The orebody is cut by a series of early east-northeast trending faults (B, T, Liscarton and Castle Faults) and then by a later northeast trending set (A, C, D, Castle and Randlestown Faults).

The late faults, which have been attributed to the reactivation of basement structures during the Variscan orogeny, have displacements of up to ~250m and truncate the ore lenses. The early faults, some of which were also later reactivated by Variscan activity, are thought to

have been active during the late Tournaisian to early Viséan because the B Fault is truncated by the 'Erosion Surface' and does not penetrate the Upper Dark Limestone in the main mine area (Ashton, 1995). The T Fault also shows evidence of several stages of movement and according to Ashton (1995) may have formed before and also moved after the formation of the Boulder Conglomerate. Ashton *et al.* (1986) and Blakeman *et al.* (2002) considered that these early faults played an important role during mineralisation.

9.2.3 Mineralisation

Mineralisation at Navan is most persistent towards the base of the Pale Beds within the basal Micrite Unit and associated dolomites. The ore occurs in stratiform to stratabound lenses, which, as mentioned in Section 9.2.2, are dislocated by Variscan faulting. In the southeastern part of the orebody, the ore lenses are truncated by the erosion surface (Figure 9.2). Mineralisation also occurs within the Boulder Conglomerate where it is referred to as the Conglomerate Group Ore (CGO, Figure 9.2); this occurs almost exclusively in the southeastern part of the orebody and accounts for less than 3% of the total ore at Navan (Anderson *et al.*, 1998).

The age of mineralisation at Navan has been controversial. Early work on the deposit (see summary by Andrew (1993)) suggested that mineralisation was syngenetic or syndiagenetic in origin and therefore occurred during the late Tournaisian to early Viséan. The occurrence of stratiform ore in the Boulder Conglomerate (Ashton *et al.*, 1992), mineralised veining (Anderson, 1990), mineralised clasts with evidence of epigenetic textures within the Boulder Conglomerate (Ford, 1996), and mineralised beds within the UDL have all been used as evidence to suggest that mineralisation spanned the formation of the Boulder Conglomerate (early Viséan to early Arundian). Peace (1999) and Peace and Wallace (2000) have argued for a later age (post-Arundian) for the mineralisation at Navan on the basis that the sulphides can be seen to have replaced stylolites, which they suggested formed at depths >800m. Based on reconstructions of the burial history, using data from Strogen *et al.* (1990), Somerville *et al.* (1992), Pickard *et al.* (1994) and Hitzman (1995b), Peace and Wallace (2000) suggested that the mineralised zones at Navan would not have reached a depth of ≥800m until the Holkerian and so they considered the mineralisation to have occurred during the Holkerian or younger. Recent work by Symons *et al.* (2002) using palaeomagnetism has also suggested a late Arundian to early Asbian date for mineralisation.

9.3 PETROGRAPHY

Several boreholes (N1446, N1445, N1455, N1544), each containing good intersections of the Boulder Conglomerate, were sampled. Drillholes that contained intersections of the 'Conglomerate Complex' were also sampled (EP11 and EP4A). These were drilled near the small satellite deposit of Clogherboy, which lies approximately 1.5 kilometres southeast of Navan (Figure 9.1).

9.3.1 Boulder Conglomerate

Hand samples

The Boulder Conglomerate is a chaotic, polymict debris flow. The clasts were dominantly derived from the Pale Beds, Shaley Pales and Waulsortian Limestone (Plate 9.1) and are enclosed in a dark matrix that varies from being predominantly micritic to argillaceous (Ford, 1996). Sand sized grains of quartz, which may have come from the Red Beds or the Shaley Pales, and bioclastic fragments also form a substantial part of the matrix (Plate 9.1).

Large cobble sized clasts of Waulsortian Limestone are common within the Boulder Conglomerate in core (Figure 9.2) and very large boulders have been encountered during mine development underground. They are commonly angular in shape, which suggests that they were probably well-cemented prior to being incorporated within the conglomerate. Many of them contain large early calcite-filled cavities, some of which have been truncated by the conglomerate matrix (Figure 9.2). These samples provide evidence of the degree of cementation of the Waulsortian Limestone at the time of its entrainment within the Boulder Conglomerate.

Thin sections

In the samples studied, the Boulder Conglomerate is both matrix and clast supported. Sand grade quartz, fossil fragments and calcareous shale dominate the matrix, although in some places a more micritic matrix is present. A common component found within the matrix is collophane (cryptocrystalline apatite). Former mudstone clasts are completely replaced by collophane and are ubiquitous throughout the samples (Plate 9.3a). Peace (1999) recorded the presence of both collophane clasts and collophane cement within the Boulder Conglomerate; however, only the former were observed within this study. The clasts replaced by collophane are usually reddish brown in PPL, isotropic in XPL (Plate 9.3b),

and have a dull blue luminescence under CL. They were up to 12mm in size and were generally subangular or subrounded in shape. Peace (1999) carried out microprobe analysis on the collophane and showed that it was F-rich and Cl-poor. Although the exact composition was not determined, Peace (1999) concluded that it was probably francolite (carbonate fluorapatite) because most marine phosphates are composed of carbonate fluorapatite. Discrete grains of apatite also occur within the matrix of the Boulder Conglomerate (Plates 9.4a and 9.4b). They may have come via sandy units in the Tournaisian succession, from the late Caledonian syenites known from the Lower Palaeozoic basement in the area (Figure 9.2) or from the Pale Beds sandstone (Rees, 1987).

Of all of the clasts contained within the Boulder Conglomerate, those of Waulsortian Limestone are the most abundant. Many are cobble sized (Plate 9.2) or larger. The early cavity-filling cements within them are well-developed (Plates 9.5a and 9.5b) and, as observed elsewhere in the Irish Midlands, the Stage D cement is the final porosity occluding cement. It is clear from the relationship between the calcite-filled cavities and the clast margins that porosity occlusion within the Waulsortian Limestone clasts had occurred prior to their incorporation within the conglomerate.

Possible evidence for a primary Waulsortian cavity, rimmed by CFC and then infilled with the matrix of the conglomerate, within the Waulsortian Limestone has been observed in hand sample (Plate 9.2). However, upon close examination of a thin section of the clast, it was concluded that it had broken cleanly along the boundary between CFC and later cements and therefore did not provide evidence of preservation of primary porosity at the time that it was incorporated into the conglomerate. Other examples of truncated calcite-filled cavities were found in thin section (Plates 9.6a and 9.6b). These cavities appear to have been totally filled by cements prior to being truncated. This supports the hypothesis that all of the porosity within the Waulsortian Limestone was occluded prior to the Boulder Conglomerate being deposited.

9.3.2 'Conglomerate Complex'

Hand samples

The 'Conglomerate Complex' is lithologically very different from the UDL within which it occurs and so is easily identified. The dark coloured matrix is predominantly argillaceous and contains an abundance of bioclastic fragments (Plate 9.7). Although dominated by

Waulsortian Limestone clasts (Plate 9.7), some of which are up to 1m in diameter (Philcox, 1989), the 'Conglomerate Complex' also contains a large quantity of Pale Beds clasts. These are more abundant than those found within the Boulder Conglomerate and tend to be larger in size. The 'Conglomerate Complex' therefore provides an ideal opportunity to study the degree of cementation of the Pale Beds at the time of their incorporation within the conglomerate.

Thin sections

Clasts of skeletal grainstone (Plate 9.8a) contained within the 'Conglomerate Complex' are likely to have come from the Pale Beds and comparison of foraminiferans contained within them and those studied by Rees (1987), suggests that they may have come from the lower parts of the Pale Beds. Calcite cements are visible within the grainstone clasts (Plate 9.8b) and indicate that porosity occlusion occurred within the Pale Beds limestones prior to their incorporation within the conglomerate. There is little evidence of mechanical breakage of the bioclasts within the Pale Beds grainstones and so these calcite cements are thought to have formed very early and to have imparted sufficient rigidity to the limestones to prevent crushing by compactional stress.

Clasts of Pale Beds containing bird's eye textures are also very common with the 'Conglomerate Complex' (Plate 9.9). They were probably derived from the basal unit of the Pale Beds, the Micrite Unit, which typically contains bird's eye micrite. Silicification of bioclasts within clasts of Waulsortian Limestone within the 'Conglomerate Complex' is also a common feature (Plate 9.10).

9.4 TIMING OF CEMENTATION OF THE TOURNAISIAN ROCKS

Porosity occlusion within the Waulsortian Limestone had already occurred by the time it was incorporated within the Boulder Conglomerate. Based on the early Viséan age of the erosion surface at Navan, this suggests that porosity occlusion within the Waulsortian Limestone in this part of the Irish Midlands was complete by the early Viséan.

Carbonate clasts from the Pale Beds, incorporated within the 'Conglomerate Complex', indicate that complete occlusion of porosity within them had occurred prior to the Arundian.

The abundance of loose sand grains within the matrix of the Boulder Conglomerate (Plate 9.3a) may also provide evidence that the siliciclastics were poorly cemented at the time of incorporation into the conglomerate.

9.5 DEPTH OF FORMATION OF THE EARLY CALCITE CEMENTS

De Brit (1988) reported a Waulsortian Limestone clast within the Boulder Conglomerate at Navan, containing a truncated early cavity that was lined with Stage B and C and some early Stage D calcite. He used this to propose that the depth of formation of the late Stage C and earliest Stage D in the Waulsortian Limestone was likely to have been between 50 and 150m (not taking compaction into account). Peace (1999) suggested that burial cementation prior to mineralisation occurred at a minimum of 400-500m.

Evidence from this study shows that cement Stages A-D were present within the Waulsortian Limestone prior to its incorporation within the Boulder Conglomerate during the Lower Viséan. The Athboy borehole, drilled approximately 12km southwest of Navan in a more basinal setting (Strogen *et al.*, 1990), provides an upper limit of ~230m (from the base of the Waulsortian Limestone to the base of the Arundian) for the maximum burial of the Waulsortian Limestone prior to its incorporation into the Boulder Conglomerate. This depth is well within the estimate of Lees and Miller (1995 p.250 Fig. 46) for the depth of formation of cements within the Waulsortian Limestone.

9.6 CONCLUSIONS

- The early calcite-filled cavities within Waulsortian Limestone clasts entrained within the Boulder Conglomerate contain the cement Stages A-D. In accordance with what has been observed throughout the Irish Midlands, Stage D is the porosity occluding cement.

- Porosity occlusion within the Waulsortian Limestone at Navan occurred prior to the inclusion of its clasts within the Boulder Conglomerate and so occurred prior to the early Viséan.

- The abundance of loose sand grains within the matrix of the Boulder Conglomerate suggest that some siliciclastic units may have been poorly cemented at the time they were incorporated within the conglomerate.

- The 'Conglomerate Complex', which occurs below the AA marker and above the Thin Bedded Unit, contains an abundance of Pale Beds clasts. It therefore provides an ideal opportunity to examine the degree of cementation of the Zn-Pb host rocks at Navan at the time of inclusion within the conglomerate.

- CL microscopy indicates that all of the remaining porosity within the Pale Beds clasts was occluded prior to inclusion within the 'Conglomerate Complex'. Microfaunal dating of the units directly below the conglomerate suggests an Arundian age date for the 'Conglomerate Complex' and therefore indicates that porosity occlusion within the Pale Beds occurred prior to this.

- Based on evidence from this study as well as data from Lees and Miller (1995 p.250 Fig. 46) and Strogen *et al.* (1990), the depth of formation of the early calcite cements within the Waulsortian Limestone at Navan is likely to have occurred within a maximum of 500m. This contradicts the depths proposed by other workers (de Brit, 1988; Peace, 1999; Peace & Wallace, 2000).

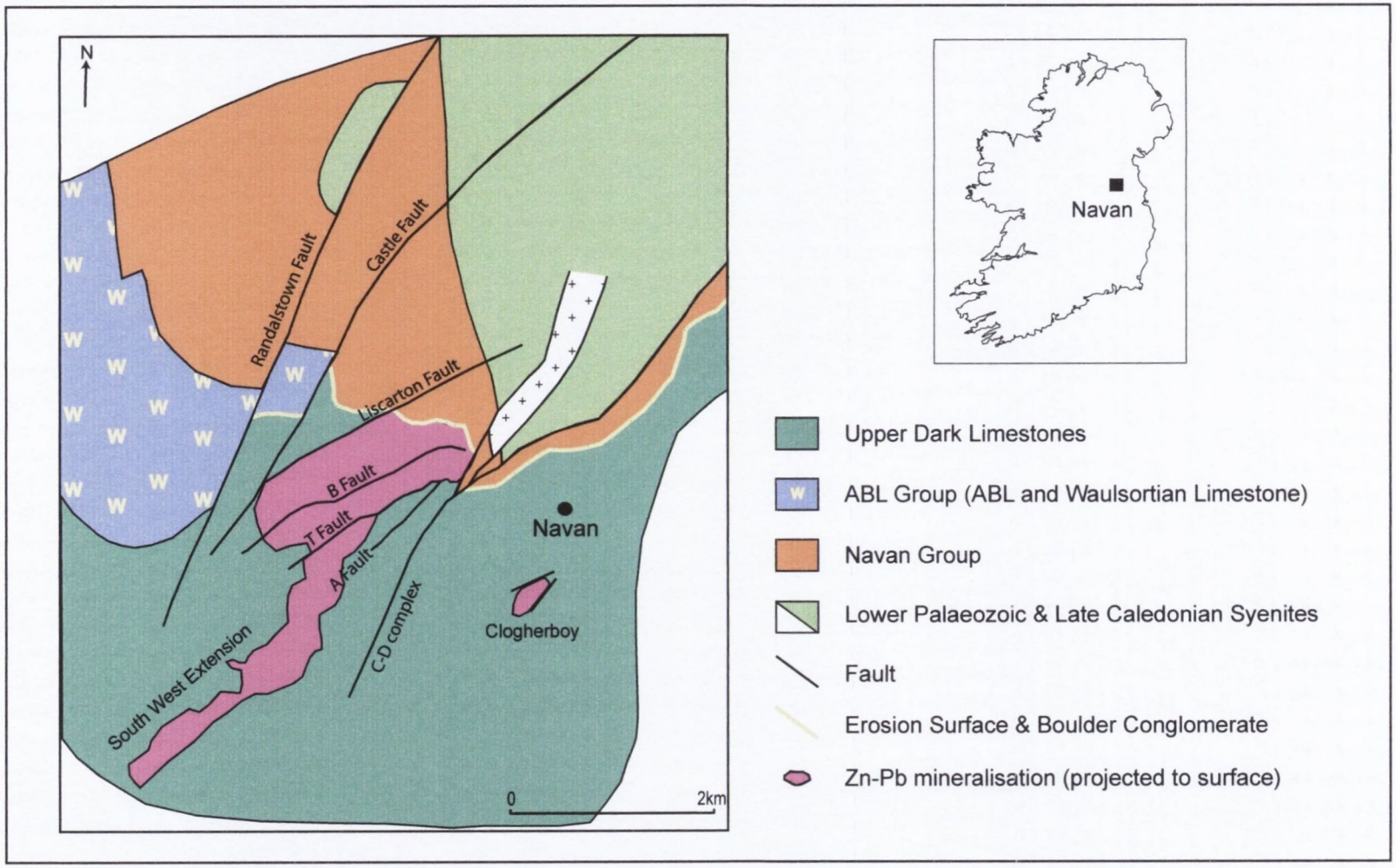

Figure 9.1 Location and geological setting of the Navan Zn-Pb deposit. Modified after Ashton (1995) and Peace *et al.* (2003).

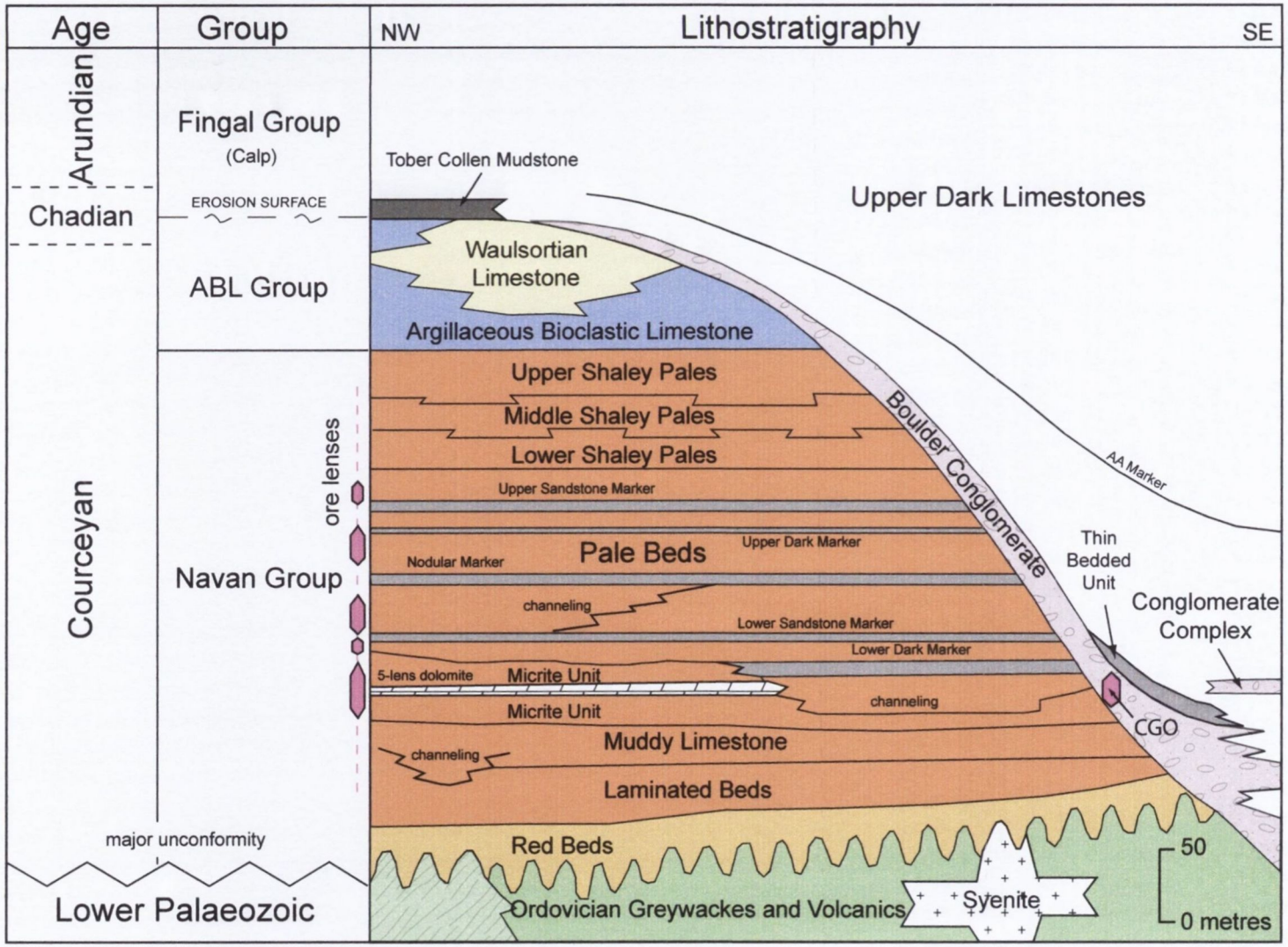

Figure 9.2 Stratigraphic sequence as seen in the Navan mine area. Modified after Ashton (1995).

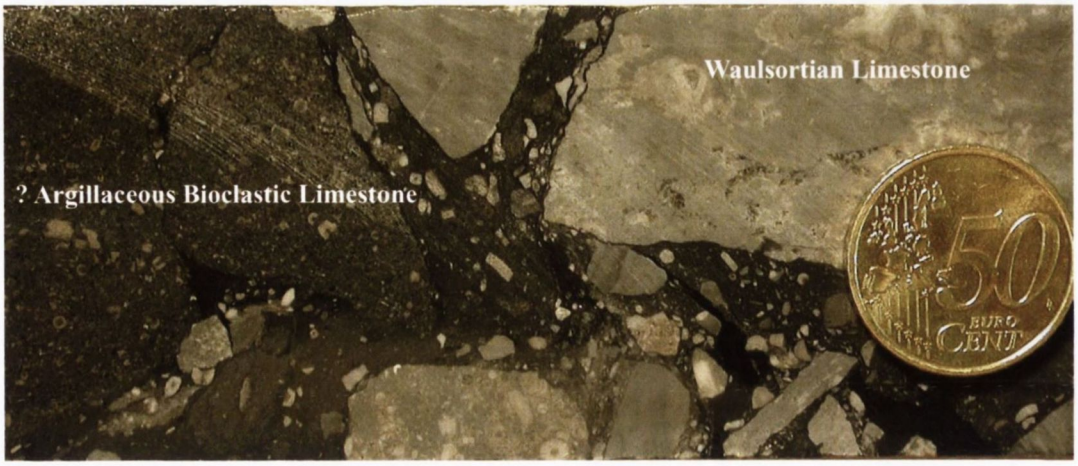

Plate 9.1: Drillcore sample of the Boulder Conglomerate from N1446 (863.9 - 864.35m). Some of the clasts found within the conglomerate are labelled. The dark coloured matrix is very argillaceous and contains many fine quartz grains and bioclastic fragments. Top to the left. Size of coin is 24mm.

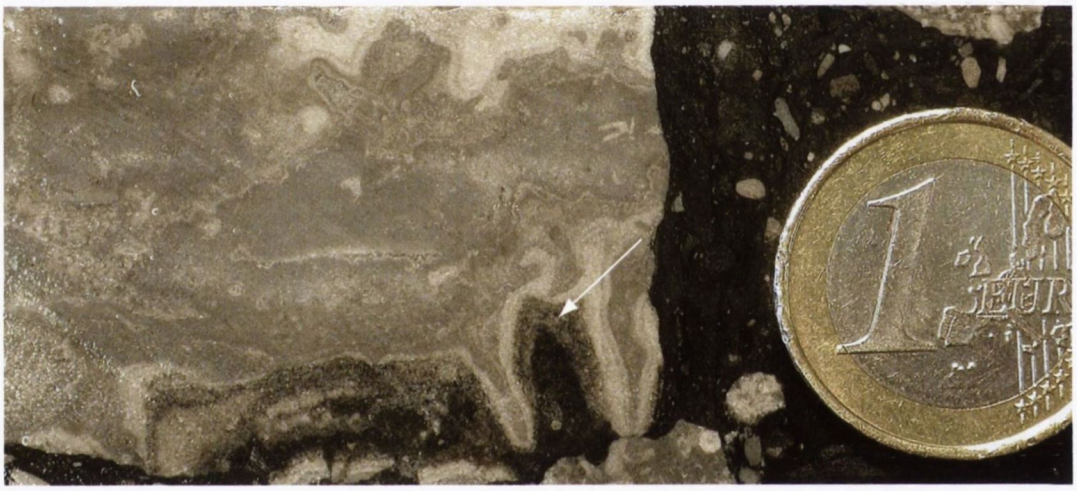

Plate 9.2: Drillcore sample of Boulder Conglomerate from N1446 (863.9 - 864.35m). A cobble sized clast of Waulsortian Limestone with a primary cavity (arrow) apparently filled by matrix. Top to the left. Size of coin is 23mm.

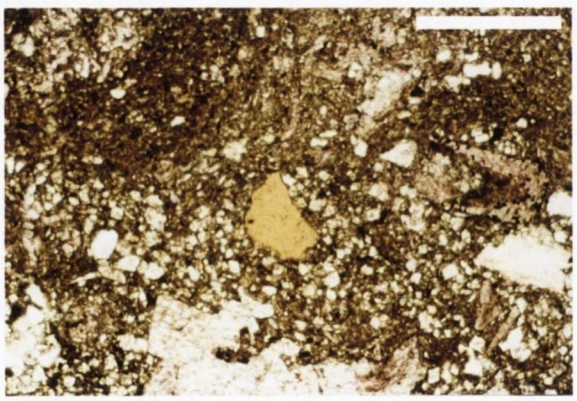

Plate 9.3a: P17617 - N1445 (779.3 - 779.48m). PPL view of the matrix of the Boulder Conglomerate containing a mudstone clast that has been replaced by collophane. Scale bar is 500µm.

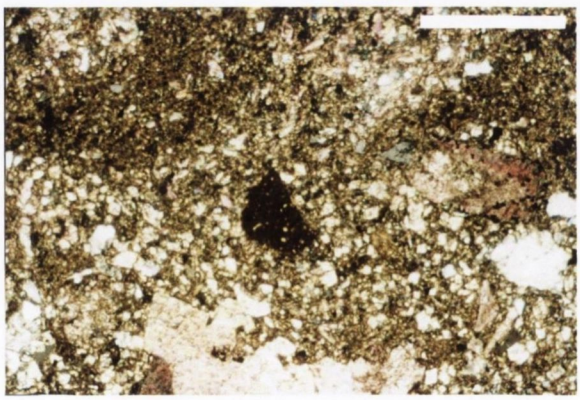

Plate 9.3b: Same view in XPL. Note the subangular shape of the clast. The collophane is isotropic in XPL. Scale bar is 500µm.

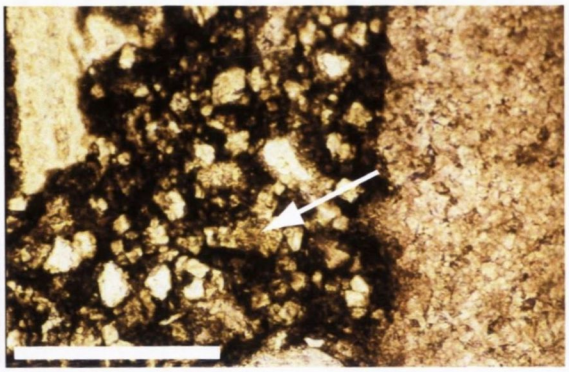

Plate 9.4a: P17617 - N1445 (779.3 - 779.48m). PPL view of the matrix of the Boulder Conglomerate and an individual grain of apatite (arrow) contained therein. Scale bar is 500µm.

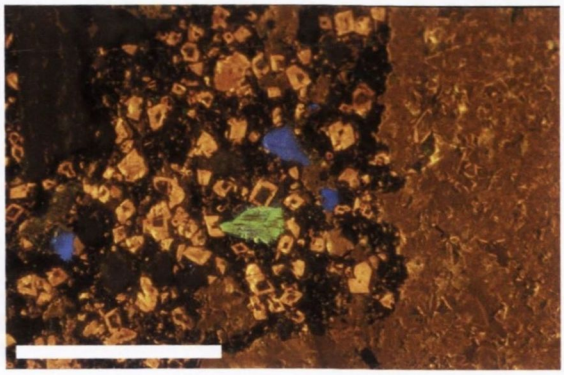

Plate 9.4b: Same view in CL. Note how the apatite grain, with its bright green luminescence, is easily located under CL. Scale bar is 500µm.

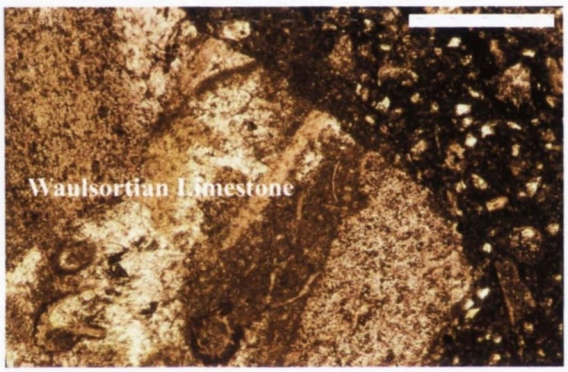

Plate 9.5a: P17621 - N1446 (863.9 - 864.35m). PPL view of a sharp edged Waulsortian Limestone clast (labelled) contained within the Boulder Conglomerate. Scale bar is 500µm.

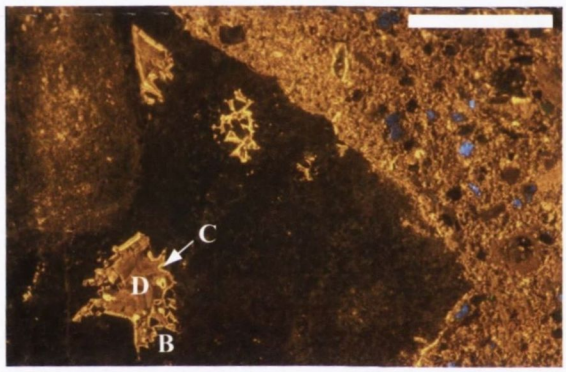

Plate 9.5b: Same view in CL. Note the presence of early calcite-filled cavities. The calcite cements (Stages B-D) in one cavity are labelled. Scale bar is 500µm.

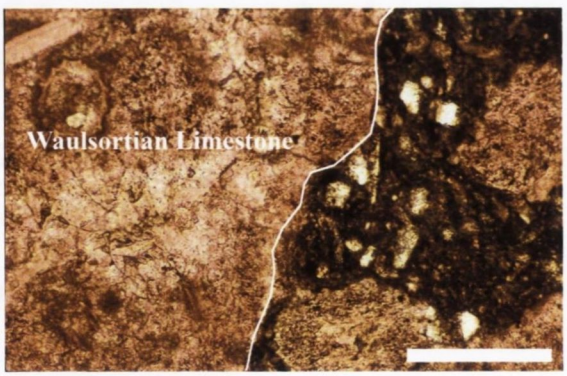

Plate 9.6a: P17621 - N1446 (863.9 - 864.35m). PPL view of the edge of a Waulsortian Limestone clast (outlined) contained within the Boulder Conglomerate. The area in the middle of the clast is an early calcite-filled cavity. Scale bar is 500µm.

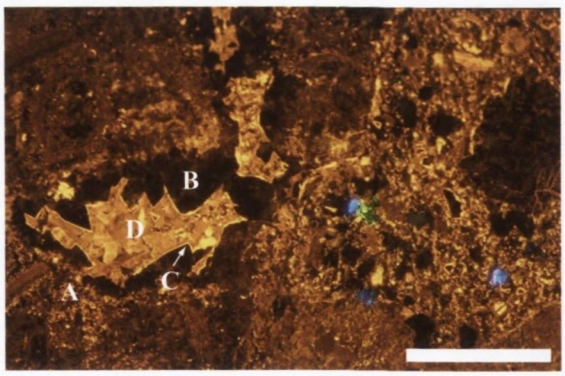

Plate 9.6b: Same view in CL. The early calcite-filled cavity, which contains cement Stages A-D (labelled), has been truncated by the matrix of the Boulder Conglomerate. These cements were clearly present prior to this clast being incorporated within the conglomerate. Scale bar is 500µm.

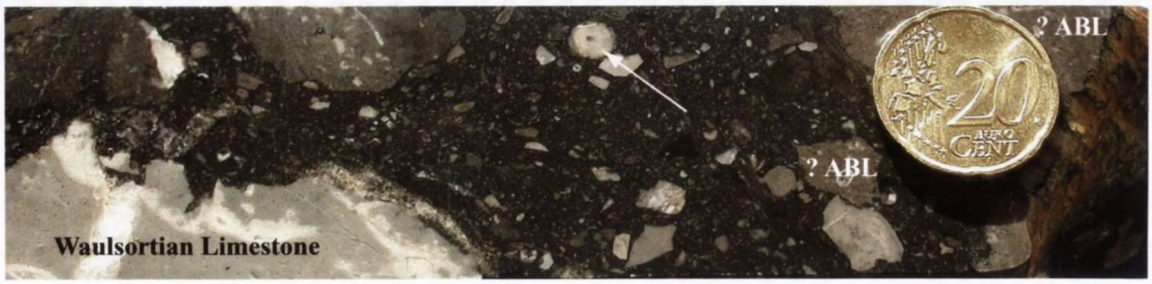

Plate 9.7: Drillcore sample of the 'Conglomerate Complex' from EP4A (195.5 - 195.9m). Some of the clasts found within the conglomerate are labelled. The dark coloured matrix is very argillaceous and contains many bioclastic fragments including crinoid ossicles (arrow). Top to the right. Size of coin is 22mm.

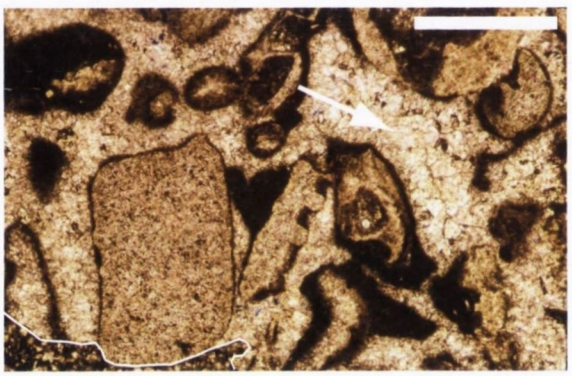

Plate 9.8a: P17626 - EP11 (473.3 - 473.6m). PPL view of the edge of a Pale Beds clast (outlined), from within the 'Conglomerate Complex'. A calcite-filled cavity is indicated (arrow). Scale bar is 500µm.

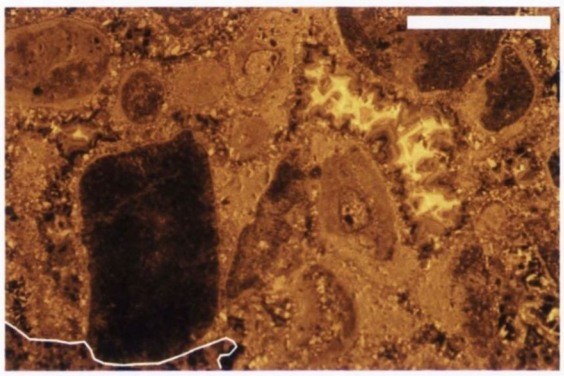

Plate 9.8b: Same view in CL. Note how the calcite cavity has been filled and the porosity occluded. These calcite cements must have formed early as they prevented any mechanical breakage of the bioclasts due to compaction. Scale bar is 500µm.

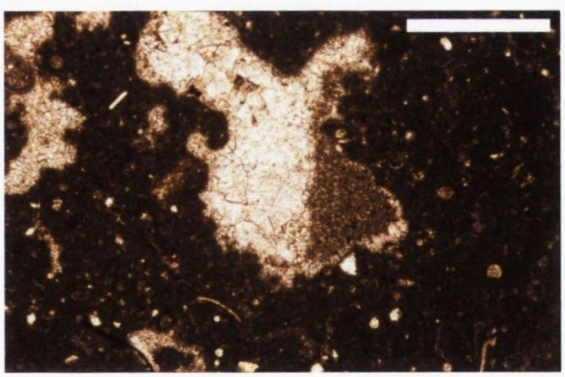

Plate 9.9: P17625 - EP4A (365.1 - 364.9m). PPL view of a Pale Beds clast (with bird's eye texture) within the 'Conglomerate Complex'. The geopetal fill shows that top of the clast is to the left. Scale bar is 500µm.

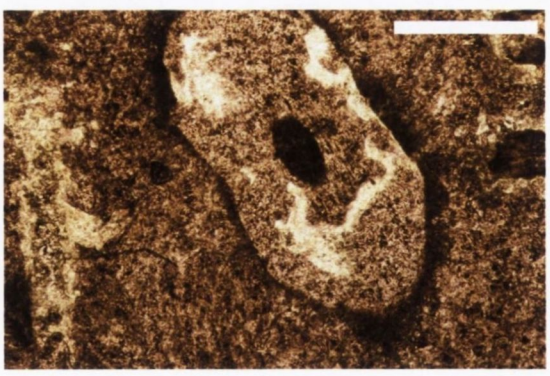

Plate 9.10: P17623 - EP4A (191.4 - 191.8m). PPL view of a clast of Waulsortian Limestone within the 'Conglomerate Complex' that contains a partially silicified crinoid ossicle. Scale bar is 500µm.

CHAPTER 10

STRATIGRAPHICAL AGE OF CEMENTATION: MOYVORE

10.1 INTRODUCTION

Drilling by Irish Base Metals and Navan Resources near the Moyvore Zn-Pb prospect, approximately 6 kilometres southeast of Ballymahon and 3 kilometres northwest of Ballymore (Figure 10.1), intersected several basic igneous dykes and sills, containing numerous Carboniferous clasts, intruded into the sub-Waulsortian succession. These intrusions are probably related to the basaltic magmatism found approximately 25 kilometres to the southeast at Croghan Hill, where both alkali basalt lavas and pyroclastic deposits are preserved. Strogen *et al.* (1996) suggested that the Croghan Hill volcanics were likely to be Arundian in age. A radiometric Ar-Ar age date of 345 Ma (S. Daly pers comm.) has been obtained for the emplacement of the Croghan Hill volcanics. The probable Arundian age of the intrusions at Moyvore provide a datum by which the porosity occlusion of the Lower Carboniferous rocks in this area can be dated. This was attempted in this study by documenting the degree of cementation of both siliciclastic and carbonate clasts within the intrusion at the time of their entrainment. Petrographic studies were concentrated on several boreholes (MV17, 3531/5, 3528/1, 3531/3 and 3531/7) that each contained good intersections of the volcanic intrusions and the sedimentary clasts entrained within them (Figure 10.1).

10.2 REGIONAL GEOLOGICAL SETTING

10.2.1 Stratigraphy

The Lower Carboniferous lithostratigraphy of the Irish Midlands, which includes the area surrounding the Moyvore prospect, was first reviewed by Philcox (1984). Previous work in the area had concentrated entirely on the Waulsortian Limestone (Nevill, 1958; Lees, 1964; King, 1984). Work by MacCarthy (1990) provided an overview of the Moyvore area and first described in detail the volcanics contained within the MV17 borehole.

The upper part of the Old Red Sandstone, the Basal Sandstones, is present in the Moyvore area (Figure 10.2). These are known to lie unconformably upon Lower Palaeozoic rocks and are Lower Carboniferous in age. Above the Basal Sandstones, the Navan Group (consisting of the Pale Beds, Upper Sandstone and Shaley Pales) is followed by the Argillaceous Bioclastic Limestones (ABL) and the Waulsortian Limestone. To the south and north of the Zn-Pb prospect at Moyvore, basinal Viséan limestones (Calp) overlie the Waulsortian Limestone. Several volcanic intrusions occur throughout the sub-Waulsortian

succession (Figure 10.2). These intrusions, termed the Shinglis Breccia Member in the MV17 drillhole by MacCarthy (1990), consist of sedimentary and igneous clasts contained within a dark green/grey fine-grained igneous matrix and are the focus of this study.

10.2.2 Structure

The area surrounding the Moyvore Zn-Pb prospect lies towards the north-western margin of the Dublin Basin (see discussion in Chapter 8). The present-day structure of the Moyvore area is characterised by a series of northwest-southeast trending faults (Figure 10.1), which are probably related to Variscan deformation and northeast-southwest trending structures, which are re-activated Caledonian structures that may have been active during the Dinantian.

10.3 PETROGRAPHY

Hand samples

The volcanic intrusions at Moyvore contain a wide range of both sedimentary and igneous clasts and therefore may be considered as being igneous breccias. The clasts include quartz pebbles (Plate 10.1), sandstone, siltstone, micrite (probably from the Pale Beds, as some contain bird's eyes), mudstone (Plate 10.2), and Waulsortian Limestone, as well as numerous buff or pale green coloured igneous fragments. The sedimentary clasts are highly variable in size, ranging from several millimetres to tens of centimetres in diameter. Generally the breccias are matrix supported. The breccia fabric is highly chaotic with no observable evidence of sorting. The igneous fragments are commonly angular and some may possibly have been glass shards (Plate 10.2). The matrix surrounding the clasts is fine-grained and usually dark green/grey in colour. It is commonly made of tiny microlites and is acicular in nature. Staining with a combination of Alizarin red S and Potassium ferricyanide indicates that the intrusions have been replaced by Fe-bearing carbonate. The contact between the intrusions and the surrounding country rock is usually very abrupt with some evidence of a chilled margin.

Thin sections

Although the intrusions have been replaced by Fe-bearing carbonate they retain the textural evidence of many of their igneous characteristics. Fe carbonate pseudomorphs of former phenocrysts are ubiquitous. Many possess six-sides and were obviously olivine (Plate 10.3), indicating that the intrusions are basic in composition. Some of the phenocrysts are

zoned (Plate 10.3). Pseudomorphs of lath-shaped phenocrysts are also common and are probably after feldspars (Plate 10.4).

Shards of what were likely to have been vitric fragments are also present. Some of them have cuspate rims (Plate 10.2) and fiamme-type textures. Fragments of pumice are also present within the intrusions. Although more commonly associated with extrusive igneous activity, pumice has been observed in intrusive igneous rocks on the island of Mull, Scotland (V. Troll pers comm.).

Large numbers of spherical shaped bodies that have an amorphous internal structure are contained within the matrix of these igneous intrusions (Plate 10.3). Many of these spheres have chilled margins (Plate 10.5), which suggest that some may be fragments of clasts/country rock that have been entrained (Plate 10.6) and partially assimilated and so exhibit a spherical outline. However, some of the spheres contain a radial internal structure (Plates 10.7a and 10.7b). These have been interpreted as spherulites, which probably resulted as a result of the devitrification of glass. The preserved internal radial fabric suggests that the spherulites were never hollow and so therefore should not be considered as lithophysae. Rare, sheared examples of these spheres have been observed (Plate 10.8). This indicates that some of these spheres were once gas filled vesicles. As vesicles usually become elongated in the direction of flow those shown in Plate 10.8 are likely to have formed while the magma was still moving.

There is strong evidence that the magma within these intrusions was quite aggressive. Features such as round embayments in quartz xenocrysts are ubiquitous (Plate 10.9). Embayments in quartz phenocrysts and xenocrysts have traditionally been interpreted in two ways: either as a product of unstable growth or as a consequence of dissolution in melt (Donaldson & Henderson, 1988). The quartz xenocrysts in the Moyvore intrusions display features typical of 'corrosion embayments' (Blackberry, 1968) such as round corners and edges, which indicate that they are probably a consequence of dissolution in melt (sharp corners and edges would indicate an element of unstable growth). Moreover, trails of two-phase fluid inclusions within the quartz xenocrysts are truncated (Plate 10.10) by these embayments, which further supports their being the result of dissolution by an aggressive magma.

The replacement of these igneous dykes and sills by Fe-bearing carbonate is more prevalent in some samples than others. In the MV17 drillhole, developments of what were once probably mica have been predominantly replaced by Fe carbonate (Plate 10.11). These micas have been replaced and expanded by the Fe carbonate in a similar way to that in which swelling clays such as smectites might behave in the presence of water. Further north of Moyvore, near Keel (Figure 10.1) tuffs occur stratigraphically above the Waulsortian Limestone and contain large brown micas (G.D. Sevastopulo pers comm.). These large micas may be similar to the micas seen in intrusions at Moyvore.

Parts of numerous Waulsortian Limestone clasts, entrained within the magmas, are replaced by large amounts of fibrous microcrystalline chalcedony (probably more correctly termed moganite) (Plates 10.12a and 10.12b). This replacement by silica is not diagenetic as areas of Waulsortian Limestone country rock away from the intrusions do not display such replacement. Commonly this replacement selectively targets the areas of the Waulsortian Limestone clasts that contain early calcite cements. It is possible that during the formation of the embayments in quartz (Plate 10.9) the magma became saturated in silica enabling the redistribution and precipitation of silica within Waulsortian Limestone clasts

There is a marked difference in the effect of the intrusions on siliciclastic and carbonate country rocks. The more siliciclastic lithologies appear to have behaved as unconsolidated sands when intruded by the igneous injections (Plate 10.13). Individual quartz grains become entrained within the matrix of these intrusions and indicate that these units were not well cemented at the time of intrusion. Conversely, the overlying carbonate lithologies remain cohesive when intruded by these magmas. Large cobbles (up to 200mm in diameter) of Waulsortian Limestone remain intact (Plate 10.14) and appear to be more robust than the siliciclastic material during the forceful igneous injections. CL microscopy of these clasts indicates that the early calcite cavity filling cements (Stages A-D) are well-developed and that porosity occlusion, by the Stage D cements, had occurred by the time these clasts were entrained (Plates 10.15a and 10.15b). This suggests that at the time of these intrusions the Waulsortian Limestone was not conducive to fluid flow except perhaps via fractures. However, as the underlying siliciclastic units were not well cemented at the time of intrusion it is probable that they retained much of their original porosity and permeability and so may have been amenable to fluid flow.

10.4 TIMING OF CEMENTATION AND IMPLICATIONS FOR FLUID FLOW

Complete occlusion of porosity within the Waulsortian Limestone had already occurred by the time these magmas were intruded. Based on the Arundian age of the Croghan Hill volcanics this suggests that porosity occlusion within the Waulsortian Limestone in this part of the Irish Midlands had occurred by the Arundian. Therefore it seems probable that the deeper palaeoaquifers during the early Viséan were confined almost entirely to the poorly cemented siliciclastic units.

10.5 MAAR-DIATREMES OR PEPERITES?

All of the intrusions located near the Moyvore Zn-Pb prospect occur within the sub-Waulsortian succession. The occurrence of clasts from both above (Waulsortian Limestone) and below (quartz pebbles probably from the Basal Sandstones, sandstone and Pale Beds micrite) the level of intrusion indicates that significant transportation of material took place during this igneous activity.

The entrainment of xenoliths of wall rock from both stratigraphically above and below is a common feature observed in diatremes, the pipe-like subsurface feeders for maars. However, the igneous intrusions near Moyvore also share many of the same characteristics as peperites (Skilling *et al.*, 2002). White *et al.* (2000) defined the word peperite as being "a genetic term applied to a rock formed essentially in situ by disintegration of magma intruding and mingling with unconsolidated or poorly consolidated, typically wet sediments". Lorenz *et al.* (2002) highlighted the difference between maar-diatremes and peperites indicating that the former occur by the ingestion of debris within melt that is later fragmented by explosive processes whereas the latter formed by *in situ* magma-sediment mingling and simultaneous fragmentation.

Studies of Cretaceous carbonatite intrusions from Namibia (Stachel *et al.*, 1994) and Permo-Carboniferous basaltic diatremes in Germany (Lorenz, 1985, 1986) have documented xenocrysts of individual round sedimentary quartz grains enclosed by magma, identical to those shown in Plate 10.13. These rounded sedimentary quartz xenocrysts are interpreted as having been enclosed by the magma prior to fragmentation. In accordance with the intrusions at Moyvore, the country rocks within which these maar-diatremes formed consisted of unconsolidated sandy sediments.

Based on this comparison with Namibian and German maar-diatremes, and the entrainment of xenoliths of wall rock from both stratigraphically above and below the level of intrusion, the Moyvore intrusions should probably be characterised as maar-diatremes rather than peperites.

10.6 CONCLUSIONS

- When intruded by basic igneous dykes and sills, siliciclastic units behave like unconsolidated sands.

- Individual grains of quartz became easily entrained within the magmas and clearly were not well cemented at the time of intrusion.

- Carbonate units behave cohesively with only large blocks of limestone becoming entrained within the magmas.

- CL microscopy of Waulsortian Limestone clasts entrained within the magmas indicates that porosity occlusion had occurred within these limestones prior to entrainment.

- Based on the 345 Ma age date for the Croghan Hill volcanics (S. Daly pers comm.) porosity occlusion within the Waulsortian Limestone at Moyvore had occurred by the early Viséan (Arundian).

- This is similar to the petrographic data from Navan, which also indicates an early Viséan age, at the latest, for porosity occlusion within the Waulsortian Limestone.

- As the underlying siliciclastic units were apparently poorly cemented at the time of intrusion it seems probable that the deeper palaeoaquifers during the early Viséan were confined almost entirely to the siliciclastic units.

- This has implications for the fluid flow models for base-metal mineralisation (see Chapter 1). Everett *et al.* (2003) suggest that porosity occluding calcite cements within the Old Red Sandstone would have been one of the inhibiting factors that would have impeded fluid migration through the sandstone unit. Data from this study contradicts

this assumption, as there clearly are examples where deeply buried sandstone units remained relatively uncemented, and therefore, by inference, amenable to fluid flow.

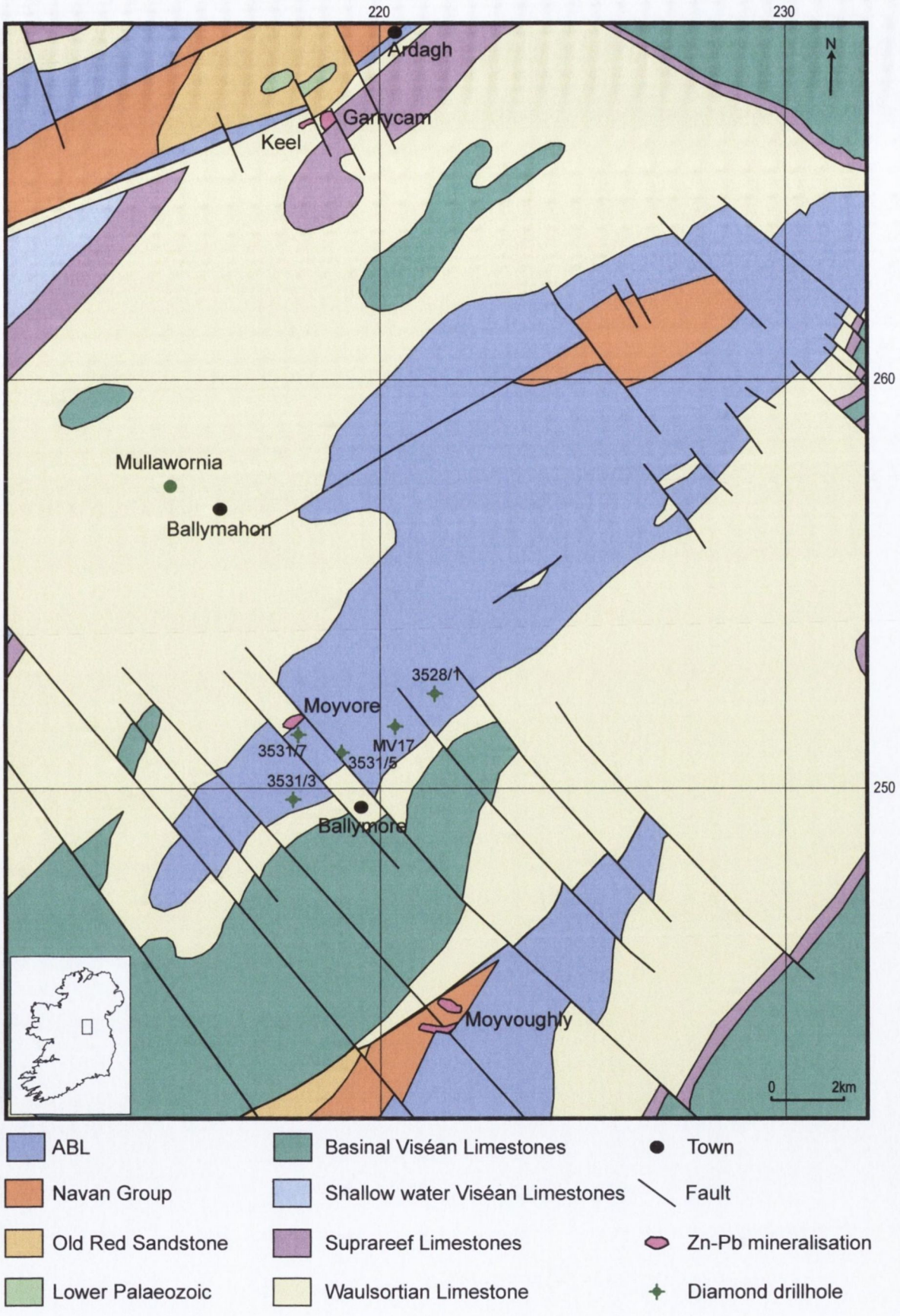

Figure 10.1 A simplified geological map of the area surrounding the Moyvore Zn-Pb prospect and the location of the drillholes studied. Grid lines refer to the Ordnance Survey of Ireland National Grid. Modified after Hitzman (1992c).

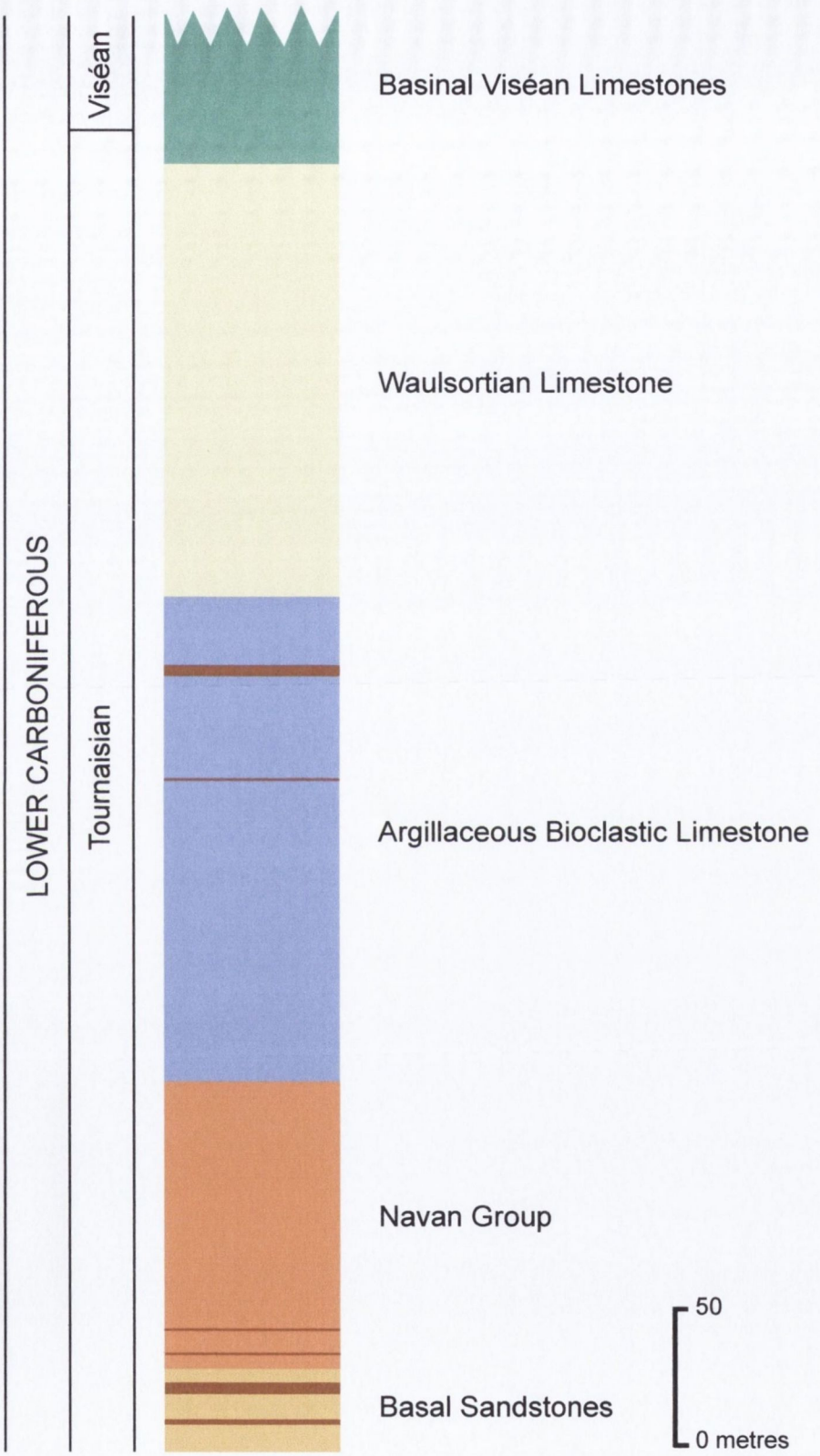

Figure 10.2 Stratigraphic section of the Moyvore prospect area based on the 3528/1 drillhole. The thin horizons shaded in brown are the volcanic intrusions.

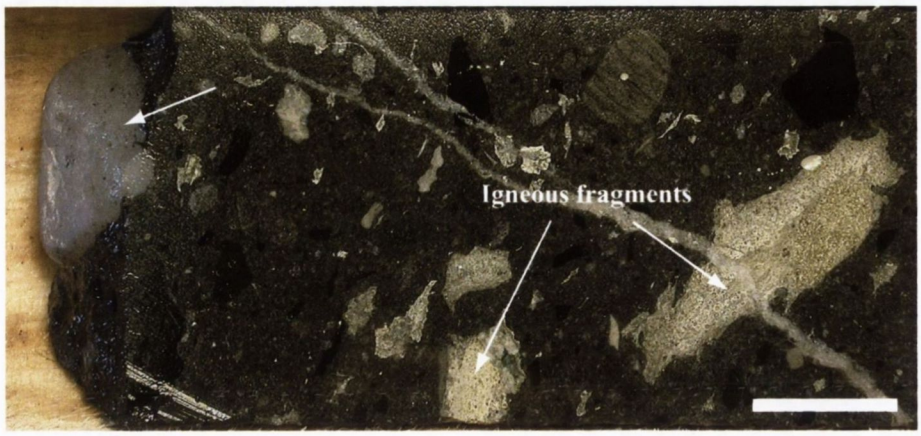

Plate 10.1: Drillcore sample from 3531/3 (155m) showing a large quartz pebble (arrow) and many igneous fragments. Scale bar is 15mm. Top to the left.

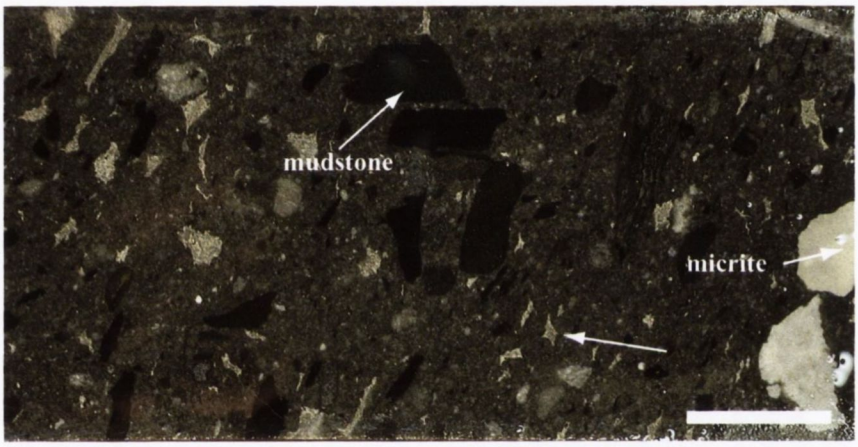

Plate 10.2: Drillcore sample from 3531/3 (156m) showing clasts of mudstone and micrite as well as many shard-like igneous fragments with cuspate rims (arrow) that are probably former vitric fragments. Scale bar is 13mm. Top to the left.

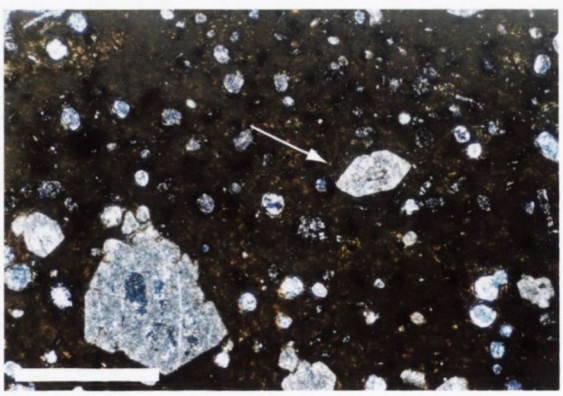

Plate 10.3: P17604 - 3531/5 (86.63- 86.6m). PPL view of a pseudomorph of a zoned phenocryst (arrow). As it has six sides it was probably olivine. This suggests that these intrusions were basic in composition. Scale bar is 500µm.

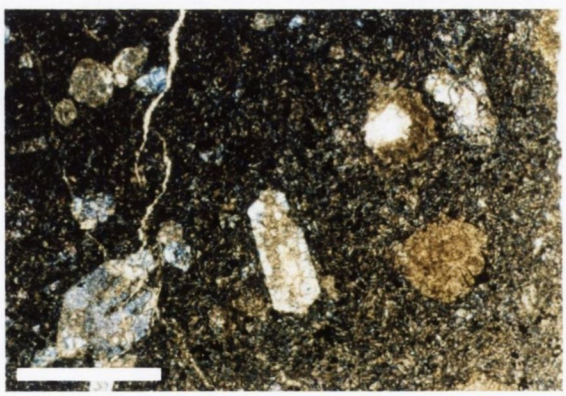

Plate 10.4: P17604 - 3531/5 (86.65-86m). PPL view of a lath-shaped pseudomorph of a probable phenocryst of feldspar. Scale bar is 500µm.

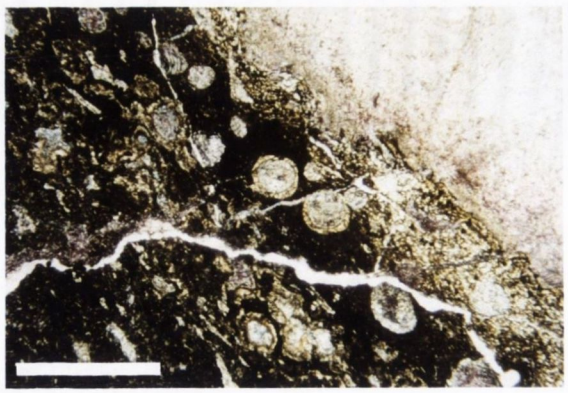

Plate 10.5: P17604 - 3531/5 (86.63-86.6m). PPL view of the spheres contained within the matrix of the intrusions. A large clast of Waulsortian Limestone is visible in the top right of the image. Scale bar is 500µm.

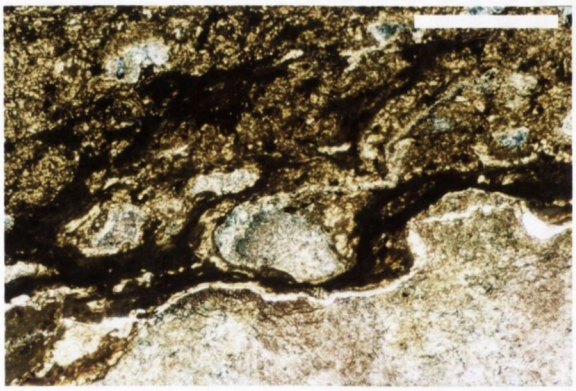

Plate 10.6: P17613 - 3531/3 (155m). PPL view of a fragment of Waulsortian Limestone indicating that some of these spheres are broken off pieces of country rock. Scale bar is 500µm.

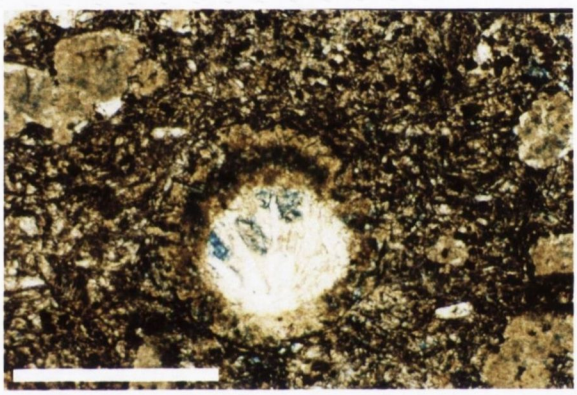

Plate 10.7a: P17603 - 3531/5 (86.65-86.63m). PPL view of a sphere with a chilled margin and an internal radial arrangement. Scale bar is 500µm.

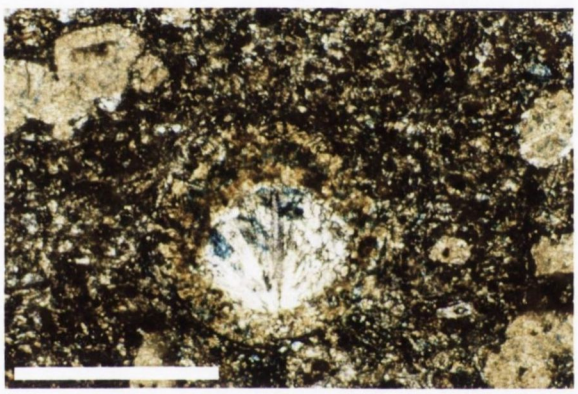

Plate 10.7b: Same view in XPL. The internal radial arrangement implies that these structures are spherulites, which probably formed as a result of the devitrification of glass. Scale bar is 500µm.

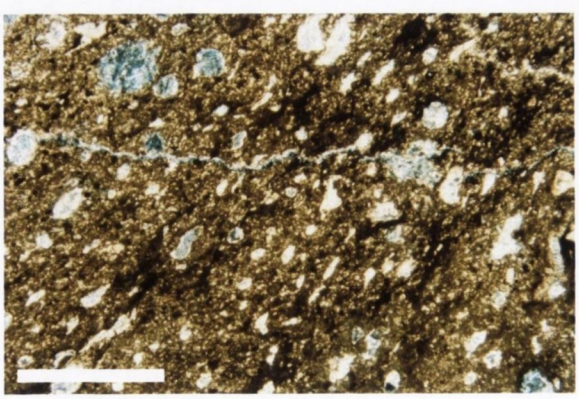

Plate 10.8: P17605 - 3531/5 (117.45-119m). PPL view of sheared spheres. This indicates that at least some of these spheres were once vesicles. Scale bar is 500µm.

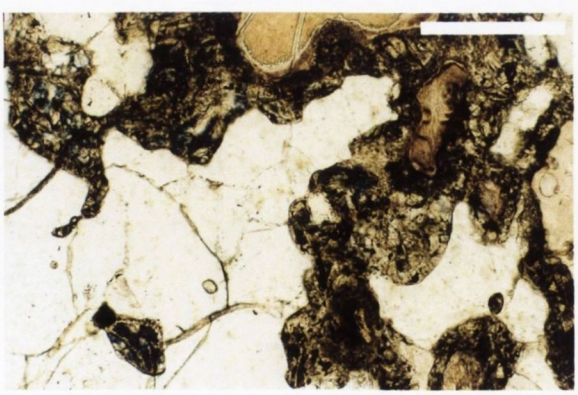

Plate 10.9: P17603 - 3531/5 (86.65-86.63m). PPL view of embayments in quartz. This suggests that the magma was undersaturated with repect to silica. Scale bar is 500µm.

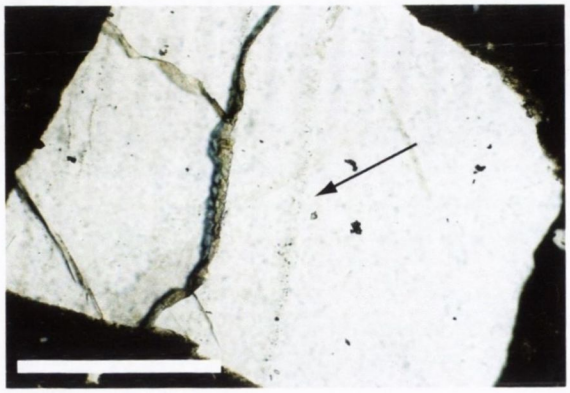

Plate 10.10: P17599 - 3531/5 (84.03m). PPL view of a large quartz grain containing a truncated trail of two-phase fluid inclusions (arrow). Scale bar is 500µm.



Plate 10.11: P17597 - MV17 (607ft). PPL view of the replacement by Fe carbonate of mica crystals contained within the intrusion. Scale bar is 500µm.

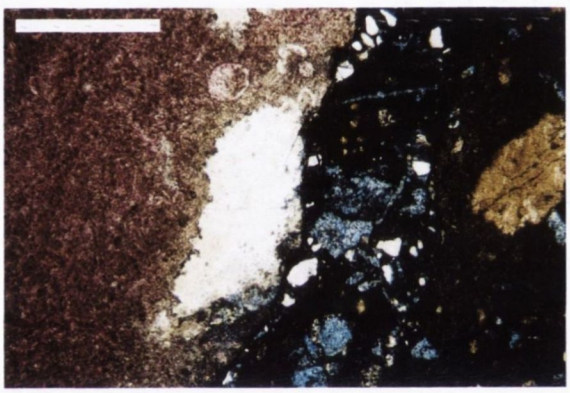

Plate 10.12a: P17595 - MV17 (595ft). PPL view of a Waulsortian Limestone clast containing silica. Scale bar is 500µm.

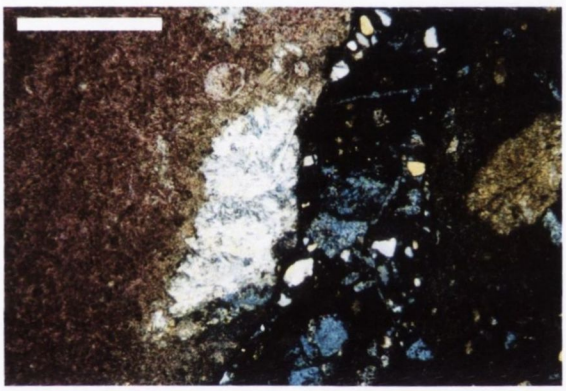

Plate 10.12b: Same view in XPL. The silica has a fibrous structure and is most likely to be chalcedony. Scale bar is 500µm.

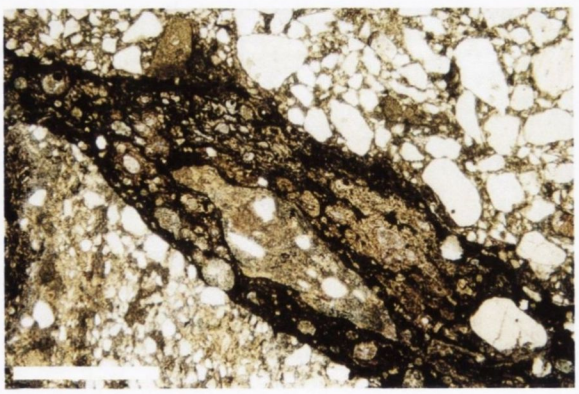

Plate 10.13: P17613 - 3531/3 (155m). PPL view of an intrusion into unconsolidated sandstone. Note the entrainment of individual sedimentary quartz grains. Scale bar is 500µm.

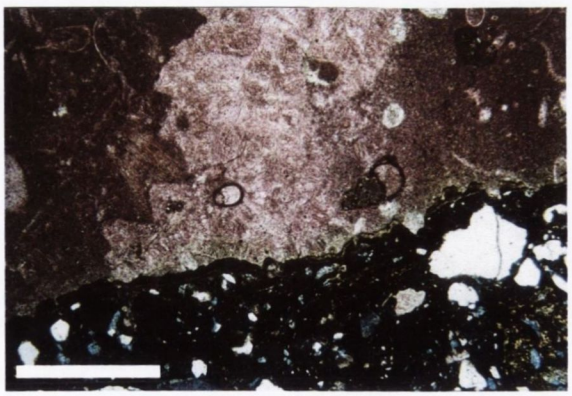

Plate 10.14: P17599 - 3531/5 (84.03m). PPL view of part of a large clast of Waulsortian Limestone that has been entrained within the intrusion. Scale bar is 500µm.

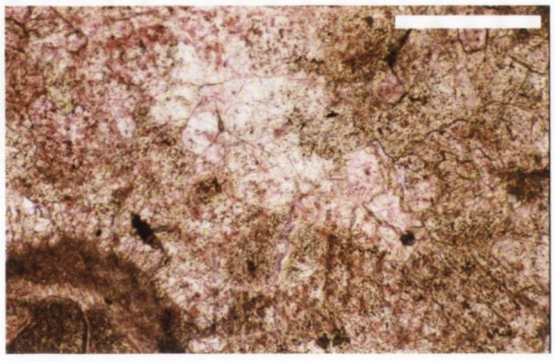

Plate 10.15a: P17596 - MV17 (606ft). PPL view of a Waulsortian Limestone clast that has been entrained within the intrusion. Scale bar is 500µm.

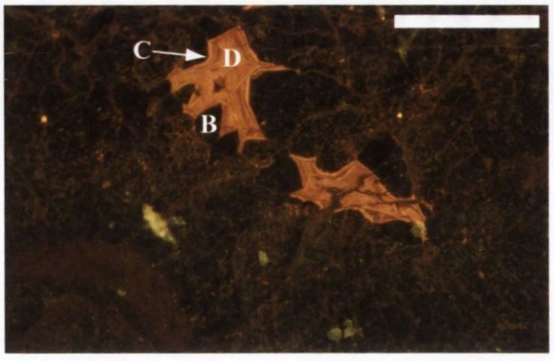

Plate 10.15b: Same view in CL. Note the presence of two early calcite-filled cavities. The calcite cements (Stages B-D) in one of the cavities have been labelled. Scale bar is 500µm.

CHAPTER 11

DISCUSSION

11.1 INTRODUCTION

The results of the preceding chapters provide some constraints on the relative timing of cementation of the precursor limestones with regards to pre-mineralisation dolomitisation in the areas studied. Microthermometric measurements and halogen data from the dolomite itself, as well as phases that both pre-date and post-date the dolomite, have also helped to constrain the thermal and chemical evolution of the dolomitising fluids. In this chapter implications of the data in terms of the depth and timing of dolomitisation/mineralisation are considered, as well as the possible fluid pathways and their bearing on the genetic models for the Irish Zn-Pb deposits.

11.2 DEPTH AND TIMING OF POROSITY OCCLUSION

As reported in all of the previous chapters, final porosity occlusion occurred within the Waulsortian Limestone as the result of the precipitation of the Stage D calcite. This cement phase pre-dated the onset of both dolomitisation and mineralisation and according to Lees and Miller ((1995) p.249 Fig. 46) probably formed within approximately 500m of the seafloor. Petrographic evidence from the Waulsortian Limestone at Navan (Chapter 9) and Moyvore (Chapter 10) prove an early Viséan age for the porosity occlusion within these areas at burial depths probably of less than 500m.

However, many workers believe this cement stage to be contemporaneous with sulphide mineralisation and/or pyrobitumen formation and to be contemporaneous with or post-date dolomitisation (Gregg *et al.*, 2001; Reed & Wallace, 2001).

Reed and Wallace (2001) maintained that Zn-Pb mineralisation at Courtbrown, Co. Limerick was contemporaneous with the development of the Stage D porosity occluding cements and that dolomitisation pre-dated their formation. Petrographic evidence from Newcastle West (Chapter 5), approximately 25 kilometres SSE of Courtbrown, has clearly shown that dolomitisation there post-dated the Stage D, porosity occluding cements and that the mineralisation was epigenetic. Great care has to be exercised in interpreting the CL petrography. Dolomite is commonly very 'particular' in what phases it replaces.

Similarly, Gregg *et al.* (2001) suggested that fine-grained dolomite (their pk1 cement) pre-dated the early calcite cements (their BCC, which includes Stage D of this study) found in

the Irish Midlands and Dublin Basin. Evidence for dolomite pre-dating early calcite cements has not been observed in any of the areas within this study. However, if this observation is correct, then based on the fluid inclusion data from Newcastle West and Subulter, which indicates that the fine-grained dolomite formed at >131°C and >105°C respectively, dolomitisation and early calcite cementation must have either occurred at substantial depths or have been the product of a high temperature hydrothermal fluid. Alternatively fine-grained dolomite formed at different depths in different places.

11.3 DOLOMITISATION – HYDROTHERMAL VERSUS BURIAL ORIGIN

Given the high temperatures of formation of the pre-mineralisation dolomite throughout all of the areas in this study, the question arises as to whether these temperatures reflect the ambient temperature of the surrounding sedimentary sequence (geothermal *sensu* Machel and Lonnee (2002)) or the introduction of a fluid that was hotter than the ambient temperature of the surrounding rocks (hydrothermal *sensu stricto* Machel and Lonnee (2002)).

The coarse-grained dolomite components of the regionally dolomitised Waulsortian Limestone in many of the areas studied contain the sweeping extinction and curved crystal faces indicative of saddle dolomite. This suggests formation at elevated temperatures in the range of 60-150°C (Radke & Mathis, 1980), which is consistent with many of the homogenisation temperatures of the fluid inclusions.

Attaining these temperatures through burial alone requires either burial beneath large sedimentary thicknesses or elevated geothermal gradients. If the temperatures simply reflect normal burial they would require burial depths of >4km (estimated using the minimum measured Th value of 110°C and a 10°C surface temperature at present day average geothermal gradients). This thickness of cover seems unlikely to have been achieved at any point prior to the late Carboniferous/early Permian Variscan inversion. This therefore suggests that Mesozoic cover, which is known to have been at least, but probably much more than 1.5km (Green *et al.*, 2000), may have been sufficient to enable these temperatures to have been attained through burial under present day average geothermal gradients.

However, it is much more likely that the high temperatures as indicated by the homogenisation data reflect formation under elevated geothermal gradients. At present there are relatively few estimates of the palaeogeothermal gradient. However, Corcoran and Clayton (2001) reported a geothermal gradient of ~51°C km^{-1} for peak burial in the late Carboniferous, based on vitrinite reflectance data from Dinantian rocks in the Athboy borehole, Co. Meath. Under this geothermal gradient the amount of cover that would have lain above the point of dolomite precipitation can be estimated at ~2km. This estimate is much more reasonable and is within the range of stratigraphic thickness attained prior to Variscan inversion.

Therefore the pre-mineralisation dolomite found throughout the Irish Midlands is believed to have formed geothermally. It is not thought to be a hydrothermal dolomite, as it is believed to have formed at or near the same temperature as the surrounding rocks. However, as much of the vitrinite reflectance data indicate higher temperatures than the fluid inclusions data, this would suggest that the dolomites were precipitated prior to peak burial.

Furthermore, given the large volume of pre-mineralisation dolomite, (a conservative estimate of >50km^3 was given by Sevastopulo and Redmond (1999)), it is difficult to imagine how the enormous volume of fluid, needed by the hydrothermal system, could form such a large body without equilibrating thermally with the country rock.

Figure 11.1 is a schematic diagram showing the minimum possible age (assuming that only conductive heat transport was involved) and depth of dolomitisation for all areas studied. It indicates that the pre-mineralisation dolomite is much younger and formed and significantly greater depths than those envisaged by other workers (Lee & Wilkinson, 2002; Wilkinson, 2003).

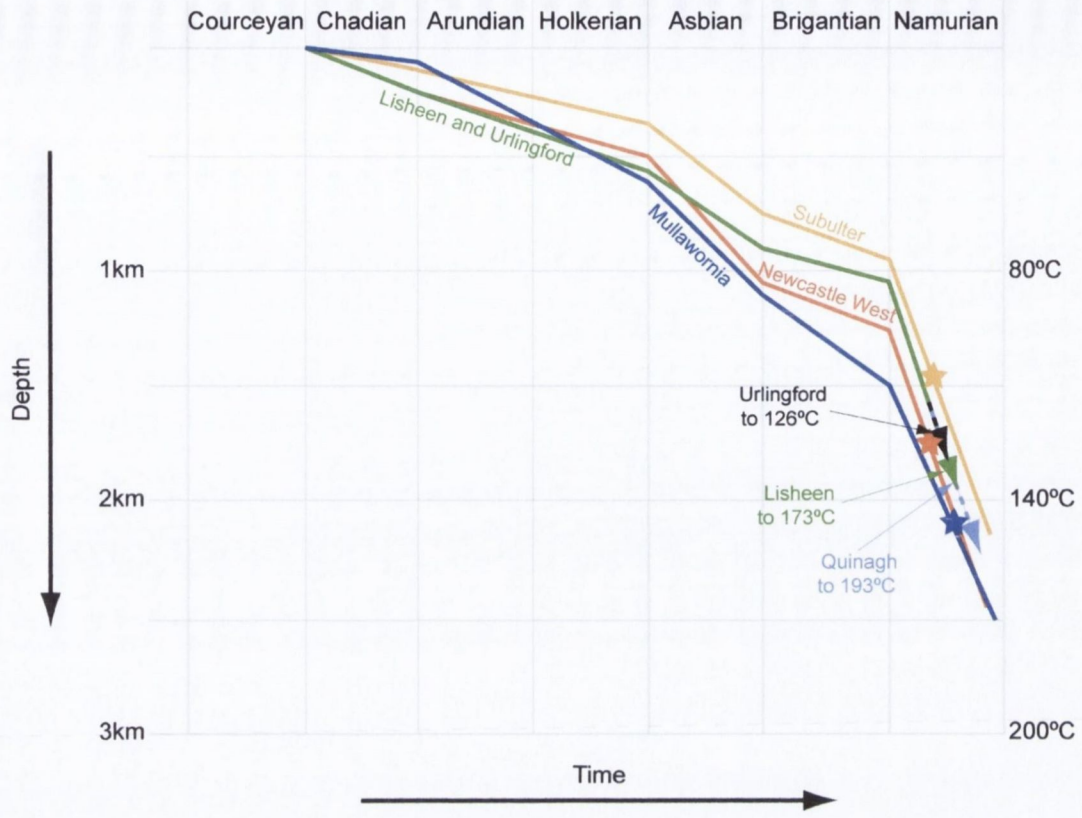

Figure 11.1 Schematic diagram showing the minimum possible age (assuming conductive heat transport only) and depth of dolomitisation for all areas studied (stars). It was constructed using: the cumulative stratigraphical thickness (not decompacted) of Tournaisian (Waulsortian and Ballysteen Limestone) to Namurian-aged rocks (data from Sevastopulo and Wyse Jackson (2001)); the depth/temperature relationship for each study area based on a uniform geothermal gradient of 60°C km^{-1} and a surface temperature of 20°C; and the minimum homogenisation temperatures for each occurrence of dolomite. In the case of Lisheen, Urlingford and Quinagh the preserved stratigraphic thickness above each of these areas is not sufficient to have generated the minimum fluid inclusion homogenisation temperatures. Therefore the arrows indicate the trajectories along which these data would plot.

11.4 STRETCHING OF FLUID INCLUSIONS

As there is evidence of substantial late Carboniferous heating (Clayton *et al.*, 1989), some authors have expressed concerns over the validity of fluid inclusion data measured in Irish Carboniferous rocks (Peace, 1999; Reed & Wallace, 2001). Also, if the increase in temperature with pressure (due to depth of burial) is greater than that of the isochore for

the inclusions, the internal pressure in the inclusions will be greater than the confining pressure and the inclusions may stretch or leak (Goldstein, 1986; Prezbindowski & Larese, 1987). This is important to consider, if the limestones within this study were buried to significant depths prior to the onset of dolomitisation.

Bodnar (2003) suggested that the most important factor that determines the ease with which fluid inclusions re-equilibrate is the mineralogy of the host phase. Fluid inclusions in dolomite, which has a Mohs hardness of 3.5 to 4, are more likely to re-equilibrate than fluid inclusions in quartz, which has a hardness of 7 and is therefore a more robust mineral (Bodnar (2003), p.8.3 Fig. 8.2). The overlap in the homogenisation temperature data from both the quartz and coarse dolomite at Newcastle West and the pre-dolomite quartz and dolomite at Subulter, suggests that there has been no stretching as a result of Variscan heating. This means that the fluid inclusion data from both areas can be considered as being reliable.

The type of re-equilibration that occurs is also related to the mineral hardness. Soft minerals tend to re-equilibrate by stretching to produce a gradual increase in homogenisation temperature as re-equilibration proceeds, whereas harder minerals maintain their original homogenisation temperature until the inclusion finally decrepitates. However, exceptions to this general trend do occur: Ulrich and Bodnar (1988) observed decrepitation of inclusions within barite (Mohs' hardness of 3); and Bodnar *et al.* (1989) found that inclusions in quartz re-equilibrated by stretching (followed by later decrepitation). A plot of inclusion size versus Th should show a positive correlation if partial re-equilibration has occurred, with softer minerals (e.g. calcite or dolomite) having a more pronounced correlation than harder minerals (e.g. quartz). Figure 11.2, which shows a plot of inclusion size versus Th, subdivided according to the host mineral, shows no positive correlation for either the dolomite or quartz data. However, the calcite data measured at Lisheen, which is interpreted as having re-equilibrated (Chapter 3), does show a slight positive correlation. The post-dolomite quartz from both Subulter and Quinagh are plotted separately as the fluids which formed these two phases are not the same and so the two quartz generations are not directly comparable.

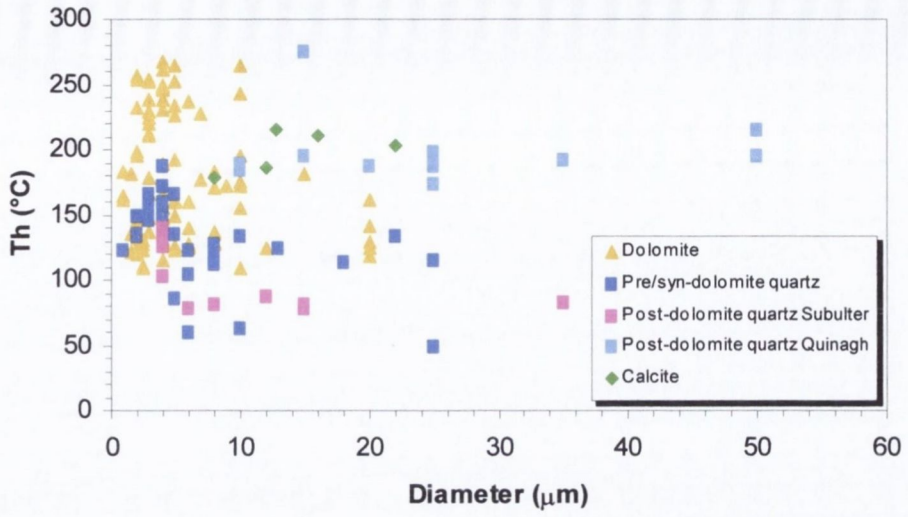

Figure 11.2 Th vs. maximum inclusion size for all inclusions measured in this study.

Re-equilibration by stretching may also be accompanied by a change in inclusion shape from irregular to that of a negative crystal (Bodnar *et al.*, 1989). Of the 156 fluid inclusion measurements made in this study only 20 came from inclusions that had a negative crystal shape. This means that >87% of the measurements made came from inclusions whose shape was not consistent with having been stretched.

Bodnar (2003) also noted that while the mineralogy of the host mineral is the most important factor in governing the pressure required to re-equilibrate fluid inclusions, the "average" pressure could vary considerably depending on the size of the individual inclusion. Bodnar *et al.* (1989) investigated the decrepitation behaviour of fluid inclusions in quartz and deduced the following relationship:

$$\textbf{Internal pressure (kbars)} = 4.26\, D^{-0.423}$$

where D is the inclusion diameter in microns. This means that the internal pressure required to re-equilibrate the inclusions in quartz in this study varies from 0.8 kbars for a 50μm inclusion, to 4.3 kbars for a 1μm inclusion (with 50μm and 1μm being the maximum and minimum diameters measured in this study). A similar relationship between inclusion size and the pressure required to initiate stretching was found in fluorite and sphalerite (Bodnar & Bethke, 1984), calcite (Prezbindowski & Larese, 1987) and to a lesser extent in barite (Ulrich & Bodnar, 1988).

11.5 TRAPPING TEMPERATURE ESTIMATION

Th data only provide an estimate of the minimum temperature of formation. The difference between Th and the trapping temperature (T_t) is dependent on the fluid pressure at the time of entrapment. This in turn is directly related to the depth of burial at which precipitation of the host mineral took place.

As outlined in Chapter 1 there are two contrasting hypothesis regarding the depth at which mineralisation/dolomitisation took place. One hypothesis is based on the evidence for synsedimentary mineralisation in the Irish Zn-Pb orefield and proposes that mineralisation and dolomitisation took place either on the seafloor or at shallow depths (within tens of metres of the seafloor). The opposing hypothesis proposes that because the majority of the mineralisation is epigenetic, mineralisation and pre-mineralisation dolomitisation occurred at a much greater depth.

If dolomitisation occurred at shallow depths (within tens of metres of the seafloor) the fluid pressures would be hydrostatic and would essentially depend on the depth of the seawater. Estimates of the water depth at Silvermines at the time of mineralisation are in the region of 300m (Samson & Russell, 1987). This would impart a maximum fluid pressure of ~30bars (0.03kbars). Given that the homogenisation pressure is ~14bars for inclusions homogenising at ~200°C and the isochoric dP/dT for high salinity fluids is ~14bar°C^{-1} (Haas, 1977), a maximum correction of about +2.1°C would be estimated.

However, if mineralisation and dolomitisation occurred at depth, the amount of fluid pressure imparted would depend on whether hydrostatic or lithostatic conditions prevailed. Twiss and Moores (1992) state that at about 3km the fluid pressure is typically equal to hydrostatic pressure. This is supported by the German Continental Deep Drilling Program where near hydrostatic pressures were measured in a 9km deep borehole (Emmermann & Lauterjung, 1997). Despite the observation that porosity occlusion within Waulsortian Limestone occurred prior to the onset of both mineralisation/dolomitisation and that permeability, except along fractures, was almost certainly minute, it remains a reasonable assumption that the succession was under conditions of hydrostatic pressure.

Hitzman and Beaty (1996) estimated that mineralisation occurred at a depth of between 0.5 and 1km. If the upper limit of their depth estimate is used (1km) and hydrostatic conditions are assumed to have prevailed at these depths, a maximum fluid pressure of ~130bars (0.13kbars) would be exerted. This implies a maximum pressure correction of +9.3°C. However, if at a depth of 1 km lithostatic conditions prevailed, the maximum fluid pressure exerted would be ~295bars (sum of the lithostatic load ~265bars and hydrostatic load ~30bars) and the pressure correction would be ~+21.1°C.

Therefore, if dolomitisation occurred at depth, the pressure corrections needed for the Th values measured in this study vary between 9.3°C and ~21.1°C depending on whether a lithostatic or hydrostatic model is assumed. Also, assuming that the fluid inclusions were in equilibrium with their surroundings, the estimation of the maximum fluid pressures for dolomitisation at depth (0.13kbars) are well below the internal pressures required to re-equilibrate the maximum and minimum sized inclusions in quartz in this study (0.8 kbars for a 50μm inclusion, and 4.3 kbars for a 1μm inclusion).

11.6 FLUID GEOCHEMISTRY

11.6.1 Source of salinity

The calculated Cl and Br composition of the fluid inclusions from all study areas are shown in Figure 11.3. Much of the data lie on the line representing the evaporation of seawater and indicate that the fluid within these inclusions is residual brine, formed by the concentration of seawater by evaporation beyond the point of halite precipitation. The data from Urlingford lie, within analytical uncertainty, on the SET and indicate that the fluid within these inclusions is seawater that has been evaporated, but not to the point of halite precipitation. The quartz data from Newcastle West (OW28 and OW24) and the post-dolomite quartz data from Quinagh lie to the left of the SET and indicate that the fluids within these inclusions may in part contain a component of a fluid, which has acquired some Cl from the dissolution of halite. The dolomite data from Quinagh and Clonmelsh lie to the right of the SET and indicate that the fluids within these inclusions probably contain a mixture of residual brine and a low salinity fluid (meteoric water or seawater). Mixing of a residual brine with ~30% of a low salinity fluid (Figure 11.3) could account for these halogen data (Carpenter, 1978). The fluids within the post-dolomite quartz from Subulter (whose maximum Br value has been plotted) are consistent with having been derived from the dissolution of halite.

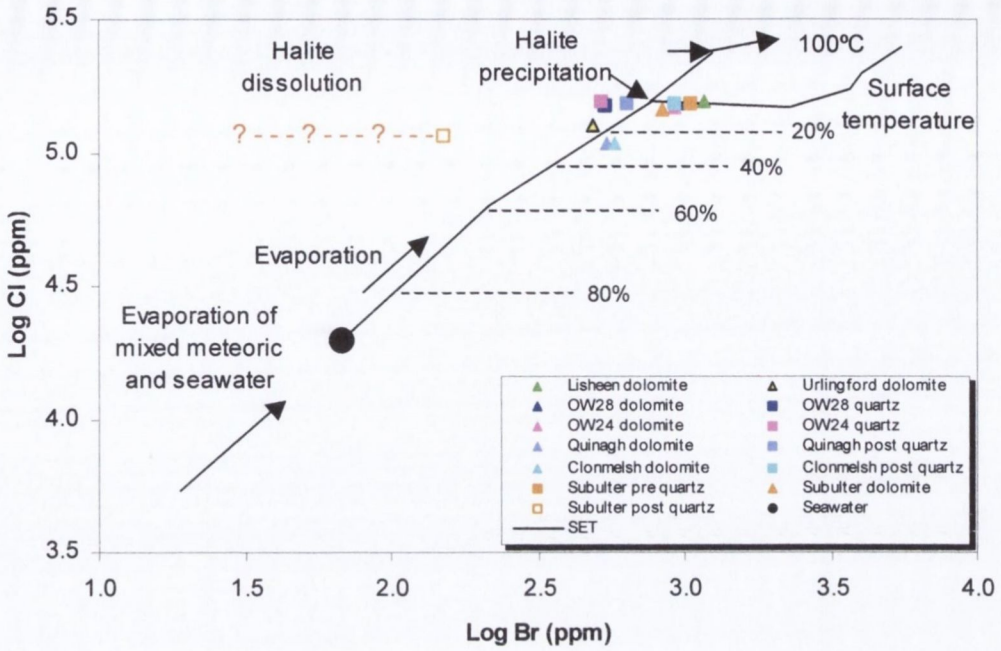

Figure 11.3 Cl and Br systematics of the fluid inclusions from all areas. Plot also shows the SET (after Carpenter (1978) and Gleeson & Yardley (2002)). Dotted lines represent mixing with a dilute fluid (meteoric or seawater) for the amount indicated.

The Na-Cl-Br systematics of the fluid inclusions from all study areas are shown in Figure 11.4. With the exception of the quartz from Newcastle West (OW28 and OW24), all of the data have Cl/Br molar ratios less than seawater. In fact, with the exception of the post-dolomite quartz from Quinagh and the dolomite from Urlingford, most samples have Cl/Br molar ratios that suggest the fluids originated as highly evaporated seawater (beyond the point of halite precipitation). In relation to the fluids associated with the Irish Zn-Pb deposits, these fluids are most similar to Fluid 2.

Many samples lie to the right of the SET and appear enriched in Na relative to seawater. Other samples lie to the left of the SET, which suggests that they are slightly depleted in Na relative to seawater. As many of these fluids originated as seawater, these variable Na concentrations can be explained as being due to Na-Ca exchange reactions. However, as some of these fluids probably represent a mixture of either residual brine and a dilute fluid (meteoric water or seawater) or residual brine and a fluid, which has acquired some Cl from the dissolution of halite, these variable Na concentrations may also be attributable to the fluid that was mixed with the residual brine, whose original Na/Br ratio is unknown.

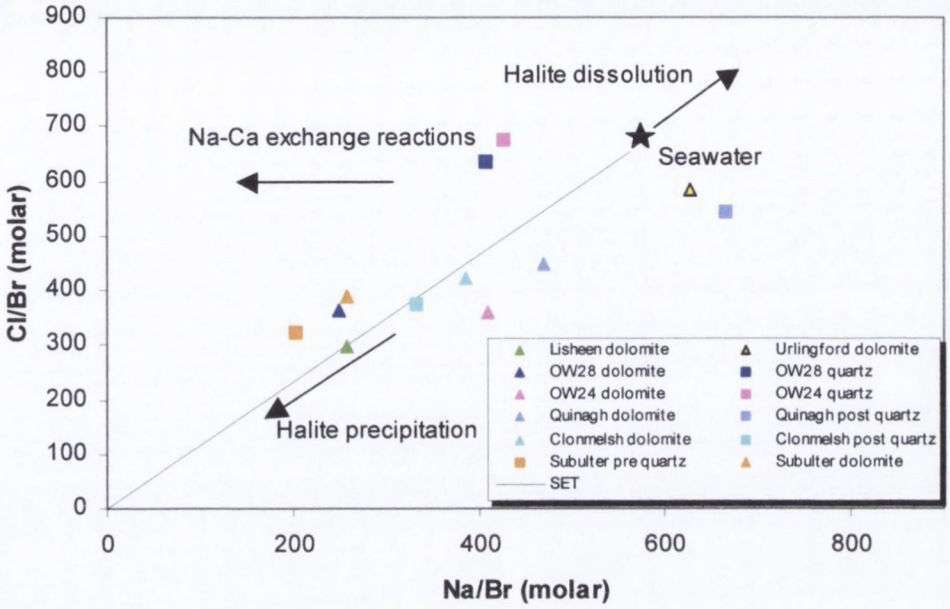

Figure 11.4 Cl-Na-Br systematics of the fluid inclusions from all areas. SET data after Kesler *et al.* (1995).

11.6.2 Modification by fluid-rock interaction

In contrast to Cl and Br, which are assumed to behave as conservative elements in solution, Na, K and Li concentrations are easily modified by fluid-rock interactions and reflect the sum of all reactions along the flow pathway and at the site of precipitation. As seen in Figure 11.3, many of the fluids within the inclusions sampled are mixtures of residual brine and either a dilute fluid or minor component of a fluid, which has acquired some Cl from the dissolution of halite. In the case of the dolomite data from Clonmelsh and Quinagh, the proportion of the dilute fluid that was mixed with the residual brine was ~30%. As the composition or origin of this dilute fluid cannot be determined, its influence on the overall composition of the residual brine is unknown. While it is conceded that dilution by this unknown fluid will alter the overall composition of the residual brine, the assumption is made that the amount of residual brine relative to the dilute component is such that any alteration will be minor. Therefore in the discussion of the modifications of these fluids by fluid-rock interaction it is assumed that these fluids began as evaporated seawater and that any deviations in the elemental compositions from those expected for seawater, are likely to reflect fluid-rock interactions.

Plots of the Na/Li weight ratios versus Cl/Br molar ratios (Figure 11.5) and Na/Li weight ratios versus Na/K weight ratios (Figure 11.6) of the inclusions from all areas show that there are significant variations in the elemental ratios both between and within the different sample areas. The Cl/Br molar ratios of all samples from all areas (with the exception of the post-dolomite quartz from Subulter) range from 299 to 675, with the majority being lower than approximately 450, and are consistent with seawater-derived fluids, evaporated beyond the point of halite precipitation. The high Cl/Br ratio of the post-dolomite quartz from Subulter is consistent with this fluid having obtained its solutes through the dissolution of halite, probably within Mesozoic evaporites.

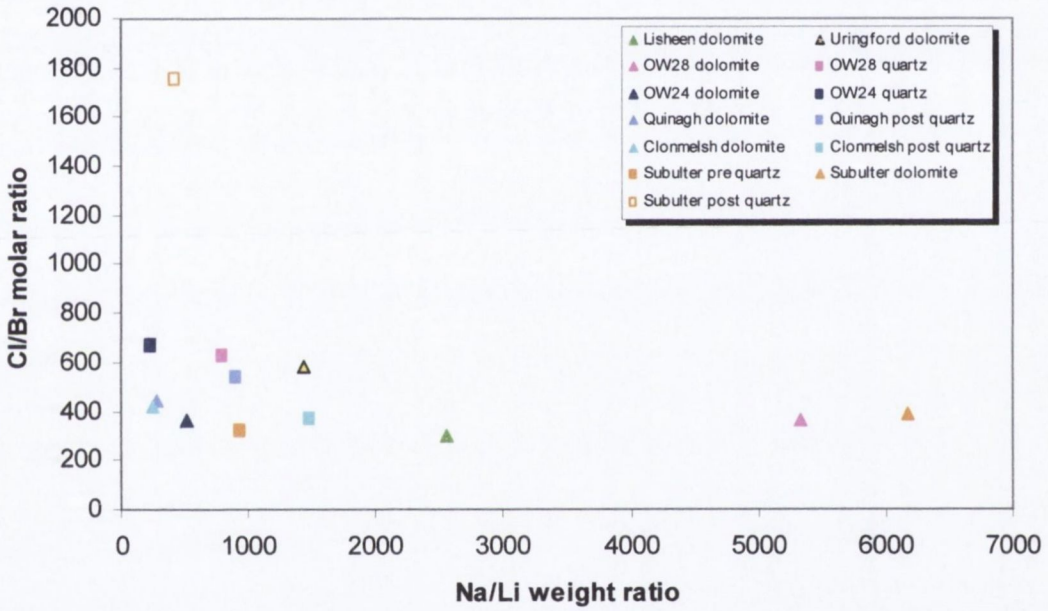

Figure 11.5 Cl/Br molar ratio vs. Na/Li weight ratio of the fluid inclusions from all areas.

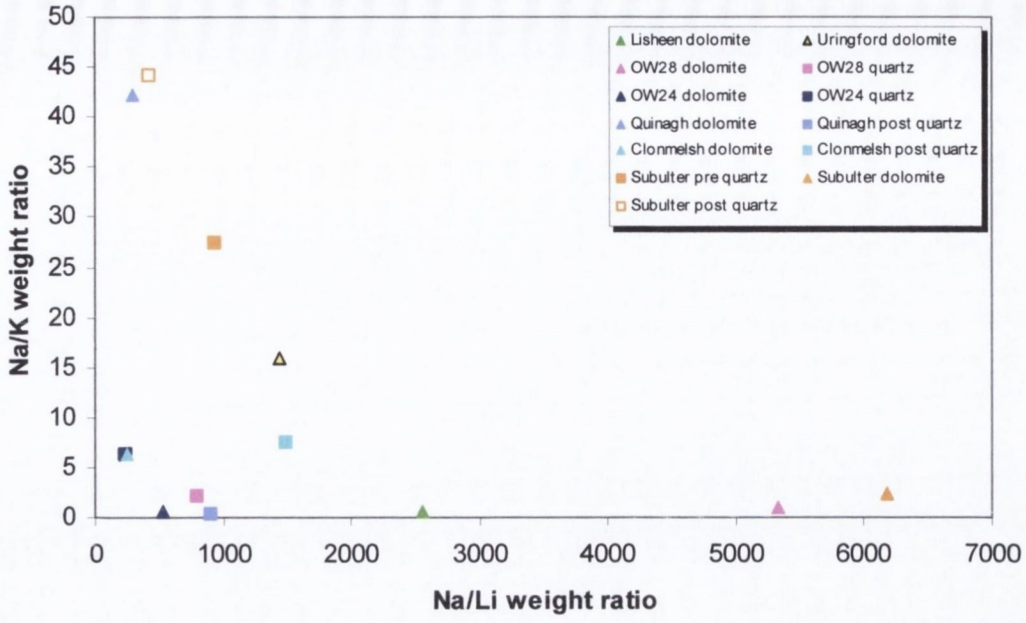

Figure 11.6 Na/K weight ratio vs. Na/Li weight ratio of the fluid inclusions from all areas.

The Na/Li and Na/K weight ratios have a broader spread than the Cl/Br ratios with the Na/Li ratios ranging from 230 to 6,180 and the Na/K ratios ranging from 0.36 to 44.23. In order to understand the evolution of the fluids within each individual study area the discussion of the Na, K and Li concentrations will carried out separately by sample area.

Lisheen

The data from Lisheen have a Na/Li weight ratio (2,556), which is very different from that expected for seawater (202,818). This suggests that the fluids within these inclusions are very much enriched in Li relative to seawater and may have undergone interaction with Li-rich lithologies. Micas and clay minerals are known to be major sources for crustal Li and are both present within the Lower Palaeozoic basement rocks in Ireland. This suggests that the dolomitising fluids at Lisheen may have undergone some interaction with the underlying basement.

The low Na/K ratio (0.63) may indicate a degree of K contamination as Banks *et al.* (2002) suggest that low Na/K ratios (<~5) are probably due to contamination from K-bearing phases not removed during cleaning. No petrographic evidence for the presence of such

contaminants was found. However, it may be possible that they were too small to have been observed.

The fluid inclusions in the coarse dolomite at Lisheen have Na and Cl concentrations (Figure 11.7) that are exactly what would be expected from seawater that had been evaporated beyond the point of halite precipitation (Fluid 2). This is consistent with the Na/Br and Cl/Br molar ratios (Figure 11.4), which suggest no exchange with Na for other cations in this sample. The Lisheen data is not plotted on Figure 11.8, as its K value is too high (81,047 ppm). However, the data indicate that the K concentrations within these inclusions are much higher than would be expected for seawater. This may be due to the albitization of K-feldspars or may be due to contamination by K-rich phases as mentioned above.

Urlingford

The data from Urlingford, which has a Na/Li ratio of 1,434, also suggests some interaction with Li-bearing lithologies, again most probably within the underlying basement rocks. The Na and K versus Cl plots (Figures 11.7 and 11.8) show that the fluids within the coarse dolomite inclusions at Urlingford had not reached the point of halite precipitation (Fluid 1) and are enriched in Na but depleted in K. This is consistent with the Na/Br and Cl/Br molar ratios (Figure 11.4), which suggest that the fluids within this sample were enriched in Na relative to seawater. As the magnitude of Na enrichment is similar to that of K depletion, it is assumed that the same process that increased the Na also depleted the K. One possible way that this might have happened is through the interaction of the fluids with Na feldspar (i.e. addition of Na, thus relative depletion of K).

Newcastle West

The quartz and dolomite from Newcastle West have Na/Li ratios ranging from 230 to 5,327 and Na/K ratios of <6.43. The Li concentrations for all Newcastle West data, with the exception of the dolomite from OW28, are high (>264 ppm) and suggest that perhaps these fluids underwent interaction with Li-rich lithologies (either clays or micas within the underlying basement rocks). The Na/K ratios that are <~5 may indicate a degree of K contamination (Banks *et al.*, 2002).

The Cl/Br molar ratios clearly indicate that two different fluids precipitated the quartz and the dolomite at Newcastle West (Figures 11.4 and 11.5). The quartz from OW24 and OW28 have Cl/Br ratios that are similar to seawater (675 and 634 respectively) but Na/Br ratios (426 and 408 respectively) that are lower than the values expected for seawater. These high Cl/Br values are likely to be the result of the addition of Cl (and Na) from another source, perhaps a component of halite dissolution. The Na and K versus Cl plots (Figures 11.7 and 11.8) indicate that the fluids within the quartz at Newcastle West had reached the point of halite precipitation and were not involved in any exchange reactions involving with Na or K. Therefore in terms of the fluids associated with the Irish Zn-Pb deposits, the fluids within the quartz at Newcastle West are thought to be equivalent to Fluid 2.

The fluid inclusions in the coarse dolomite from OW28 have Na and Cl concentrations (Figure 11.7) that are exactly what would be expected from seawater that had been evaporated beyond the point of halite precipitation (Fluid 2). However, although not plotted on Figure 11.8, the K concentration (17,380 ppm) within these inclusions is much higher than would be expected for seawater. Na and Cl concentrations (Figure 11.7) for the dolomite from OW24 show that the fluids are enriched in Na and although not shown in Figure 11.8, they are also very much enriched in K. As mentioned above, low Na/K ratios may indicate the contamination of these samples by K-bearing phases (Banks *et al.*, 2002). However, albitization of K-feldspars may also account for the high K concentrations of the dolomite from both boreholes. The increase in Na in the dolomite from OW24 may suggest interaction with Na-feldspar.

North Co. Cork

The pre-dolomite quartz and coarse dolomite from North Cork have similar Cl/Br ratios (325 and 390 respectively) but very different Na/Li (929 and 6,180 respectively) and Na/K (27.4 and 2.32 respectively) ratios. The Li concentration within the pre-dolomite quartz inclusions (219 ppm) is orders of magnitude greater than the concentration within the dolomite inclusions (33 ppm) and suggests that the fluid that precipitated the pre-dolomite quartz underwent significantly more interaction with Li-rich lithologies (possibly within the basement rocks) than the dolomitising fluid. They both have Na and Cl concentrations (Figure 11.7) comparable with seawater that had been evaporated beyond the point of halite precipitation (Fluid 2). However, the K and Cl concentrations (Figure 11.8) show

that while the coarse dolomite plots along the SET, the pre-dolomite quartz is depleted in K. This may indicate that that the pre-dolomite bearing fluid interacted with Na feldspar, whereas the dolomite-bearing fluid did not.

The post-dolomite quartz has a Cl/Br molar (1,754) ratio that is consistent with the dissolution of evaporites. The Na/Li and Na/K ratios are 417 and 44.23 respectively. Interestingly, the Li concentration of the fluids within the post-dolomite quartz inclusions is very high (539 ppm). The Na and K versus Cl plots (Figures 11.7 and 11.8) show that the fluids within the post-dolomite quartz have a Na concentration similar to that of evaporated seawater but are depleted in K. As these fluids are thought to be the result of the dissolution of Mesozoic aged evaporites, the fluid-rock interactions that caused the depletion in K must have occurred either within the evaporites themselves or within lithologies stratigraphically higher than the Waulsortian Limestone in which the quartz crystals occur. Developments of gypsum, anhydrite and halite are known to have occurred within the Permo-Triassic rocks in Ireland (Wilson *et al.*, 2001). However, there is no record of the precipitation of K-salts anywhere in Ireland. Therefore the K depletion within these fluids must have come from interaction with the rocks along the flow pathway. The incorporation of K into clay minerals such as illite may have reduced the K in these fluids or perhaps the interaction with Na feldspar. Similarly, as these fluids are not thought to have interacted with basement lithologies, the high Li concentration within these fluid inclusions must reflect fluid-rock interactions within lithologies stratigraphically above the Waulsortian Limestone. However, any attempt to indicate possible sources of these high Li concentrations would be purely speculative.

Co. Carlow

The Cl/Br ratios of the quartz and dolomite samples from Carlow are broadly similar in that they are all less than seawater and with the exception of the post-dolomite quartz from Quinagh, plot in the region expected for the composition of seawater evaporated beyond the point of halite precipitation (Fluid 2). The Na/Li and Na/K ratios range from 247 to 1,485 and 0.36 to 42.28 respectively.

The Na and K versus Cl plots (Figures 11.7 and 11.8) of the quartz data from Clonmelsh indicate that the fluids within the quartz inclusions had Na and K concentrations similar to that of seawater. However, the dolomite data show a very minor enrichment in Na (Figure

11.7) consistent with the Cl/Br ratios (Figure 11.4), and an increase in the K concentration relative to seawater (Figure 11.8). This large K increase may be due to the albitization of K-feldspar or interaction with clay minerals (e.g. illite).

The Na and K versus Cl plots (Figures 11.7 and 11.8) of the dolomite from Quinagh show that the fluids within these inclusions were enriched in Na and depleted in K. However, the magnitude of Na enrichment is not matched by the decrease in K. Therefore the concentrations of Na and K in this fluid were, at least in part, controlled by different exchange reactions. The data from the quartz at Quinagh are not shown in either of the Na and K versus Cl plots, as their Na (121,796 ppm) and K (197,679 ppm) concentrations are too large. The data do suggest that the fluids within the quartz inclusions at Quinagh are massively enriched in both Na and K. This is consistent with the Cl/Br and Na/Br data (Figure 11.4), which indicated that the quartz-bearing fluids were greatly enriched in Na. However, the low Na/K ratios (0.36) and may suggest the contamination of these samples by K-bearing phases. It should also be noted that the charge balance for the quartz from Quinagh was poor and indicated an excess in cations.

Interestingly the F values for the coarse dolomite at both Quinagh and Clonmelsh (0.155 and 0.21 mg/L respectively) are orders of magnitude larger than the F data from other areas within this study (Appendix D). This is probably related to the cubes of fluorite that post-date the coarse dolomite that were found with the samples from Quinagh. Li values for the dolomite at both Quinagh and Clonmelsh (953 and 967 ppm respectively) are the highest in the dataset and probably reflect interaction of the parental fluids with the underlying granitic basement, which in this area, is known to contain extensive economically-important spodumene-bearing pegmatites (O'Connor *et al.*, 1991).

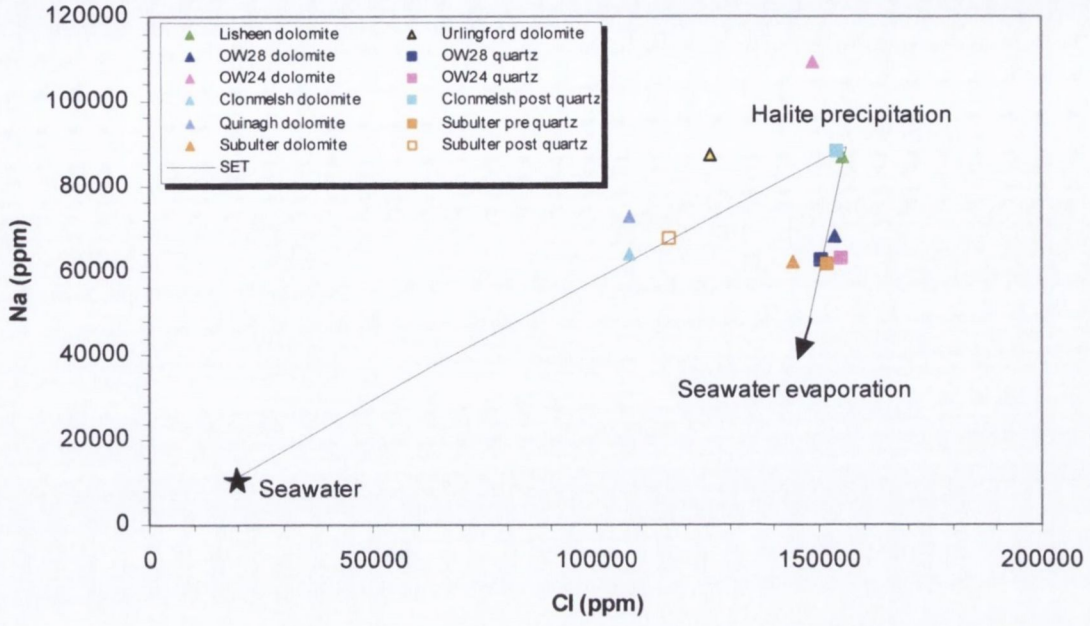

Figure 11.7 Calculated Na vs. Cl composition of the fluid inclusions from all study areas. SET after (Fontes & Matray, 1993a).

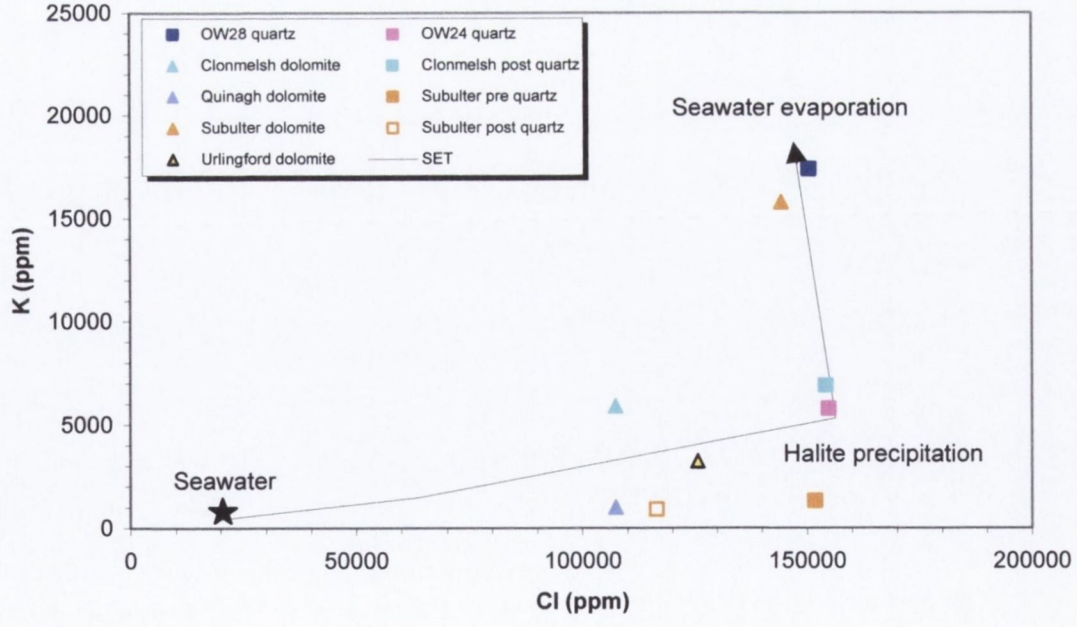

Figure 11.8 Calculated K vs. Cl composition of the fluid inclusions from all study areas. SET after (Fontes & Matray, 1993a).

Discussion

The evidence from the composition of fluid inclusions from the many of the areas within this study indicates that the fluids involved in pre-mineralisation dolomitisation and quartz precipitation were residual brines (or mixtures of residual brines and either: a low salinity fluid; or a fluid that acquired some Cl from the dissolution of halite), formed by the evaporation of seawater past the point of halite precipitation.

The Na and K concentrations of these fluids vary both within and between the different study areas and probably reflect varying degrees of interaction with feldspars and clay minerals, probably within the underlying Old Red Sandstone (± the Lower Palaeozoic basement). Li concentrations in the majority of the fluid inclusions are substantially higher than those expected for seawater and since neither limestone nor feldspar are viable sources of crustal Li, may indicate that many of these dolomitising fluids underwent interaction with the underlying Lower Palaeozoic basement. Figure 11.9 is a summary diagram of the fluid-rock interaction pathways of both the dolomitising and quartz-bearing fluids from all of the areas studied.

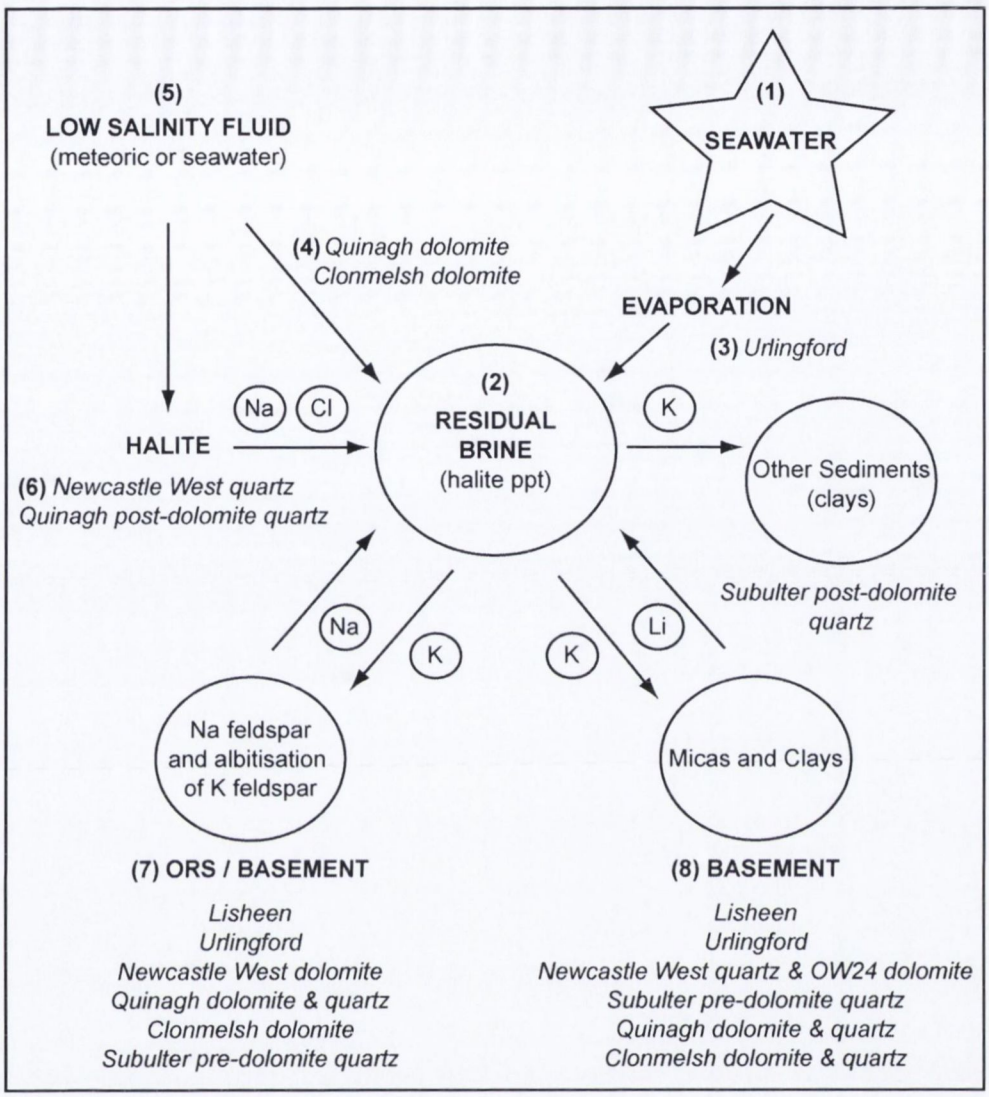

Figure 11.9 A schematic summary diagram of the fluid-rock interaction pathways of the dolomitising and quartz-bearing fluids from all areas studied. The majority of fluids began as seawater (1) that was subsequently evaporated beyond the point of halite precipitation to form residual brine (2). Exceptions to this include: the dolomite at Urlingford (3), which shows evidence for seawater having been evaporated, but not to the point of halite precipitation; the dolomite from both Quinagh and Clonmelsh (4) which shows evidence for the residual brine having mixed with a component of either meteoric or seawater (5); and the quartz from Newcastle West and Quinagh (6), which both show evidence for a component of halite dissolution. The Na, K and Li concentrations of the residual brines show evidence for later modification by fluid-rock interaction within the underlying Old Red Sandstone (7) and/or Lower Palaeozoic basement (8).

Therefore these data are consistent with the modelled parental fluid values, which suggested that these fluids underwent significant fluid-rock interaction. The Li concentrations confirm the interaction of many of these fluids with the underlying Lower Palaeozoic basement, which is consistent with the density-driven convection model (Russell, 1978, 1986).

However, there remains a fundamental problem with the interpretation of this data. If these fluids did genuinely originate as residual brines, evaporated past the point of halite precipitation, where are all the evaporites? Given the large amounts of fluid needed to dolomitise such a vast area (>50km^3 as estimated by Sevastopulo and Redmond (1999)), there would have been extensive evaporite deposits generated.

However, there is very little geological evidence for the existence of evaporites in Ireland during the Tournaisian, which makes the halogen geochemistry and geological data difficult to reconcile. Phillips and Sevastopulo (1986) noted the occurrence of evaporites of >1m, which are restricted to the north Midlands, areas west of Navan and northwest of the Longford Down Inlier. Minor developments are also known to have existed in the northwest near Lough Key (Sevastopulo & Wyse Jackson, 2001) and in the southeast near Wexford (Carter & Wilbur, 1986). However, no extensive evaporite deposits are known to have existed in the southern or eastern parts of the Irish Midlands (Phillips & Sevastopulo, 1986). Gypsum beds do occur within Asbian-Brigantian aged rocks in the northwest of Ireland (Grennan, 1992), but this would have implications for the age of dolomitisation/mineralisation.

Therefore there remain two possibilities: either the age of mineralisation/dolomitisation is younger than thought (i.e. younger than the late Tournaisian); or the halogen geochemistry data and its underlying assumptions are questionable.

11.7 MECHANISMS FOR FLUID FLOW

As the primary porosity within the Waulsortian Limestone was occluded prior to the onset of both dolomitisation and mineralisation it was unlikely to have been amenable to fluid flow, unless fractured. Therefore other mechanisms must have been available to enable the magnesium and ore-bearing fluids to move through these well-cemented limestones.

As mentioned in the discussion of the regionally dolomitised Waulsortian Limestone at Lisheen in this study (Chapter 3, Section 3.3), analysis of the fine-grained 'black tops' dolomite using SEM has shown that there is evidence for a large amount of intercrystal porosity within these dolomites and perhaps some intergrain porosity also. This microporosity may have provided a mechanism for fluids to move through these rocks.

Similarly, the occurrence of fine-grained dolomite rhombs along a dissolution seams that cross-cut the early calcite cements at Newcastle West (Chapter 5, Section 5.3), implies that at least during the earliest stages of dolomitisation the magnesium-bearing fluids exploited these structures as conduits.

Other workers have suggested other mechanisms that may have enabled fluid flow within these well-cemented limestones. Gregg *et al.* (2001) have speculated that an early replacive dolomite (their pk1), which they suggest occurred prior to complete cementation and porosity occlusion in the Waulsortian Limestone, increased the porosity and permeability of the Waulsortian Limestone and so enabled later fluid flow associated with late diagenetic dolomitisation (their pk2) and sulphide mineralisation to occur. Moreover, Everett *et al.* (1999a) have suggested that CO_2 may have played an important role in generating acidity in the mineralising fluid by hydrolysis, thereby providing a mechanism for the mineralising fluids to dissolve and replace the carbonate lithosome. However, although CO_2-bearing inclusions have been reported from both Navan and Lower Palaeozoic feeder veins (Everett *et al.*, 1999a), as well as from the Irish Midlands (Wilkinson, 2003), their occurrence still remains relatively uncommon.

11.8 GENETIC MODELS

As fluid inclusion data (Samson & Russell, 1983, 1987; Banks & Russell, 1992; Banks *et al.*, 2002) strongly suggest that two fluids were involved in the formation of the Irish Zn-Pb deposits, the basin compaction model (Lydon, 1986), which assumes the involvement of only one fluid, is probably no longer valid. Therefore in terms of the three models discussed in Chapter 1, only the density-driven convection model (Russell, 1978, 1986) and the topographically driven flow model (Hitzman & Beaty, 1996) remain.

There is little doubt that the fluids involved in the Irish deposits interacted with the Lower Palaeozoic basement (± the Precambrian crystalline basement), which acted as the main

source for the metals (Everett *et al.*, 2003). This eliminates the Old Red Sandstone as a possible source for the metals in the Irish ore-field as suggested in the topographically driven flow model (Hitzman & Beaty, 1996) and lends strong support in favour of the density-driven convection model (Russell, 1978, 1986). Based on these conclusions and the observation that alteration in the Old Red Sandstone diminished away from structural conduits, Everett *et al.* (2003) discounted the Old Red Sandstone as a possible efficient regional aquifer.

However, work by L. Chapman (pers. comm.) has shown, contrary to work by Mallon (1997), that alteration in the Old Red Sandstone occurs in many locations throughout the Irish Midlands, irrespective of whether there is a deposit in the vicinity or not, and that this alteration is not necessarily fault or fracture-related.

Also, a degree of lateral flow within the Old Red Sandstone cannot be discounted as work from this study at Moyvore (Chapter 10) has shown that, at least locally, sandstones retained much of their original porosity and permeability longer than coeval carbonates and so may have formed aquifers. This contrasts with what is observed within the carbonate lithologies, which cemented quickly and were unlikely to be amenable to fluid flow, unless fractured. This highlights the danger in assuming that the Old Red Sandstone was impermeable at the time of mineralisation.

Therefore, while it seems likely that many aspects of the density-driven convection model are consistent with much of the recent work on the Irish Zn-Pb deposits, there may be elements of the topographically driven flow model, such as local lateral fluid flow within the Old Red Sandstone, that will need to be considered. It is possible that in addition to the vertical fluid flow in the density-driven convection model, which is primarily focused along reactivated Caledonian structures, a component of lateral flow within the Old Red Sandstone may also have occurred.

CHAPTER 12

CONCLUSIONS

12.1 REGIONAL CONCLUSIONS

- Pre-mineralisation dolomitisation (Regional Dolomite) post-dated the final porosity occlusion within the Waulsortian Limestone.

- Fine-grained grey dolomite occurred during the initial stages of dolomitisation and commonly selectively replaced the micrite and bryozoan material. Replacement by this dolomite was generally mimetic.

- Texturally later coarse-grained white dolomite has a similar luminescence to the fine-grained dolomite and is both a replacive and open space filling dolomite. Replacement by this dolomite is non-mimetic, with the dolomite crystals being orders of magnitude greater than the precursor calcite phase.

- In many of the areas studied, the coarse-grained white dolomite displays the curved crystal faces and sweeping extinction indicative of saddle dolomite, which suggests formation at elevated temperatures in the range of 60-150°C (Radke & Mathis, 1980).

- Fluid inclusion data confirm that coarse-grained white dolomite formed from high temperature (>100°C), very saline (>17wt% combined NaCl and $CaCl_2$ equivalent) fluids (Figure 12.1).

- The pre-mineralisation dolomitisation is believed to have formed geothermally. It is not believed to be a hydrothermal dolomite, as it is thought to have formed at or near the same temperature as the surrounding rocks. Vitrinite reflectance data indicate higher temperatures than the fluid inclusions data and suggest that the dolomites were precipitated prior to peak burial.

- There is no evidence from this study for the re-equilibration of fluid inclusions in dolomite by stretching.

- Stable isotope data indicate that that there is no south to north trend in the $\delta^{18}O$ values of the Regional Dolomite.

- Petrographically identical dolomite from two different areas may have distinctly different isotopic signatures (Figure 12.2).

- The modelled $\delta^{18}O$ values of the parental fluids of the coarse-grained white dolomite indicate that the fluids within all areas underwent a significant amount of fluid-rock interaction.

- Halogen data indicate that the fluids responsible for dolomitisation in the majority of areas studied, were residual brines (or a mixture of residual brine and a low salinity fluid), formed by the evaporation of seawater past the point of halite precipitation. In relation to the fluids involved in the formation of the Irish Zn-Pb deposits, the dolomitising fluids are most similar to Fluid 2.

- Na and K concentrations of the dolomitising fluids indicate that these fluids underwent interaction with feldspars and clay minerals, probably within the Old Red Sandstone.

- Li concentrations are substantially higher than those expected for seawater and indicate that many of these dolomitising fluids probably underwent interaction with the underlying basement lithologies.

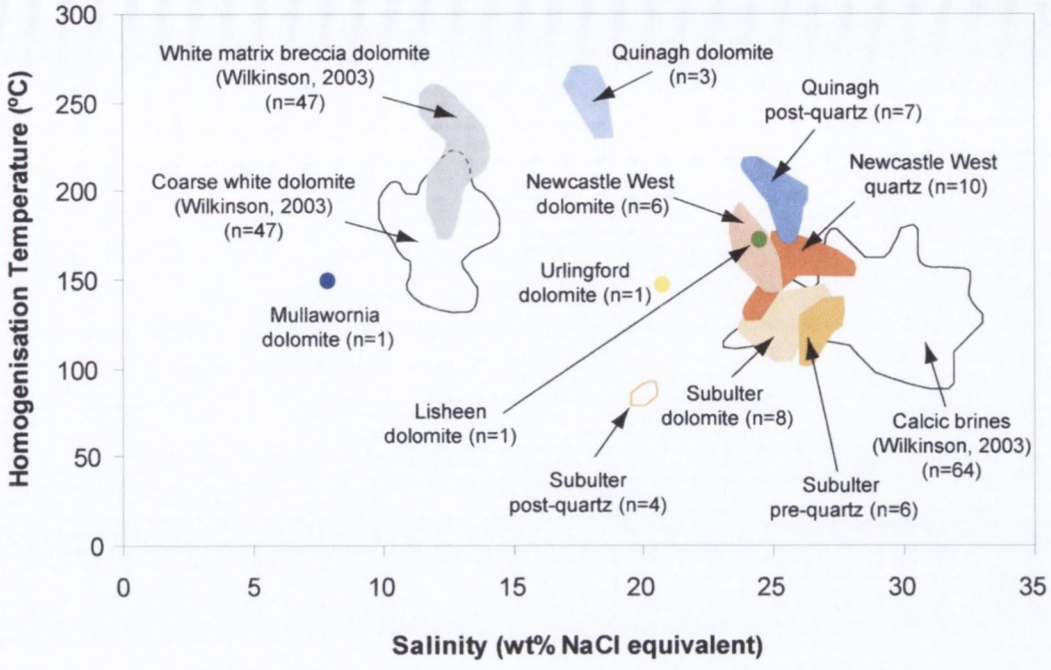

Figure 12.1 Fluid inclusion data from the coarse white dolomite component of the dolomitised Waulsortian Limestone and Ballysteen Limestone. Also plotted are data from quartz generations that both pre-date and post-date the dolomite. Note that the salinities of the dolomite data in this study are very different from those measured by Wilkinson (2003) for coarse white dolomite and white matrix breccia dolomite from the south and west Irish Midlands. There is however, some overlap in the data from this study with the calcic brines measured by Wilkinson (2003) from the Asbian-aged Ballyadams Formation. Note that in order to include the Wilkinson (2003) data salinity values measured in this study were converted to wt% NaCl equivalent. However, as final ice melting temperatures lower than -21.2°C cannot strictly be modelled using the NaCl-H_2O binary system, salinity values above ~23 wt% NaCl equivalent are very approximate.

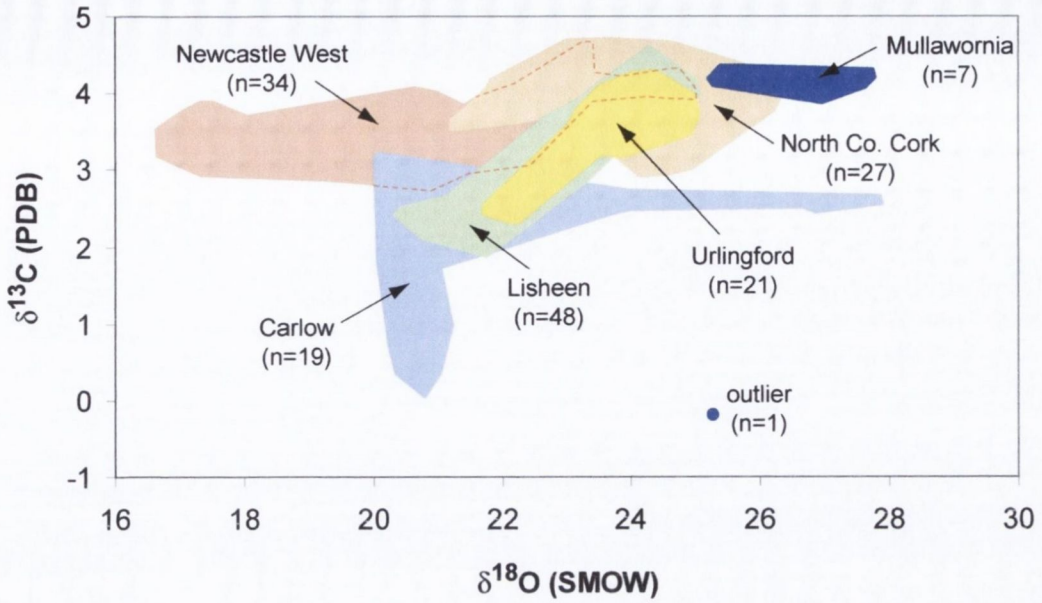

Figure 12.2 Stable isotope data from the fine-grained and coarse-grained components of the dolomitised Waulsortian Limestone and Ballysteen Limestone.

12.2 STUDY AREA SPECIFIC CONCLUSIONS

- A dolomite type, termed 'black tops' dolomite, occurs at both Lisheen and Urlingford. Petrographic evidence suggests that it may be a geopetal dolomite. Examination of this dolomite under the SEM has shown evidence for a large amount of intercrystal porosity and perhaps some intergrain porosity also. This microporosity may have provided a mechanism for fluid movement through these rocks.

- The coarse-grained dolomite component of the Regional Dolomite does not always replace a precursor coarsely crystalline limestone component as has been previously suggested (Wilkinson & Earls, 2000). Petrographic data from both Lisheen and Carlow has provided evidence for the coarse-grained dolomite being an open-space filling dolomite and not the replacement of a precursor phase.

- There is an overlap in the homogenisation temperature data from both the quartz and coarse dolomite at Newcastle West and the pre-dolomite quartz and dolomite at Subulter. This is taken as good evidence to suggest that there has been no stretching as a result of Variscan heating and means that the fluid inclusion data from both areas can be considered as being reliable.

- Inferred homogenisation temperature data for the fine-grained dolomite at Newcastle West suggests formation at temperatures >131°C. This temperature is substantially hotter than the <50°C suggested by other workers (Wright *et al.*, 2000; Gregg *et al.*, 2001) for the fine-grained dolomite found in the Irish Midlands and the Dublin Basin and indicates that dolomitisation could not have occurred by the circulation of seawater during early diagenesis.

- At least during the initial stages of dolomitisation at Newcastle West, dissolution seams may have been exploited as conduits, enabling the Mg bearing fluids to move through the well-cemented limestone.

- The halogen data contradict the petrographic, fluid inclusion and modelled parental fluid data, which all indicated that the same fluid precipitated both the coarse dolomite and the quartz at Newcastle West.

- The intermediate stage between partial dolomitisation and pervasive dolomitisation was observed in North Co. Cork where fine-grained dolomite was seen replacing CFC cements.

- Inferred homogenisation temperature data for the fine-grained dolomite at Subulter suggests formation at temperatures >105°C. This temperature is substantially hotter than the <50°C suggested by other workers (Wright *et al.*, 2000; Gregg *et al.*, 2001) for the fine-grained dolomite found in the Irish Midlands and the Dublin Basin and indicates that dolomitisation could not have occurred by the circulation of seawater during early diagenesis.

- Mesozoic fluids involved in halite dissolution were probably involved in the precipitation of the post-dolomite quartz crystals at Subulter. High Cl/Br and Na/Br molar ratios are consistent with these fluids having sourced their solutes by the dissolution of evaporites.

- Large vugs that occur within pervasively dolomitised Ballysteen Limestone at Carlow are not the amplification by dolomitisation of pre-existing calcite-filled cavities within

the limestone lithosome, as in contrast to the Waulsortian Limestone there are no 'stromatactis-like' cavities within the Ballysteen Limestone.

- The coarse pink dolomite from Carlow is isotopically different from that studied from Lisheen or North Co. Cork. This suggests that not all of the pink dolomite found throughout the Irish Midlands is the same or indeed that it formed from the same fluid.

- Bitumen occurs within large secondary cavities within the Waulsortian Limestone at Mullawornia. Petrographic examination of the bitumen indicates that it was emplaced as a liquid after the host limestone was cemented. Feeder veins to the secondary cavities appear to been also exploited by the bitumen-bearing fluids

- Mesophase textures exhibited by the bitumens at Mullawornia probably formed at temperatures much lower than those derived by experiment (350°C). They are more likely to have developed as a result of peak Variscan burial (~250°C).

- Petrographic data from Navan indicates that final porosity occlusion of the Waulsortian Limestone had occurred prior to the entrainment of its clasts within the Boulder Conglomerate and so occurred prior to the early Viséan.

- Similarly, all of the remaining porosity within the Pale Beds was occluded prior to its entrainment within the Arundian aged 'Conglomerate Complex'.

- Studies of the relationship between basic igneous intrusions and carbonate and siliciclastic country rocks at Moyvore, has shown that, at least locally, sandstones retained much of their original porosity and permeability longer than coeval carbonates and so may have formed aquifers, whereas carbonate lithologies were cemented quickly and were unlikely to be amenable to fluid flow, unless fractured.

12.3 FURTHER WORK

Worthwhile further work on the dolomitising fluids and their relation to base-metal mineralisation should include:

- A thorough investigation of the validity of the underlying assumption of halogen geochemistry, that Cl and Br remain conservative in solution.

- Further investigation into the assumption that the Cl and Br concentrations of seawater have not altered through geological time.

- Conclusively establishing the origin for the excess chlorinity in the mineralising and dolomitising brines. If as suggested in this study, highly evaporated seawater (residual brine) was responsible for dolomitisation and data from other workers (Gleeson *et al.*, 1999; Banks *et al.*, 2002) indicate that evaporated seawater was responsible for mineralisation, work needs to be done to provide either: geological evidence for the existence of extensive evaporites during the Lower Carboniferous; or other mechanisms for the generation of the high salinities.

REFERENCES

ALLAN, J. R., BEATY, D. W., STURTEVANT, R. G., HITZMAN, M. W. & SHEARLEY, E. 1992. The origin of regional dolomite in the Waulsortian of southeastern Ireland: implications for ore deposition. *Geological Society of America, Abstracts with Programs*, **24,** A354.

ANDERSON, I. K. 1990. *Ore depositional processes in the formation of the Navan zinc/lead deposit, Co. Meath*. Unpublished Ph.D. thesis, University of Strathclyde.

ANDERSON, I. K., ASHTON, J. H., J., B. A., FALLICK, A. E. & RUSSELL, M. J. 1998. Ore depositional processes in the Navan Zn-Pb deposit, Ireland. *Economic Geology*, **93,** 535-563.

ANDERSON, K., ASHTON, J., EARLS, G., HITZMAN, M. & TEAR, S. 1995. *Irish carbonate-hosted Zn-Pb deposits*. Society of Economic Geologists Guidebook Series. 296pp.

ANDREW, C. J. 1986a. The tectono-stratigraphic controls to mineralisation in the Silvermines area, Co. Tipperary, Ireland. *In*: ANDREW, C. J., CROWE, R.W. A., FINLAY, S., PENNELL, W. M., AND PYNE, J. F. (eds). *Geology and genesis of mineral deposits in Ireland*. Irish Association for Economic Geology, 377-418.

— 1992. Basin development chronology of the lowermost Carboniferous strata in the Irish north-Central Midlands. *In*: BOWDEN, A., EARLS, G., O'CONNOR, P., and PYNE, J. (eds). *The Irish Minerals Industry 1980-1990*. Irish Association of Economic Geology, 143-169.

— 1993. Mineralisation in the Irish Midlands. *In*: PATRICK, R. A. D., and POLYA, D. A. (eds). *Mineralisation in the British Isles*. Chapman and Hall London, 208-269.

ANDREW, C. J. & ASHTON, J. H. 1985. Regional setting, geology and metal distribution patterns of Navan orebody, Ireland. *Transactions of the Institution of Mining and Metallurgy*, **94,** B66-93.

ANDREW, C. J., CROWE, R.W. A., FINLAY, S., PENNELL, W. M., AND PYNE, J. F. 1986b. *Geology and genesis of mineral deposits in Ireland.* Irish Association for Economic Geology, Dublin. 709pp.

ASHBY, D. F. 1939. The geological succession and petrology of the Carboniferous volcanic area of Co. Limerick. *Proceedings of the Geologist's Association*, **50,** 324-330.

ASHTON, J. H. 1995. Guide to the geology of the Navan orebody. *In*: ANDERSON, K., ASHTON, J., EARLS, G., HITZMAN, M., and TEAR, S. (eds). *Irish carbonate-hosted Zn-Pb deposits*. Society of Economic Geologists Guidebook Series, **21,** 151-168.

ASHTON, J. H., BLACK, A., GERAGHTY, J., HOLDSTOCK, M. & HYLAND, E. 1992. The geological setting and metal distribution pattern of the Zn-Pb-Fe mineralization in the Navan Boulder Conglomerate. *In*: BOWDEN, A., EARLS, G., O'CONNOR, P., and PYNE, J. (eds). *The Irish Minerals Industry 1980-1990.* Irish Association of Economic Geology, 171-210.

ASHTON, J. H., DOWNING, D. T. & FINLAY, S. 1986. The geology of the Navan Orebody. *In*: ANDREW, C. J., CROWE, R.W. A., FINLAY, S., PENNELL, W. M., AND PYNE, J. F. (eds). *Geology and genesis of mineral deposits in Ireland.* Irish Association for Economic Geology, 243-280.

ASHTON, J. H., HOLDSTOCK, M. P., GERAGHTY, J. F., O'KEEFFE, W. G., MATINEZ, N., PEACE, W. & PHILCOX, M. E. 2003. The Navan orebody - discovery and geology of the South West Extension. *In*: KELLY, J. G., ANDREW, C. J., ASHTON, J. H., BOLAND, M. B., EARLS, G., FUSCIARDI, L., and STANLEY, G. (eds). *Europe's Major Base Metal Deposits.* Irish Association for Economic Geology, 405-436.

AZAROUAL, M., FOUILLAC, C. & MATRAY, J. M. 1997. Solubility of silica polymorphs in electrolyte solutions, I. Activity coefficient of aqueous silica from 25° to 250°C, Pitzer's parameterisation. *Chemical Geology*, **140,** 155-165.

BANKS, D. A. 1985. A fossil hydrothermal assemblage from the Tynagh lead-zinc deposit in Ireland. *Nature*, **313,** 128-131.

— 1986. Hydrothermal chimneys and fossil worms from the Tynagh lead-zinc deposit, Ireland. *In*: ANDREW, C. J., CROWE, R.W. A., FINLAY, S., PENNELL, W. M., AND PYNE, J. F. (eds). *Geology and genesis of mineral deposits in Ireland.* Irish Association for Economic Geology, 441-448.

BANKS, D. A., BOYCE, A. J. & SAMSON, I. M. 2002. Constraints on the origins of fluids forming Irish Zn-Pb-Ba deposits: Evidence from the composition of fluid inclusions. *Economic Geology*, **97,** 471-480.

BANKS, D. A. & RUSSELL, M. J. 1992. Fluid mixing during ore deposition at the Tynagh base-metal deposit, Ireland. *European Journal of Mineralogy*, **4,** 921-931.

BANKS, D. A. & YARDLEY, B. W. D. 1992. Crush-leach analysis of fluid inclusions in small natural and synthetic samples. *Geochimica et Cosmochimica Acta*, **56,** 245-248.

BLACKBERRY, B. A. 1968. Convolute zoning of plagioclase phenocrysts in Miocene volcanics from the Western Santa Monica Mountains, California. *American Mineralogist*, **53,** 954-962.

BLAKEMAN, R. J., ASHTON, J. H., BOYCE, A. J., FALLICK, A. E. & RUSSELL, M. J. 2002. Timing of interplay between hydrothermal and surface fluids in the Navan Zn + Pb orebody, Ireland: Evidence from metal distribution trends, mineral textures and $\delta^{34}S$ analyses. *Economic Geology*, **97,** 73-91.

BOAST, A. M., COLEMAN, M. L. & HALLS, C. 1981a. Textural and stable isotope evidence for the genesis of the Tynagh base metal deposit, Ireland. *Economic Geology*, **76,** 27-55.

BODNAR, R. J. 1993. Revised equation and table for determining the freezing point depression of H_2O-NaCl solutions. *Geochimica et Cosmochimica Acta*, **57,** 683-684.

— 2003. Re-equilibration of fluid inclusions. *In*: SAMSON, I. M., ANDERSON, A., and MARSHALL, D. (eds). *The analysis and interpretation of fluid inclusions*. Mineralogical Association of Canada Short Course, **32,** 213-231.

BODNAR, R. J. & BETHKE, P. M. 1984. Systematics of stretching of fluid inclusions I: Fluorite and sphalerite at 1 atmosphere confining pressure. *Economic Geology*, **79,** 141-161.

BODNAR, R. J., BINNS, P. R. & HALL, D. L. 1989. Synthetic fluid inclusions - VI. Quantitative evaluation of the decrepitation behaviour of fluid inclusions in quartz at one atmosphere confining pressure. *Journal of Metamorphic Geology*, **7,** 229-242.

BORTHWICK, J. & HARMON, R. S. 1982. A note regarding ClF_3 as an alternative to BrF_5 for oxygen isotope analysis. *Geochimica et Cosmochimica Acta*, **46,** 1665-1668.

BOTTRELL, S. H., YARDLEY, B. W. D. & BUCKLEY, F. 1988. A modified crush-leach method for the analysis of fluid inclusion electrolytes. *Bulletin of Mineralogy*, **111,** 279-290.

BOWDEN, A., EARLS, G., O'CONNOR, P. & PYNE, J. 1992. *The Irish Minerals Industry 1980-1990*. Irish Association of Economic Geology, Dublin. 434pp.

BOYCE, A. J., ANDERTON, R. & RUSSELL, M. J. 1983b. Rapid subsidence and early Carboniferous base-metal mineralisation in Ireland. *Transactions of the Institution of Mining and Metallurgy*, **92,** B55-66.

BOYCE, A. J., COLEMAN, M. L. & RUSSELL, M. J. 1983a. Formation of fossil hydrothermal chimneys and mounds from Silvermines, Ireland. *Nature*, **306,** 545-550.

BOYCE, A. J., LITTLE, C. T. S. & RUSSELL, M. J. 2003. A new fossil vent biota in the Ballynoe baryte deposit, Silvermines, Ireland: evidence for intracratonic sea-floor hydrothermal activity about 352 Ma. *Economic Geology*, **98,** 649-656.

BRAND, U. 1982. The oxygen and carbon isotope composition of Carboniferous fossil components; sea-water affects. *Sedimentology*, **29,** 139-147.

BRUCKSCHEN, P., OESMANN, S. & VEIZER, J. 1999. Isotope stratigraphy of the European Carboniferous: proxy signals for ocean chemistry, climate and tectonics. *Chemical Geology*, **161,** 127-163.

BURRUSS, R. C. 1991. Practical aspects of fluorescence microscopy of petroleum inclusions. *In*: BARKER, C. E., and KOPP, O. (eds). *Qualitative and quantitative applications*. SEPM Short Course, **25,** 1-7.

— 2003. Petroleum fluid inclusions, an introduction. *In*: SAMSON, I. M., ANDERSON, A., and MARSHALL, D. (eds). *The analysis and interpretation of fluid inclusions*. Mineralogical Association of Canada Short Course, **32,** 159-174.

CAMPBELL, K. J. M. 1988. *The geology of the area around Mallow, Co. Cork*. Unpublished MSc.thesis, University of Dublin.

CARBONI, V., WALSH, J. J., STEWART, D. R. A. & GÜVEN, J. F., 2003. Timing and geometry of normal faults and associated structures at the Lisheen Zn/Pb deposit, Ireland - investigating their role in the transport and the trapping of metals, *in* ELIOPOULOS, D. G.,(eds)., Proceedings of the 7th Biennial SGA Meeting: Athens, Millpress, Rotterdam, 665-668.

CARPENTER, A. B. 1978. Origin and chemical evolution of brines in sedimentary basins. *Oklahoma Geological Survey Circular*, **79,** 60-77.

CARTER, J. S. & WILBUR, D. G. 1986. The geological setting of Zn mineralisation near Duncormick in the Wexford Permo-Carboniferous outlier. *In*: ANDREW, C. J., CROWE, R.W. A., FINLAY, S., PENNELL, W. M., AND PYNE, J. F. (eds). *Geology and genesis of mineral deposits in Ireland*. Irish Association for Economic Geology, 471-474.

CAULFIELD, J. B. D., LEHURAY, A. P. & RYE, D. M. 1986. A review of lead and sulphur isotope investigations of Irish sediment-hosted base-metal deposits with new data from the Keel, Ballinalack, Moyvoughly and Tatestown deposits. *In*: ANDREW, C. J., CROWE, R.W. A., FINLAY, S., PENNELL, W. M., AND PYNE, J. F. (eds). *Geology and genesis of mineral deposits in Ireland.* Irish Association for Economic Geology, 591-624.

CHACKO, T., COLE, D. R. & HORITA, J. 2001. Equilibrium oxygen, hydrogen and carbon isotope fractionation factors applicable to geologic systems. *In*: VALLEY, J. W., and COLE, D. R. (eds). *Stable Isotope Geochemistry*. Mineralogical Society of America, **43,** 1-62.

CHOWNS, T. M. & ELKINS, J. E. 1974. The origin of quartz geodes and cauliflower cherts through the silicification of anhydrite nodules. *Journal of Sedimentary Petrology*, **44,** 885-903.

CLAYTON, G., HAUGHEY, N., SEVASTOPULO, G. D. & BURNETT, R. 1989. *Thermal maturation levels in the Devonian and Carboniferous rocks of Ireland.* Geological Survey of Ireland. 36pp.

CLAYTON, R. N., GOLDSMITH, J. R., KAREL, K. J., MAYEDA, T. K. & NEWTON, R. C. 1975. Limits on the effect of pressure on isotopic fractionation. *Geochimica et Cosmochimica Acta*, **39,** 1197-1201.

COLLINS, A. G. 1975. *The geochemistry of oilfield waters*. Elsevier, New York. 496pp.

CORCORAN, D. V. & CLAYTON, G. 2001. Interpretation of vitrinite reflectance profiles in sedimentary basins, onshore and offshore Ireland. *In*: SHANNON, P. M., HAUGHTON, P. D. W., and CORCORAN, D. V. (eds). *The Petroleum Exploration of Ireland's Offshore Basins*. Geological Society, London, Special Publications, **188,** 61-90.

CRAIG, H. 1961. Isotopic variations in meteoric waters. *Science*, **133,** 1702-1703.

CRAWFORD, M. L. 1981. Phase equilibria in aqueous fluid inclusions. *In*: HOLLISTER, L. S., and CRAWFORD, M. L. (eds). *Fluid inclusions: applications to petrology.* Mineralogical Association of Canada Short Course, **6,** 75-100.

CREAN, E. 1987. *The Lower Carboniferous geology of south County Longford.* Unpublished MSc.thesis, University of Dublin.

CRISS, R. E. 1999. *Principles of stable isotope distribution.* University Oxford Press, New York. 254pp.

CRUISE, M. D. 2000. *Iron oxide and associated base metal mineralisation in the Central Midlands Basin, Ireland.* Unpublished Ph.D. thesis, University of Dublin.

CZERNIAKOWSKI, L. A., LOHMANN, K. C. & WILSON, J. L. 1984. Closed-system marine burial diagenesis: Isotopic data from the Austin Chalk and its components. *Sedimentology*, **31,** 863-877.

DALY, J. S. 2001. Precambrian. *In*: HOLLAND, C. H. (eds). *The geology of Ireland.* Dunedin Academic Press Edinburgh, 7-45.

DALY, J. S., VAN DEN BERG, R. & FLOWERDEW, M. J. 2002. Precambrian and lower crustal geology of Ireland in relation to Carboniferous-hosted base metal mineralisation. *Basement controls on mineralisation in the Irish orefield*, Irish Association of Economic Geology.

DAVIS, D. W., LOWENSTEIN, T. K. & SPENCER, R. J. 1990. Melting behaviour of fluid inclusions in laboratory grown halite crystals in the systems NaCl-H_2O, NaCl-KCl-H_2O, NaCl-$MgCl_2$-H_2O and NaCl-$CaCl_2$-H_2O. *Geochimica et Cosmochimica Acta*, **54,** 591-601.

DE BRIT, T. J. 1988. *The diagenetic and structural relationships of veins from Lower Carboniferous Limestones, Counties Longford and Westmeath, Ireland.* Unpublished Ph.D. thesis, University of Dublin.

DIAMOND, L. W. 2003. Systematics of H_2O inclusions. *In*: SAMSON, I. M., ANDERSON, A., and MARSHALL, D. (eds). *The analysis and interpretation of fluid inclusions*. Mineralogical Association of Canada Short Course, **32,** 55-79.

DICKSON, J. A. D. 1966. Carbonate identification and genesis as revealed by staining. *Journal of Sedimentary Petrology*, **36,** 491-505.

DICKSON, J. A. D. & COLEMAN, M. L. 1980. Changes in carbon and oxygen isotope composition during limestone diagenesis. *Sedimentology*, **27,** 107-118.

DICKSON, J. A. D., SMALLEY, P. C., RÅHEIM, A. & STIJFHOORN 1990. Intracrystalline carbon and oxygen isotope variation in calcite revealed by laser microsampling. *Geology*, **18,** 809-811.

DIXON, P. R., LEHURAY, A. P. & RYE, D. M. 1990. Basement geology and tectonic evolution of Ireland as deduced from Pb isotopes. *Journal of the Geological Society, London*, **147,** 121-132.

DONALDSON, C. H. & HENDERSON, C. M. B. 1988. A new interpretation of round embayments in quartz crystals. *Mineralogical Magazine*, **52,** 27-33.

DOVE, P. M. & RIMSTIDT, J. D. 1994. Silica-water interactions. *In*: HEANEY, P. J., PREWITT, C. T., and GIBBS, G. V. (eds). *Silica: physical behaviour, geochemistry and materials applications*. Reviews in Mineralogy, **29,** 259-308.

DOYLE, E. & BOWDEN, A. A. 1995. Field guide to the Galmoy zinc-lead deposits, Co. Kilkenny. *In*: ANDERSON, K., ASHTON, J., EARLS, G., HITZMAN, M., and TEAR, S. (eds). *Irish carbonate-hosted Zn-Pb deposits*. Society of Economic Geologists Guidebook Series, **21,** 139-145.

DOYLE, E., BOWDEN, A. A., JONES, G. V. & STANLEY, G. A. 1992. The geology of the Galmoy zinc-lead deposits, Co. Kilkenny. *In*: BOWDEN, A., EARLS, G., O'CONNOR, P., and PYNE, J. (eds). *The Irish Minerals Industry 1980-1990*. Irish Association of Economic Geology, 211-225.

DRIESNER, T. 1997. The effect of pressure on deuterium-hydrogen fractionation in high-temperature water. *Science*, **277,** 791-794.

EMMERMANN, R. & LAUTERJUNG, J. 1997. The German Continental Deep Drilling Program KTB: Overview and major results. *Journal of Geophysical Research*, **102,** 18179-18201.

EMO, G. T. 1986. Some considerations regarding the styles of mineralisation at Harberton Bridge, Co. Kildare. *In*: ANDREW, C. J., CROWE, R.W. A., FINLAY, S., PENNELL, W. M., AND PYNE, J. F. (eds). *Geology and genesis of mineral deposits in Ireland.* Irish Association for Economic Geology, 461-470.

EVERETT, C. E., RYE, D. M. & ELLAM, R. M. 2003. Source or sink? An assessment of the role of the Old Red Sandstone in the genesis of the Irish Zn-Pb deposits. *Economic Geology*, **98,** 31-50.

EVERETT, C. E., RYE, D. M., WILKINSON, J. J., BOYCE, A. J., ELLAM, R. M., FALLICK, A. E. & GLEESON, S. A. 1999b. The genesis of Irish-type Zn-Pb deposits: Characterisation and origin of the principle ore fluid. *In*: STANLEY, C. J. (eds). *Mineral deposits: Processes and Processing*. Balkema Rotterdam, 854-848.

EVERETT, C. E., WILKINSON, J. J. & RYE, D. M. 1999a. Fracture-controlled fluid flow in the Lower Palaeozoic basement rocks of Ireland: implications for the genesis of Irish-type Zn-Pb deposits. *In*: MCCAFFREY, K. J. W., LONERGAN, L., WILKINSON, J. (eds). *Fractures, Fluid Flow and Mineralisation*. Geological Society, London, Special Publications, **155,** 247-276.

EYRE, S. L. 1998. *Geochemistry of dolomitisation and Zn-Pb mineralisation in the Rathdowney Trend, Ireland.* Unpublished Ph.D. thesis, Imperial College London.

EYRE, S. L., WILKINSON, J. J., STANLEY, C. J. & BOYCE, A. J. 1996. Geochemistry of dolomitisation and zinc-lead mineralisation in the Rathdowney Trend, Ireland. *Geological Society of America, Abstracts with Programs*, **28,** A210-211.

FALLICK, A. E., ASHTON, J. H., J., B. A., ELLAM, R. M. & RUSSELL, M. J. 2001. Bacteria were responsible for the magnitude of the world-class hydrothermal base metal sulphide orebody at Navan, Ireland. *Economic Geology*, **96,** 885-890.

FLEMING, B. A. & CRERAR, D. A. 1982. Silicic acid ionization and calculation of silica solubility at elevated temperature and pH. *Geothermics*, **11,** 15-29.

FOLK, R. L. & PITTMAN, J. S. 1971. Length-slow chalcedony: a new testament for vanished evaporites. *Journal of Sedimentary Petrology*, **41,** 1045-1058.

FONTES, J. C. & MATRAY, J. M. 1993a. Geochemistry and origin of formation brines from the Paris Basin, France 1. Brines associated with Triassic salts. *Chemical Geology*, **109,** 149-175.

FOOT, F. J. & O'KELLY, J. 1865. *Explanation to accompany Sheets 98, 99, 108 and 109 of the one-inch maps of the Geological Survey of Ireland.* Hodges and Smith, Dublin.

FORD, C. V. 1996. *The integration of petrologic and isotopic data from the Boulder Conglomerate to determine the age of the Navan orebody, Ireland.* Unpublished Ph.D. thesis, University of Glasgow.

FORD, M. 1987. Practical application of the sequential balancing technique: an example from the Irish Variscides. *Journal of the Geological Society of London*, **144,** 881-885.

FOURNIER, R. O. 1983. A method of calculating quartz solubilities in aqueous sodium chloride solutions. *Geochimica et Cosmochimica Acta*, **47,** 579-586.

FOURNIER, R. O. & POTTER, R. W. 1982. An equation correlating the solubility of quartz in water from 25°C to 900°C at pressures up to 10,000 bars. *Geochimica et Cosmochimica Acta*, **47,** 579-586.

FOURNIER, R. O., ROSENBAUER, R. J. & BISCHOFF, J. L. 1982. The solubility of quartz in aqueous sodium chloride solution at 350°C and 180 to 500 bars. *Geochimica et Cosmochimica Acta*, **46,** 1975-1978.

FRIEDMAN, I. & O'NEIL, J. R. 1977. Compilation of stable isotope fractionation factors of geochemical interest. *USGS Professional Paper*, **440-KK**.

FUSCIARDI, L. P., GÜVEN, J. F., STEWART, D. R. A., CARBONI, V. & WALSH, J. J. 2003. The geology and genesis of the Lisheen Zn-Pb deposit, Co. Tipperary, Ireland. *In*: KELLY, J. G., ANDREW, C. J., ASHTON, J. H., BOLAND, M. B., EARLS, G., FUSCIARDI, L., and STANLEY, G. (eds). *Europe's Major Base Metal Deposits.* Irish Association for Economic Geology, 455-481.

GALLAGHER, S. J. & SOMERVILLE, I. D. 1997. Late Dinantian (Lower Carboniferous) platform carbonate stratigraphy of the Buttevant area north Co. Cork, Ireland. *Geological Journal*, **32,** 313-335.

GALLAGHER, V., BOYCE, A. J., FALLICK, A. E. & MÖHR, P. J. 1992. An isotopic study of the Harberton Bridge Fe-Zn-Pb deposit, County Kildare, and its implications for metallogenesis in Ireland. *In*: BOWDEN, A., EARLS, G., O'CONNOR, P., and PYNE, J. (eds). *The Irish Minerals Industry 1980-1990.* Irish Association of Economic Geology, 261-272.

GARVEN, G. 1985. The role of regional fluid flow in the genesis of the Pine point deposit. *Economic Geology*, **80,** 307-324.

GARVEN, G. & FREEZE, R. A. 1984a. Theoretical analysis of the role of groundwater flow in the genesis of stratabound ore deposits: 1. Mathematical and numerical model. *American Journal of Science*, **284,** 1085-1124.

— 1984b. Theoretical analysis of the role of groundwater flow in the genesis of stratabound ore deposits: 2. Quantitative results. *American Journal of Science*, **284,** 1125-1174.

GATLEY, S., SOMERVILLE, I. D., MORRIS, J. H., SLEEMAN, A. G. & EMO, G. in press. *Geology of Galway - Offaly, and adjacent parts of Westmeath, Tipperary, Laois, Clare and Roscommon; a geological description to accompany the bedrock geology 1:100,000 scale map series, Sheet 15, Galway-Offaly with contributions by W. Cox, T. Hunter-Williams and R. van den Berg and E. Sweeney.* Geological Survey of Ireland.

GILLIES, D. 1987. *Diagenetic history of the Waulsortian buildups (Dinantian), Craven Basin, N.W. England.* Unpublished Ph.D. thesis, University of Edinburgh.

GIVEN, R. K. & LOHMANN, K. C. 1985. Derivation of the original isotopic composition of Permian marine cements. *Journal of Sedimentary Petrology*, **55,** 430-439.

GIZE, A. P. 1986. The development of a thermal mesophase in bitumens from high temperature ore deposits. *In*: DEAN, W. E. (eds). *Proceedings of the Denver Region Exploration Geologists Society Symposium, Organics and Ore Deposits*, 137-151.

GLEESON, S. A. 2003. Bulk analysis of electrolytes in fluid inclusions. *In*: SAMSON, I. M., ANDERSON, A., and MARSHALL, D. (eds). *The analysis and interpretation of fluid inclusions*. Mineralogical Association of Canada Short Course, **32,** 233-246.

GLEESON, S. A., BANKS, D. A., EVERETT, C. E., WILKINSON, J. J., SAMSON, I. M. & BOYCE, A. J. 1999. Origin of mineralising fluids in Irish-type deposits: Constraints from halogens. *In*: STANLEY, C. J. (eds). *Mineral deposits: Processes and Processing*. Balkema Rotterdam, 857-860.

GLEESON, S. A. & YARDLEY, B. W. D. 2002. Veins and mineralisation in basement rocks: the role of penetration of sedimentary fluids. *In*: STOBER, I., and BUCHER, K. (eds). *Water-rock interaction*. Kluwer Academic Publishers.

GOLDSTEIN, R. H. 1986. Reequilibration of fluid inclusions in low-temperature calcium-carbonate cement. *Geology*, **14,** 792-795.

— 2003. Petrographic analysis of fluid inclusions. *In*: SAMSON, I. M., ANDERSON, A., and MARSHALL, D. (eds). *The analysis and interpretation of fluid inclusions*. Mineralogical Association of Canada Short Course, **32,** 9-53.

GOLDSTEIN, R. H. & REYNOLDS, T. J. 1994. Systematics of fluid inclusions in diagenetic minerals. *SEPM Short Course*, **31,** 199pp.

GRAHAM, J. R. 1983. Analysis of the Upper Devonian Munster Basin, an example of a fluvial distributary system. *In*: COLLINSON, J. D., and LEWIN, J. (eds). *Special Publication of the International Association of Sedimentologists*, **6,** 473-483.

— 2001. Variscan Structures. *In*: HOLLAND, C. H. (eds). *The geology of Ireland* Edinburgh, 313-330.

GREEN, P. F., DUDDY, I. R., HEGARTY, K. A., BRAY, R. J., SEVASTOPULO, G., CLAYTON, G. & JOHNSTON, D. 2000. The post-Carboniferous evolution of Ireland: evidence from Thermal History Reconstruction. *Proceedings of the Geologist's Association*, **111,** 307-320.

GREGG, J. A., SHELTON, K. L., JOHNSON, A. W., SOMERVILLE, I. D. & WRIGHT, W. R. 2001. Dolomitisation of the Waulsortian Limestone (Lower Carboniferous) in the Irish Midlands. *Sedimentology*, **48,** 745-766.

GRENNAN, E. 1992. The Glangevlin gypsum deposit, Co. Cavan. *In*: BOWDEN, A., EARLS, G., O'CONNOR, P., and PYNE, J. (eds). *The Irish Minerals Industry 1980-1990*. Irish Association of Economic Geology, 317-325.

HAAS, J. L. 1977. Thermodynamic properties of the coexisting phases and thermochemical properties of the NaCl component in boiling NaCl solutions. *U.S Geological Survey Bulletin*, **1421-B**.

HALLIDAY, A. N. & MITCHELL, J. G. 1983. K-Ar ages of clay concentrates from Irish orebodies and their bearing on the timing of mineralization. *Transactions of the Royal Society of Edinburgh*, **74,** 1-14.

HANOR, J. S. 1987. Origin and migration of subsurface sedimentary brines. *SEPM Short Course*, **21,** 247pp.

HARDY, R. & TUCKER, M. 1988. X-ray diffraction of sediments. *In*: TUCKER, M. (eds). *Techniques in sedimentology*. Blackwell Science, 191-228.

HAYNES, F. M. 1985. Determination of fluid inclusion composition by sequential freezing. *Economic Geology*, **80,** 1436-1439.

HELGESON, H. C., KIRKHAM, D. H. & FLOWERS, G. C. 1981. Theoretical prediction of the thermodynamic behavior of aqueous electrolytes at high pressures and temperatures: IV. Calculation of activity coefficients, osmotic coefficients, and apparent molal and standard and relative partial molal properties to 600°C and 5 KB. *American Journal of Science*, **281,** 1249-1516.

HITZMAN, M. 1995a. Geological setting of the Irish Zn-Pb-(Ba-Ag) orefield. *In*: ANDERSON, K., ASHTON, J., EARLS, G., HITZMAN, M., and TEAR, S. (eds). *Irish carbonate-hosted Zn-Pb deposits*. Society of Economic Geologists Guidebook Series, **21,** 3-23.

— 1995b. Mineralization in the Irish Zn-Pb-(Ba-Ag) orefield. *In*: ANDERSON, K., ASHTON, J., EARLS, G., HITZMAN, M., and TEAR, S. (eds). *Irish carbonate-hosted Zn-Pb deposits*. Society of Economic Geologists Guidebook Series, **21,** 25-61.

HITZMAN, M. W., ALLAN, J. R. & BEATY, D. W. 1998. Regional dolomitisation of the Waulsortian Limestone in southeastern Ireland; evidence of large scale fluid flow driven by the Hercynian Orogeny. *Geology*, **26,** 547-550.

HITZMAN, M. W. & BEATY, D. W. 1996. The Irish Zn-Pb-(Ba) orefield. *Society of Economic Geologist's Special Publication*, **4,** 112-143.

HITZMAN, M. W., CONNOR, P. O. O., SHEARLEY, E., SCHAFFALITZKY, C., BEATY, D. W., ALLAN, J. R. & THOMPSON, T. 1992. Discovery and geology of the Lisheen Zn-Pb-Ag prospect, Rathdowney Trend, Ireland. *In*: BOWDEN, A., EARLS, G., O'CONNOR,

P., and PYNE, J. (eds). *The Irish Minerals Industry 1980-1990.* Irish Association of Economic Geology, 227-246.

HITZMAN, M. W., REDMOND, P. & BEATY, D. W. 2002. The carbonate-hosted Lisheen Zn-Pb-Ag deposit, County Tipperary, Ireland. *Economic Geology*, **97,** 1627-1655.

HOEFS, J. 2001. *Stable isotope geochemistry.* Springer-Verlag, Berlin. 201pp.

HOLLAND, C. H. 2001. *The geology of Ireland.* Dunedin Academic Press, Edinburgh. 531pp.

HORITA, J., COLE, D. R., POLYAKOV, V. B. & DRIESNER, T. 2002. Experimental and theoretical study of pressure effects on hydrogen isotope fractionation in the system brucite-water at elevated temperatures. *Geochimica et Cosmochimica Acta*, **66,** 3769-3788.

HORITA, J., COLE, D. R. & WESOLOWSKI, D. J. 1993b. The activity-composition relationship of oxygen and hydrogen isotopes in aqueous salt solutions: II. Vapor-liquid water equilibration of mixed salt solutions from 50 to 100°C and geochemical implications. *Geochimica et Cosmochimica Acta*, **57,** 4703-4711.

— 1995. The activity-composition relationship of oxygen and hydrogen isotopes in aqueous salt solutions: III. Vapor-liquid water equilibration of NaCl solutions to 350°C. *Geochimica et Cosmochimica Acta*, **59,** 1139-1151.

HORITA, J., DRIESNER, T. & COLE, D. R. 1999. Pressure effect on hydrogen isotope fractionation between brucite and water at elevated temperatures. *Science*, **286,** 1545-1547.

HORITA, J., WESOLOWSKI, D. J. & COLE, D. R. 1993a. The activity-composition relationship of oxygen and hydrogen isotopes in aqueous salt solutions: I. Vapor-liquid water equilibration of single salt solutions from 50 to 100°C. *Geochimica et Cosmochimica Acta*, **57,** 2797-2817.

HUDSON, J. D. 1977. Stable isotopes and limestone lithification. *Journal of the Geological Society, London*, **133,** 637-660.

HUDSON, R. G. S. & PHILCOX, M. E. 1965. The Lower Carboniferous stratigraphy of the Buttevant area, Co. Cork. *Proceedings of the Royal Irish Academy*, **64B,** 65-79.

JACKA, A. D. 1974. Replacement of fossils by length-slow chalcedony and associated dolomitization. *Journal of Sedimentary Petrology*, **44,** 421-427.

JOHNSTON, J. D. 1999. Regional fluid flow and the genesis of Irish Carboniferous base metal deposits. *Mineralium Deposita*, **34,** 571-598.

JOHNSTON, J. D., COLLER, D., MILLAR, G. & CRITCHLEY, M. F. 1996. Basement structural controls on Carboniferous-hosted base metal mineral deposits in Ireland. *In*: STROGEN, P., SOMERVILLE, I.D., JONES, G.LI. (eds). *Recent advances in Lower Carboniferous geology*. Geological Society, London, Special Publications, **151,** 1-21.

JONES, B., LUTH, R. W. & MACNEIL, A. J. 2001. Powder X-Ray diffraction analysis of homogeneous and heterogeneous sedimentary dolostones. *Journal of Sedimentary Research*, **71,** 790-799.

JONES, G. V. & BRAND, S. F. 1986. The setting, styles of mineralization and mode of origin of the Ballinalack Zn-Pb deposit. *In*: ANDREW, C. J., CROWE, R.W. A., FINLAY, S., PENNELL, W. M., AND PYNE, J. F. (eds). *Geology and genesis of mineral deposits in Ireland*. Irish Association for Economic Geology, 355-376.

KELLY, J. G., ANDREW, C. J., ASHTON, J. H., BOLAND, M. B., EARLS, G., FUSCIARDI, L. & STANLEY, G. 2003. *Europe's Major Base Metal Deposits*. Irish Association for Economic Geology. 551pp.

KELLY, W. C. & NISHIOKA, G. K. 1985. Precambrian oil inclusions in late veins and the role of hydrocarbons in copper mineralization at White Pine, Michigan. *Geology*, **13,** 334-337.

KESLER, S. E., APPOLD, M. S., MARTINI, A. M., WALTHER, L. M., HUSTON, T. J. & KYLE, J. R. 1995. Na-Cl-Br systematics of mineralising brines in Mississippi Valley-type deposits. *Geology*, **23,** 641-644.

KESLER, S. E., MARTINI, A. M., APPOLD, M. S., WALTER, L. M., HUSTON, T. J. & FURMAN, F. C. 1996. Na-Cl-Br systematics of fluid inclusions from Mississippi Valley-type deposits, Appalachian Basin: Constraints on solute origin and migration paths. *Geochimica et Cosmochimica Acta*, **60,** 225-233.

KING, D. E. 1984. *A diagenetic history of the Waulsortian Limestones, Eastern Midlands and Dublin Basin, Republic of Ireland.* Unpublished MSc. thesis, State University of New York at Stony Brook.

KVENVOLDEN, K. A. & ROEDDER, E. 1971. Fluid inclusions in quartz crystals from South-West Africa. *Geochimica et Cosmochimica Acta*, **35,** 1209-1229.

LAND, L. S. 1983. The application of stable isotopes to studies of the origin of dolomite and to problems of diagenesis of clastic sediments. *In*: ARTHUR, M. A. (eds). *Stable isotopes in sedimentary geology*. Society of Economic Paleontologists and Mineralogists Short Course, **10,** 4.1-4.22.

LAND, L. S. & PREZBINDOWSKI, D. R. 1981. The origin and evolution of the saline water, Lower Cretaceous carbonates, south-central Texas, USA. *Journal of Hydrology*, **54,** 51-74.

LEE, M. J. & WILKINSON, J. J. 2002. Cementation, hydrothermal alteration and Zn-Pb mineralization of carbonate breccias in the Irish Midlands: Textural evidence from the Cooleen Zone, near Silvermines, County Tipperary. *Economic Geology*, **97,** 653-662.

LEES, A. 1964. The structure and origin of the Waulsortian (Lower Carboniferous) "Reefs" of West Central Eire. *Philosophical Transactions of the Royal Society, London*, **740,** 483-531.

LEES, A., HALLET, V. & HIBO, D. 1985. Facies variation in Waulsortian buildups, Part 1; A model from Belgium. *Geological Journal*, **20,** 133-158.

LEES, A. & MILLER, J. 1995. Waulsortian banks. *In*: C.L.V. MONTY, D. W. J. B., P.H. BRIDGES AND B.R. PRATT. (eds). *Carbonate Mud-Mounds - their origin and evolution*. Special Publication of the International Association of Sedimentologists, **23,** 191-271.

LEHURAY, A. P., CAULFIELD, J. B. D., RYE, D. M. & DIXON, P. R. 1987. Basement controls on sediment-hosted Pb-Zn deposits: a lead isotope study of Carboniferous mineralisation in Central Ireland. *Economic Geology*, **82,** 1695-1709.

LIND, I. L. 1993. Stylolites in chalk from leg 130, Ontong Java Plateau. *In*: W.H., B., W., K. J., and A, M. L. (eds). *Mineral deposit modelling*. Geological Association of Canada, 289-314.

LORD, J. 1999. *Aspects of the palaeoecology and palaeoenvironmental setting of Waulsortian carbonate buildups in Ireland*. Unpublished Ph.D. thesis, University of Dublin.

LORENZ, V. 1985. Maars and diatremes of phreatomagmatic origin, a review. *Transactions of the Geological Society of South Africa*, **88,** 459-470.

— 1986. On the growth of maars and diatremes and its relevance to the formation of tuff-rings. *Bulletin of Volcanology*, **48,** 265-274.

LORENZ, V., ZIMANOWSKI, B. & BUETTNER, R. 2002. On the formation of deep-seated subterranean peperite-like magma-sediment mixtures. *Journal of Volcanology and Geothermal Research*, **114,** 107-118.

LOWTHER, J. M., BALDING, A. B., DUNPHY, S. & MCEVOY, F. M. 1999. The Galmoy mine: Some geological aspects of development from 1995 to 1999. *In*: STANLEY, C. J. (eds). *Mineral deposits: Processes and Processing*. Balkema Rotterdam, 881-884.

LUMSDEN, D. N. 1979. Discrepancy between time-section and X-ray estimates of dolomite in limestone. *Journal of Sedimentary Petrology*, **49,** 429-436.

LYDON, J. W. 1986. Models for the generation of metalliferous hydrothermal systems within sedimentary rocks, and their applicability to Irish Carboniferous Zn-Pb deposits. *In*: ANDREW, C. J., CROWE, R. W. A., FINLAY, S., PENNEL, W. M., and PYNE, J. F. (eds). *Geology and genesis of minerals deposits in Ireland.* Irish Association of Economic Geology Dublin, 555-577.

MACCARTHY, F. J. 1990. *The Lower Carboniferous geology of parts of Counties Longford and Westmeath, Central Ireland.* Unpublished Ph.D. thesis, University of Dublin.

MACDERMOT, C. V. & SEVASTOPULO, G. D. 1972. Upper Devonian and Lower Carboniferous setting of Irish mineralisation. *Geological Survey of Ireland Bulletin*, **1,** 267-280.

MACHEL, H. G. & LONNEE, J. 2002. Hydrothermal dolomite - a product of poor definition and imagination. *Sedimentary Geology*, **152,** 163-171.

MALIVA, R. G. 1986. Quartz geodes: early diagenetic silicified anhydrite nodules related to dolomitisation. *Journal of Sedimentary Petrology*, **57,** 1054-1059.

MALLON, A. J. 1997. *Petrological and mineralogical characteristics of the Old Red Sandstone facies rocks beneath base metal deposits as a guide to the setting of mineralisation in the Irish Midlands.* Unpublished Ph.D. thesis, University College Cork.

MARSHALL, D. J. 1988. *Cathodoluminescence of geological materials.* Unwin Hyman, Boston. 146pp.

MARSHALL, J. D. 1992. Climatic and oceanographic isotopic signals from the carbonate rock record and their preservation. *Geological Magazine*, **129,** 143-160.

MARSHALL, W. L. & CHEN, C. T. A. 1982. Amorphous silica solubilities V. Predictions of solubility behavior in aqueous mixed electrolyte solutions to 300°C. *Geochimica et Cosmochimica Acta*, **46,** 289-291.

MARSHALL, W. L. & WARAKOMSKI, J. M. 1980. Amorphous silica solubilities. II. Effect of aqueous salt solutions at 25°C. *Geochimica et Cosmochimica Acta*, **44,** 915-924.

MATSUHISA, Y., GOLDSMITH, J. R. & CLAYTON, R. N. 1979. Oxygen isotopic fractionation in the system quartz-albite-anorthite-water. *Geochimica et Cosmochimica Acta*, **43,** 1131-1140.

MAX, M. D. & RODDICK, J. C. 1989. Age of metamorphism in the Rosslare Complex, S.E. Ireland. *Proceedings of the Geologist's Association*, **100,** 113-121.

MCCAFFREY, M. A., LAZAR, B. & HOLLAND, H. D. 1987. The evaporation path of seawater and the coprecipitation of Br^- and K^+ with halite. *Journal of Sedimentary Petrology*, **57,** 928-937.

MCCREA 1950. On the isotopic chemistry of carbonates and a palaeo-temperature scale. *Journal of Chemical Physics*, **18,** 849-857.

MERRIMAN, R. J. & KEMP, S. J. 1997. Correlating clay mineral reaction progress with organic maturity indicators. *Clay mineral evolution, basin maturity and mudrock properties*, British Geological Survey, Nottingham, UK, 41-42.

MEYERS, W. J. 1974. Carbonate cement stratigraphy of the Lake Valley Formation (Mississippian) Sacramento Mountains, New Mexico. *Journal of Sedimentary Petrology*, **44,** 837-861.

— 1977. Chertification in the Mississippian Lake Valley Formation, Sacramento Mountains, New Mexico. *Sedimentology*, **24,** 75-105.

— 1978. Carbonate cements: their regional distribution and interpretation in Mississippian limestones of southwestern New Mexico. *Sedimentology*, **25,** 371-400.

MEYERS, W. J. & LOHMANN, K. C. 1985. Isotope geochemistry of regionally extensive calcite zones and marine components in Mississippian limestones, New Mexico. *In*: SCHNEIDERMANN, N., and HARRIS, P. M. (eds). *Carbonate cements*. Society of Economic Paleontologists and Mineralogists Special Publication, **36,** 223-240.

MILLS, H., HALLIDAY, A. N., ASHTON, J. H., ANDERSON, I. K. & RUSSELL, M. J. 1987. Origin of a giant orebody at Navan, Ireland. *Nature*, **327,** 223-226.

MOLDOVANYI, E. P. & LOHMANN, K. C. 1984. Isotopic and petrographic record of phreatic diagenesis: Lower Cretaceous Sligo and Cupido Formations. *Journal of Sedimentary Petrology*, **54,** 972-985.

MUNZ, I. A. 2001. Petroleum inclusions in sedimentary basins: systematics, analytical methods and applications. *Lithos*, **55,** 195-212.

NADEN, J., 1996. CalcicBrine 1.5: a Microsoft Excel 5.0 Add-in for calculating salinities from microthermometric data in the system NaCl-$CaCl_2$-H_2O, PACROFI VI: Wisconsin, Program with Abstracts, 97-98.

NAGY, Z. R., BECKER, S., GREGG, J. M., SHELTON, K. L., JOHNSON, A. W., SOMERVILLE, I. D. & WRIGHT, W. R., 2002. Early dolomitisation, brine migration and hydrothermal dolomite in the Lower Carboniferous platform carbonates of the southeast Irish Midlands, International conference on the geometry and petrogenesis of dolomite hydrocarbon reservoirs (final programme and abstracts): London.

NAGY, Z. R., SOMERVILLE, I. D., BECKER, S. P., GREGG, J. A., WRIGHT, W. R. & SHELTON, K. L. 2001. Petrology and biostratigraphy of carbonate rocks from the ?lower to upper Visean (Lower Carboniferous) Milford Formation, County Carlow, Ireland. *Geological Society of America, Abstracts with Programs*, **33,** A443.

NEVILL, W. E. 1958. Carboniferous knoll reefs of East Central Ireland. *Proceedings of the Royal Irish Academy*, **59,** 285-303.

NICOLAIDES, S. & WALLACE, M. W. 1997. Pressure dissolution and cementation in an Oligo-Miocene non-tropical limestone (Clifton Formation), Otway Basin, Victoria. *In*: N.P, J., and J.A, C. (eds). *Cool water carbonates*. Society of Economic Paleontologists and Mineralogists Special Publication, **56,** 249-261.

NOLAN, S. C. 1986. *The Carboniferous geology of the Dublin area.* Unpublished Ph.D. thesis, University of Dublin.

— 1989. The style and timing of Dinantian synsedimentary tectonics in the eastern part of the Dublin Basin, Ireland. *In*: ARTHURTON, R. S., GUTTERRIDGE, P., and NOLAN, S. C. (eds). *The role of tectonics in Devonian and Carboniferous sedimentation in the British Isles*. Yorkshire Geological Society Occasional Publication, **6,** 83-98.

OAKES, C. S., BODNAR, R. J. & SIMONSON, L. M. 1990. The system $NaCl\text{-}CaCl_2\text{-}H_2O$: I. The ice liquidus at 1 atm total pressure. *Geochimica et Cosmochimica Acta*, **54,** 603-610.

O'CONNOR, P. J., AFTALION, M. & KENNAN, P. S. 1989. Isotopic U-Pb ages of zircon and monazite from the Leinster Granite, S.E. Ireland. *Geological Magazine*, **126,** 725-728.

O'CONNOR, P. J., V., G. & KENNAN, P. S. 1991. Genesis of lithium pegmatites from the Leinster Granite Margin, southeast Ireland: geochemical constraints. *Geological Journal*, **26,** 295-305.

O'KEEFFE, W. G. 1986. Age and postulated source rocks for mineralisation in central Ireland, as indicated by lead isotopes. *In*: ANDREW, C. J., CROWE, R.W. A., FINLAY, S., PENNELL, W. M., AND PYNE, J. F. (eds). *Geology and genesis of mineral deposits in Ireland.* Irish Association for Economic Geology, 617-624.

O'REILLY, B. M., READMAN, P. W. & MURPHY, T. 1999. Gravity lineaments and Carboniferous-hosted base metal deposits of the Irish Midlands. *In*: MCCAFFREY, K. J. W., LONERGAN, L., WILKINSON, J. (eds). *Fractures, Fluid Flow and Mineralisation*. Geological Society, London, Special Publications, **155,** 313-321.

PARNELL, J., MONSON, B. & GENG, A. 1996. Maturity and petrography of bitumens in the Carboniferous of Ireland. *International Journal of Coal Petrology*, **29,** 23-38.

PEACE, W. 1999. *Carbonate-hosted Zn-Pb mineralisation, Upper Pale Beds, Navan, Ireland.* Unpublished Ph.D. thesis, University of Melbourne.

PEACE, W. M. & WALLACE, M. W. 2000. Timing of mineralization at the Navan Zn-Pb deposit: A post Arundian age for Irish mineralization. *Geology*, **28,** 711-714.

PEACE, W. M., WALLACE, M. W., HOLDSTOCK, M. P. & ASHTON, J. H. 2003. Ore textures within the U lens of the Navan Zn-Pb deposit, Ireland. *Mineralium Deposita*, **38,** 568-584.

PETTKE, T. & DIAMOND, L. W. 1995. Rb-Sr isotopic analysis of fluid inclusions in quartz: evaluation of bulk extraction procedures and geochromometer systematics using synthetic fluid inclusions. *Geochimica et Cosmochimica Acta*, **59,** 4009-4027.

PHILCOX, M. E. 1964. Compartment Deformation near Buttevant, Co. Cork, Ireland, and its relation to the Variscan Thrust Front. *Scientific Proceedings of the Royal Dublin Society*, **2,** 1-11.

— 1984. *Lower Carboniferous lithostratigraphy of the Irish Midlands.* Irish Association for Economic Geology, Dublin. 89pp.

— 1989. The mid-Dinantian unconformity at Navan, Ireland. *In*: ARTHURTON, R. S., GUTTERRIDGE, P., and NOLAN, S. C. (eds). *The role of tectonics in Devonian and Carboniferous sedimentation in the British Isles.* Yorkshire Geological Society Occasional Publication, **6,** 67-81.

PHILLIPS, W. E. A. & SEVASTOPULO, G. D. 1986. The stratigraphic and structural setting of the Irish mineral deposits. *In*: ANDREW, C. J., CROWE, R.W. A., FINLAY, S., PENNELL, W. M., AND PYNE, J. F. (eds). *Geology and genesis of mineral deposits in Ireland.* Irish Association for Economic Geology, 1-30.

PICKARD, N. A. H., JONES, G. L. I., REES, J., SOMERVILLE, I. D. & STROGEN, P. 1992. Lower Carboniferous (Dinantian) stratigraphy and structure of the Walterstown-Kentstown area, Co. Meath, Ireland. *Geological Journal*, **27,** 35-38.

PICKARD, N. A. H., REES, J., STROGEN, P., SOMERVILLE, I. D. & JONES, G. L. I. 1994. Controls on the evolution and the demise of Lower Carboniferous platforms, northern margin of the Dublin Basin, Ireland. *Geological Journal*, **29,** 93-117.

POPP, B. N., ANDERSON, T. F. & SANDBERG, P. A. 1986. Brachiopods as indicators of original isotopic compositions in some Paleozoic limestones. *Geological Society of America Bulletin*, **97,** 1262-1269.

PRACHT, M. 1997. *Geology of Kerry-Cork; a geological description to accompany the bedrock geology 1:100,000 scale map series, Sheet 21, Kerry-Cork with contributions by G. Wright, G. Stanley, K. Claringbold and W.P. Warren.* Geological Survey of Ireland

PREZBINDOWSKI, D. R. & LARESE, R. E. 1987. Experimental stretching of fluid inclusions in calcite - Implications for diagenetic studies. *Geology*, **15,** 333-336.

RADKE, B. M. & MATHIS, R. L. 1980. On the formation and occurrence of saddle dolomite. *Journal of Sedimentary Petrology*, **50,** 1149-1168.

RAILSBACK, L. B. 1993b. Intergranular pressure dissolution in a Plio-Pleistocene grainstone buried no more than 30 metres: Shoofy oolite, southwestern Idaho. *Carbonates and Evaporites*, **8,** 163-169.

REDMOND, P. B. 1997. *Structurally controlled mineralisation and hydrothermal dolomitisation at the Lisheen Zn-Pb-Ag deposit, County Tipperary, Ireland.* Unpublished MSc.thesis, University of Dublin.

REED, C. P. & WALLACE, M. W. 2001. Diagenetic evidence for an epigenetic origin of the Courtbrown Zn-Pb deposit, Ireland. *Mineralium Deposita*, **36,** 428-441.

REES, J. 1987. *The Carboniferous geology of the Boyne Valley area, Ireland.* Unpublished Ph.D. thesis, University of Dublin.

RIMSTIDT, J. D. 1997b. Gangue mineral transport and deposition. *In*: BARNES, H. L. (eds). *Geochemistry of hydrothermal ore deposits.* John Wiley & Sons, New York, 487-515.

RITTENHOUSE, G. 1967. Bromine in oil-field waters and its use in determining possibilities of origin of these waters. *American Association of Petroleum Geologists Bulletin*, **51,** 2430-2440.

RIZZI, G. 1993. *The sedimentology and petrography of Lower Carboniferous limestones and dolomites; host rocks to the Navan zinc-lead deposit, Ireland.* Unpublished Ph.D. thesis, University of Glasgow.

ROBINSON, B. W. & KUSAKABE, M. 1975. Quantitative preparation of sulfur dioxide for $^{34}S/^{32}S$ analyses from sulfides by combustion with cuprous oxide. *Analytical Chemistry*, **47,** 1179-1181.

ROEDDER, E. 1958. Technique for the extraction and partial chemical analysis of fluid filled inclusions from minerals. *Economic Geology*, **53,** 235-269.

— 1984. Fluid Inclusions. *In*: RIBBE, P. H. (eds). *Reviews in Mineralogy Volume 12.* Mineralogical Society of America, **12,** 646.

ROEDDER, E., INGRAM, B. & HALL, W. E. 1963. Studies of fluid inclusions, III. Extractions and quantitative analysis of fluid inclusions in the milligram range. *Economic Geology*, **58,** 620-643.

RUSSELL, M. J. 1978. Downward-excavating hydrothermal cells and Irish type ore deposits: importance of an underlying thick Caledonian prism. *Transactions of the Institution of Mining and Metallurgy*, **87,** B168-171.

— 1986. Extension and convection: a genetic model for the Irish Carboniferous base metal and barite deposits. *In*: ANDREW, C. J., CROWE, R.W. A., FINLAY, S., PENNELL, W. M., AND PYNE, J. F. (eds). *Geology and genesis of mineral deposits in Ireland.* Irish Association for Economic Geology, 545-554.

SALTZMAN, M. R. 2002. Carbon and oxygen isotope stratigraphy of the Lower Mississippian (Kinderhookian-early Osagean), western United States: Implications for seawater chemistry and glaciation. *Geological Society of America Bulletin*, **114,** 96-108.

SAMSON, I. M. & RUSSELL, M. J. 1983. Fluid inclusion data from Silvermines base-metal-baryte deposits, Ireland. *Transactions of the Institution of Mining and Metallurgy*, **92,** B67-71.

— 1987. Genesis of the Silvermines zinc-lead-barite deposit, Ireland: Fluid inclusion and stable isotope evidence. *Economic Geology*, **82,** 371-394.

SAMSON, I. M. & WALKER, R. T. 2000. Cryogenic raman spectroscopic studies in the system NaCl-$CaCl_2$-H_2O and implications for low-temperature phase behavior in aqueous fluid inclusions. *The Canadian Mineralogist*, **38,** 35-43.

SCHOLLE, P. & ARTHUR, M. 1980. Carbon isotope fluctuations in Cretaceous pelagic limestones: Potential stratigraphic and petroleum exploration tool. *American Association of Petroleum Geologists Bulletin*, **64,** 67-87.

SEVASTOPULO, G. D. 2001. Carboniferous (Silesian). *In*: HOLLAND, C. H. (eds). *The geology of Ireland.* Dunedin Academic Press Edinburgh, 298-312.

SEVASTOPULO, G. D. & REDMOND, P. 1999. Age of mineralisation of carbonate-hosted, base metal deposits in the Rathdowney Trend, Ireland. *In*: MCCAFFREY, K. J. W., LONERGAN, L., and WILKINSON, J. J. (eds). *Fractures, Fluid Flow and Mineralisation.* Geological Society, London, Special Publications, **155,** 303-311.

SEVASTOPULO, G. D. & WYSE JACKSON, P. N. 2001. Carboniferous (Dinantian). *In*: HOLLAND, C. H. (eds). *The geology of Ireland.* Dunedin Academic Press Edinburgh, 241-289.

SHARP, Z. D. 1990. A laser-based microanalytical method for the in-situ determination of oxygen isotope ratios of silicates and oxides. *Geochimica et Cosmochimica Acta*, **54,** 1353-1357.

SHEARLEY, E., REDMOND, P., GOODMAN, R. & KING, M. 1995. A guide to the Lisheen Zn-Pb deposit. *In*: ANDERSON, K., ASHTON, J., EARLS, G., HITZMAN, M., and TEAR, S. (eds). *Irish carbonate-hosted Zn-Pb deposits.* Society of Economic Geologists Guidebook Series, **21,** 123-137.

SHEARLEY, E., REDMOND, P., KING, M. & GOODMAN, R. 1996. Geological controls on mineralization and dolomitisation of the Lisheen Zn-Pb-Ag deposit, Co. Tipperary, Ireland. *In*: STROGEN, P., SOMERVILLE, I.D., JONES, G.LI. (eds). *Recent advances in Lower Carboniferous geology.* Geological Society, London, Special Publications, **151,** 23-35.

SHEPHARD-THORN, E. R. 1963. The Carboniferous limestone succession in north-west County Limerick. *Proceedings of the Royal Irish Academy*, **62B,** 267-294.

SHEPHERD, T., RANKIN, A. H. & ALDERTON, D. H. M. 1985. *A practical guide to fluid inclusion studies.* Blackie, Glasgow and London. 239pp.

SHEPPARD, S. M. F. 1986. Characterization and isotopic variations in natural waters. *In*: RIBBE, P. H. (eds). *Stable isotopes in high temperature geological processes.* Mineralogical Society of America, **16,** 165-181.

SINGER, D. A. 1995. World class base and precious metal deposits - a quantitative analysis. *Economic Geology*, **90,** 88-104.

SKILLING, I. P., WHITE, J. D. L. & MCPHIE, J. 2002. Peperite: a review of magma-sediment mingling. *Journal of Volcanology and Geothermal Research*, **114,** 1-17.

SLEEMAN, A. G. & MCCONNELL, B. 1995. *A geological description of East Cork, Waterford and adjoining parts of Tipperary and Limerick to accompany the bedrock geology 1:100,000 scale map series, Sheet 22, East Cork-Waterford with contributions by K. Claringbold, P. O'Connor, W.P. Warren and G. Wright.* Geological Survey of Ireland

SLEEMAN, A. G. & PRACHT, M. 1999. *Geology of the Shannon Estuary; a geological description of the Shannon Estuary region including parts of Clare, Limerick and Kerry, to accompany the bedrock geology 1:100,000 scale map series, Sheet 17, Shannon Estuary with contributions by K. Claringbold, G. Stanley, J. Deakin, G. Wright, O. Bloetjes and R. Creighton.* Geological Survey of Ireland

SOMERVILLE, I. D. & JONES, G. L. L. 1985. The Courceyan stratigraphy of the Pallaskenry Borehole, Co. Limerick, Ireland. *Geological Journal*, **20,** 377-400.

SOMERVILLE, I. D. & STROGEN, P. 1992. Ramp sedimentation in the Dinantian limestones of the Shannon Trough, Co. Limerick, Ireland. *Sedimentary Geology*, **79,** 59-75.

SOMERVILLE, I. D., STROGEN, P. & JONES, G. L. L. 1992. Biostratigraphy of Dinantian limestones and associated volcanic rocks in the Limerick Syncline, Ireland. *Geological Journal*, **27,** 201-220.

SPENCER, R. J., MOLLER, N. & WEARE, J. H. 1990. The prediction of mineral solubilities in natural waters: A chemical equilibrium model for the Na-K-Ca-Mg-Cl-SO_4-H_2O system at temperatures below 25°C. *Geochimica et Cosmochimica Acta*, **54,** 575-590.

SPERBER, C. M., WILKINSON, B. H. & PEACOR, D. R. 1984. Rock composition, dolomite stoichiometry and rock/water reactions in dolomitic carbonate rocks. *Journal of Geology*, **92,** 609-622.

STACHEL, T., LORENZ, V. & STANISTREET, I. G. 1994. Gross Brukkaros (Namibia) - an enigmatic crater fill reinterpreted as due to Cretaceous caldera evolution. *Bulletin of Volcanology*, **56,** 386-397.

STASIUK, L. D. & SNOWDEN, L. R. 1997. Fluorescence micro-spectrometry of synthetic and natural fluid inclusions: crude oil chemistry, density and application to petroleum migration. *Applied Geochemistry*, **12,** 229-241.

STERN, M. J., SPINDEL, W. & MONSE, E. U. 1968. Temperature dependence of isotope effects. *Journal of Chemical Physics*, **48,** 2908.

STROGEN, P. 1974. The sub-Palaeozoic basement in central Ireland. *Nature*, **250,** 562-563.

STROGEN, P., JONES, G. L. & SOMERVILLE, I. D. 1990. Stratigraphy and sedimentology of Lower Carboniferous (Dinantian) boreholes from West Co. Meath, Ireland. *Geological Journal*, **25,** 103-137.

STROGEN, P., SOMERVILLE, I. D., PICKARD, N. A. H., JONES, G. L. & FLEMING, M. 1996. Controls on ramp, platform and basinal sedimentation in the Dinantian of the Dublin Basin and Shannon Trough, Ireland. *In*: STROGEN, P., SOMERVILLE, I.D., JONES. G.LI. (eds). *Recent advances in Lower Carboniferous geology*. Geological Society, London, Special Publications, **151,** 263-279.

SYMONS, D. T., SMETHURST, M. T. & ASHTON, J. H. 2002. Palaeomagnetism of the Navan Zn-Pb deposit, Ireland. *Economic Geology*, **97,** 997-1012.

TAYLOR, H. P. 1997. Oxygen and hydrogen isotope relationships in hydrothermal mineral deposits. *In*: BARNES, H. L. (eds). *Geochemistry of hydrothermal ore deposits*. John Wiley & Sons, New York, 231-302.

TAYLOR, S. 1984. Structural and palaeotopographic controls of lead-zinc mineralization in the Silvermines Orebodies, Republic of Ireland. *Economic Geology*, **79,** 529-548.

TIETZSCH-TYLER, D. & SLEEMAN, A. G. 1994. *Geology of Carlow-Wexford; a geological description to accompany the bedrock geology 1:100,000 scale map series, Sheet 19, Carlow-Wexford with contributions by B.J. McConnell, E.P. Daly, A.M. Flegg, P.J. O'Connor and W.P. Warren*. Geological Survey of Ireland

TRUDE, K. J. & WILKINSON, J. J. 2001. A mineralogical and fluid inclusion study of the Harberton Bridge Fe-Zn-Pb deposit, County Kildare, Ireland. *Journal of the Geological Society, London*, **158,** 37-46.

TUCKER, M. & WRIGHT, V. P. 1990. *Carbonate Sedimentology*. Blackwell Science, Oxford. 482pp.

TWISS, R. J. & MOORES, E. M. 1992. *Structural geology*. W.H. Freeman and Company, New York. 532pp.

ULRICH, M. R. & BODNAR, R. J. 1988. Systematics of stretching of fluid inclusions II: Barite at 1 atm confining pressure. *Economic Geology*, **83,** 1037-1046.

VAN DEN BERG, R. & DALY, J. S. 2001. Assessing the reliability of high grade xenoliths as lower crustal samples: an example from Central Ireland. *Journal of Conference Abstracts*, **6,** 363.

VAN DEN KERKHOF, A. M. & HEIN, U. F. 2001. Fluid inclusion petrography. *Lithos*, **55,** 27-47.

VANKO, D. A., BODNAR, R. J. & STERNER, S. M. 1988. Synthetic fluid inclusions: VII Vapor-saturated halite solubility in part of the system $NaCl\text{-}CaCl_2\text{-}H_2O$, with application to fluid inclusions from oceanic hydrothermal systems. *Geochimica et Cosmochimica Acta*, **52,** 2451-2456.

VEIZER, J., ALA, D., AZMY, K., BRUCKSCHEN, P., BUHL, D., BRUHN, F., CARDEN, G. A. F., DIENER, A., EBNETH, S., GOGGERIS, Y., JASPER, T., KORTE, C., PAWELLEK, F., PODLAHA, O. G. & STRAUSS, H. 1999. ^{87}Sr / ^{86}Sr, $\delta^{13}C$ and $\delta^{18}O$ evolution of Phanerozoic seawater. *Chemical Geology*, **161,** 59-88.

VEIZER, J., BRUCKSCHEN, P., PAWELLEK, F., DIENER, A., PODLAHA, O. G., CARDEN, G. A. F., JASPER, T., KORTE, C., STRAUSS, H., AZMY, K. & ALA, D. 1997. Oxygen isotope evolution of Phanerozoic seawater. *Palaeogeography, Palaeoclimatology, Palaeoecology*, **132,** 159-172.

WALSHAW, R. D. & MENUGE, J. F. 1997. Rb-Sr analysis of sphalerite from Irish Carboniferous-hosted base metal deposits. *In*: HENDRY, J. P., CAREY, P. F., PARNELL, J., RUFFELL, A. H., and WORDEN, R. H. (eds). *Geofluids II - Contributions to the Second International Conference of Fluid Evolution, Migration and Interaction in Sedimentary Basins and Orogenic Belts* Belfast, 63-64.

WHITE, J. D. L., MCPHIE, J. & SKILLING, I. P. 2000. Peperite: a useful genetic term. *Bulletin of Volcanology*, **62,** 65-66.

WHITE, J. L. 1976. Mesophase mechanism in the formation of the microstructure of petroleum coke. *In*: DEVINEY, M. L., and O'GRADY, T. M. (eds). *Petroleum derived carbons*. American Chemical Society Symposium Series, **21,** 282-314.

WILKINSON, J. J. 2001. Fluid inclusions in the hydrothermal ore deposits. *Lithos*, **55,** 229-272.

— 2003. On diagenesis, dolomitisation and mineralisation in the Irish Zn-Pb orefield. *Mineralium Deposita*, **38,** 968-983.

WILKINSON, J. J., BOYCE, A. J., EVERETT, C. E. & LEE, M. J. 2003. Timing and depth of mineralisation in the Irish Zn-Pb orefield. *In*: KELLY, J. G., ANDREW, C. J., ASHTON, J. H., BOLAND, M. B., EARLS, G., FUSCIARDI, L., and STANLEY, G. (eds). *Europe's Major Base Metal Deposits*. Irish Association for Economic Geology, 483-497.

WILKINSON, J. J. & EARLS, G. 2000. A high-temperature origin for black dolomite matrix breccias in the Irish Zn-Pb orefield. *Mineralogical Magazine*, **64,** 1077-1096.

WILSON, H. E., REID, R. E. H., PARNELL, J. & SMITH, R. A. 2001. Permian and Mesozoic. *In*: HOLLAND, C. H. (eds). *The geology of Ireland*. Dunedin Academic Press Edinburgh, 331-351.

WRIGHT, W. R. 2001. *Dolomitisation, fluid-flow and mineralisation of the Lower Carboniferous rocks of the Irish Midlands and Dublin Basin regions*. Unpublished Ph.D. thesis, University College Dublin.

WRIGHT, W. R., JOHNSON, A. W., SHELTON, K. L., SOMERVILLE, I. D. & GREGG, J. M. 2000. Fluid migration and rock interactions during dolomitisation of the Dinantian Irish Midlands and Dublin Basin. *Journal of Geochemical Exploration*, **69-70,** 159-164.

WRIGHT, W. R., SOMERVILLE, I. D., GREGG, J. M., SHELTON, K. L. & JOHNSON, A. W. 2001. Application of regional dolomite cement CL (cathodoluminescence) microstratigraphy to the genesis of the Zn-Pb mineralization in Lower Carboniferous rocks, Ireland: similarities to the southeast Missouri Pb-Zn district? *In*: HAGNI, D. (eds). *Studies on ore deposits, mineral economics and applied mineralogy: with emphasis on Mississippi Valley-type base metal and carbonate-related ore deposits*. University of Missouri-Rolla Press, Rolla, USA, 1-17.

YANATIEVA, O. K. 1946. Polythermal solubilities in the systems $CaCl_2$-$MgCl_2$-H_2O and $CaCl_2$-NaCl-H_2O. *ZHURNAL PRIKLADNOI KHIMII*, **19,** 709-722 (in Russian).

APPENDICES

APPENDIX A

SAMPLE CATOLOGUE

Appendix A: Sample Catalogue

TCD Number	Borehole	Depth (m)	Type of sample	Comments
P16777	Newcastle West OW/28 67	297.71 - 297.75	Thin section	Most of photos
P16778	Newcastle West OW/28 67	297.61 - 297.63	Thin section	Dissolution seam containing dolomite
P16779	Newcastle West OW/28 67	297.54 - 297.58	Thin section	Relationship between quartz and Stage E cements
P16780	Newcastle West OW/28 67	297.5 - 297.54	Thin section	Most good quartz and dolo relationship examples
P16781	Newcastle West OW/28 67	297.45-297.5	Thin section	Limestone/dolomite contact
P16782	Newcastle West OW/28 67	297.42 - 297.45	Thin section	
P16783	Newcastle West OW/28 67	297.40 - 297.44	Thin section	
P16784	Newcastle West OW/28 67	297.39 - 297.35	Thin section	
P16785	Newcastle West OW/28 67	297.31 - 297.27	Thin section	
P17500	Lisheen LK 2258-38	249.60 - 249.80	Thin section	Ossicle & both bry & dolo in brachiopod
P17501	Lisheen LK 2258-38	121.20 - 122.53	Thin section	
P17502	Lisheen LK 2258-38	121.20 - 122.53	Thin section	Calcite in centre of cavity
P17503	Lisheen LK 2258-38	121.20 - 122.53	Thin section	
P17504	Lisheen LK 2258-38	112.44 - 112.75	Thin section	X-cutting 2nd dolomite
P17505	Lisheen LK 2258-38	112.44 - 112.75	Thin section	Dolo rhombs order of mag bigger
P17506	Lisheen LK 2258-38	183.65 - 184	Thin section	
P17507	Lisheen LK 2258-38	172.20 - 172.65	Thin section	X-cutting vein & lots pyrite & poro
P17508	Lisheen LK 2258-38	112.44 - 112.75	Thin section	Dolomite replacing blocky calcite veins
P17509	Lisheen LK 2258-38	112.44 - 112.75	Thin section	Weird fossil
P17510	Lisheen LK 2258-38	46.50 - 46.75	Thin section	
P17511	Lisheen LK 2258-38	46.50 - 46.75	Thin section	
P17512	Lisheen LK 2258-38	164.2 - 164.45	Thin section	
P17513	Quarry at Lisheen (GR 21453 16187)	Sample A	Thin section	Partially replaced Waulsortian
P17514a	Quarry at Lisheen (GR 21453 16187)	Sample B	Thin section	Amplexus coral
P17514b	Quarry at Lisheen (GR 21453 16187)	Sample B	Thin section	Amplexus coral
P17515	Lisheen LK 310 c	356.3 - 356.45	Thin section	
P17516	Lisheen LK 310 d	361.0 - 361.25	Thin section	
P17517	Lisheen LK 310 e	364.68 - 364.9	Thin section	Pyrite
P17518	Lisheen LK 310 f	371.2 - 371.35	Thin section	Pyrite
P17519	Lisheen LK 310 g	373.2-373.45	Thin section	
P17520	Newcastle West OW/28 67	297.5	Thin section & plaquette	Limestone / dolomite contact
P17521	Lisheen LK 3262-18 a	203 - 203.62	Thin section	X-cutting 2nd dolomite
P17522	Lisheen LK 3262-18 b	203 - 203.62	Thin section	Banded calcite with dolo along a stylolite

Appendix A: Sample Catalogue

TCD Number	Borehole	Depth (m)	Type of sample	Comments
P17523	Lisheen LK 3262-18 c	203 - 203.62	Thin section	Pyrite CD replacing space with ECC
P17524	Lisheen LK 3262-18 d	203 - 203.62	Thin section	Later calcite vein x-cutting dolo
P17525	Lisheen LK 3262-18	108.09 - 108.3	Thin section	Breccia fill + bright blue material?
P17526	Lisheen LK 3262-18	46.87 - 46.23	Thin section	
P17527a	Lisheen LK 2258-38	121.2 - 122.65	Thin section	
P17527b	Lisheen LK 2258-38	121.2 - 122.65	SI Plaquette	
P17528a	Lisheen LK 2258-38	73.9 - 74.15	Thin section	
P17528b	Lisheen LK 2258-38	73.9 - 74.15	SI Plaquette	
P17529a	Lisheen LK 2258-38	73.9 - 74.15	Thin section	
P17529a	Lisheen LK 2258-38	73.9 - 74.15	SI Plaquette	
P17530a	Lisheen LK 2258-38	no depth	Thin section	
P17530b	Lisheen LK 2258-38	no depth	SI Plaquette	
P17531a	Lisheen LK 2258-38	121.2 - 122.53	Thin section	
P17531b	Lisheen LK 2258-38	121.2 - 122.53	SI Plaquette	
P17532a	Lisheen LK 3262-18	203 - 203.62	Thin section	
P17532b	Lisheen LK 3262-18	203 - 203.62	SI Plaquette	
P17533a	Lisheen LK 3262-18	112.44 - 112.75	Thin section	
P17533b	Lisheen LK 3262-18	112.44 - 112.75	SI Plaquette	
P17534a	Lisheen LK 3262-18	203 - 203.62	Thin section	
P17534b	Lisheen LK 3262-18	203 - 203.62	SI Plaquette	
P17535a	Lisheen LK 3262-18	203 - 203.62	Thin section	
P17535b	Lisheen LK 3262-18	203 - 203.62	SI Plaquette	
P17536a	Newcastle West OW/28 67	no depth	Thin section	
P17536b	Newcastle West OW/28 67	no depth	SI Plaquette	
P17537a	Newcastle West OW/28 67	no depth	Thin section	
P17537b	Newcastle West OW/28 67	no depth	SI Plaquette	
P17538a	Newcastle West OW/28 67	no depth	Thin section	
P17538b	Newcastle West OW/28 67	no depth	SI Plaquette	
P17539a	Lisheen LK 2258-38	172.2 - 172.65	Thin section	
P17539b	Lisheen LK 2258-38	172.2 - 172.65	SI Plaquette	
P17540a	Newcastle West OW/28 67	no depth	T/S	
P17540b	Newcastle West OW/28 67	no depth	SI Plaquette	
P17541a	Lisheen LK 2258-38	112.44 - 112.75	Thin section	

Appendix A: Sample Catalogue

TCD Number	Borehole	Depth (m)	Type of sample	Comments
P17541b	Lisheen LK 2258-38	112.44 - 112.75	SI Plaquette	
P17542a	Lisheen LK 3262-18	203 - 203.62	Thin section	
P17542b	Lisheen LK 3262-18	203-203.62	SI Plaquette	
P17543a	Lisheen LK 3262-18	203 - 203.62	Thin section	
P17543b	Lisheen LK 3262-18	203 - 203.62	SI Plaquette	
P17544a	Fermoy (Curtin's Farm) 3626-01	91.95 - 92.15	Thin section	Partially dolomitised WMC. Geopetal fills
P17544b	Fermoy (Curtin's Farm) 3626-01	91.95 - 92.15	SI Plaquette	
P17545a	Fermoy (Curtin's Farm) 3626-02	54 - 54.1	Thin section	Large ossicle, large dolomite vug
P17545b	Fermoy (Curtin's Farm) 3626-02	54 - 54.1	SI Plaquette	
P17546a	Fermoy (Curtin's Farm) 3626-02	100.07 - 100.43	Thin section	Dolomite veining. CD replacment of Stage D
P17546b	Fermoy (Curtin's Farm) 3626-02	100.07 - 100.43	SI Plaquette	
P17547a	Fermoy (Curtin's Farm) 3626-02	100.63 - 100.83	Thin section	Partially dolomitised WMC
P17547b	Fermoy (Curtin's Farm) 3626-02	100.63 - 100.83	SI Plaquette	Was never drilled for SI
P17548	Fermoy (Curtin's Farm) 3626-02	99.12 - 99.29	SI Plaquette	
P17549a	Mallow (Lag) 3537-04	71.7 - 71.88	Thin section	1st time to see qtz & dolomite in CFC. Rhombopora present
P17549b	Mallow (Lag) 3537-04	71.7 - 71.88	SI Plaquette	
P17550a	Mallow (Lag) 3537-04	68.86 - 69	Thin section	Quartz in CFC. Lots of CFC
P17550b	Mallow (Lag) 3537-04	68.86 - 69	SI Plaquette	
P17551a	Mallow (Lag) 3537-04	79.83 - 80.26	Thin section	Dolo in CFC. Late calcite veins x-cutting dolomite
P17551b	Mallow (Lag) 3537-04	79.83 - 80.26	SI Plaquette	
P17552a	Mallow (Ballybeg) 3536-06	155.8 - 156.1	Thin section	Veins containing dolomite breccia. x-cutting 2nd dolo
P17552b	Mallow (Ballybeg) 3536-06	155.8 - 156.1	SI Plaquette	
P17553a	Subutler Quarry (GR 1443 1042)	-	Thin section	Pre-dolomite quartz and post dolomite quartz
P17553b	Subutler Quarry (GR 1443 1042)	-	SI Plaquette	
P17554a	Subutler Quarry (GR 1443 1042)	-	Thin section	More abundant pre-dolomite quartz
P17554b	Subutler Quarry (GR 1443 1042)	-	SI Plaquette	
P17555a	Mallow (Lag) 3537-04	58.6 - 59.28	Thin section	Nice zoned calcite xls - replaced by dolo. 2nd dolo
P17555b	Mallow (Lag) 3537-04	58.6 - 59.28	SI Plaquette	
P17556a	Urlingford 3246-15	136.55 - 136.58	Thin section	Black tops texture
P17556b	Urlingford 3246-15	136.55 - 136.58	SI Plaquette	Black tops texture
P17557a	Urlingford 3246-15	136.58 - 136.62	Thin section	Black tops texture
P17557b	Urlingford 3246-15	136.58-136.62	SI Plaquette	Black tops texture
P17558	Urlingford 3246-15	136.64 - 136.68	SI Plaquette	Black tops texture

Appendix A: Sample Catalogue

TCD Number	Borehole	Depth (m)	Type of sample	Comments
P17559	Urlingford 3246-15	136.68 - 136.74	SI Plaquette	Black tops texture
P17560a	Lisheen LK 2258-38	73.9 - 74.15	Thin section	
P17560b	Lisheen LK 2258-38	73.9 - 74.15	SI Plaquette	
P17561a	Lisheen LK 2258-38	121.2 - 122.53	Thin section	
P17561b	Lisheen LK 2258-38	121.2 - 122.53	SI Plaquette	
P17562a	Quarry at Lisheen (GR 21453 16187)	-	Thin section	
P17562b	Quarry at Lisheen (GR 21453 16187)	-	SI Plaquette	
P17563a	Lisheen LK 3262-18	203 - 203.62y	Thin section	
P17563b	Lisheen LK 3262-18	203 - 203.62y	SI Plaquette	
P17564a	Lisheen LK 3262-18	203 - 203.62x	Thin section	
P17564b	Lisheen LK 3262-18	203 - 203.62x	SI Plaquette	
P17565	Lisheen LK 3262-18	203 - 203.62	SI Plaquette	
P17566	Lisheen LK 3262-18	203 - 203.62z	SI Plaquette	
P17567	Lisheen LK 2258-38	73.9 - 74.15b	SI Plaquette	
P17568	Lisheen LK 2258-38	121.2 - 122.53	SI Plaquette	
P17569	Quarry at Lisheen (GR 21453 16187)	-	SI Plaquette	
P17570	Quarry at Lisheen (GR 21453 16187)	-	SI Plaquette	
P17571	Lisheen LK 3262-18	203 - 203.62	SI Plaquette	
P17572	Newcastle West OW/24 4	37.30	SI Plaquette	
P17573a	Newcastle West OW/24 11	73.45	SI Plaquette	
P17573b	Newcastle West OW/24 11	73.45	Thin section	
P17574	Newcastle West OW/24 12	77.70	SI Plaquette	
P17575	Newcastle West OW/24 13	81.70	SI Plaquette	
P17576a	Newcastle West OW/24 14	85.30	Thin section	
P17576b	Newcastle West OW/24 14	85.30	SI Plaquette	
P17577	Newcastle West OW/24 17	98.70	SI Plaquette	
P17578	Newcastle West OW/24 18	103.20	SI Plaquette	
P17579	Newcastle West OW/24 19	107.90	SI Plaquette	
P17580	Newcastle West OW/24 20	113.15	SI Plaquette	
P17581	Newcastle West OW/24 21	116.8 - 117.0	SI Plaquette	
P17582	Newcastle West OW/24 60	283.24 - 283.5	SI Plaquette	
P17583	Newcastle West OW/24 66	309.3 - 309.6	SI Plaquette	
P17584	Newcastle West OW/24 67	312.6 - 312.63	SI Plaquette	

Appendix A: Sample Catalogue

TCD Number	Borehole	Depth (m)	Type of sample	Comments
P17585	Newcastle West OW/24 103	468 - 468.35	SI Plaquette	
P17586	Newcastle West OW/24 103	468 - 468.35	SI Plaquette	
P17587	Newcastle West OW/24 110	498.32 - 498.68	SI Plaquette	
P17588	Newcastle West OW/24 61	287.9 - 288.18	SI Plaquette	
P17589	Newcastle West OW/24 17	98.70	SI Plaquette	
P17590	Lisheen LK 318	71.75 - 71.85	Thin section	
P17591	Lisheen LK 318	73.35 - 73	Thin section	
P17592	Lisheen LK 318	107.16 - 107.4	Thin section	
P17593	Lisheen LK 318	140.1 - 141.05	Thin section	
P17594	Lisheen LK 318	144.1 - 144	Thin section	
P17595	Moyvore MV17 - Shinglis Breccia	595ft	Thin section	Fibrous clasts
P17596	Moyvore MV17 - Shinglis Breccia	606ft	Thin section	WMC with early cavities with Stages A-D
P17597	Moyvore MV17 - Shinglis Breccia	607ft	Thin section	Chlorite, flbrous clasts
P17598	Moyvore MV17 - Shinglis Breccia	636ft	Thin section	
P17599	Moyvore 3531/5	84.03	Thin section	
P17600	Moyvore 3531/5	84.3	Thin section	
P17601	Moyvore 3531/5	84.63	Thin section	
P17602	Moyvore 3531/5	84.8	Thin section	
P17603	Moyvore 3531/5	86.65 - 86.63	Thin section	Vesicles - radial texture, pseudomorphs, embayments in qtz
P17604	Moyvore 3531/5	86.63 - 86.6	Thin section	Pseudomorphs
P17605	Moyvore 3531/5	119 - 117.45	Thin section	Sheared vesicles
P17606	Moyvore 3531/5	119 - 117.45	Thin section	
P17607	Moyvore 3531/5	122.1	Thin section	
P17608	Moyvore 3531/5	137.65 - 138.05	Thin section	
P17609	Moyvore 3528/1	47.1 - 47.95	Thin section	
P17610	Moyvore 3528/1	88 - 88.5	Thin section	
P17611	Moyvore 3528/1	288.4 - 288.8	Thin section	Contact with intrusion
P17612	Moyvore 3528/1	315 - 315.5	Thin section	Injection into loose sandstone
P17613	Moyvore 3531/3	155	Thin section	Best sample for overall igneous features
P17614	Moyvore 3531/3	156	Thin section	
P17615	Navan N1445	775.55 - 775.35	Thin section	
P17616	Navan N1445	775.8 - 775.55	Thin section	Abundance of qtz - some spicules some authigenic
P17617	Navan N1445	779.3 - 779.48	Thin section	Contains apatite

Appendix A: Sample Catalogue

TCD Number	Borehole	Depth (m)	Type of sample	Comments
P17618	Navan N1445	785.3 - 785.65	Thin section	
P17619	Navan N1455	761.7 - 761.55	Thin section	Typical top WMC bryozoans
P17620	Navan N1455	763.75 - 763.5	Thin section	Michelinia corals
P17621	Navan N1446	863.9 - 864.35	Thin section	
P17622	Navan N1544	978.3 - 978.5	Thin section	Michelinia and ankerite rich
P17623	Navan (Clogherboy) EP4A	191.4 - 191.8	Thin section	
P17624	Navan (Clogherboy) EP4A	195.5 - 195.9	Thin section	
P17625	Navan (Clogherboy) EP4A	365.1 - 364.9	Thin section	Bird's eye micrite clast and dolomite clast
P17626	Navan (Clogherboy) EP11	473.3 - 473.6	Thin section	Healed conglomerate - fully cemented clasts
P17627	Navan N1445	762.8 - 762.95	Thin section	Typical bird's eye micrite
P17628	Navan N1445	779.48 - 779.6	Thin section	
P17629	Navan N1445	818 - 818.15	Thin section	
P17630	Navan N1445	897.55 - 897.8	Thin section	Collophane rich, it is seen replacing grains
P17631	Navan N1455	765.73 - 765.68	Thin section	Some collophane
P17632	Quinagh Borehole (Q31)	158.5	Thin section	Silicified fossils
P17633	Quinagh Borehole (Q30)	152.5	Thin section	Early calcite cements
P17634	Quinagh Borehole (Q21)	98.5	Thin section	
P17635	Quinagh Borehole	36.8 - 37	Thin section	grey organic dolomite (+ qtz) as geopetal fill below CD
P17636	Urlingford 3246-15	144.7	Thin section	Black tops texture
P17637	Mullawornia Quarry (GR 2130 2590)	-	Thin section	large secondary cavity with abundant bitumen
P17638	Mullawornia Quarry (GR 2130 2590)	-	Thin section	Brachiopod with spines replaced by bitumen
P17639	Mullawornia Quarry (GR 2130 2590)	-	Thin section	large secondary cavity with no bitumen + lots Fe dolomite
P17640	Mullawornia Quarry (GR 2130 2590)	-	Thin section	bitumen rich

APPENDIX B

STABLE ISOTOPE DATA

Appendix B: Stable Isotope Data - Carbonates

Sample No.	Drillhole	Depth (m)	Phase sampled	$\delta^{18}O$ (SMOW)	$\delta^{18}O$ (PDB)	$\delta^{13}C$ (PDB)	Mean $\delta^{18}O$	$\sigma\ \delta^{18}O$	Mean $\delta^{13}C$	$\sigma\ \delta^{13}C$	AP/Con	Comment
LISHEEN												
SD 13	LK 2258-38	121.2 - 122.53	stage D	23.07	-7.61	2.89	**24.50**	1.19	**2.61**	0.57	AP	
SD 14	LK 2258-38	121.2 - 122.53	stage D	22.80	-7.87	2.29					AP	
SD 1	LK 3262-18	203 - 203.62 (a)	stage D	23.42	-7.27	2.14					AP	
SD 2	LK 3262-18	203 - 203.62 (a)	stage D	23.97	-6.73	2.00					AP	
SD 3	LK 3262-18	203 - 203.62 (a)	stage D	23.33	-7.35	2.05					AP	Contains FeS_2?
SD 4	LK 3262-18	203 - 203.62 (b)	stage D	25.17	-5.57	2.60					AP	
SD 5	LK 3262-18	203 - 203.62 (b)	stage D	25.40	-5.34	2.60					AP	
SD 6	LK 3262-18	203 - 203.62 (b)	stage D	26.04	-4.73	3.17					AP	
SD 7	LK 3262-18	203 - 203.62 (b)	stage D	24.61	-6.11	2.63					AP	
SD 8	LK 3262-18	203 - 203.62 (a)	stage D	24.71	-6.02	2.87					AP	
SD 9	LK 3262-18	203 - 203.62 (a)	stage D	25.37	-5.38	2.68					AP	
SD 11	LK 3262-18	203 - 203.62 (c)	stage D	23.76	-6.93	2.82					AP	
SD 12	LK 3262-18	203 - 203.62 (c)	stage D	25.28	-5.46	2.33					AP	
SD 15	LK 3262-18	203 - 203.62 (x)	stage D	24.08	-6.63	1.98					AP	
SD 16	LK 3262-18	203 - 203.62 (x)	stage D	23.62	-7.07	2.53					AP	
SD 18	LK 3262-18	203 - 203.62 (y)	stage D	24.17	-6.53	1.94					AP	
SD 10	LK 2258-38	249.6 - 249.8	stage D	27.63	-3.18	4.19					AP	
SD 17	Quarry at Lisheen	Outcrop (GR 21453 16187)	stage D	24.54	-6.17	3.32					AP	
CFC 1	LK 2258-38	73.9 - 74.15 (a)	CFC	26.32	-4.45	3.17	**25.66**	0.71	**3.21**	0.13	AP	
CFC 2	LK 2258-38	73.9 - 74.15 (a)	CFC	26.39	-4.39	3.35					AP	
CFC 3	LK 2258-38	73.9 - 74.15 (a)	CFC	26.27	-4.50	3.17					AP	
CFC 4	LK 2258-38	73.9 - 74.15 (b)	CFC	24.39	-6.33	3.13					AP	
CFC 5	LK 2258-38	73.9 - 74.15 (b)	CFC	26.51	-4.27	3.23					AP	
CFC 6	LK 2258-38	73.9 - 74.15 (b)	CFC	25.91	-4.85	3.41					AP	
CFC 7	LK 2258-38	73.9 - 74.15 (a)	CFC	25.05	-5.68	3.10					Con	
CFC 8	LK 2258-38	73.9 - 74.15 (b)	CFC	25.71	-5.04	3.24					Con	
CFC 9	LK 2258-38	73.9 - 74.15 (b)	CFC	25.13	-5.60	3.30					Con	
CFC 11	LK 2258-38	73.9 - 74.15 (b)	CFC	25.31	-5.44	2.97					AP	
Mic 1	Quarry at Lisheen	Outcrop (GR 21453 16187)	micrite	26.91	-3.88	3.74	**26.71**	0.53	**3.57**	0.20	AP	
Mic 2	Quarry at Lisheen	Outcrop (GR 21453 16187)	micrite	27.02	-3.77	3.60					AP	
Mic 3	Quarry at Lisheen	Outcrop (GR 21453 16187)	micrite	27.48	-3.33	3.24					AP	
Mic 4	Quarry at Lisheen	Outcrop (GR 21453 16187)	micrite	26.73	-4.05	3.63					AP	
Mic 5	Quarry at Lisheen	Outcrop (GR 21453 16187)	micrite	26.62	-4.16	3.77					AP	
Mic 6	Quarry at Lisheen	Outcrop (GR 21453 16187)	micrite	25.92	-4.84	3.23					AP	
Mic 7	Quarry at Lisheen	Outcrop (GR 21453 16187)	micrite	27.31	-3.49	3.71					AP	
Mic 8	Quarry at Lisheen	Outcrop (GR 21453 16187)	micrite	26.27	-4.50	3.59					AP	
Mic 9	Quarry at Lisheen	Outcrop (GR 21453 16187)	micrite	26.16	-4.61	3.66					AP	

Appendix B: Stable Isotope Data - Carbonates

Sample No.	Drillhole	Depth (m)	Phase sampled	$\delta^{18}O$ (SMOW)	$\delta^{18}O$ (PDB)	$\delta^{13}C$ (PDB)	Mean $\delta^{18}O$	$\sigma\ \delta^{18}O$	Mean $\delta^{13}C$	$\sigma\ \delta^{13}C$	AP/Con	Comment
Dol mic 1	LK 3262-18	203 - 203.62	fine-grained dolomite	23.49	-7.20	3.81	**23.36**	0.64	**3.66**	0.33	AP	
Dol mic 2	LK 3262-18	203 - 203.62	fine-grained dolomite	23.19	-7.49	3.83					AP	
Dol mic 3	LK 3262-18	203 - 203.62	fine-grained dolomite	23.59	-7.10	3.97					AP	
Dol mic 4	LK 3262-18	203 - 203.62	fine-grained dolomite	23.32	-7.36	3.69					AP	
Dol mic 5	LK 3262-18	203 - 203.62	fine-grained dolomite	22.65	-8.01	3.29					AP	
Dol mic 6	LK 3262-18	203 - 203.62 (y)	fine-grained dolomite	23.09	-7.59	3.63					AP	
Dol mic 7	LK 3262-18	203 - 203.62 (y)	fine-grained dolomite	23.46	-7.23	3.85					AP	
Dol mic 8	LK 3262-18	203 - 203.62 (y)	fine-grained dolomite	23.39	-7.29	3.97					AP	
Dol mic 9	LK 3262-18	203 - 203.62 (y)	fine-grained dolomite	23.39	-7.29	3.93					AP	
Dol mic 17	LK 3262-18	203 - 203.62 (a)	fine-grained dolomite	23.05	-7.63	3.57					Con	
Dol mic 18	LK 3262-18	203 - 203.62 (a)	fine-grained dolomite	23.10	-7.58	3.46					Con	
Dol mic 19	LK 3262-18	203 - 203.62 (a)	fine-grained dolomite	22.58	-8.08	3.52					AP	
Dol mic 20	LK 3262-18	203 - 203.62 (a)	fine-grained dolomite	22.88	-7.79	3.39					Con	
Dol mic 21	LK 3262-18	203 - 203.62 (a)	fine-grained dolomite	23.21	-7.47	3.62					Con	
Dol mic 22	LK 3262-18	203 - 203.62 (a)	fine-grained dolomite	22.84	-7.83	3.40					Con	
Dol mic 23	LK 3262-18	203 - 203.62 (b)	fine-grained dolomite	22.63	-8.04	3.33					Con	
Dol mic 24	LK 3262-18	203 - 203.62 (b)	fine-grained dolomite	22.68	-7.99	3.18					Con	
Dol mic 25	LK 3262-18	203 - 203.62 (b)	fine-grained dolomite	23.33	-7.35	3.47					Con	
Dol mic 10	LK 2258-38	249.6 - 249.8	fine-grained dolomite	23.06	-7.62	3.15					AP	
Dol mic 11	LK 2258-38	249.6 - 249.8	fine-grained dolomite	23.05	-7.63	3.25					AP	
Dol mic 12	LK 2258-38	249.6 - 249.8	fine-grained dolomite	24.09	-6.61	3.63					AP	
Dol mic 13	LK 2258-38	249.6 - 249.8	fine-grained dolomite	24.92	-5.81	4.15					AP	
Dol mic 14	LK 2258-38	249.6 - 249.8	fine-grained dolomite	24.96	-5.77	3.97					AP	
Dol mic 15	Quarry at Lisheen	Outcrop (GR 21453 16187)	fine-grained dolomite	24.23	-6.48	4.51					AP	
Dol mic 16	Quarry at Lisheen	Outcrop (GR 21453 16187)	fine-grained dolomite	23.93	-6.77	4.00					AP	
2nd Dolo 1	LK 2258-38	112.44 - 112.75 (a)	x-cutting dolomite	23.09	-7.59	3.14	**22.37**	0.90	**2.92**	0.46	Con	
2nd Dolo 2	LK 2258-38	112.44 - 112.75 (a)	x-cutting dolomite	23.30	-7.38	3.01					Con	
2nd Dolo 3	LK 2258-38	112.44 - 112.75 (b)	x-cutting dolomite	23.33	-7.35	2.97					AP	
2nd Dolo 4	LK 2258-38	112.44 - 112.75 (a)	x-cutting dolomite	23.09	-7.59	3.30					AP	
Dol spar 5	LK 2258-38	121.2 - 122.53	dolomitised spar	23.04	-7.64	3.43					Con	
Dol spar 6	LK 2258-38	121.2 - 122.53	dolomitised spar	22.83	-7.84	3.24					Con	
Dol spar 7	LK 2258-38	121.2 - 122.53	dolomitised spar	22.47	-8.19	3.26					AP	
Dol spar 8	LK 2258-38	121.2 - 122.53	dolomitised spar	20.77	-9.83	2.19					AP	
Dol spar 9	LK 2258-38	121.2 - 122.53	dolomitised spar	21.72	-8.91	1.99					AP	
Dol spar 1	LK 3262-18	203 - 203.62 (x)	dolomitised spar	22.42	-8.24	2.36					AP	
Dol spar 2	LK 3262-18	203 - 203.62 (x)	dolomitised spar	22.75	-7.92	3.52					AP	
Dol spar 3	LK 3262-18	203 - 203.62 (x)	dolomitised spar	22.58	-8.08	3.11					AP	
Dol spar 4	LK 3262-18	203 - 203.62 (x)	dolomitised spar	23.64	-7.05	3.48					AP	
CD 6	LK 2258-38	73.9 - 74.15 (a)	coarse white dolomite	21.12	-9.48	2.55					Con	
CD 7	LK 2258-38	73.9 - 74.15 (a)	coarse white dolomite	20.45	-10.14	2.39					AP	
CD 9	LK 2258-38	73.9 - 74.15 (a)	coarse white dolomite	22.18	-8.47	3.24					AP	

Appendix B: Stable Isotope Data - Carbonates

Sample No.	Drillhole	Depth (m)	Phase sampled	$\delta^{18}O$ (SMOW)	$\delta^{18}O$ (PDB)	$\delta^{13}C$ (PDB)	Mean $\delta^{18}O$	σ $\delta^{18}O$	Mean $\delta^{13}C$	σ $\delta^{13}C$	AP/Con	Comment
CD 10	LK 2258-38	73.9 - 74.15 (a)	coarse white dolomite	21.28	-9.34	2.36					Con	
CD 11	LK 2258-38	73.9 - 74.15 (a)	coarse white dolomite	20.84	-9.77	2.28					Con	
CD 1	LK 3262-18	203 - 203.62	coarse white dolomite	22.73	-7.94	3.41					AP	
CD 2	LK 3262-18	203 - 203.62	coarse white dolomite	22.43	-8.23	3.04					AP	
CD 3	LK 3262-18	203 - 203.62	coarse white dolomite	22.76	-7.91	2.94					AP	
CD 4	LK 3262-18	203 - 203.62	coarse white dolomite	22.72	-7.95	3.03					AP	
CD 5	LK 3262-18	203 - 203.62	coarse white dolomite	23.05	-7.63	2.87					AP	
NEWCASTLE WEST												
CD 1	OW 24/4	37.30	coarse white dolomite	19.31	-11.25	2.93	**18.76**	1.82	**3.28**	0.34	AP	
CD 2	OW 24/4	37.30	coarse white dolomite	20.57	-10.03	3.28					AP	
CD 3	OW 24/65	304.9 - 305.15	coarse white dolomite	22.33	-8.33	3.12					AP	
CD 9	OW 24/67	312.6 - 312.63	coarse white dolomite	21.39	-9.23	3.01						
CD 10	OW 24/67	312.6 - 312.63	coarse white dolomite	20.78	-9.83	2.80						
CD 11	OW 24/82	377.4 - 377.7	coarse white dolomite	19.74	-10.84	2.91						
CD 12	OW 24/82	377.4 - 377.7	coarse white dolomite	20.02	-10.57	2.87						
CD 13	OW 28/41	85.0	coarse white dolomite	16.78	-13.70	3.47						
CD 14	OW 28/41	84.0	coarse white dolomite	17.08	-13.41	3.36						
CD 15	OW 28/41	87.0	coarse white dolomite	16.75	-13.74	3.27						
CD 16	OW 28/41	87.0	coarse white dolomite	17.41	-13.09	3.00						
CD 4	OW 28 /67	297.63	coarse white dolomite	17.60	-12.91	3.62					AP	
CD 5	OW 28 /67	297.63	coarse white dolomite	17.84	-12.68	3.70					Con	
CD 6	OW 28 /67	297.63	coarse white dolomite	17.18	-13.32	3.70					Con	
CD 7	OW 28 /67	297.81	coarse white dolomite	17.44	-13.07	3.82					Con	
CD 8	OW 28 /67	297.81	coarse white dolomite	17.98	-12.54	3.62					Con	
Dol mic 1	OW 24/14	85.30	fine-grained dolomite	23.30	-7.38	4.60	**22.91**	1.22	**4.07**	0.19	AP	
Dol mic 2	OW 24/14	85.30	fine-grained dolomite	22.73	-7.93	4.21					AP	
Dol mic 3	OW 24/14	85.30	fine-grained dolomite	23.35	-7.33	4.18					AP	
Dol mic 4	OW 24/14	85.30	fine-grained dolomite	22.23	-8.42	4.05					AP	
Dol mic 10	OW 24/17	98.70	fine-grained dolomite	20.85	-9.76	3.94					AP	Bleached
Dol mic 19	OW 24/17	98.70	fine-grained dolomite	21.24	-9.38	3.77					AP	
Dol mic 5	OW 24/18	103.20	fine-grained dolomite	22.84	-7.82	3.89					AP	Bleached
Dol mic 6	OW 24/18	103.20	fine-grained dolomite	22.55	-8.11	3.99					AP	Bleached
Dol mic 7	OW 24/18	103.20	fine-grained dolomite	23.35	-7.33	4.19					AP	Bleached
Dol mic 16	OW 24/19	107.90	fine-grained dolomite	21.69	-8.95	3.86					AP	
Dol mic 17	OW 24/19	107.90	fine-grained dolomite	20.61	-10.00	3.99					AP	
Dol mic 11	OW 24/20	113.15	fine-grained dolomite	23.90	-6.80	4.15					AP	
Dol mic 15	OW 24/66	309.3 - 309.6	fine-grained dolomite	24.87	-5.86	3.98					AP	
Dol mic 18	OW 24/67	312.3 - 312.63	fine-grained dolomite	24.20	-6.51	4.02					AP	
Dol mic 20	OW 24/103	468 - 468.35	fine-grained dolomite	24.42	-6.30	4.22					AP	

Appendix B: Stable Isotope Data - Carbonates

Sample No.	Drillhole	Depth (m)	Phase sampled	$\delta^{18}O$ (SMOW)	$\delta^{18}O$ (PDB)	$\delta^{13}C$ (PDB)	Mean $\delta^{18}O$	$\sigma\ \delta^{18}O$	Mean $\delta^{13}C$	$\sigma\ \delta^{13}C$	AP/Con	Comment
Dol mic 12	OW 24/110	504 - 505.18	fine-grained dolomite	24.04	-6.66	4.03					AP	
Dol mic 13	OW 24/110	504 - 505.18	fine-grained dolomite	23.29	-7.39	3.96					AP	
Dol mic 14	OW 24/110	504 - 505.18	fine-grained dolomite	22.94	-7.73	4.17					AP	
CFC 1	OW 24/14	85.30	CFC	23.51	-7.18	3.97	**23.85**	1.79	**4.14**	0.24	AP	
CFC 2	OW 24/14	85.30	CFC	24.72	-6.01	4.17					AP	
CFC 3	OW 24/14	85.30	CFC	24.13	-6.58	4.47					AP	
CFC 4	OW 24/14	85.30	CFC	23.68	-7.01	4.25					AP	
CFC 5	OW 24/18	103.20	CFC	22.39	-8.27	4.45					AP	
CFC 6	OW 24/18	103.20	CFC	21.25	-9.37	4.37					AP	
CFC 8	OW 24/20	113.15	CFC	24.52	-6.19	4.00					AP	
CFC 7	OW 24/21	116.8 - 117.0	CFC	27.59	-3.22	4.57					AP	Crinoid ossicle
CFC 9	OW 28 /67	301.60	CFC	23.10	-7.57	3.94					AP	
CFC 10	OW 28 /67	301.60	CFC	23.03	-7.65	3.83					Con	
CFC 11	OW 28 /67	301.60	CFC	26.27	-4.50	4.03					Con	
CFC 12	OW 28 /67	301.60	CFC	25.63	-5.12	3.99					Con	
CFC 13	OW 28 /67	301.60	CFC	21.59	-9.04	3.96					Con	
CFC 14	OW 28 /67	301.60	CFC	22.52	-8.14	3.99					Con	
Mic 1	OW 24/18	103.20	micrite	22.06	-8.58	4.27	**22.36**	4.08	**3.83**	0.42	AP	
Mic 2	OW 24/61	287.9 - 288.18	micrite	27.50	-3.30	4.36					AP	
Mic 3	OW 24/61	287.9 - 288.18	micrite	27.26	-3.54	4.35					AP	
Mic 4	OW 24/61	287.9 - 288.18	micrite	27.23	-3.57	4.34					AP	
Mic 13	OW 24/61	287.9 - 288.18	micrite	27.52	-3.29	3.20					AP	
Mic 5	OW 28/67	301.60	micrite	19.46	-11.11	3.69					AP	
Mic 6	OW 28/67	301.60	micrite	18.95	-11.61	3.60					AP	
Mic 7	OW 28/67	301.60	micrite	19.36	-11.20	3.50					AP	
Mic 8	OW 28/67	301.60	micrite	19.21	-11.35	3.50					AP	
Mic 10	OW 28/67	301.60	micrite	18.92	-11.63	3.61					AP	
Mic 12	OW 28/67	301.60	micrite	18.47	-12.07	3.67					Con	
SD 14	OW 24/4	37.30	stage D	24.29	-6.42	3.46	**24.71**	1.13	**3.29**	0.73	AP	
SD 15	OW 24/4	37.30	stage D	24.29	-6.42	2.13					AP	
SD 1	OW 24/11	73.45	stage D	24.88	-5.85	2.43					AP	
SD 4	OW 24/11	73.45	stage D	24.94	-5.80	2.66					AP	
SD 5	OW 24/11	73.45	stage D	25.45	-5.30	3.28					AP	
SD 6	OW 24/11	73.45	stage D	23.81	-6.89	2.17					AP	
SD 11	OW 24/12	77.70	stage D	23.56	-7.13	3.07					AP	
SD 12	OW 24/12	77.70	stage D	26.74	-4.04	3.94					AP	
SD 13	OW 24/13	81.70	stage D	25.20	-5.54	3.03					AP	
SD 2	OW 24/14	85.30	stage D	23.30	-7.38	2.88					AP	
SD 3	OW 24/14	85.30	stage D	24.24	-6.47	3.60					AP	

Appendix B: Stable Isotope Data - Carbonates

Sample No.	Drillhole	Depth (m)	Phase sampled	$\delta^{18}O$ (SMOW)	$\delta^{18}O$ (PDB)	$\delta^{13}C$ (PDB)	Mean $\delta^{18}O$	$\sigma\ \delta^{18}O$	Mean $\delta^{13}C$	$\sigma\ \delta^{13}C$	AP/Con	Comment
SD 7	OW 24/18	103.20	stage D	25.03	-5.70	4.69					AP	
SD 8	OW 24/18	103.20	stage D	25.14	-5.60	3.76					AP	
SD 9	OW 24/18	103.20	stage D	25.24	-5.50	4.29					AP	
SD 10	OW 24/18	103.20	stage D	23.49	-7.20	3.18					AP	
SD 19	OW 24/60	283.24 - 283.5	stage D	26.93	-3.87	3.27					AP	
SD 16	OW 24/67	312.3 - 312.63	stage D	25.67	-5.08	3.34					AP	
SD 17	OW 24/103	468 - 468.35	stage D	24.87	-5.85	4.53					AP	
SD 18	OW 24/103	468 - 468.35	stage D	22.42	-8.24	2.76					AP	
MALLOW												
CFC 4	3537- 04	68.86 - 69	CFC	25.62	-5.14	2.69	**26.14**	0.86	**3.18**	0.49	AP	
CFC 5	3537- 04	68.86 - 69	CFC	24.65	-6.07	2.91					AP	
CFC 6	3537- 04	71.7 - 71.88	CFC	26.99	-3.80	4.09					AP	
CFC 1	3537- 04	79.83 - 80.26	CFC	26.55	-4.23	3.25					AP	
CFC 2	3537- 04	79.83 - 80.26	CFC	26.70	-4.08	3.14					AP	
CFC 3	3537- 04	79.83 - 80.26	CFC	26.32	-4.45	2.97					AP	
SD 3	3537- 04	68.86 - 69	stage D	24.10	-6.60	3.43	**25.75**	1.21	**3.54**	0.43	AP	
SD 4	3537- 04	71.7 - 71.88	stage D	26.88	-3.91	4.00					AP	
SD 1	3537- 04	79.83 - 80.26	stage D	25.64	-5.11	3.00					AP	
SD 2	3537- 04	79.83 - 80.26	stage D	26.36	-4.41	3.71					AP	
Pink Dol 1	Subutler	Outcrop (GR 1443 1042)	late pink dolomite	22.95	-7.72	4.15	**24.19**	0.87	**4.42**	0.21	AP	
Pink Dol 2	Subutler	Outcrop (GR 1443 1042)	late pink dolomite	24.37	-6.34	4.58					AP	
Pink Dol 3	Subutler	Outcrop (GR 1443 1042)	late pink dolomite	24.47	-6.25	4.37					AP	
Pink Dol 4	Subutler	Outcrop (GR 1443 1042)	late pink dolomite	24.98	-5.75	4.58					AP	
CD 1	3537- 04	58.6 - 59.28	coarse white dolomite	24.67	-6.05	3.34	**23.96**	0.93	**3.50**	0.60	AP	
CD 2	3537- 04	58.6 - 59.28	coarse white dolomite	23.96	-6.74	3.12					AP	
CD 3	3537- 04	58.6 - 59.28	coarse white dolomite	24.54	-6.17	3.36					AP	
CD 4	3536- 06	155.8 - 156.1	coarse white dolomite	24.20	-6.51	2.97					AP	
CD 5	3536- 06	155.8 - 156.1	coarse white dolomite	24.89	-5.84	3.06					AP	
CD 6	Subutler	Outcrop (GR 1443 1042)	coarse white dolomite	22.30	-8.35	4.02					AP	
CD 7	Subutler	Outcrop (GR 1443 1042)	coarse white dolomite	23.13	-7.54	4.61					AP	
Dol mic 5	3537- 04	58.6 - 59.28	fine-grained dolomite	24.20	-6.50	3.81	**23.52**	0.95	**4.21**	0.35	AP	
Dol mic 6	3537- 04	58.6 - 59.28	fine-grained dolomite	24.23	-6.48	3.85					AP	
Dol mic 1	3537- 04	71.7 - 71.88	fine-grained dolomite	23.98	-6.72	4.47					AP	
Dol mic 2	3537- 04	71.7 - 71.88	fine-grained dolomite	24.57	-6.15	4.60					AP	
Dol mic 3	3537- 04	71.7 - 71.88	fine-grained dolomite	21.91	-8.73	4.10					AP	
Dol mic 4	3537- 04	71.7 - 71.88	fine-grained dolomite	23.76	-6.93	4.64					AP	

Appendix B: Stable Isotope Data - Carbonates

Sample No.	Drillhole	Depth (m)	Phase sampled	$\delta^{18}O$ (SMOW)	$\delta^{18}O$ (PDB)	$\delta^{13}C$ (PDB)	Mean $\delta^{18}O$	$\sigma\ \delta^{18}O$	Mean $\delta^{13}C$	$\sigma\ \delta^{13}C$	AP/Con	Comment
Dol mic 7	3536- 06	155.8 - 156.1	fine-grained dolomite	22.11	-8.54	3.64					AP	
Dol mic 8	3536- 06	155.8 - 156.1	fine-grained dolomite	24.31	-6.40	4.39					AP	
Dol mic 9	Subutler	Outcrop (GR 1443 1042)	fine-grained dolomite	23.29	-7.39	4.39					AP	
Dol mic 10	Subutler	Outcrop (GR 1443 1042)	fine-grained dolomite	22.82	-7.85	4.25					AP	
Mic 1	3537- 04	71.7 - 71.88	micrite	26.58	-4.20	4.08	**26.58**	-	**4.08**	-	AP	
FERMOY												
SD 1	3626-01	91.95 - 92.15	stage D	27.56	-3.25	3.60	**28.11**	0.78	**3.64**	0.06	AP	
SD 2	3626-01	91.95 - 92.15	stage D	28.66	-2.18	3.68					AP	
Mic 6	3626-02	54 - 54.10	micrite	28.66	-2.18	4.06	**26.44**	1.30	**3.57**	0.47	AP	
Mic 1	3626-02	99.12 - 99.29	micrite	25.79	-4.97	3.79					AP	Bleached
Mic 2	3626-02	99.12 - 99.29	micrite	26.22	-4.55	2.74					AP	Bleached
Mic 3	3626-02	100.07 - 100.43	micrite	24.71	-6.02	3.36					AP	Bleached
Mic 4	3626-02	100.07 - 100.43	micrite	26.63	-4.15	3.64					AP	Bleached
Mic 5	3626-02	100.07 - 100.43	micrite	26.63	-4.15	3.81					AP	
CFC 3	3626-02	54 - 54.10	CFC	28.04	-2.78	3.93	**27.89**	0.59	**3.66**	0.50	AP	
CFC 2	3626-01	91.95 - 92.15	CFC	28.38	-2.45	3.97					AP	
CFC 1	3626-02	99.12 - 99.29	CFC	27.24	-3.56	3.08					AP	
LCV 1	3626-02	99.12 - 99.29	late calcite vein	25.89	-4.87	3.00	**25.89**	-	**3.00**	-	AP	
CD 6	3626-02	54 - 54.10	coarse white dolomite	22.89	-7.78	3.98	**22.93**	0.86	**3.76**	0.20	AP	
CD 1	3626-02	99.12 - 99.29	coarse white dolomite	23.72	-6.97	3.60					AP	
CD 2	3626-02	99.12 - 99.29	coarse white dolomite	22.96	-7.71	3.76					AP	
CD 3	3626-02	100.07 - 100.43	coarse white dolomite	21.30	-9.33	3.58					AP	
CD 4	3626-02	100.07 - 100.43	coarse white dolomite	23.23	-7.45	4.03					AP	
CD 5	3626-02	100.07 - 100.43	coarse white dolomite	23.46	-7.23	3.62					AP	
Dol mic 1	3626-02	54 - 54.10	fine-grained dolomite	25.18	-5.56	3.75	**25.54**	0.85	**3.66**	0.48	AP	
Dol mic 2	3626-01	91.95 - 92.15	fine-grained dolomite	26.32	-4.45	4.11					AP	Brownish
Dol mic 3	3626-01	91.95 - 92.15	fine-grained dolomite	26.16	-4.61	3.80					AP	
Dol mic 4	3626-01	91.95 - 92.15	fine-grained dolomite	24.52	-6.20	2.99					AP	
URLINGFORD												
BT 1	3246-15	136.55 - 136.58	black tops	23.27	-7.41	3.57	**23.34**	0.09	**3.52**	0.08	AP	
BT 2	3246-15	136.64 - 136.68	black tops	23.41	-7.28	3.46					AP	

Appendix B: Stable Isotope Data - Carbonates

Sample No.	Drillhole	Depth (m)	Phase sampled	$\delta^{18}O$ (SMOW)	$\delta^{18}O$ (PDB)	$\delta^{13}C$ (PDB)	Mean $\delta^{18}O$	$\sigma\ \delta^{18}O$	Mean $\delta^{13}C$	$\sigma\ \delta^{13}C$	AP/Con	Comment
CD 1	3246-15	136.58 - 136.62	coarse white dolomite	23.40	-7.28	3.19	**23.67**	1.30	**3.21**	0.59	AP	
CD 2	3246-15	136.58 - 136.62	coarse white dolomite	22.20	-8.45	2.36					AP	
CD 3	3246-15	136.68 - 136.74	coarse white dolomite	24.89	-5.84	3.92					AP	
CD 4	3246-15	136.68 - 136.74	coarse white dolomite	24.82	-5.91	3.50					AP	
CD 5	3246-15	136.64 - 136.68	coarse white dolomite	21.81	-8.83	2.49					AP	
CD 6	3246-15	136.64 - 136.68	coarse white dolomite	23.60	-7.09	3.27					AP	
CD 7	3246-15	136.64 - 136.68	coarse white dolomite	24.97	-5.76	3.73					AP	
RD 1	3246-15	136.58 - 136.62	fine-grained dolomite	23.60	-7.09	3.97	**23.71**	0.37	**3.80**	0.29	AP	
RD 2	3246-15	136.58 - 136.62	fine-grained dolomite	23.75	-6.94	3.85					AP	
RD 3	3246-15	136.55 - 136.58	fine-grained dolomite	24.34	-6.37	4.20					AP	
RD 4	3246-15	136.55 - 136.58	fine-grained dolomite	23.98	-6.72	3.82					AP	
RD 5	3246-15	136.64 - 136.68	fine-grained dolomite	23.44	-7.24	3.80					AP	
RD 6	3246-15	136.64 - 136.68	fine-grained dolomite	23.84	-6.86	3.22					AP	
RD 7	3246-15	136.64 - 136.68	fine-grained dolomite	23.07	-7.60	3.47					AP	
RD 8	3246-15	136.68 - 136.74	fine-grained dolomite	23.23	-7.45	3.69					AP	
RD 9	3246-15	136.68 - 136.74	fine-grained dolomite	24.05	-6.65	3.49					AP	
RD 10	3246-15	136.68 - 136.74	fine-grained dolomite	23.61	-7.08	4.03					AP	
RD 11	3246-15	136.68 - 136.74	fine-grained dolomite	24.08	-6.63	4.18					AP	
RD 12	3246-15	136.68 - 136.74	fine-grained dolomite	23.57	-7.12	3.83					AP	
CARLOW												
CD 1	Quinagh	36.8 - 37	coarse white dolomite	21.16	-9.46	1.03	**20.80**	0.66	**1.58**	0.95	AP	
CD 2	Quinagh	77.28 - 77.58	coarse white dolomite	21.03	-9.58	0.53					AP	
CD 3	Quinagh	77.28 - 77.58	coarse white dolomite	20.80	-9.80	0.15					AP	
CD 4	Quinagh	77.28 - 77.58	coarse white dolomite	20.47	-10.13	0.36					AP	
CD 5	Quinagh	36.8 - 37	coarse white dolomite	22.40	-8.25	2.13					AP	
CD 6	Clonmelsh	Outcrop (GR 2724 1702)	coarse white dolomite	20.36	-10.24	2.10					AP	
CD 7	Clonmelsh	Outcrop (GR 2724 1702)	coarse white dolomite	21.10	-9.52	1.80					AP	
CD 8	Clonmelsh	Outcrop (GR 2724 1702)	coarse white dolomite	20.22	-10.37	1.85					AP	
CD 9	Clonmelsh	Outcrop (GR 2724 1702)	coarse white dolomite	20.18	-10.41	1.80					AP	
CD 11	Quinagh	77.28 - 77.58	coarse white dolomite	20.93	-9.68	2.45					AP	
CD 12	Quinagh	77.28 - 77.58	coarse white dolomite	20.13	-10.46	3.16					AP	
RD 1	Quinagh	36.8 - 37	fine-grained dolomite	23.84	-6.86	2.57	**25.15**	1.67	**2.56**	0.05	AP	
RD 2	Quinagh	36.8 - 37	fine-grained dolomite	24.03	-6.68	2.54					AP	
RD 3	Quinagh	77.28 - 77.58	fine-grained dolomite	24.01	-6.70	2.57					AP	
RD 4	Quinagh	77.28 - 77.58	fine-grained dolomite	23.85	-6.85	2.52					AP	
RD 5	Clonmelsh	Outcrop (GR 2724 1702)	fine-grained dolomite	27.79	-3.03	2.59					AP	
RD 6	Clonmelsh	Outcrop (GR 2724 1702)	fine-grained dolomite	26.74	-4.04	2.56					AP	
RD 7	Clonmelsh	Outcrop (GR 2724 1702)	fine-grained dolomite	24.08	-6.62	2.66					AP	

Appendix B: Stable Isotope Data - Carbonates

Sample No.	Drillhole	Depth (m)	Phase sampled	$\delta^{18}O$ (SMOW)	$\delta^{18}O$ (PDB)	$\delta^{13}C$ (PDB)	Mean $\delta^{18}O$	$\sigma\ \delta^{18}O$	Mean $\delta^{13}C$	$\sigma\ \delta^{13}C$	AP/Con	Comment
RD 8	Clonmelsh	Outcrop (GR 2724 1702)	fine-grained dolomite	26.88	-3.90	2.50					AP	
Pink Dol 1	Clonmelsh	Outcrop (GR 2724 1702)	late pink dolomite	16.05	-14.42	1.40	**16.00**	0.11	**1.41**	0.05	AP	
Pink Dol 2	Clonmelsh	Outcrop (GR 2724 1702)	late pink dolomite	16.08	-14.39	1.47					AP	
Pink Dol 3	Clonmelsh	Outcrop (GR 2724 1702)	late pink dolomite	15.87	-14.58	1.37					AP	
MULLAWORNIA												
BRC1	Mullawornia	Outcrop (GR 2130 2590)	bitumen-related calcite	27.90	-2.92	1.85	**28.30**	0.30	**2.47**	0.89		TCD
BRC2	Mullawornia	Outcrop (GR 2130 2590)	bitumen-related calcite	28.56	-2.28	1.58						TCD
BRC3	Mullawornia	Outcrop (GR 2130 2590)	bitumen-related calcite	28.48	-2.35	3.38						TCD
BRC4	Mullawornia	Outcrop (GR 2130 2590)	bitumen-related calcite	28.27	-2.56	3.06						TCD
Mic 1	Mullawornia	Outcrop (GR 2130 2590)	micrite	27.53	-3.28	3.99	**27.91**	0.70	**4.10**	0.21		TCD
Mic 2	Mullawornia	Outcrop (GR 2130 2590)	micrite	28.29	-2.54	4.13						TCD
Mic 3	Mullawornia	Outcrop (GR 2130 2590)	micrite	27.70	-3.11	4.20						TCD
Mic 4	Mullawornia	Outcrop (GR 2130 2590)	micrite	26.88	-3.91	3.77						TCD
Mic 5	Mullawornia	Outcrop (GR 2130 2590)	micrite	27.50	-3.31	3.97						TCD
Mic 6	Mullawornia	Outcrop (GR 2130 2590)	micrite	28.83	-2.02	4.39						TCD
Mic 7	Mullawornia	Outcrop (GR 2130 2590)	micrite	28.67	-2.18	4.27						TCD
CD 1	Mullawornia	Outcrop (GR 2130 2590)	coarse white dolo (zone 4)	27.65	-1.78	4.16	**26.45**	1.10	**3.61**	1.54		TCD
CD 2	Mullawornia	Outcrop (GR 2130 2590)	coarse white dolo (zone 3)	25.82	-3.55	4.28						TCD, orange
CD 3	Mullawornia	Outcrop (GR 2130 2590)	coarse white dolo (zone 3)	25.26	-4.09	-0.19						TCD, orange
CD 4	Mullawornia	Outcrop (GR 2130 2590)	coarse white dolo (zone 4)	27.68	-1.74	4.22						TCD
CD 5	Mullawornia	Outcrop (GR 2130 2590)	coarse white dolo (zone 3)	25.40	-3.95	4.27						TCD, orange
CD 6	Mullawornia	Outcrop (GR 2130 2590)	coarse white dolo (zone 3)	26.93	-2.48	3.94						TCD, orange
CD 7	Mullawornia	Outcrop (GR 2130 2590)	coarse white dolo (zone 4)	27.50	-1.92	4.08						TCD
CD 8	Mullawornia	Outcrop (GR 2130 2590)	coarse white dolo (zone 4)	25.33	-4.02	4.14						TCD

Appendix B: Stable Isotope Data - Pyrite

LineNo.	Sample No.	Drillhole	Depth (m)	Phase sampled	$\delta^{34}S$ (CDT)	Morphology	Mean $\delta^{34}S$	$\sigma\ \delta^{34}S$
NEWCASTLE WEST								
SA8368	2	OW24 / 20	113.5	pyrite	8.39	cubic	**7.4**	**2.60**
SA8372	6	OW24 / 81	370.8 - 371.1	pyrite	8.34	cubic		
SA8371	5	OW24 / 82	377.4 - 377.7	pyrite	8.30	cubic		
SA8369	3	OW24 / 83	377.65 - 377.9	pyrite	9.15	cubic		
SA8370	4	OW24 / 106	479.3 - 479.7	pyrite	2.14	bedded/shaley		
SA8367	1	OW24 / 110	498.32 - 498.68	pyrite	8.00	cubic		
SA8374	4 (re-run)	OW24 / 106	479.3 - 479.7	pyrite	2.35	bedded/shaley		

Appendix B: Stable Isotope Data - Quartz

Sample No.	Drillhole	Depth (m)	Phase sampled	Delta 1	Delta 2	$\delta^{18}O$ (SMOW)	Mean $\delta^{18}O$	$\sigma\ \delta^{18}O$	Comment
NEWCASTLE WEST									
1	OW 28 / 67	297.45-297.5	quartz	-25.93	-18.84	19.4	**19.2**	**0.37**	
2	OW 28 / 67	297.45-297.5	quartz	-26.02	-18.92	19.3			
3	OW 28 / 67	297.45-297.5	quartz	-26.05	-18.75	19.5			
4	OW 28 / 67	297.45-297.5	quartz	-25.98	-18.97	19.3			
5	OW 28 / 67	297.45-297.5	quartz	-26.33	-19.06	19.1			
6	OW 28 / 67	297.45-297.5	quartz	-25.93	-18.92	19.3			
7	OW 28 / 67	297.45-297.5	quartz	-25.98	-18.88	19.3			
8	OW 28 / 67	297.45-297.5	quartz	-25.99	-18.94	19.3			
9	OW 28 / 67	297.45-297.5	quartz	-26.00	-18.76	19.5			
10	OW 28 / 67	297.45-297.5	quartz	-26.00	-19.16	19.0			
11	OW 28 / 67	297.45-297.5	quartz	-26.00	-18.82	19.4			
12	OW 28 / 67	297.45-297.5	quartz	-25.94	-18.96	19.2			
13	OW 28 / 67	297.45-297.5	quartz	-25.97	-19.06	19.2			
14	OW 28 / 67	297.45-297.5	quartz	-25.98	-19.77	18.4			
1	OW 24 / 4	37.30	black quartz	-26.00	-19.14	19.3			
2	OW 24 / 4	37.30	black quartz	-25.91	-18.71	19.8			
3	OW 24 / 4	37.30	black quartz	-25.96	-20.08	18.3			
4	OW 24 / 4	37.30	black quartz	-25.95	-19.45	19.0			
5	OW 24 / 4	37.30	black quartz	-25.88	-18.78	19.7			
6	OW 24 / 4	37.30	black quartz	-25.93	-20.01	18.4			
7	OW 24 / 4	37.30	black quartz	-25.87	-19.05	19.4			
8	OW 24 / 4	37.30	black quartz	-26.00	-19.69	18.7			
9	OW 24 / 4	37.30	black quartz	-25.97	-18.83	19.6			
10	OW 24 / 4	37.30	black quartz	-25.99	-19.32	19.1			
11	OW 24 / 4	37.30	black quartz	-25.95	-19.52	18.9			
12	OW 24 / 4	37.30	black quartz	-25.93	-19.23	19.2			
13	OW 24 / 4	37.30	black quartz	-26.00	-19.41	19.0			
14	OW 24 / 4	37.30	black quartz	-25.92	-19.67	18.8			
15	OW 24 / 4	37.30	black quartz	-25.97	-19.40	19.0			

Appendix B: Stable Isotope Data - Quartz

Sample No.	Drillhole	Depth (m)	Phase sampled	Delta 1	Delta 2	$\delta^{18}O$ (SMOW)	Mean $\delta^{18}O$	$\sigma\ \delta^{18}O$	Comment
MALLOW									
1	Subutler	Outcrop (GR 1443 1042)	Post dolomite quartz	-25.85	-16.91	21.62	**20.72**	**0.60**	
2	Subutler	Outcrop (GR 1443 1042)	Post dolomite quartz	-25.88	-17.96	20.52			
3	Subutler	Outcrop (GR 1443 1042)	Post dolomite quartz	-25.87	-17.16	21.36			
4	Subutler	Outcrop (GR 1443 1042)	Post dolomite quartz	-25.82	-17.60	20.90			
5	Subutler	Outcrop (GR 1443 1042)	Post dolomite quartz	-26.00	-18.89	19.56			
6	Subutler	Outcrop (GR 1443 1042)	Post dolomite quartz	-25.98	-16.84	21.70			
7	Subutler	Outcrop (GR 1443 1042)	Post dolomite quartz	-25.86	-17.84	20.65			
8	Subutler	Outcrop (GR 1443 1042)	Post dolomite quartz	-25.81	-17.51	21.00			
9	Subutler	Outcrop (GR 1443 1042)	Post dolomite quartz	-25.71	-17.99	20.50			
10	Subutler	Outcrop (GR 1443 1042)	Post dolomite quartz	-25.79	-17.51	20.88			
11	Subutler	Outcrop (GR 1443 1042)	Post dolomite quartz	-25.84	-17.76	20.74			
12	Subutler	Outcrop (GR 1443 1042)	Post dolomite quartz	-25.86	-17.20	21.32			
13	Subutler	Outcrop (GR 1443 1042)	Post dolomite quartz	-25.86	-18.54	19.93			
14	Subutler	Outcrop (GR 1443 1042)	Post dolomite quartz	-25.93	-18.36	20.12			
15	Subutler	Outcrop (GR 1443 1042)	Post dolomite quartz	-25.87	-18.51	19.96			
16	Subutler	Outcrop (GR 1443 1042)	Post dolomite quartz	-25.91	-18.26	20.22			
17	Subutler	Outcrop (GR 1443 1042)	Post dolomite quartz	-25.81	-17.34	21.18			
18	Subutler	Outcrop (GR 1443 1042)	Post dolomite quartz	-25.94	-17.64	20.86			
1	Subutler	Outcrop (GR 1443 1042)	Pre dolomite quartz	10.36	8.63	17.29	**17.93**	**0.71**	
2	Subutler	Outcrop (GR 1443 1042)	Pre dolomite quartz	10.26	9.09	17.75			
3	Subutler	Outcrop (GR 1443 1042)	Pre dolomite quartz	10.44	9.50	18.16			
4	Subutler	Outcrop (GR 1443 1042)	Pre dolomite quartz	10.60	10.41	19.08			? May be post dol qtz
5	Subutler	Outcrop (GR 1443 1042)	Pre dolomite quartz	10.03	8.49	17.14			7.6E-10 + 1.5‰
6	Subutler	Outcrop (GR 1443 1042)	Pre dolomite quartz	10.03	9.49	18.15			6.6E-10 + 2‰
CARLOW									
1	Quinagh borehole	36.8 - 37	Post dolomite quartz	10.50	10.26	18.93	**20.28**	**0.95**	
2	Quinagh borehole	36.8 - 37	Post dolomite quartz	10.49	10.47	19.15			

Appendix B: Stable Isotope Data - Quartz

Sample No.	Drillhole	Depth (m)	Phase sampled	Delta 1	Delta 2	$\delta^{18}O$ (SMOW)	Mean $\delta^{18}O$	$\sigma\ \delta^{18}O$	Comment
3	Quinagh borehole	36.8 - 37	Post dolomite quartz	10.59	11.74	20.42			
4	Quinagh borehole	36.8 - 37	Post dolomite quartz	10.64	12.30	20.99			
5	Quinagh borehole	36.8 - 37	Post dolomite quartz	10.75	12.79	21.49			
6	Quinagh borehole	36.8 - 37	Post dolomite quartz	10.75	11.19	19.87			
7	Quinagh borehole	36.8 - 37	Post dolomite quartz	10.56	12.60	21.30			
8	Quinagh borehole	36.8 - 37	Post dolomite quartz	10.30	11.43	20.11			
1	Quinagh borehole	36.8 - 37	Pre dolomite quartz	10.47	12.45	21.15	**20.16**	**0.77**	1.8E-9 + 0.23‰
2	Quinagh borehole	36.8 - 37	Pre dolomite quartz	10.28	11.66	20.35			1.2E-9 + 1‰
3	Quinagh borehole	36.8 - 37	Pre dolomite quartz	10.08	10.70	19.38			1.05E-9 + 1‰
4	Quinagh borehole	36.8 - 37	Pre dolomite quartz	10.75	11.09	19.77			0.9E-10 + 1.2‰

APPENDIX C

FLUID INCLUSION DATA AND HISTOGRAMS

Appendix C: Fluid Inclusion Data

Sample Number	Location	Size (μm)	(ψ_{liquid})	Shape	Th	Tfm	Tm_{ice}	Tm_h	XNaCl	$XCaCl_2$	Ca/Na	Total Salinity
NEWCASTLE WEST												
OW 28 Dolomite 5.1.1	CD rhomb	20	0.9	negative	161.6	-49	-22.5	-11.3	21.2	3.6	0.3	24.8
OW 28 Dolomite 5.2.2	CD rhomb	4	0.9	oblate	188.5	-52	-22	-11	22.3	2.3	0.2	24.6
OW 28 Dolomite 5.2.3	CD rhomb	8	0.85	anhedral	170.5	-54.2	-23.5	-11.5	19.5	6.3	0.6	25.7
OW 28 Dolomite 5.3.4a	CD rhomb	5	0.85	irregular	159.5							
OW 28 Dolomite 5.3.4b	CD rhomb	5	0.85	subangular	162							
OW 28 Dolomite 5.4.5	CD rhomb	10	0.9	elongate	171.7	-55	-23	-10.1	20.5	4.9	0.5	25.4
OW 28 Dolomite 5.4.6a	CD rhomb	4	0.85	irregular	149	-52	-24	-10.6	18.6	7.5	0.8	26.1
OW 28 Dolomite 5.4.6b	CD rhomb	3	0.85	elongate	148.4							
OW 28 Dolomite 5.4.6c	CD rhomb	2	0.85	elongate	195.1							
OW 28 Dolomite 5.4.6d	CD rhomb	2	0.85	oblate	198.7							
OW 24 Dolomite M1b	CD rhomb	15	0.9	negative	181	-54.4	-21.9	-11.9	22.5	2.0	0.8	24.5
OW 24 Dolomite M1a	CD rhomb	10	0.9	rectangular	175.9	-53.8						
OW 24 Dolomite M2a	CD rhomb	6	0.9	irregular	124.8							
OW 24 Dolomite M2b	CD rhomb	8	0.9	rectangular	136.8							
OW 24 Dolomite M2c	CD rhomb	3	0.9	rounded	166.8							
OW 24 Dolomite M3a	CD rhomb	10	0.9	square	195.8							
OW 24 Dolomite M3b	CD rhomb	4	0.9	square	166.2							
OW 28 Qtz 1.5.7	Quartz	4	0.8	irregular	187.4							
OW 28 Qtz 3.1.7a	Quartz	4	0.8	irregular	147.7	-52	-24	-23.4	17.1	7.8	0.9	24.8
OW 28 Qtz 3.1.7b	Quartz	3	0.8	oblate	145.5							
OW 28 Qtz 3.1.7c	Quartz	3	0.8	rounded	166.2							
OW 24 Qtz 11.C1	Quartz	4	0.9	rounded	171.6	-52.3	-24.5	-24.1	16.1	9.0	1.1	25.1
OW 24 Qtz 11.C2	Quartz	4	0.9	rounded	130.7	-50.7	-22.8	-22.4	19.3	4.6	0.5	23.9
OW 24 Qtz 11.C3	Quartz	4	0.9	rounded	159.3	-51.2	-25.8	-24.9	13.7	11.8	1.6	25.6
OW 24 Qtz 11.C4	Quartz	4	0.9	rounded	157.2	-54.2	-26.1	-25.7	13.2	12.4	1.8	25.6
OW 24 Qtz 11.C5	Quartz	3	0.9	rounded	155.1	-53.5	-26	-25.6	13.3	12.2	1.7	25.6
OW 24 Qtz 11.C6	Quartz	3	0.9	rounded	155.5	-52.3	-28.7	-25.8	9.7	16.4	3.2	26.1
OW 24 Qtz 11.C7	Quartz	3	0.9	rounded	159.8	-51.6	-25.8	-24.9	13.7	11.8	1.6	25.6

Appendix C: Fluid Inclusion Data

Sample Number	Location	Size (μm)	(ψ_{liquid})	Shape	Th	Tfm	Tm_{ice}	Tm_h	XNaCl	$XCaCl_2$	Ca/Na	Total Salinity
OW 24 Qtz 11.C8	Quartz	3	0.9	square	161.4	-50.9	-27.7	-24.9	11.0	15.0	2.6	26.1
OW 24 Qtz 11.C9	Quartz	3	0.9	irregular	161.3							
OW 24 Qtz 11.C10	Quartz	3	0.9	rounded	154.3							
OW 24 Qtz 11.C11	Quartz	5	0.95	negative	166.1	-50.3	-26.3	-25	13.0	12.8	1.9	25.8
OW 24 Qtz 11.C12	Quartz	5	0.9	rounded	166.5							
MALLOW												
Dolomite A 1	Inner zone	8	0.8	rhombic	134.7	-50.5	-23.1					
Dolomite B 3.2.1	Inner zone	4	0.8	rhombic	137.4							
Dolomite B 3.2.2	Inner zone	10	0.8	negative	155.2							
Dolomite D 3.2.1	Inner zone	6	0.9	negative subhedral	140.4	< -49.2						
Dolomite D 3.2.2	Inner zone	6	0.9	subhedral	160.1							
Dolomite D 3.2.3	Inner zone	4	0.9	subhedral	155							
Dolomite E 5.2.1	Inner zone	20	0.8	negative	141.5	-55	-27.2					
Dolomite E 5.2.2	Inner zone	5	0.8	elongate	126.2							
Dolomite E 5.2.3	Inner zone	4	0.8	rhombic	130.7							
Dolomite E 5.2.4	Inner zone	6	0.8	elongate	128.2							
Dolomite E 5.2.5	Inner zone	4	0.8	rhombic	126							
Dolomite F 3.1	Inner zone	12	0.8	rectangular	124	-54	-22.5	-26.7	10.8	12.1	2.1	22.9
Dolomite G 3.1	Inner zone	20	0.9	negative	125	-54.8	-23.6	-26.5	11.5	12.1	2.0	23.6
Dolomite E1.1	Outer zone	2	0.85	square	134.8							
Dolomite E 1.2	Outer zone	2.5	0.9	irregular	123.1							
Dolomite D 1.1	Inner zone	2.5	0.9	rectangular	127.7			-26.2				
Dolomite D 1.2	Inner zone	1.5	0.9	rounded	120.9							
Dolomite D 1.3	Inner zone	1.5	0.9	rounded	134.7							
Dolomite D 2.1	Inner zone	2	0.9	irregular	123.1							
Dolomite D 2.2	Inner zone	8	0.9	irregular	129.8	-54.6						
Dolomite D 2.3	Inner zone	4	0.9	irregular	127							
Dolomite G 1.1	Inner zone	20	0.85	irregular	119.2	-54.3		-27.5				
Dolomite G 1.2.1	Inner zone	2	0.9	square	132.4							

Appendix C: Fluid Inclusion Data

Sample Number	Location	Size (μm)	(ψ_{liquid})	Shape	Th	Tfm	Tm_{ice}	Tm_h	XNaCl	$XCaCl_2$	Ca/Na	Total Salinity
Dolomite G 1.2.2	Inner zone	2	0.9	rounded	124.6							
Dolomiite G 1.2.3	Inner zone	2	0.9	elongate	120.5							
Dolomite G 2.1	Inner zone	4	0.9	negative	115.9							
Dolomite G 3.1b	Outer zone	5	0.9	square	123.5	-54.3	-25.4	-26.2	12.5	12.2	1.8	24.7
Dolomite G 4.1	Inner zone	10	0.85	negative	109.2	-54.4	-24.6	-27.2	17.6	6.0	0.6	23.7
Dolomite G 4.2.1	Outer zone	20	0.9	negative	129.3	-54.7	-22.6	-23.4	16.0	8.0	0.9	24.0
Dolomite G 4.2.2	Outer zone	8	0.9	negative	127.8	-54.7	-23.4	-24.2	10.6	13.4	2.4	24.0
Post dolo Qtz A 1.2	Vug	15	0.9	elongate	82	-54.2	-16.5	-26.2	9.7	9.5	1.8	19.2
Post dolo Qtz A 1.3	Vug	35	0.9	irregular	83.4	-53	-16.5					
Post dolo Qtz B 1e	Vug	6	0.9	elongate	78.3							
Post dolo Qtz A 1.2	Vug	12	0.9	negative (6-sided)	87.4	-55	-17					
Post dolo Qtz C 3	Vug	15	0.9	irregular	78							
Post dolo Qtz A 1.1	Vug	8	0.9	negative (6-sided)	82.1	-55	-16.4					
Post dolo Qtz Ba	Vug - 2nd trail	4	0.9	irregular	126							
Post dolo Qtz Bb	Vug - 2nd trail	4	0.9	rounded	132.5							
Post dolo Qtz Bc	Vug - 2nd trail	4	0.9	rounded	140.5							
Post dolo Qtz Bd	Vug - 2nd trail	4	0.9	rounded	103.1							
Pre dolo qtz D.2	Predates dol	1	0.85	elongate	123.5							
Pre dolo qtz D.4	Predates dol	2	0.8	elongate	149							
Pre dolo qtz D.5	Predates dol	2	0.85	elongate	134.8							
Pre dolo qtz D.6	Predates dol	2	0.85	elongate	133.9							
Pre dolo qtz D.B1	Predates dol	13	0.85	elongate	125.2	-54	-26.1	? -25				
Pre dolo qtz D.B3	Predates dol	6	0.85	rounded	105	-54.2	-26.2					
Pre dolo qtz F.A.1	Predates dol	5	0.9	square	135.4	-54.4	-27.6	-30.2	7.3	17.7	4.6	25.0
Pre dolo qtz F.A.2.1	Predates dol	8	0.9	rounded	127.4	-54.7	-27.9					
Pre dolo qtz F.A.2.2	Predates dol	10	0.9	rounded	134.5	-54.8	-27.9					
Pre dolo qtz F.A.2.3	Predates dol	22	0.9	irregular	134	-54.6		-30.3				
Pre dolo qtz F.A.3	Predates dol	6	0.9	negative (6-sided)	122.7	-54.7	-27.4					

Appendix C: Fluid Inclusion Data

Sample Number	Location	Size (μm)	(ψ_{liquid})	Shape	Th	Tfm	Tm_{ice}	Tm_h	XNaCl	$XCaCl_2$	Ca/Na	Total Salinity
CARLOW												
Dolomite A1	CD rhomb	10	0.8	irregular	264.7	-48	-13.4	-25	10.2	6.8	1.3	17.0
Dolomite A2	CD rhomb	5	0.8	irregular	234	-50.1	-14.8	-24.5	11.6	6.5	1.1	18.1
Dolomite A3	CD rhomb	5	0.8	rounded	265	-54	-14.5	-22.9	14.3	3.6	0.5	18.0
Dolomite B1	CD rhomb	5	0.85	irregular	192.7							
Dolomite C1.1	Inner zone	2	0.8	elongate	232.5							
Dolomite C1.2	Inner zone	3	0.8	elongate	219.5							
Dolomite D1	CD rhomb	4	0.85	elongate	267							
Dolomite E1.1	Inner zone	4	0.8	negative	230.6							
Dolomite E1.2	Inner zone	7	0.8	irregular	228.1							
Dolomite E1.3	Inner zone	3	0.8	rounded	229.8							
Dolomite E1.4	Inner zone	3	0.8	rounded	211							
Dolomite E1.5	Inner zone	3	0.8	rounded	212.6							
Dolomite E1.6	Inner zone	10	0.75	irregular	243							
Dolomite E1.7	Inner zone	3	0.8	rounded	211							
Dolomite E1.8	Inner zone	3	0.8	oblate	224.4							
Dolomite E2.1	CD rhomb	2	0.8	rounded	257.6							
Dolomite E2.2	CD rhomb	5	0.8	rounded	226							
Dolomite E2.3	CD rhomb	2	0.8	rounded	253.4							
Dolomite E2.4	CD rhomb	3	0.8	irregular	253.2							
Dolomite E3.1	CD rhomb	3	0.8	irregular	251.8							
Dolomite E3.2	CD rhomb	4	0.8	negative	248.1							
Dolomite E3.3	CD rhomb	4	0.8	rounded	246.5							
Dolomite E3.4	CD rhomb	3	0.8	rounded	238.6							
Dolomite E3.5	CD rhomb	4	0.8	irregular	249.5							
Dolomite E3.6	Outer zone	4	0.8	irregular	239.2							
Dolomite E3.7	Outer zone	4	0.8	elongate	262.2							
Dolomite E4.1	Inner zone	5	0.8	rectangular	252.6	-49.8						
Quartz A1	Post dolo vug qtz	50	0.8	irregular	214.7	-54.6	-22.7	-16.5	20.2	4.2	0.4	24.4

Appendix C: Fluid Inclusion Data

Sample Number	Location	Size (μm)	(ψ_{liquid})	Shape	Th	Tfm	Tm_{ice}	Tm_h	XNaCl	$XCaCl_2$	Ca/Na	Total Salinity
Quartz A2	Post dolo vug qtz	25	0.85	elongate	174	-54.8	-25	-16.5	16.3	9.9	1.2	26.2
Quartz A3.1	Post dolo vug qtz	10	0.85	elongate	185							
Quartz A3.2	Post dolo vug qtz	35	0.85	irregular	193	-54.2	-25.5					
Quartz A3.3	Post dolo vug qtz	15	0.85	irregular	275	-54.1						
Quartz A3.4	Post dolo vug qtz	20	0.85	elongate	187.2	-54.9	-25.4					
Quartz A3.5	Post dolo vug qtz	15	0.85	irregular	195	-54						
Quartz A4	Post dolo vug qtz	50	0.9	elongate	196.1	-53.3	-24.2	-22.9	16.8	8.2	0.9	25.1
Quartz A5.1	Post dolo vug qtz	25	0.9	elongate	187.3	-53.2						
Quartz A5.2	Post dolo vug qtz	25	0.9	elongate	195.4	-52						
Quartz A5.3	Post dolo vug qtz	25	0.9	elongate	198.3	-53.3	-25.8	-22.8	14.1	11.7	1.6	25.9
Quartz A5.4	Post dolo vug qtz	10	0.9	rounded	190	-52.7	-24.6	-23.9	15.9	9.2	1.1	25.2
CxHy inclusions					**Th 1**	**Th 2**	**Tm 1**					
Quartz OI CA1	Qtz within fg dolo	25	0.85	elongate	115.2	24.7	-86.5					
Quartz OI CA2	Qtz within fg dolo	18	0.85	negative	114	27.4	-85.4					
Quartz OI CA3	Qtz within fg dolo	8	0.85	rounded	112.4	25.2	-85.7					
Quartz OI CB1	Qtz within fg dolo	12	0.9	irregular	88.3	39.2	-85.6					
Quartz OI CB2	Qtz within fg dolo	8	0.9	irregular	119.1	14.4	-85.9					
Quartz OI CC1	Qtz within fg dolo	25	0.85	irregular	49.7		-85.6					
Quartz OI CC2	Qtz within fg dolo	5	0.9	rounded	86.3	45.9	-85.6					
Quartz OI CC3	Qtz within fg dolo	6	0.85	rounded	59.4		-86					
Quartz OI CC4	Qtz within fg dolo	10	0.9	elongate	62.8		-85.6					
LISHEEN												
Dolomite J1.a	CD rhomb	7	0.85	negative	177			-6.8				
Dolomite J1.c	CD rhomb	8	0.85	negative	183.4							
Dolomite J1.d	CD rhomb	6	0.9	negative	236.2	<-47.7						
Dolomite J2.a	CD rhomb	9	0.9	rectangular	172.6	-53.2	-23.3	-11	19.8	5.7	0.5	25.6
Calcite JA.a	Stage D calcite	12.8	0.7	irregular	215.4	-53.2	-3.1					

Appendix C: Fluid Inclusion Data

Sample Number	Location	Size (μm)	(ψ_{liquid})	Shape	Th	Tfm	Tm_{ice}	Tm_h	XNaCl	$XCaCl_2$	Ca/Na	Total Salinity
Calcite JA.b	Stage D calcite	22	0.7	irregular	203.5	-54.6						
Calcite JA.c	Stage D calcite	8	0.9	rounded	178.1							
Calcite JA.d	Stage D calcite	12	0.9	rounded	185.5	-54.6						
Calcite JA.e	Stage D calcite	16	0.9	rounded	211							
URLINGFORD												
Dolomite HA.1	CD rhomb	4	0.9	rectangular	147.9	-49.2	-17.6	-20.8	20.7			20.7
Dolomite HA.6	CD rhomb	1.5	0.9	square	181							
Dolomite HA.7	CD rhomb	3	0.9	elongate	136.5							
Dolomite HA.3	CD rhomb	2.5	0.9	square	131.1							
Dolomite HB.1	Outer Zone	2	0.9	rounded	133.7							
Dolomite HA.4	Outer Zone	6	0.9	irregular	126.2							
Dolomite HA.2	CD rhomb 2nd trail	2.5	0.9	irregular	110.9							
Dolomite HA.3	CD rhomb 2nd trail	2.5	0.9	irregular	110							
Dolomite HA.4	CD rhomb 2nd trail	2.5	0.9	irregular	110.4							
MULLAWORNIA												
Dolomite A1	CD rhomb - Zone 3 (Fe)	5	0.9	rectangular	149.9		-5		7.9			7.9
Dolomite A2	CD rhomb - Zone 3 (Fe)	2	0.9	rounded	146							
Dolomite B1	CD rhomb - Zone 3 (Fe)	1	0.9	rounded	182.9							
Dolomite B2	CD rhomb - Zone 3 (Fe)	3	0.9	rectangular	178.9							
Dolomite B3	CD rhomb - Zone 4	1	0.9	rounded	165.3							
Dolomite B4	CD rhomb - Zone 4	1	0.9	rectangular	161.9							

Appendix C: Fluid Inclusion Histograms

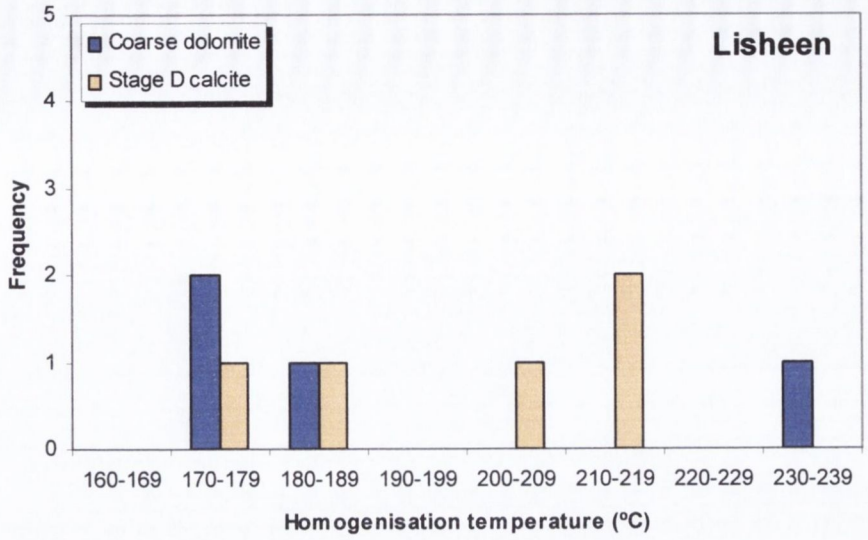

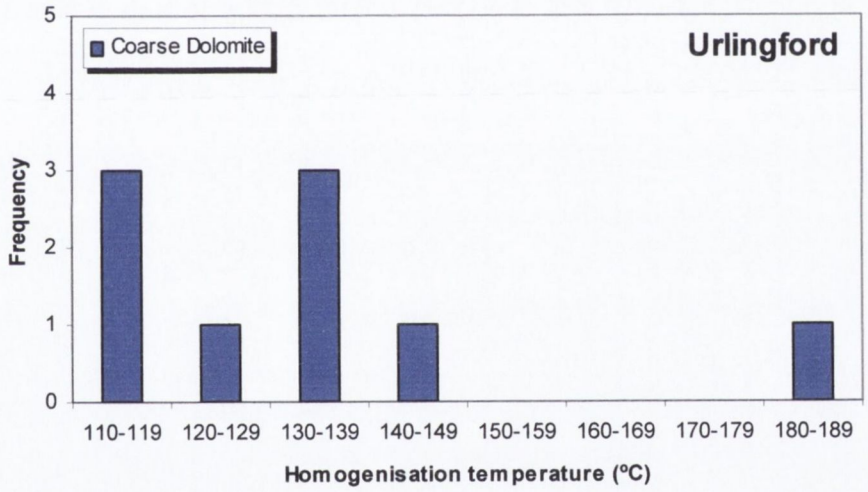

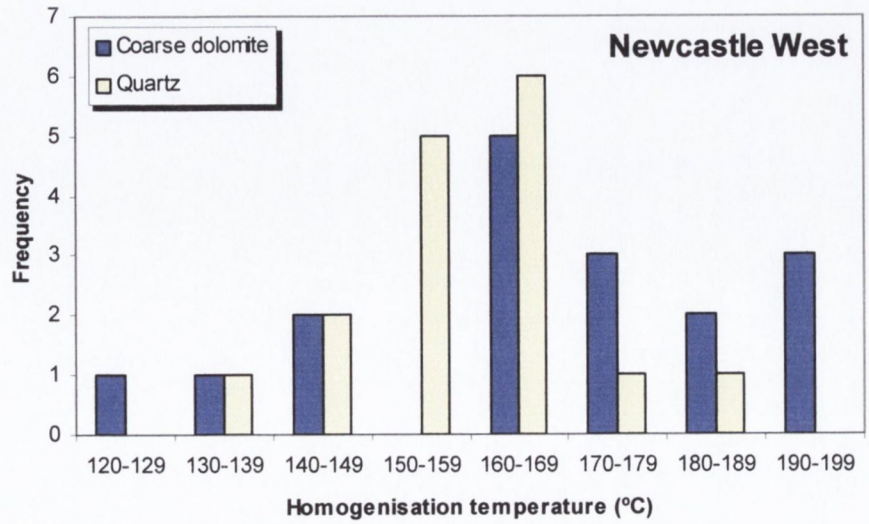

Appendix C: Fluid Inclusion Histograms

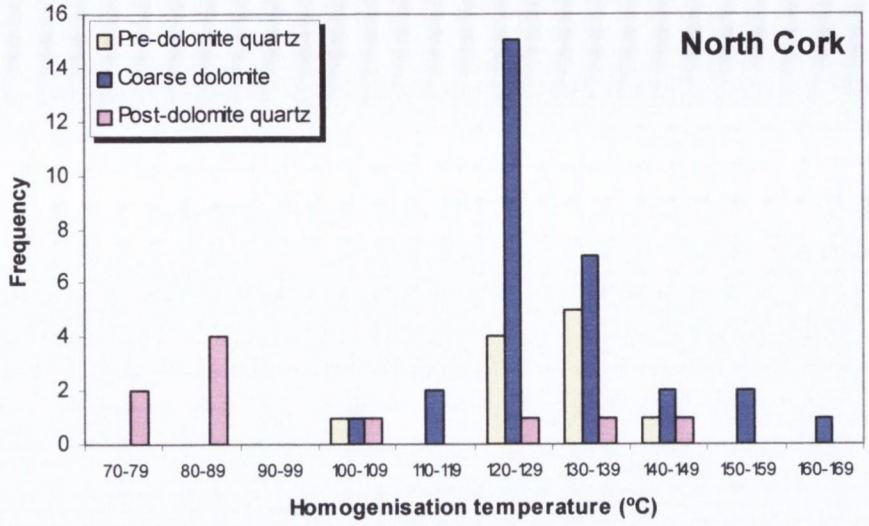

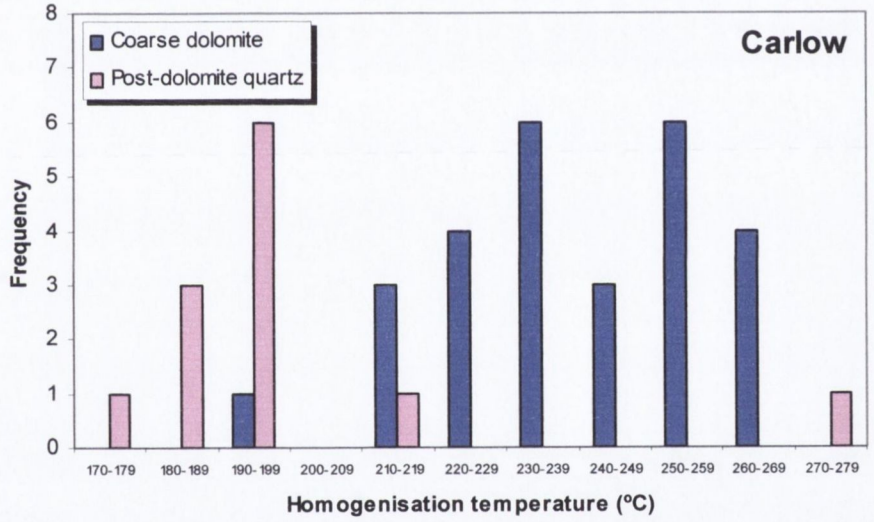

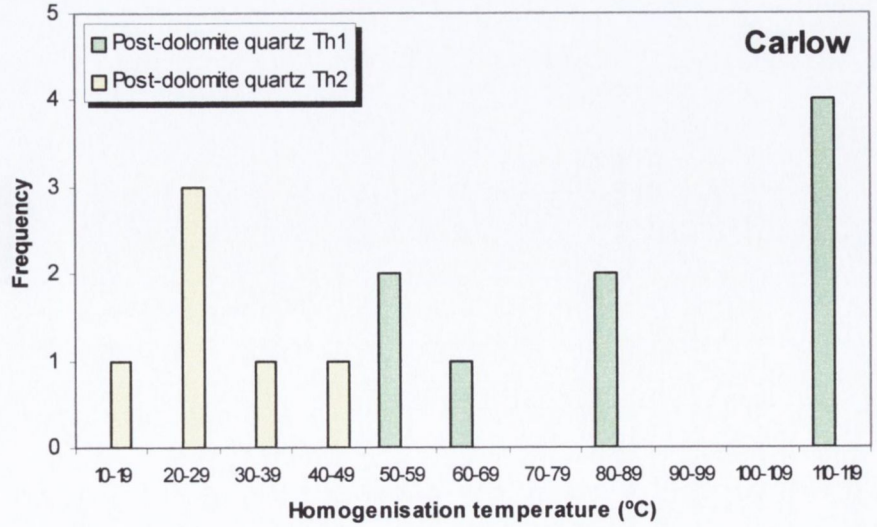

Appendix C: Fluid Inclusion Histograms

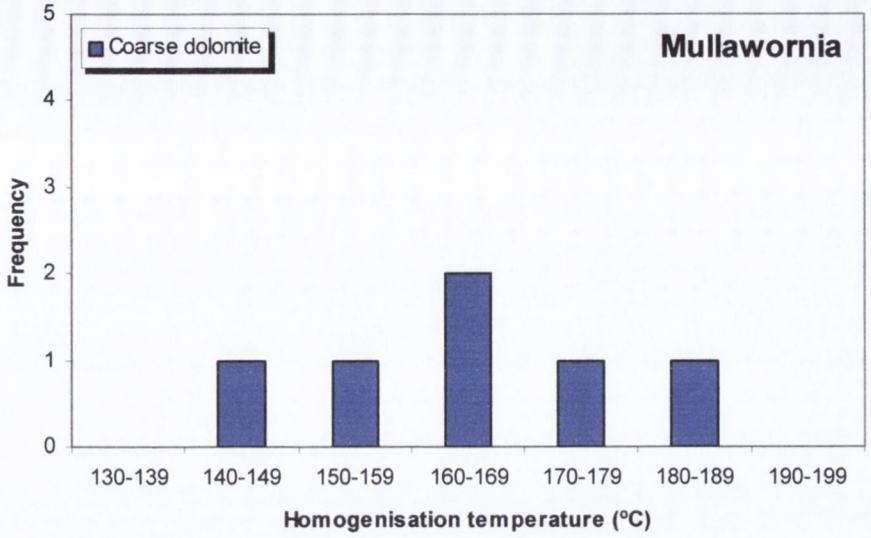

APPENDIX D

CRUSH-LEACH DATA

Appendix D: Crush Leach Data

			Measured values							Calculated values										
Sample	**Mineral**	**Salinity***	**Cl mg/L**	**Br mg/L**	**F mg/L**	**SO_4 mg/L**	**Na ppm**	**K ppm**	**Li mg/L**	**Cl/Br molar**	**Na/Br molar**	**Na/Li wt ratio**	**Na/K wt ratio**	**Cl ppm**	**Br ppm**	**Na ppm**	**K ppm**	**Li ppm**	**Log Cl ppm**	**Log Br ppm**	**Charge Balance**
Newcastle West																					
OW24	Quartz	25.5	4.31	0.014	n.a.	n.a.	1.8	0.16	0.025	675	426	230	6.43	154733	517	63230	5770	913	5.19	2.71	
OW28	Quartz	24.8	2.32	0.008	n.a.	n.a.	1.0	0.27	0.004	634	408	789	2.12	150485	535	62681	17380	264	5.18	2.73	
OW24	Dolomite	24.5	4.48	0.028	**0.005**	0.13	3.3	3.33	0.021	361	409	520	0.58	148665	928	109079	110405	696	5.17	2.97	1.8
OW28	Dolomite	25.3	21.62	0.134	0.01	0.29	9.6	5.20	0.006	364	250	5327	1.09	153519	951	68374	36921	43	5.19	2.98	0.9
Lisheen																					
LK 2258-38	Dolomite	25.6	6.90	0.052	0.038	0.12	3.9	3.60	0.005	299	258	2556	0.63	155340	1171	86675	81047	113	5.19	3.07	1.3
North Cork																					
Subulter	Pre dol qtz	25	3.46	0.024	**0.005**	0.31	1.4	**0.03**	**0.005**	325	203	929	27.40	151699	1053	61452	1317	219	5.18	3.02	0.6
Subulter	Dolomite	23.8	21.61	0.125	0.009	0.70	9.3	2.36	**0.005**	390	259	6180	2.32	144417	835	62215	15771	33	5.16	2.92	0.7
Subulter	Post dol qtz	19.2	3.89	**0.005**	**0.005**	0.10	2.3	**0.03**	0.018	1754	1572	417	44.23	116505	150	67652	898	539	5.07	2.18	0.9
Carlow																					
Quinagh	Dolomite	17.7	3.18	0.016	0.155	0.08	2.2	**0.03**	0.025	448	470	287	42.28	107403	540	72907	1013	844	5.03	2.73	0.9
Quinagh	Post dol qtz	25.4	2.42	0.010	**0.005**	0.71	1.9	3.10	0.007	545	664	906	0.36	154126	638	121796	197679	446	5.19	2.80	2.0
Clonmelsh	Dolomite	17.7	12.92	0.069	0.21	0.18	7.7	0.71	0.103	422	387	247	6.34	107403	574	63760	5902	856	5.03	2.76	0.9
Clonmelsh	Post dol qtz	25.4	12.52	0.075	**0.005**	1.82	7.2	0.56	0.016	376	332	1485	7.51	154126	923	88121	6892	197	5.19	2.97	0.8
Urlingford																					
LK 3246-15	Dolomite	20.7	3.10	0.012	0.029	0.26	2.2	0.08	**0.005**	583	626	1434	15.85	125607	486	87407	3237	202	5.10	2.69	1.0

* Salinity given in combined weight % NaCl and CaCl2 equivalent except for Urlingford data which is given in weight % NaCl equivalent.

Values in bold are the detection limits for the elements concerned and indicate a maximum value for these samples. The maximum error for each sample is 5%.

n.a. = not analysed.

APPENDIX E

XRD TRACES

Appendix E: XRD Traces

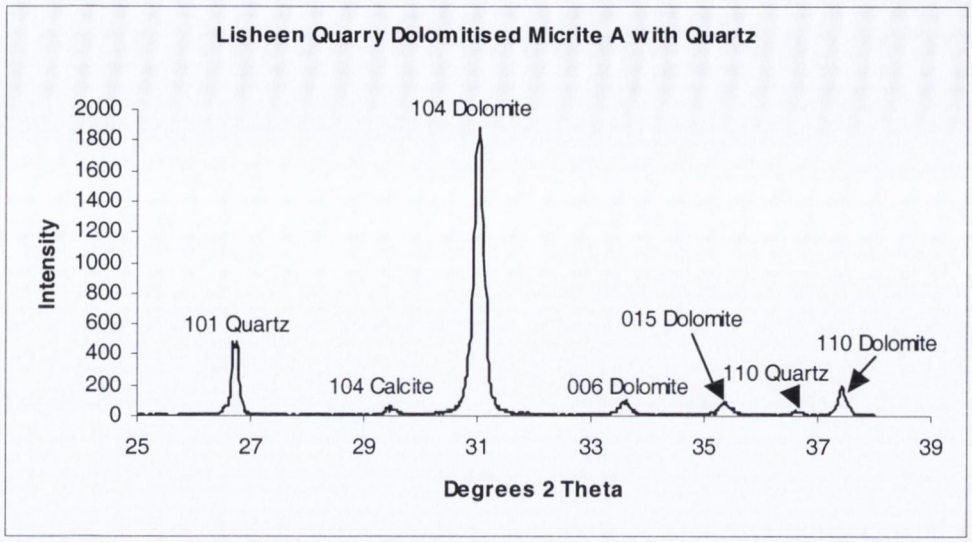

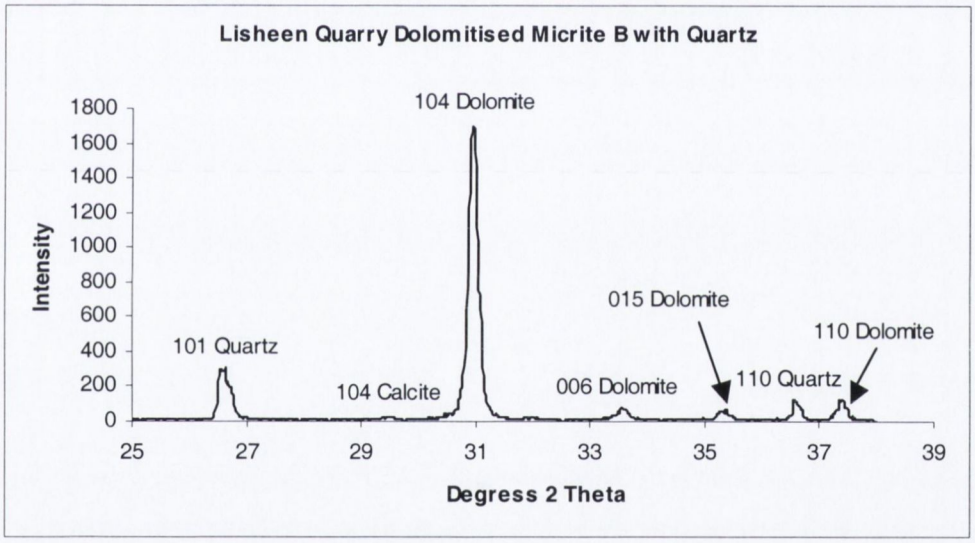

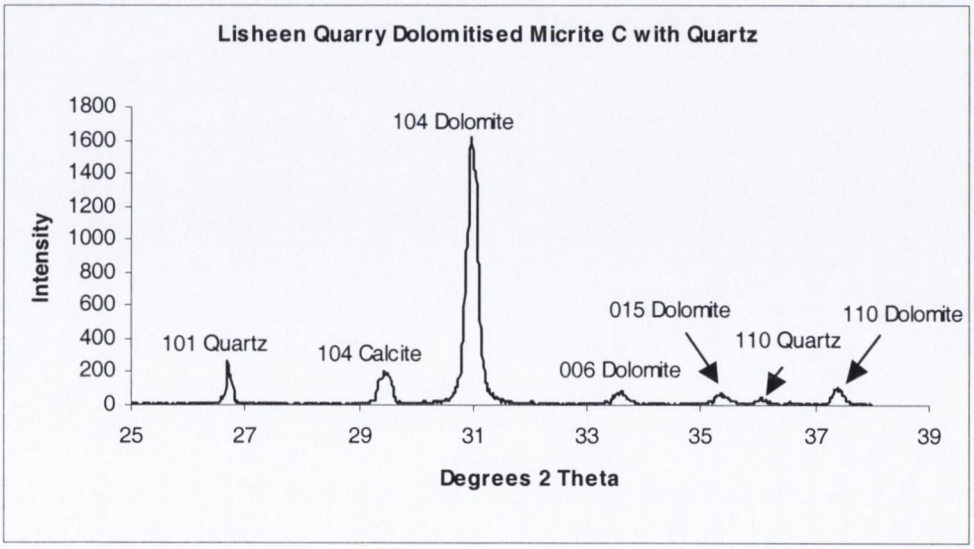

Appendix E: XRD Traces

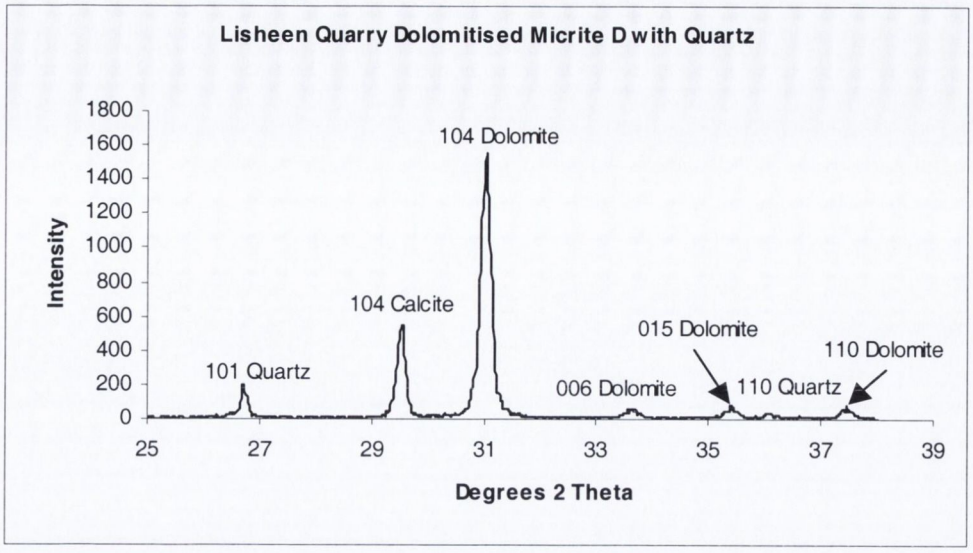

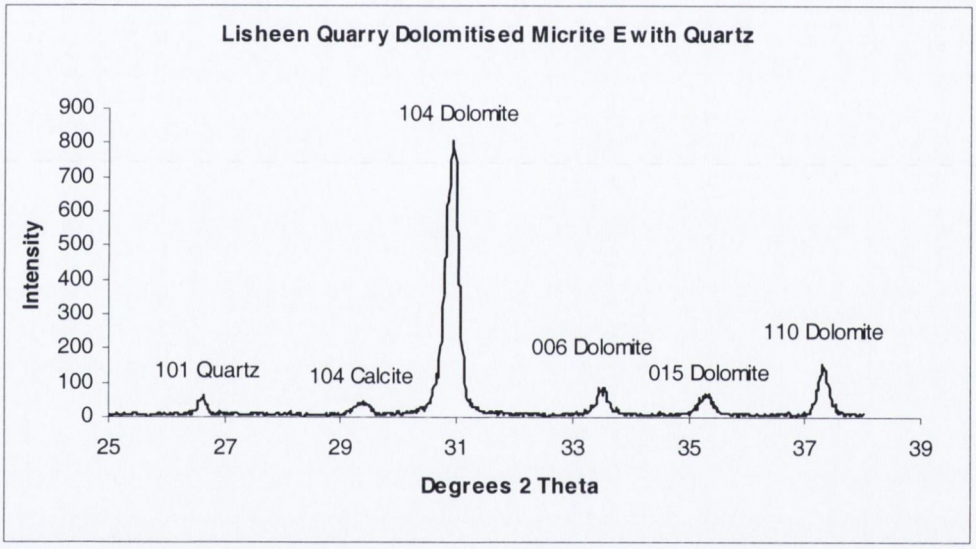

APPENDIX F

DRILLHOLE DATA FROM THE RATHDOWNEY TREND

Appendix F: Drillhole data from the Rathdowney Trend

Drillhole Number	Easting	Northing	Dip	Azimuth	EOH (m)	Regional Dolomite (Y/N)
00-3158-16	241250	189440	90	0	17	N
00-3158-17	241400	190200	90	0	36	N
01-2258-38	220901.8	169288.1	80	8	265	N
1650-02	241209	187801	90	0	75.29	N
1650-03	241615	188582	90	0	43.59	N
1650-04	241522	187857	90	0	59.74	N
1650-05	241275	187637	90	0	78.33	N
1650-06	241050	188409	90	0	38.71	N
1650-07	240741	188415	90	0	66.45	N
1650-08	241064	188313	90	0	44.2	N
1650-09	235030	184867	90	0	44.5	N
1650-10	235321	185014	90	0	111.25	N
1650-11	241146	187754	90	0	93.57	N
1650-12	241061	187795	90	0	96.32	N
1650-13	241148	187805	90	0	90.53	N
1650-14	241145	187723	90	0	99.97	N
1650-15	241140	187680	90	0	105.46	N
1650-16	241214	187767	90	0	81.08	N
1650-17	241066	187751	90	0	102.72	N
1650-18	241136	187912	90	0	92.66	N
1650-19	240969	187931	90	0	108.81	N
1650-20	240311	187284	90	0	239.88	N
1650-21	240753	187257	90	0	156.97	N
1650-22	241050	187172	90	0	99.06	N
1650-23	241061	187494	90	0	119.48	N
1650-24	240468	188529	90	0	96.01	N
1650-25	240737	188170	90	0	117.65	N
1650-26	240904	188270	90	0	114.6	N
1650-27	240921	187229	90	0	106.98	N
1650-28	240749	188609	90	0	53.34	N
1650-29	240894	188030	90	0	88.7	N
1650-30	240903	187458	90	0	131.67	N
1650-31	241233	187180	90	0	58.52	N
1650-32	241060	187011	90	0	94.49	N
1650-33	241051	187333	90	0	104.24	N
1650-34	240900	187778	90	0	142.34	N
1650-35	241070	187606	90	0	135.94	N
1650-36	241223	188164	90	0	90.22	N
1650-37	240937	187014	90	0	81.08	N
1650-38	241420	188346	90	0	38.4	N
1650-39	241691	187021	90	0	117.96	N
1650-40	241386	186693	90	0	84.12	N
1650-41	241373	187447	90	0	38.4	N
1650-42	241924	187306	90	0	30.18	N
1650-43	236230	184774	90	0	62.48	N
1650-44	242124	186776	90	0	68.88	N
1650-45	242429	186232	90	0	135.64	N
1650-46	240462	187928	90	0	162.15	N
1650-47	241520	187207	90	0	32.61	N
1650-48	241986	185781	90	0	153.01	N
1650-49	240333	186364	90	0	118.26	N
1650-50	237606	187221	90	0	132.59	N

Appendix F: Drillhole data from the Rathdowney Trend

Drillhole Number	Easting	Northing	Dip	Azimuth	EOH (m)	Regional Dolomite (Y/N)
1650-51	236673	185978	90	0	197.21	N
1650-52	235562	185661	90	0	84.43	N
1650-53	237799	186771	90	0	191.41	N
1650-54	237152	185153	90	0	227.38	N
1650-55	239554	187123	90	0	150.88	N
1650-56	236738	186691	90	0	156.97	N
1650-57	237539	183956	90	0	208.48	N
1650-58	240344	185331	90	0	157.28	N
1650-59	236222	183714	90	0	163.37	N
1650-60	238376	185833	90	0	153.01	N
1650-61	239099	185057	90	0	198.42	N
1650-62	242151	188719	90	0	12.19	N
1650-63	239850	187870	90	0	135.9	N
1650-64	242640	186510	90	0	74.7	N
1650-65	236740	184280	90	0	169.2	N
1650-66	238000	184640	90	0	190.2	N
1653-01	230643	176098	90	0	54.9	N
1653-02	230215	175444	90	0	41.7	N
1653-03	231593	176878	90	0	264	N
1653-04	232206	178498	90	0	40	N
1653-05	231922	178666	90	0	92.6	N
1653-06	232705	180926	90	0	74.4	N
1653-07	230936	176041	90	0	209.7	N
1653-08	230539	175265	90	0	123.7	N
1653-09	231550	177101	90	0	191	N
1653-10	231776	176876	90	0	382.8	N
1653-11	231320	176889	90	0	1143	N
1653-12	231581	176658	90	0	318.2	N
1653-13	232206	177362	90	0	446.5	N
1653-14	232119	177965	90	0	178.3	N
1653-15	232421	179153	90	0	83.5	N
1653-16	232649	180364	90	0	102.1	N
1653-17	233189	179795	90	0	232.6	N
1653-18	232880	178590	90	0	290.7	N
1653-21	231700	177440	90	0	150.9	N
1653-22	231200	176650	90	0	150.9	N
1653-23	231880	177450	90	0	257.8	N
1653-24	232720	176550	90	0	546	N
1653-25	232050	176460	90	0	479.5	N
3158-01	238430	189510	90	0	9.5	N
3158-02	238724	187971	90	0	126.2	N
3158-03	238627	188812	90	0	62.8	N
3158-04	239736	189116	90	0	50.5	N
3158-05	243943	188885	90	0	162	N
3158-06	244590	190120	90	0	245.4	N
3158-07	244740	191760	90	0	29.3	N
3158-08	245030	191640	90	0	57.3	N
3158-09	243540	188270	90	0	253	N
87-1652-01	234033	182633	90	0	132.6	N
87-1652-02	233354	182393	90	0	38.25	N
87-3263-03	242950	187740	90	0	26	N
90-3263-08	242598	187412	90	0	35	N

Appendix F: Drillhole data from the Rathdowney Trend

Drillhole Number	Easting	Northing	Dip	Azimuth	EOH (m)	Regional Dolomite (Y/N)
90-3263-09	242416	187614	90	0	15.3	N
90-3263-10	242832	187172	90	0	45.7	N
90-3263-11	242717	187295	90	0	39	N
91-2069-01	208120	163670	90	0	49	N
91-2069-04	208490	163700	90	0	78.4	N
91-2069-05	208600	164130	90	0	15.2	N
91-2069-06	211530	161930	90	0	45.5	N
91-2069-07	208660	164485	90	0	21	N
91-2069-08	211500	162110	90	0	45.5	N
91-2069-09	211140	160980	90	0	29	N
91-2069-10	208455	163540	90	0	10.6	N
91-2258-08	219142.8	168697.03	90	0	229.2	N
91-2447-03	214451	164777	90	0	90.05	N
91-3262-06	219783.12	166465.03	90	0	423	N
92-2069-11	208180	163615	90	0	159.1	N
92-2069-12	214590	161430	90	0	76	N
92-2218-03	241838	184119	90	0	93	N
92-2218-04	242020	183988	90	0	215	N
92-2447-09	216762	166456	90	0	24	N
93-1652-11	237930	180006	90	0	16.7	N
93-2258-26	218357.64	168195.11	90	0	180.7	N
93-2447-11	218046.55	167797.48	90	0	36.5	N
96-2069-17	211500	163560	90	0	100.9	N
97-3263-13	243400	185860	90	0	34	N
98-2069-19	212510	161115	90	0	75	N
98-2069-20	213370	161100	90	0	92	N
98-3158-11	246380	194320	90	0	82	N
98-3688-01	241450	177570	90	0	14	N
98-3688-02	241380	177970	90	0	15	N
98-3688-03	241380	178590	90	0	17	N
98-3688-04	239820	178160	90	0	16	N
99-1650-79	240190	186910	90	0	60	N
99-1650-80	241760	186580	90	0	137	N
99-2447-28	214248.8	166962.4	90	0	49	N
99-2447-29	214251.6	166383.7	90	0	68	N
99-2447-30	213401.5	166773.1	90	0	26	N
00-1652-17	235000	178800	90	0	599	Y
00-2218-13	238920	180230	90	0	538	Y
00-3158-13	243200	189600	90	0	32	Y
00-3158-14	243860	190030	90	0	221	Y
00-3158-15	244340	190640	90	0	236	Y
00-3262-19	221641	168800	80	0	235.7	Y
00-3667-03A	233990	176100	90	0	709	Y
00-3667-04	234080	176370	90	0	737	Y
01-1650-81	237300	185654	90	0	247	Y
01-2258-39	220092.6	169957.8	90	180	182	Y
01-2258-40	218430	167900	60	60	91.5	Y
01-2447-31	215551.5	167385.7	90	0	106	Y
01-3263-18	243520	186320	90	0	160	Y
01-3263-19	243520	186300	90	0	442	Y
02-1578-04	217050	154160	80	180	530.5	Y
1650-01	241229	187592	90	0	75.9	Y

Appendix F: Drillhole data from the Rathdowney Trend

Drillhole Number	Easting	Northing	Dip	Azimuth	EOH (m)	Regional Dolomite (Y/N)
87-1652-03	234151	182110	90	0	157	Y
87-3263-01	243011	187039	90	0	181.6	Y
87-3263-02	242807	187201	90	0	75	Y
90-2258-01	218527.72	167423.3	90	0	98.75	Y
90-2258-02	218571.08	167817.78	90	0	62	Y
90-2447-01	217939.59	167375.03	90	0	48	Y
90-2448-01	218779.55	167106.52	90	0	86.15	Y
90-2448-02	218089.39	165749	90	0	60.05	Y
90-3263-04	243003	187676	90	0	56.7	Y
90-3263-05	242933	187352	90	0	32.5	Y
90-3263-06	243067	187852	90	0	102.2	Y
90-3263-07	242776	187234	90	0	53	Y
91-2069-02	207975	164100	90	0	28.1	Y
91-2069-03	208560	163450	90	0	54.1	Y
91-2258-06	219134.55	168216.61	90	0	195	Y
91-2258-07A	219099.14	168097.28	90	0	199.3	Y
91-2447-02	216157	164980	90	0	89.05	Y
91-2447-04	216156	165167	90	0	91.05	Y
91-2447-05	216122	165486	90	0	93	Y
91-2447-06	214660	165435	90	0	80	Y
91-2448-05	218489	163998	90	0	152.5	Y
91-3262-10	220081.64	168620.8	90	0	198	Y
91-3262-11	221488.94	166136.06	90	0	61	Y
91-3262-12	222385.83	166198.22	90	0	81.5	Y
92-1652-04	234583	180206	90	0	461.4	Y
92-1652-05	237857	182935	90	0	383.9	Y
92-1652-06	237870	182514	90	0	463.7	Y
92-1652-07	237853	182057	90	0	511.5	Y
92-1652-08	237913	181528	90	0	501.7	Y
92-2069-13	214080	161100	90	0	144	Y
92-2069-14	212430	159920	90	0	131	Y
92-2218-01	242379	184658	90	0	165.5	Y
92-2218-02	241899	184214	90	0	173.8	Y
92-2258-09	218712.22	168260.67	90	0	150	Y
92-2258-10	218666.4	167384.6	90	0	66	Y
92-2258-11	218789.62	167343.66	90	0	94.6	Y
92-2258-12	218917	168249.83	90	0	178.5	Y
92-2258-13	219067.58	167373.27	90	0	130.5	Y
92-2258-14	219175.78	167371.69	90	0	171	Y
92-2258-15	219141.19	167249.55	90	0	147	Y
92-2258-16	218959.48	167349.97	90	0	123	Y
92-2258-17	219211.39	167852.62	90	0	209	Y
92-2258-18	219091.16	167496.09	90	0	167	Y
92-2258-19B	218972	167861	90	0	185	Y
92-2447-07	216187	164822	60	0	64	Y
92-2447-08	217300	167110	90	0	76	Y
92-2447-10	213970	165564	90	0	89.9	Y
92-3263-12	242894	186032	90	0	147.4	Y
93-1652-09	237893	180935	90	0	524.4	Y
93-1652-10	236818	181158	90	0	526.7	Y
93-2258-20	218783.58	167854.37	90	0	115.1	Y
93-2258-25	218138.94	167904.47	90	0	28.5	Y

Appendix F: Drillhole data from the Rathdowney Trend

Drillhole Number	Easting	Northing	Dip	Azimuth	EOH (m)	Regional Dolomite (Y/N)
93-2258-27	218300	167700	90	0	68	Y
93-2258-28	219925	171500	90	0	107	Y
93-2258-29	221300	170640	90	0	176	Y
93-2258-30	221230	170010	90	0	239	Y
93-2447-12	217953	167693	90	0	49.2	Y
93-2447-13	218163.97	168195.86	90	0	153	Y
93-2447-15	217300	167630	90	0	67.1	Y
93-2447-17	216694	165531	90	0	88.4	Y
93-2448-17	217284	166154	90	0	45.6	Y
96-1578-01	214000	156850	90	0	526	Y
96-1578-01B	214000	156850	88	0	546	Y
96-1578-02	217570	159360	90	0	508	Y
96-1652-12	236510	182210	90	0	398.4	Y
96-2069-18	211510	164040	90	0	57.65	Y
96-2218-07	240640	183520	90	0	395.2	Y
96-2218-08	238990	182090	90	0	434.3	Y
96-2258-27A	219081.4	168180	90	0	173.7	Y
96-2447-14	216606.151	165031.372	90	0	202	Y
96-2447-15A	217081.183	165004	90	0	37.6	Y
96-2448-18	218352.232	165170.064	90	0	230.3	Y
96-3262-14a	221940	169797	90	0	269.5	Y
96-3262-16	219675	161462	90	0	319	Y
97-1652-13	235320	178190	90	0	637	Y
97-3263-14	243160	185980	90	0	133	Y
97-3263-15	243790	187070	90	0	40	Y
97-3263-16	243480	187220	90	0	340	Y
97-3667-01	234890	177550	90	0	694	Y
98-1650-69	241200	187410	90	0	82	Y
98-1650-70	241080	185920	90	0	127	Y
98-1650-71	241110	187460	90	0	109	Y
98-1650-72	240610	187630	90	0	175	Y
98-1650-73	240730	187800	90	0	172	Y
98-1652-14	238070	179820	90	0	650	Y
98-2069-21	213320	160115	90	0	136	Y
98-2069-22	211220	160020	90	0	171	Y
98-2069-23	211200	160145	90	0	115.2	Y
98-2218-09	238820	183033	90	0	385	Y
98-2218-10	240400	184330	90	0	205	Y
98-2258-31	218340	168780	90	0	190	Y
98-2258-32	218330	168540	90	0	196.8	Y
98-2258-33	216910	168230	90	0	125.3	Y
98-2258-34	216332.31	168984	90	0	37	Y
98-2258-35	218090.14	170870.27	90	0	66.3	Y
98-2258-36	218685	168800	90	0	218.7	Y
98-2258-37	219100	169230	90	0	221	Y
98-2447-19	217643.39	168213.43	90	0	101	Y
98-2447-20	217740.61	168552.83	90	0	146	Y
98-2447-21	216969.75	167987.62	90	0	119	Y
98-2447-22	216129.6	167963.41	90	0	98	Y
98-2447-23	216951.06	167682.48	90	0	68	Y
98-2447-24	217078.1	167600.84	90	0	59	Y
98-2447-25	217303.61	167904.38	90	0	44.35	Y

Appendix F: Drillhole data from the Rathdowney Trend

Drillhole Number	Easting	Northing	Dip	Azimuth	EOH (m)	Regional Dolomite (Y/N)
98-2447-26	217763.09	168095.27	90	0	113.9	Y
98-2447-27	217763.08	168095.26	60	180	94	Y
98-3158-10	244440	189270	90	0	265	Y
98-3158-12	246200	192975	90	0	289	Y
98-3262-17	221260	161415	90	0	373	Y
98-3262-18	221420	168600	90	0	269.5	Y
98-3321-01	221590	159955	90	0	274	Y
98-3688-05	237290	177935	90	0	591	Y
99-1578-03	217516	154462	80	150	532	Y
99-1650-74	239060	186975	90	0	99	Y
99-1650-75	239060	187075	90	0	172.5	Y
99-1650-76	240650	187060	90	0	130	Y
99-1650-77	238300	186200	90	0	147	Y
99-1650-78	236760	185500	90	0	245	Y
99-1652-15	236420	179850	90	0	648	Y
99-1652-16	237300	181850	90	0	554	Y
99-2218-11	240000	181380	90	0	310	Y
99-2218-12	239780	184140	90	0	251	Y
99-2448-20	217490.4	165772.9	85	191	91	Y
99-3263-17	243275	185600	90	0	721	Y
99-3667-02	234380	176230	90	0	727	Y